

1993

# Magmatism, Deformation And Mesothermal Metasomatism: Interpretation Of Aluminosilicate Mineral Assemblages In The Cargo Muchacho Mountains, Southeastern California

Eric Olinder Owens

Follow this and additional works at: <https://ir.lib.uwo.ca/digitizedtheses>

---

## Recommended Citation

Owens, Eric Olinder, "Magmatism, Deformation And Mesothermal Metasomatism: Interpretation Of Aluminosilicate Mineral Assemblages In The Cargo Muchacho Mountains, Southeastern California" (1993). *Digitized Theses*. 2199.  
<https://ir.lib.uwo.ca/digitizedtheses/2199>

This Dissertation is brought to you for free and open access by the Digitized Special Collections at Scholarship@Western. It has been accepted for inclusion in Digitized Theses by an authorized administrator of Scholarship@Western. For more information, please contact [tadam@uwo.ca](mailto:tadam@uwo.ca), [wlsadmin@uwo.ca](mailto:wlsadmin@uwo.ca).

The author of this thesis has granted The University of Western Ontario a non-exclusive license to reproduce and distribute copies of this thesis to users of Western Libraries. Copyright remains with the author.

Electronic theses and dissertations available in The University of Western Ontario's institutional repository (Scholarship@Western) are solely for the purpose of private study and research. They may not be copied or reproduced, except as permitted by copyright laws, without written authority of the copyright owner. Any commercial use or publication is strictly prohibited.

The original copyright license attesting to these terms and signed by the author of this thesis may be found in the original print version of the thesis, held by Western Libraries.

The thesis approval page signed by the examining committee may also be found in the original print version of the thesis held in Western Libraries.

Please contact Western Libraries for further information:

E-mail: [libadmin@uwo.ca](mailto:libadmin@uwo.ca)

Telephone: (519) 661-2111 Ext. 84796

Web site: <http://www.lib.uwo.ca/>

Magmatism, Deformation and Mesothermal Metasomatism:  
Interpretation of Aluminosilicate Mineral Assemblages in the  
Cargo Muchacho Mountains, Southeastern Calif.

by

Eric Olinder Lytle Owens

Department of Geology

Submitted in partial fulfilment  
of the requirements for the degree of  
Doctor of Philosophy

Faculty of Graduate Studies  
The University of Western Ontario  
London, Ontario  
November, 1992

©Eric Olinder Lytle Owens 1992



National Library  
of Canada

Acquisitions and  
Bibliographic Services Branch

395 Wellington Street  
Ottawa, Ontario  
K1A 0N4

Bibliothèque nationale  
du Canada

Direction des acquisitions et  
des services bibliographiques

395, rue Wellington  
Ottawa (Ontario)  
K1A 0N4

*Your file* *Votre référence*

*Our file* *Notre référence*

**The author has granted an irrevocable non-exclusive licence allowing the National Library of Canada to reproduce, loan, distribute or sell copies of his/her thesis by any means and in any form or format, making this thesis available to interested persons.**

**L'auteur a accordé une licence irrévocable et non exclusive permettant à la Bibliothèque nationale du Canada de reproduire, prêter, distribuer ou vendre des copies de sa thèse de quelque manière et sous quelque forme que ce soit pour mettre des exemplaires de cette thèse à la disposition des personnes intéressées.**

**The author retains ownership of the copyright in his/her thesis. Neither the thesis nor substantial extracts from it may be printed or otherwise reproduced without his/her permission.**

**L'auteur conserve la propriété du droit d'auteur qui protège sa thèse. Ni la thèse ni des extraits substantiels de celle-ci ne doivent être imprimés ou autrement reproduits sans son autorisation.**

ISBN 0-315-81274-5

**Canada**





FRONTISPIECE. View of the aluminosilicate assemblages at Micataic Hill, looking NE. K, Kyanite Zone; MM, magnetite subzone, Muscovite Zone; MB, biotite subzone, Muscovite Zone; F, Feldspar Zone. Dark layer between MM and MB is granoblastic quartz-tourmaline.

## ABSTRACT

Aluminosilicate mineral assemblages, with more than 30%  $\text{Al}_2\text{O}_3$  and less than 2%  $\text{CaO}+\text{Na}_2\text{O}+\text{K}_2\text{O}$ , occur on the western flank of the Cargo Muchacho Mountains, southeastern California. The aluminosilicate mineral assemblages are shallow-dipping tabular zones locally more than 100 m in total thickness. From bottom to top, they are: a.) the Feldspar Zone, with quartz-oligoclase-K-feldspar-biotite-epidote-magnetite, b.) the Muscovite Zone, with quartz-muscovite-biotite-magnetite-tourmaline-apatite, and c.) the Kyanite Zone, with quartz-kyanite-muscovite-magnetite-rutile-tourmaline-apatite (with or without andalusite, pyrophyllite, staurolite, lazulite, and specularite) occur in the Kyanite Zone.

The host rocks are fine grained quartzofeldspathic gneiss of the Tumco Formation, and Jurassic intrusive rocks. The latter are 173 Ma quartz diorite, a 173-160 Ma metaluminous to peraluminous suite of hornblende-biotite granodiorite, granite porphyry, and muscovite-biotite granite. and post-160 Ma pegmatite and aplite. Emplacement of the 173-160 Ma series coincided with deformation along low angle shear zones, and was accompanied by late magmatic albitization and muscovitization. Cross cutting relationships indicate development of the aluminosilicate assemblages occurred during the emplacement of the 173-160 Ma intrusive suite.

Bulk rock and mineral compositions vary regularly from quartzofeldspathic gneiss of the Tumco Formation into the

Kyanite Zone. Bulk rock  $\text{Al}_2\text{O}_3$ ,  $\text{TiO}_2$ ,  $\text{P}_2\text{O}_5$ , Ga and V increase from the gneiss across the Feldspar and Muscovite Zones, into the Kyanite Zone, whereas the transition metal oxides and alkali and alkaline earth oxides decrease in this same direction. Feldspar and mica become more aluminous, suggesting bulk rock control on mineral composition. The paragonite content of muscovite increases, and  $\text{Fe}/(\text{Fe}+\text{Mg})$  of biotite decreases into the Kyanite Zone. Tourmaline is schorl-dravite, with a low uvite component, and with increasing Fe from core to rim. The compositions of biotite and tourmaline, in conjunction with the transition from biotite-bearing assemblages to magnetite-bearing assemblages are consistent with progressive oxidation from the feldspar-bearing assemblages into the kyanite-bearing assemblages.

Mineral paragenesis, the fracture and vein occurrence of the minerals, and mineral equilibria in the zones of aluminosilicate mineral assemblages indicate development via early pervasive replacement by oxidizing, low to moderate pH fluids which removed most major cations from the Kyanite and Muscovite Zones. Cross-cutting S-C fabrics containing aluminosilicate mineral assemblages suggest pervasive replacement evolved to later shear zone-hosted replacement. Mineral equilibria indicate pressures and temperatures of aluminosilicate formation at about 5 Kb and  $550^\circ\text{C}$ , and suggest the source for the fluids was likely the 173-160 Ma metaluminous-peraluminous intrusive suite.

## ACKNOWLEDGEMENTS

Input on various aspects of the material contained herein came from a number of individuals. To those people, I extend my appreciation. Further thanks go to Dr. Robert W Hodder, my thesis supervisor, for guiding me through what sometimes seemed a morass of information, and helping me to keep the final goal in perspective. Thanks also go to the persons on my examining committee for many useful critical comments and thoughts: Drs. W.R. Church and W.S. Fyfe of the Geology Department at UWO, Dr. R.A. Secco of the Geophysics Department at JWO, and Dr. R.G. Wiese of Mount Union College. Drs. Lawrence P. Kennedy and Margery D. Osborne provided the impetus for this work: without them this project would not have gotten off the ground. In addition, thanks go to Joe Sawyer of American Girl Mining Corp. for allowing access to the property and, later, for providing access for a field excursion to the American Girl Mine.

I want to express my gratitude and love, first to my wife, Laurel, for her support and help when such things were needed, and to our daughter, Elaine, who reminded me of the truly important things in life. It is to them, and to "Eduardo", that I dedicate this thesis. Last, but not least, love and appreciation is sent to my parents, Betty Ericson and Arnold Owens, for their support throughout the duration of this project.

## TABLE OF CONTENTS

	Page
CERTIFICATE OF EXAMINATION . . . . .	ii
ABSTRACT . . . . .	iii
ACKNOWLEDGEMENTS . . . . .	v
TABLE OF CONTENTS . . . . .	vi
LIST OF TABLES . . . . .	ix
LIST OF PHOTOGRAPHIC PLATES . . . . .	x
LIST OF FIGURES . . . . .	xi
LIST OF APPENDICES . . . . .	xiv
CHAPTER ONE -- INTRODUCTION . . . . .	1
1.1. Statement of the Problem . . . . .	1
1.2. Previous Work . . . . .	5
1.3. Methods . . . . .	7
CHAPTER TWO -- REGIONAL GEOLOGY . . . . .	8
2.1. General Statement . . . . .	8
2.2. Pre-Mesozoic Geology . . . . .	8
2.3. Mesozoic and Cenozoic Geology . . . . .	11
2.4. General Geology of the Cargo Muchacho Mountains . . . . .	14
CHAPTER THREE - MESOZOIC AND TERTIARY COUNTRY ROCKS . . . . .	20
3.1. General Statement . . . . .	20
3.2. Tumco Formation . . . . .	20
3.3. Intrusive Rocks . . . . .	34
3.3.1. Regional Correlation . . . . .	34
3.3.2. Quartz Diorite . . . . .	35
3.3.3. Hornblende-biotite Granodiorite . . . . .	36
3.3.3.1. Field and Textural Relationships . . . . .	36
3.3.3.2. Feldspar Composition . . . . .	44
3.3.3.3. Biotite Composition . . . . .	47
3.3.3.4. Garnet Composition . . . . .	47
3.3.3.5. Origin of Mineral and Textural Variation . . . . .	48
3.3.4. Granite Porphyry . . . . .	50
3.3.5. Muscovite-Biotite Granite . . . . .	52
3.3.5.1. Field and Textural Relationships . . . . .	52
3.3.5.2. Feldspar Composition . . . . .	56
3.3.5.3. Muscovite Composition . . . . .	57
3.3.5.4. Biotite Composition . . . . .	60
3.3.5.5. Late to Post-Magmatic Changes . . . . .	60
3.3.6. Pegmatite and Aplite . . . . .	61
3.3.7. Compositional Variation and Magma Type . . . . .	62
3.4. Miocene Dacite . . . . .	62
3.5. Summary . . . . .	65

CHAPTER FOUR - MINERAL AND TEXTURAL VARIATION IN THE ZONES OF ALUMINOSILICATE ASSEMBLAGES . . .	68
4.1. General Statement . . . . .	68
4.2. Gross Characteristics . . . . .	72
4.2.1. Feldspar Zone . . . . .	72
4.2.2. Muscovite Zone . . . . .	75
4.2.3. Kyanite Zone . . . . .	78
4.2.4. Relationships to Intrusive Rocks . . . . .	84
4.3. Mineral, Textural and Compositional Variation . . . . .	85
4.3.1. Quartz . . . . .	85
4.3.2. Feldspar . . . . .	86
4.3.3. Muscovite . . . . .	87
4.3.4. Biotite . . . . .	100
4.3.5. Magnetite . . . . .	110
4.3.6. Kyanite . . . . .	110
4.3.7. Tourmaline and Apatite . . . . .	114
4.3.8. Garnet . . . . .	119
4.3.9. Rutile . . . . .	120
4.3.10. Trace Minerals . . . . .	125
4.4. Mineral Paragenesis . . . . .	125
4.5. Summary . . . . .	130
CHAPTER FIVE - STRUCTURE . . . . .	135
5.1. General Statement . . . . .	135
5.2. Domainal Analysis: Fabric Characteristics and Orientation . . . . .	136
5.2.1. Domain One: Foliated to Gneissic Fabric . . . . .	141
5.2.2. Domain Two: Schistose, Mylonitic and Crenulated Fabrics . . . . .	143
5.2.2.1. General Characteristics . . . . .	143
5.2.2.2. Foliation Characteristics and orientation . . . . .	151
5.2.2.3. Lineation Characteristics and Orientation . . . . .	153
5.2.2.4. D <sub>2</sub> Movement Direction . . . . .	154
5.2.3. Domain Three: Granoblastic Fabrics . . . . .	159
5.3. Post D <sub>2</sub> Deformation . . . . .	160
5.4. Summary . . . . .	163
CHAPTER SIX - MOBILITY OF MAJOR AND TRACE ELEMENTS . . . . .	167
6.1. General Statement . . . . .	167
6.2. Distribution of Elements . . . . .	167
6.2.1. Silicon . . . . .	170
6.2.2. Aluminum, Gallium, and Phosphorus . . . . .	170
6.2.3. Alkali and Alkaline Earth Oxides . . . . .	171
6.2.4. Transition Metals . . . . .	174
6.2.5. Ti, Zr, Nb, Y, and V . . . . .	175

6.3. Element Gains and Losses . . . . .	181
6.3.1. Methods . . . . .	181
6.3.2. Compositional Changes in the Feldspar and Kyanite Zones . . . . .	187
6.3.3. Compositional Changes in the Muscovite Zone . . . . .	190
6.4. Summary . . . . .	195
 CHAPTER 7 - MINERAL COMPOSITION, EQUILIBRIA AND CONDITIONS OF ALUMINOSILICATE FORMATION . . . . .	 200
7.1. General Statement . . . . .	200
7.2. Pervasive Metasomatism . . . . .	200
7.2.1. Bulk Rock Control on Mineral Composition . . . . .	200
7.2.2. Hydrolysis Reactions . . . . .	201
7.2.3. Oxidation Reactions . . . . .	207
7.2.4. pH of Fluids Affecting Hydrolysis Reactions . . . . .	209
7.2.5. Oxygen Fugacity . . . . .	209
7.3. Mylonite-Hosted Metasomatism . . . . .	215
7.3.1. Mineral Composition . . . . .	215
7.3.2. Deformation-Induced Mineral Reaction . . . . .	216
7.4. Evidence for a Magmatic Component to the Fluids . . . . .	218
7.5. Pressure and Temperature . . . . .	219
7.5.1. Pressure . . . . .	222
7.5.2. Two-Feldspar Thermometry . . . . .	223
7.5.3. Garnet-Biotite Thermometry . . . . .	223
7.5.4. Interpretation of Thermometry . . . . .	228
7.6. Summary . . . . .	231
 CHAPTER 8 - CONCLUSIONS . . . . .	 233
APPENDIX A. . . . .	237
APPENDIX B. . . . .	246
APPENDIX C. . . . .	251
APPENDIX D . . . . .	317
BIBLIOGRAPHY . . . . .	322
VITA . . . . .	341

**LIST OF TABLES**

Table	Description	Page
5-1	Average Fabric Orientations, Vitrifax Hill, Micatalc Hill, and Hedges . . . . .	142
7-1	Two-Feldspar Geothermometry . . . . .	224
7-2	Garnet-Biotite Geothermometry . . . . .	225



## LIST OF PHOTOGRAPHIC PLATES

Plate	Description	Page
1	Characteristics of the quartzofeldspathic gneiss and quartz diorite . . . . .	28
2	Characteristics of granodiorite and granite porphyry . . . . .	42
3	Characteristics of muscovite-biotite granite and pegmatite . . . . .	55
4	Characteristic textures of the Feldspar Zone .	74
5	Characteristics of the Musovite and Kyanite Zones . . . . .	77
6	Characteristics of the Kyanite Zone . . . . .	80
7	Characteristics of minerals and textures of the zones of aluminosilicate mineral assemblages .	83
8	Textural relationships of kyanite and tourmaline . . . . .	113
9	Kinematic indicators, Micatalc Hill . . . . .	158

## LIST OF FIGURES

Figure	Description	Page
2-1	Location and regional geology . . . . .	10
2-2	Geology of the Cargo Muchacho Mountains . . . . .	16
3-1	Geology of Micatalc Hill and Vitrifax Hill . . . . .	22
3-2	Geologic cross sections of Micatalc Hill and Vitrifax Hill . . . . .	24
3-3	Geology of the Hedges area . . . . .	26
3-4	Composition of K-feldspar from the country rocks . . . . .	31
3-5	Composition of biotite from the country rocks . . . . .	33
3-6	Detailed geologic relationships between muscovite-biotite granite and granodiorite at Micatalc Hill . . . . .	39
3-7	Composition of plagioclase from the intrusive rocks . . . . .	46
3-8	Composition of muscovite from muscovite-biotite granite . . . . .	59
3-9	Whole rock composition of the intrusive rocks . . . . .	64
4-1	Variation of modal mineralogy, zones of aluminosilicate mineral assemblages . . . . .	71
4-2	Composition of K-feldspar from the Feldspar Zone . . . . .	89
4-3	Composition of plagioclase from the zones of aluminosilicate mineral assemblages . . . . .	91
4-4	Composition of muscovite from the zones of aluminosilicate mineral assemblages . . . . .	95
4-5	Paragonite content of muscovite from the zones of aluminosilicate mineral assemblages . . . . .	97
4-6	Fe+Mg in white mica from the zones of alumino- silicate mineral assemblages . . . . .	99

4-7	Fe/(Fe+Mg) vs. Fe in white mica and biotite from the aluminosilicate assemblages . . . . .	102
4-8	Composition of biotite in the zones of aluminosilicate mineral assemblages . . . . .	104
4-9	Fe/(Fe+Mg) vs. Al-vi in biotite from the zones of aluminosilicate mineral assemblages . . . . .	107
4-10	Variation of Fe/(Fe+Mg) in micas at Micatalc Hill . . . . .	109
4-11	Tourmaline compositions on a molecular Al-Fe-Mg diagram . . . . .	116
4-12	Variation in composition from core to rim in tourmaline . . . . .	118
4-13	Composition of garnet in the zones of aluminosilicate mineral assemblages and hornblende-biotite granodiorite . . . . .	122
4-14	Variation in composition from core to rim in garnet . . . . .	124
4-15	Paragenetic sequence of minerals in the zones of aluminosilicate mineral assemblages . . . . .	127
5-1	Subdivision of domains at Micatalc Hill and Vitrifax Hill . . . . .	138
5-2	Subdivision of domains at Hedges . . . . .	140
5-3	Lower hemisphere stereographic projection, S <sub>1</sub> and S <sub>2</sub> at Micatalc Hill . . . . .	145
5-4	Lower hemisphere stereographic projection, S <sub>1</sub> and S <sub>2</sub> at Hedges . . . . .	147
5-5	Lower hemisphere stereographic projection, S <sub>1</sub> at Vitrifax Hill . . . . .	149
5-6	Lower hemisphere stereographic projection, L <sub>2</sub> at Micatalc Hill and Hedges . . . . .	156
5-7	Lower hemisphere stereographic projection, S <sub>1</sub> in Domain 3 at Vitrifax Hill . . . . .	162
6-1	Major element composition of the zones of aluminosilicate mineral assemblages . . . . .	169

6-2	Abundance of alkali and alkaline earth elements in the zones of aluminosilicate assemblages . . . . .	173
6-3	Abundance of transition metals in the zones of aluminosilicate assemblages . . . . .	177
6-4	Ti, Zr, V, Y, and Nb variation in the zones of aluminosilicate assemblages . . . . .	180
6-5	Isocon diagrams for the Feldspar and Kyanite Zones . . . . .	184
6-6	Isocon diagrams for the Muscovite Zone . . . . .	186
6-7	Transposed quartz veinlet in mylonitic Muscovite Zone . . . . .	189
6-8	Element gains and losses for the Feldspar Zone and Kyanite Zone . . . . .	192
6-9	Element gains and losses for the Muscovite Zone . . . . .	194
7-1	Activity-activity diagram for the $K_2O-Na_2O-Al_2O_3-SiO_2-H_2O$ system . . . . .	204
7-2	Annite composition as a function of pH and oxidation potential . . . . .	211
7-3	Temperature- $\log(fO_2)$ diagram . . . . .	213
7-4	Sample locations for temperature calculations . . . . .	227
7-5	Pressure-temperature diagram for the kyanite-bearing rocks . . . . .	230

**LIST OF APPENDICES**

<b>Appendix</b>		<b>Page</b>
APPENDIX 1	ROCK SAMPLES AND MODAL ANALYSES . . . .	240
APPENDIX 2	WHOLE ROCK X-RAY FLOURESCENCE ANALYSES .	249
APPENDIX 3	ELECTRON MICROPROBE ANALYSES, MINERAL FORMULA RECALCULATION AND GEOTHERMOMETER DERIVATIONS . . . . .	254
APPENDIX 4	FOLIATION AND LINEATION DATA . . . . .	317

## CHAPTER ONE -- INTRODUCTION.

### 1.1. Statement of the Problem.

Quartz-kyanite granofels, containing greater than 30%  $Al_2O_3$ , and less than 2% total  $CaO+Na_2O+K_2O$ , occurs at three sites along the west flank of the Cargo Muchacho Mountains, southeastern California. These aluminum-rich rocks are part of a mineral assemblage sequence which is hosted in variably deformed Jurassic metasedimentary and meta-igneous rocks, and which occurs along strike with two of the gold deposits in the range. Regional metamorphic rocks contain the assemblage quartz-plagioclase-K-feldspar-biotite-epidote-magnetite, with minor hornblende, chlorite, carbonate and garnet. These rocks grade into the assemblage quartz-plagioclase-biotite-epidote-magnetite, which grades into the assemblage quartz-muscovite-biotite-magnetite. The latter assemblage contains local high contents of tourmaline and apatite, as well as a low content of garnet. The muscovite-bearing rocks in turn grade into the aluminum-rich rocks, with the assemblage quartz-kyanite-muscovite-magnetite, which also contains local tourmaline, rutile, apatite, lazulite, andalusite, hematite, limonite after pyrite, and pyrophyllite.

The  $Al_2O_3$  content of the kyanite-bearing rocks represents an enrichment of 2 to 3 times over that of "average" continental crust (Fyfe et. al., 1978; Hyndman, 1972). Because the solubility of aluminum-rich phases is low in near-neutral pH fluids, aluminum is considered a relatively immobile element

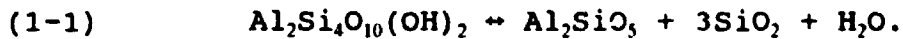
under most conditions in the continental crust (Hem and Roberson, 1967; Meyer and Hemley, 1967; Sokolova and Khodakovskiy, 1977). Enrichment is therefore not thought to occur by addition of aluminum to the rocks, but by the removal of other, more reactive cations from the rocks (Guilbert and Parks, 1986; Kerrich et. al., 1987). Such enrichment may occur in environments under a wide variety of pressure and temperature conditions. Well known among these is the weathering environment, where silicate decomposition results in the concentration of aluminum and the formation of bauxite and other products of soils (Norton, 1973; Meillon, 1978).

This process of cation removal by fluid-rock interaction is known as hydrogen-ion metasomatism, and has been studied extensively at relatively low pressures and temperatures (Hemley, 1959; Hemley and Jones, 1964; Shade, 1974; Helgeson, 1974; Hemley et. al., 1980). Experimental work in the system  $K_2O-Na_2O-Al_2O_3-SiO_2-H_2O$  indicate that continued reaction of a quartz-feldspar rock with low pH fluids results in the production of mineral phases progressively richer in aluminum and depleted in alkali ions. These experiments were originally performed to explain mineral zonation around quartz veins at Butte, Montana, which, from vein outward, consists of kaolinite, white mica, and feldspar. The results, however, have been commonly applied to alteration zones of a wide range of sizes from a variety ore deposits, including epithermal precious and base metal deposits, porphyry deposits, and massive sulfide deposits (Burnham, 1962; Geiger, 1963;

Gustafson and Hunt, 1975; Beane and Titley, 1980; Henley et. al., 1984; Steefel and Atkinson, 1984; Berger and Bethke, 1985; Stoffregen, 1987; Marquis et. al., 1990). Concentration of aluminum in these alteration zones is reflected in the mineral assemblages, variously containing kaolinite, dickite, white mica, topaz, pyrophyllite and andalusite, depending on temperature of formation.

Although no experimental data exists for pressures and temperatures above about 1 to 2 Kb and 350°C, thermodynamic studies indicate that the same relationships hold at least up to 500°C and 6 Kb (Wise, 1974; Wintsch, 1975b; Bowers, et. al., 1986). As such, the occurrence of aluminum-rich mineral assemblages in metamorphic rocks has stimulated debate about the genesis of these assemblages. Numerous workers have presented evidence that aluminum enrichment occurred at relatively low pressures and temperatures, during hydrothermal alteration or weathering, and was subsequently metamorphosed to new aluminous assemblages stable at higher metamorphic pressures and temperatures (Sykes and Moody, 1978; Valliant et. al., 1983; Schmidt, 1985; Ririe, 1990). The mineralogical changes are governed by dehydration reactions, which are common in prograde regional metamorphism (Fyfe et. al., 1978). Minerals stable at low pressure and temperature, such as kaolinite, dickite, and pyrophyllite, form assemblages stable at higher temperatures and pressures, as with the conversion of pyrophyllite to andalusite or kyanite:





In contrast, other workers have presented evidence that aluminum-enrichment through hydrogen-ion metasomatism has occurred at relatively high pressures and temperatures in a variety of environments. Some occurrences can be directly related to some stage of magma emplacement where cation removal is accomplished by late magmatic fluids (Gresens, 1971; Wise, 1974; Dillon, 1976; Vernon et. al. 1987). Other sites are not as clearly defined genetically, but suggest origins at relatively deep crustal sites (Kerrick et. al., 1987). The presence of high-aluminum mineral assemblages in shear zones has been noted by Banerji (1981) and Tourigny et. al. (1989), and suggests deformation played a role in the formation of such assemblages.

The purpose of the present study is to examine the aluminosilicate assemblages in the Cargo Muchacho Mountains in light of the experimental and thermodynamic work discussed above: do these assemblages represent metamorphism of a sedimentary sequence which contained primary compositional differences or do they represent the products of aluminum-enrichment before, during or after peak metamorphism? Evidence that the latter may have occurred includes the small size of the aluminosilicate assemblages, the spatial relationships of the assemblages to plutonic rocks and shear zones in the range, and the presence of aluminosilicate assemblages in the plutonic rocks. In addition, although the Tumco Formation

is layered, with quartzite, mafic gneiss, and marble, the great bulk of the formation consists of relatively uniform, fine grained quartzofeldspathic gneiss. The relatively sharp progression of mineral and compositional changes over small distances in the aluminosilicate assemblages is thus an uncommon and localized feature within the Tumco Formation.

### 1.2. Previous Work.

The first formal geologic study of the Cargo Muchacho Mountains was undertaken by Henshaw (1942), as part of an evaluation of the state's resources by the California Division of Mines. The basic relationships and terminology initiated in that study are for the most part in use today. The country rock into which the intrusive rocks were emplaced was defined as the Tumco Formation, thought to be of Precambrian age, and consisting primarily of quartzofeldspathic gneiss. The kyanite-bearing rocks and associated white mica schist, were given the name Vitrifax Formation, and its origin was ascribed to metamorphism of pelitic rocks or to contact metasomatism. Henshaw recognized the existence of major low angle faults and showed that they hosted gold mineralization in the range.

Dillon (1976) provided considerable detail on the magmatic and structural history of the range. U-Pb age determinations showed the granitic orthogneisses are Jurassic. Quartz diorite, however, remained undated, and was tentatively assigned a Proterozoic age. A Proterozoic age was also proposed for the Tumco Formation, similar to the conclusions

of Henshaw (1942). Parallelism of the fabric elements in the Cargo Muchacho Mountains to that of the Chocolate Mountains Thrust Fault, 15 Km to the north, led Dillon (1976) to conclude that metamorphism and thrusting were contemporaneous. The kyanite-bearing rocks were thought to have arisen as a result of contact metasomatism of the Tumco Formation by Jurassic granites.

Branham (1988) studied the geology and alteration in and around the American Girl Mine. Emplacement of granites and movement along the American Girl Fault, which hosts the gold deposit, were thought to be partly contemporaneous, and that movement along the American Girl Fault was both normal and reverse. It was suggested that the aluminosilicate assemblages, which occur along strike with the American Girl Mine, was earlier than main stage gold mineralization. Fluid inclusion data from one sample of quartz-kyanite granulites yielded homogenization temperatures of 280°C (Branham, 1988).

The Al-hornblende geobarometry work of Hayes (1989) put the depth of crystallization of the quartz diorite at 22 Km (6 Kb), and Murphy et. al. (1990) and Tosdal and Wooden (1991) provided U-Pb zircon data which indicates it is about 173 Ma. These workers suggest that the intrusive rocks are part of a regionally extensive calc-alkaline to mildly alkaline Jurassic batholith. In addition, Tosdal and Haxel (1987) and Tosdal (1990) concluded that normal movement along the American Girl Fault during the Jurassic suggests extension may have been an important aspect of this magmatism.

### 1.3. Methods.

Detailed mapping in and around the aluminosilicate mineral assemblages occurred during 1987, 1988 and 1989. Data acquired in the field and from the examination of about 200 thin sections is the basis for evaluating lithologic, mineralogic and temporal relationships. Thirty-six rock samples of the aluminosilicate assemblages and intrusive rocks were analyzed by X-Ray Fluorescence (XRF) in order to provide information on the nature of compositional changes which occurred during formation. Individual mineral grains were analyzed by electron microprobe, and include 35 K-feldspar, 150 plagioclase, 150 white mica, 140 biotite, 90 garnet, and 65 tourmaline analyses. This data is used in geothermometry and in the evaluation of the conditions of aluminosilicate formation.

## CHAPTER TWO -- REGIONAL GEOLOGY.

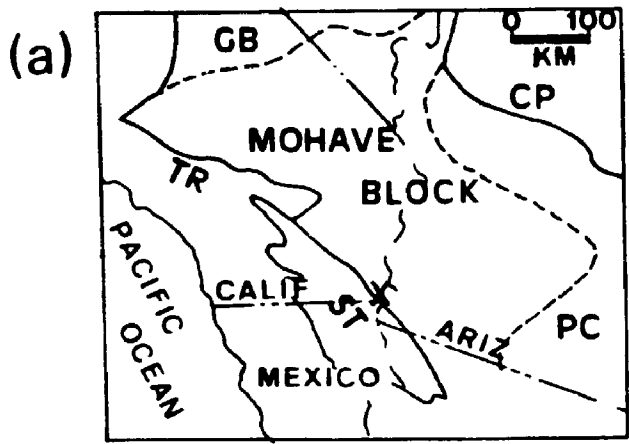
### 2.1. General Statement.

The Cargo Muchacho Mountains are in the extreme southeast corner of California, within the Mojave Desert block of the southern Basin and Range Province (Fig. 2-1). They are within the upper plate of the east-striking Chocolate Mountains Thrust Fault, a major Laramide structure approximately 15 Km to the north of the range. The southern Basin and Range consists of variably deformed Proterozoic to Cenozoic igneous, sedimentary and metamorphic rocks. These are overlain by relatively unlithified Quaternary and Recent marine and fluvial sedimentary rocks and basalt flows. The geologic history is of an active continental margin, changing character throughout Proterozoic and Phanerozoic times (Dickinson, 1981a). Present geologic relationships in the Cargo Muchacho Mountains are dominantly those of Mesozoic and early Cenozoic events.

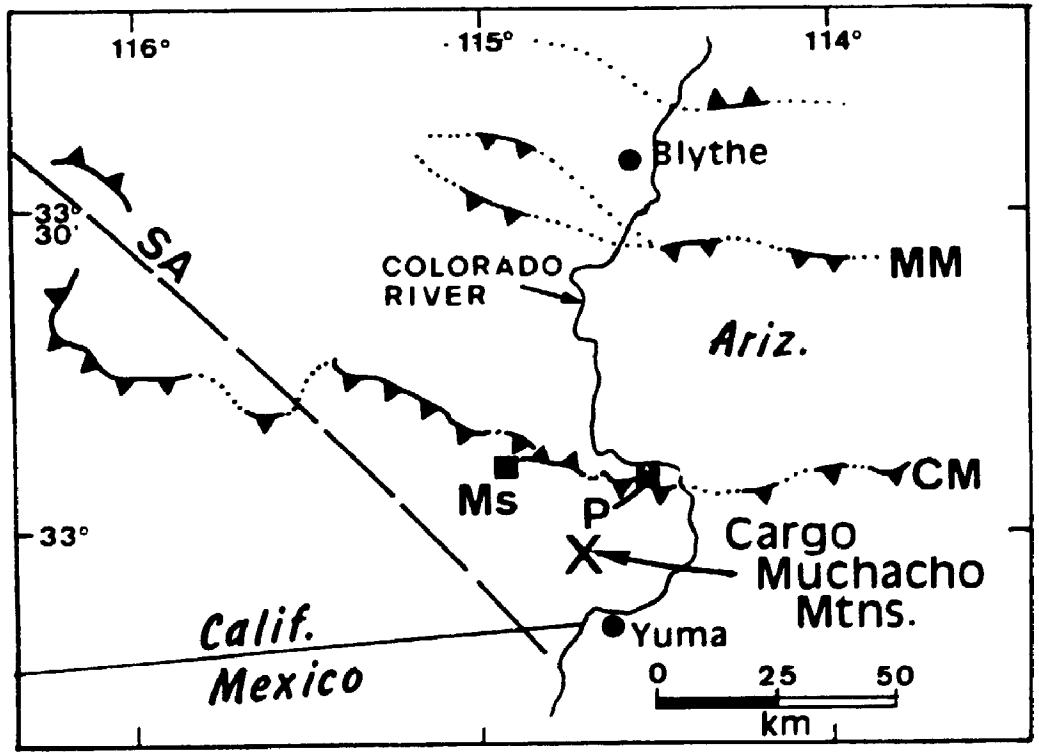
### 2.2. Pre-Mesozoic Geology.

Oldest exposed rocks in the region are Proterozoic quartzofeldspathic gneisses, migmatites, mafic gneiss and granitic rocks, with apparent U/Pb ages of 1.44 to 1.7 Ga (Olmsted et. al., 1973; Dillon, 1976; Garner, et. al. 1982). Rapikivi granites in the region are thought to be part of a 1.4 to 1.5 Ma anorogenic suite of granites extending from Wisconsin to southern California (Silver et. al., 1977). Metamorphic grade increases from greenschist in central Arizona to granulite in

**FIGURE 2-1. a.)** Location of the Cargo Muchacho Mountains. Symbols: **CP**, Colorado Plateau; **GB**, Great Basin; **PC**, Porphyry Copper Block; **ST**, Salton Trough; **X**, location of the Cargo Muchacho Mountains. **b.)** Location of major Laramide low angle faults and the San Andreas Fault in the southern Colorado River Basin. Symbols: dot-solid lines with teeth are late Cretaceous thrust faults; **CM**, trace of the Chocolate Mountains-Vincent Thrust Fault; **MM**, trace of the Mule Mountains Thrust Fault; **Ms**, Mesquite Mine; **P**, Picacho Mine; **SA**, trace of the easternmost fault of the San Andreas Fault System. Compiled from Haxel and Dillon (1978), Wilkins (1984), Haxel et. al. (1985), and Tosdal (1986b).



(b)



southern Nevada. In the lower Colorado River region, the rocks are part of a belt of upper amphibolite-grade metamorphic rocks, with high thermal gradients of 50°C/Km determined from mineral geothermometry (Thomas et. al., 1988).

Late Proterozoic and Paleozoic carbonate and clastic rocks are exposed over much of the southern Basin and Range and Colorado Plateau. These platformal deposits reflect a change from an active margin to a trailing edge, Atlantic-type margin (Dickinson, 1981a). However, no Paleozoic rocks have been positively identified in the lower Colorado River region. The nearest known exposures of Paleozoic cratonal rocks are 150 km north of the Cargo Muchacho Mountains in the Big Maria Mountains, the Plomosa Mountains, and Little San Bernardino Mountains, to the east in Arizona, and to the south in Mexico (Hamilton, 1987). To explain the absence of Paleozoic rocks, Coney (1981) has speculated on the presence of post-Paleozoic suspect terrains, and Anderson and Silver (1979) have proposed the existence of a major Mesozoic left-lateral transcurrent fault, the Mohave-Sonora Megashear.

### **2.3. Mesozoic and Cenozoic Geology.**

Mesozoic rocks in the Colorado River region indicate a change from a passive margin to an Andean-style subduction zone, culminating in the Laramide Orogeny from 80 Ma to 40 Ma (Coney, 1981; Dickinson, 1981a). The timing and styles of magmatism and metamorphism varied across the southern Basin and Range Province. Magmatism and regional metamorphism to



upper greenschist and lower amphibolite facies began in the Triassic in California, became more widespread during the Jurassic, and led to the emplacement of the regionally extensive Jurassic calc-alkaline batholith of Tosdal and Wooden (1991). With time, this activity migrated eastward, culminating in Arizona during the early Paleocene. Most of the magmatism, with associated with porphyry copper deposits, were emplaced during the latter half of this interval, as about 90% of Laramide magmatism occurred from 75 Ma to 50 Ma (Damon et. al., 1981). The latest Cretaceous and earliest Tertiary were accompanied by emplacement of peraluminous granitic rocks over much of the southern Basin and Range (Haxel et. al., 1984).

In contrast to the Paleozoic, Mesozoic sedimentary rocks are predominantly fluvial and continental red-beds. Triassic strata in the Mojave Block consist of early marine to continental clastic and carbonate sequences which changed with time to coarse clastic and volcanoclastic rocks through the Jurassic (Hamilton, 1987; Walker, 1987). No early to middle Mesozoic rocks have been positively identified in the lower Colorado River region. Metamorphosed clastic rocks of inferred late Mesozoic age, the Orocopia Schist and the Winterhaven Formation, are exposed in the Chocolate Mountains and Peter Kane Mountains, about 20 Km north of the Cargo Muchacho Mountains (Dillon, 1976; Haxel, 1977; Haxel et. al., 1985). Recent studies of the late Jurassic(?) to Cretaceous McCoy Mountains Formation and the Jurassic(?) Winterhaven Formation

indicate that later Mesozoic sedimentary rocks occur in ESE-striking structural basins, now with WNW antiformal patterns (Harding and Coney, 1985; Frost and Okaya, 1986).

Deformation accompanying metamorphism and magmatism included both compressional and extensional faulting beginning at least in the Jurassic (Dillon, 1976; Tosdal and Haxel, 1987; Dickinson, 1981a). The most prominent of these structures are regionally extensive east-striking Laramide thrust faults, including the Chocolate Mountains Thrust Fault and the Mule Mountains Thrust Fault (Fig. 2-1). Isotopic ages, in conjunction with cross cutting relationships, indicate north-east-directed movement along these thrusts occurred between 87 and 65 Ma (Tosdal, 1986b).

Cessation of subduction led to the onset of extensional tectonics in the Cenozoic and the inception of the San Andreas Fault system, which began around 29 Ma (Dickinson, 1981b; Crowell, 1981). Low angle normal faults, or detachment faults, became widespread throughout the southwestern U.S., beginning about 26 Ma and continuing to about 14 Ma (Rehrig, 1982). Although none have been positively identified in the Cargo Muchacho Mountains, detachment surfaces host gold mineralization at the Picacho Mine in the Peter Kane Mountain area, 15 Km to the northeast. High angle normal faults began after the mid-Miocene, giving rise to the current physiographic relationships of the Basin and Range.

Cenozoic magmatism is characterized by widespread explosive volcanism, represented in the lower Colorado River

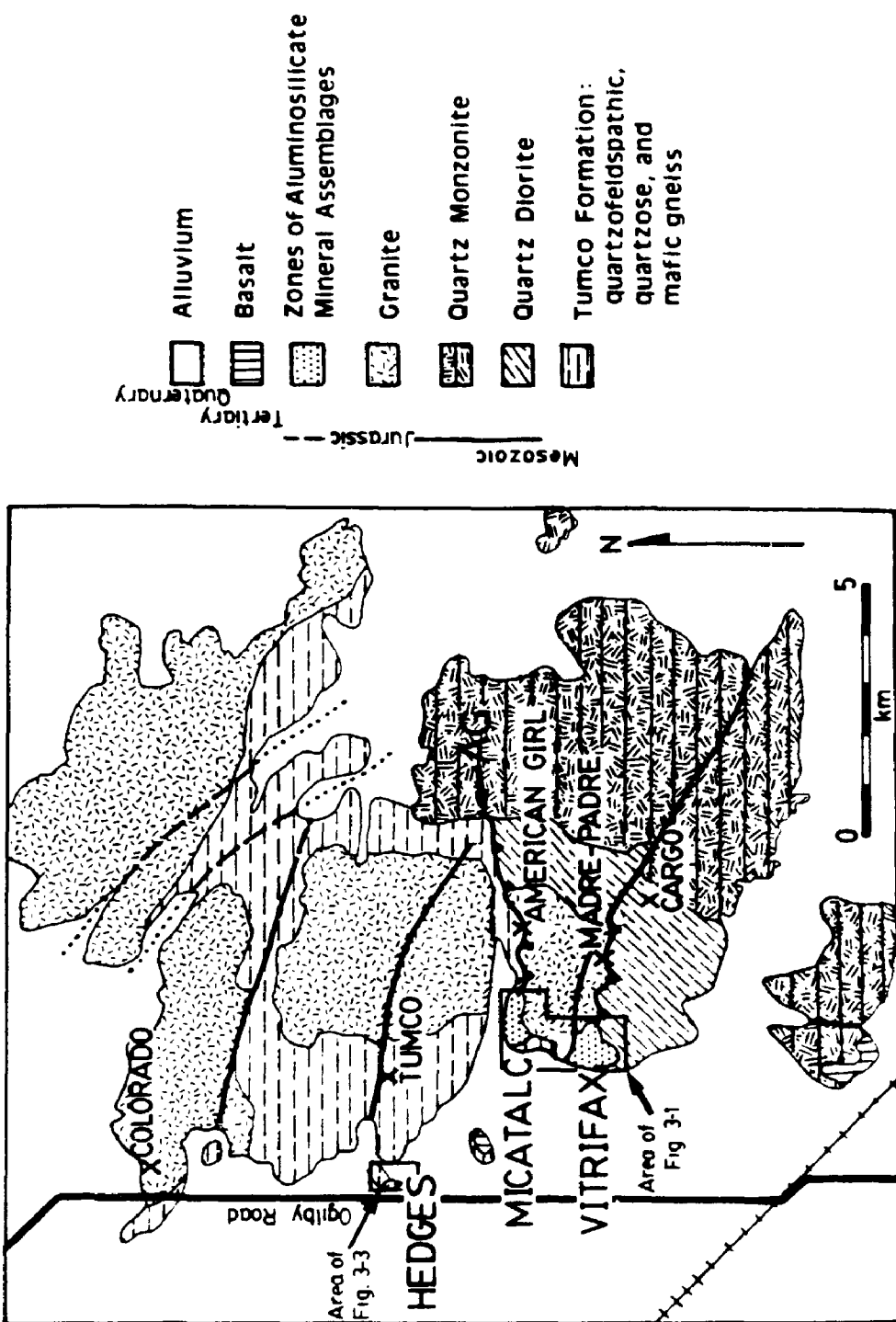
region by the 32 Ma Quechan volcanics and 26.2 Ma Ferguson Wash ignimbrite (Dillon, 1976; Crowe, 1978). This changed to predominantly basalt-rhyolite volcanism from about 19 Ma to 13 Ma (Murray, 1982), with the most recent basalt flows at about 5 Ma (Dillon, 1976). Interbedded with these rocks are continental conglomerates and other coarse clastic rocks, plus finer grained shallow marine deposits in basins.

#### **2.4. General Geology of the Cargo Muchacho Mountains.**

The Cargo Muchacho Mountains are underlain primarily by Jurassic foliated diorite to granite which has intruded Mesozoic quartzofeldspathic gneiss of the Tumco Formation (Fig.2-2). These rocks are variably folded and metamorphosed to epidote-amphibolite facies. Foliation generally dips less than 30° to the SSW. Foliation-parallel shear zones, which host gold deposits, occupy major east-west drainages in the central part of the range. Zones of aluminosilicate minerals occur at the western ends of 3 of these valleys, at Hedges (Tumco Valley), Micatahc (American Girl Canyon), and Vitrifax (Madre-Padre Valley). Unmetamorphosed dacite, thought to be mid-Tertiary in age, cross cuts the aluminosilicate assemblages and basalt flows occur on the flanks of the range.

The oldest rocks in the area, the Tumco Formation, are fine grained quartz-feldspar-biotite-epidote-magnetite gneiss, with minor marble, quartzite, mafic gneiss and schist, and metaconglomerate. Both Dillon (1976) and Branham (1988) indicate a significant volcanoclastic component to the gneiss.

**FIGURE 2-2.** General geology of the Cargo Muchacho Mountains. Heavy solid lines are faults. Low angle faults are shown with teeth on the upper plate. AG is the American Girl Fault. X's locate past and present Au mines. Location of the detailed geologic maps of Figs. 3-1 and 3-3 are shown. Compiled from Dillon (1976) and Tosdal (1986a).



- Alluvium
  - Basalt
  - Zones of Aluminosilicate Mineral Assemblages
  - Granite
  - Quartz Monzonite
  - Quartz Diorite
  - Tumco Formation: quartzofeldspathic, quartzose, and mafic gneiss
- Mesozoic  
 Jurassic  
 Tertiary  
 Quaternary

Although Dillon (1976) and Henshaw (1942) suggested a Precambrian age based upon lithologic similarity to other gneisses in the region, U-Pb isotopic ratios in zircons indicate a Mesozoic age for the protolith (Tosdal, pers. communication, 1990).

The Tumco Formation has been intruded by Jurassic quartz diorite, quartz monzonite, and granite, the latter with 3 phases: a hypidiomorphic granular phase, a porphyritic phase and a leucocratic, pegmatitic phase. The first two phases are mutually intrusive into one another. These plutonic rocks are part of three regionally extensive intrusive suites, based on U-Pb age determinations (Dillon, 1976; Murphy et. al., 1990; Tosdal and Wooden, 1991). The earlier, 173 Ma suite consists of diorite-monzodiorite (quartz diorite and quartz monzonite on Fig. 2-2), part of a Middle to Late Jurassic, calc-alkaline diorite to granite batholith. The granite is part of a second, more differentiated suite, at 160-173 Ma, and pegmatite (see Fig. 3-3) is part of a 158-160 Ma leucocratic granite suite.

Metamorphic grade is epidote-amphibolite facies in all pre-Tertiary rocks, whereas it is greenschist facies in Tertiary dacite. Foliation-parallel mylonitic fabrics of shear zones overprint metamorphic fabric, and the parallelism of metamorphic and mylonitic fabrics led Dillon (1976) to conclude that metamorphism and mylonitization were contemporaneous and related to the Laramide Chocolate Mountains Thrust Fault. However, field relationships and K/Ar ages indicate

that both metamorphism and mylonitization began in the Jurassic (Tosdal, 1986a and 1990).

Faults are mainly east trending, south-dipping, low angle faults and NNW-trending high angle faults. The low angle faults are mylonitic shear zones, sub-parallel to the regional metamorphic fabric. The NNW-striking faults are of two types. The first type contains mylonitic fabrics similar to the low angle structures and the second type contains fault gouge and breccia characteristic of brittle behavior at shallower crustal levels. The latter appear to be younger, offsetting all rock units. Some, if not most, of these are probably related to the San Andreas Fault system (Dillon, 1976).

Gold occurs in quartz veins and disseminations in foliated intrusive rocks and quartzofeldspathic gneiss (Henshaw, 1942; Dillon, 1976; Branham, 1988). The quartz veins are in low angle shear zones, as in the American Girl Fault (Fig. 2-2), although shear zones appear to be absent from the Tumco Camp, historically the most productive of the camps. Within the veins, quartz is the dominant gangue mineral, usually with carbonate, chlorite, epidote, tourmaline, sericite and biotite, and rare fluorite, orthoclase, magnetite, hematite, apatite, topaz, zircon and sphene. Pyrite is the most abundant sulfide mineral, with minor chalcopyrite. A temporal sequence is indicated by Branham (1988) in which minor deposition of gold occurred during early ductile deformation, with the alteration assemblage K-feldspar-biotite-magnetite-epidote. This was followed by brittle

deformation and mainstage gold deposition associated with the propylitic assemblage quartz-chlorite-pyrite-sericite-chalcopyrite.



## **CHAPTER THREE -- MESOZOIC AND TERTIARY COUNTRY ROCKS.**

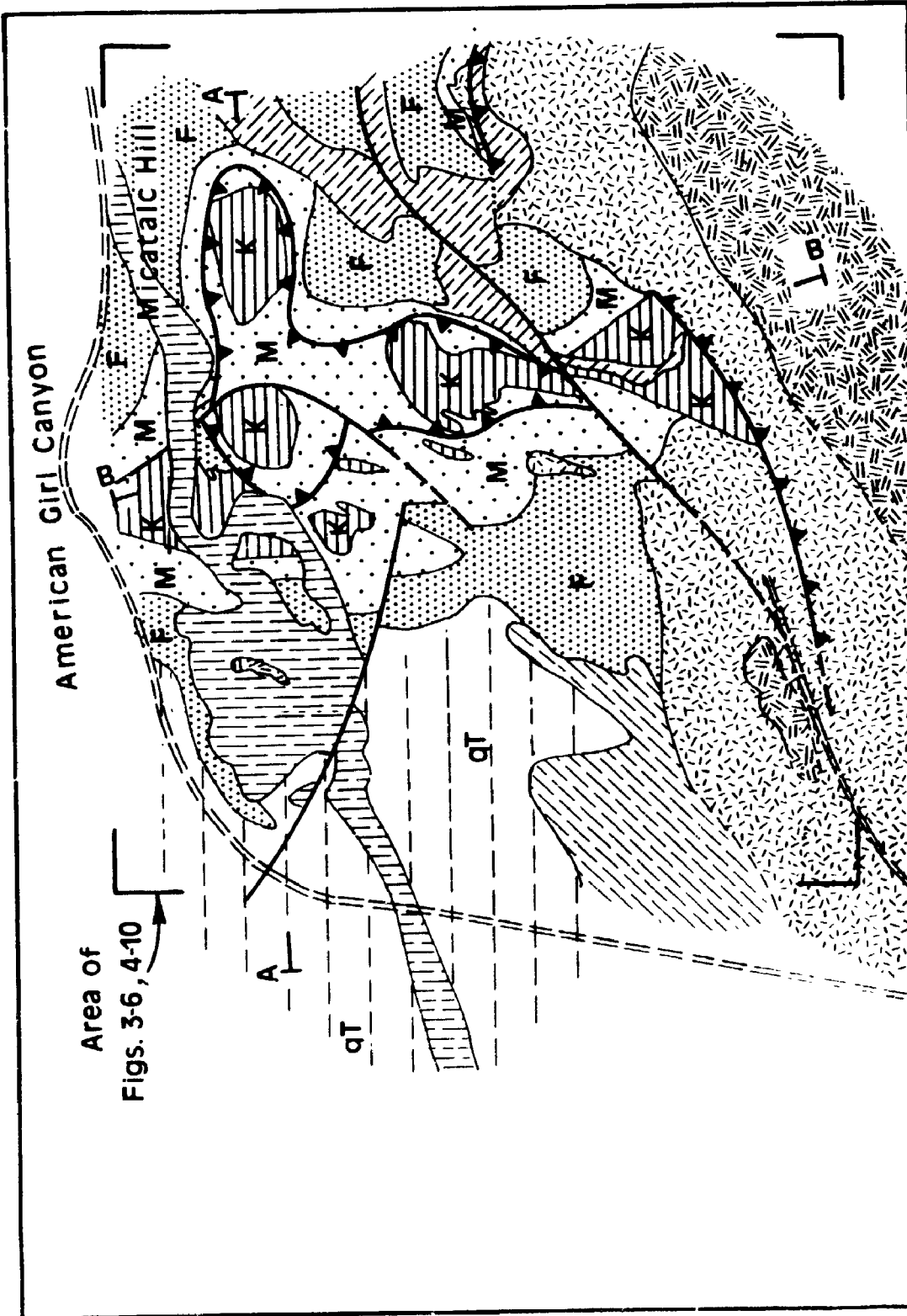
### **3.1. General Statement.**

In the thesis area, the country rocks which host the zones of aluminosilicate mineral assemblages are variably deformed quartzofeldspathic gneiss, quartzite, and mafic gneiss of the Tumco Formation, and foliated quartz diorite, granodiorite and granite (Figs. 3-1 to 3-3). Low angle, foliation-parallel shear zones cross cut these rocks, including the zones of aluminosilicate assemblages. Age relationships are sometimes obscure because many contacts are concordant to the regional foliation, but this work, in conjunction with that from Dillon (1976) and Branham (1988), gives considerable detail to relative ages.

### **3.2. Tumco Formation.**

The Tumco Formation is primarily quartzofeldspathic gneiss, with minor quartzite and quartz-epidote-hornblende granofels. Quartzofeldspathic gneiss contains the assemblage quartz-microcline-albite-oligoclase-biotite-epidote-magnetite. Subrounded to angular, matrix-supported clasts, 2 cm to 15 cm long, comprise up to 10% of the gneiss (Plate 1a). Compositional and textural layering are uncommon, but generally concordant with the penetrative fabric, which dips 30° south. This layering may be sharp or diffuse (Plate 1b), the sharper contacts occurring where quartz-rich, mica-poor layers alternate with mica-rich gneiss. Rounded quartz grains in some of these layers suggest a sedimentary origin for some

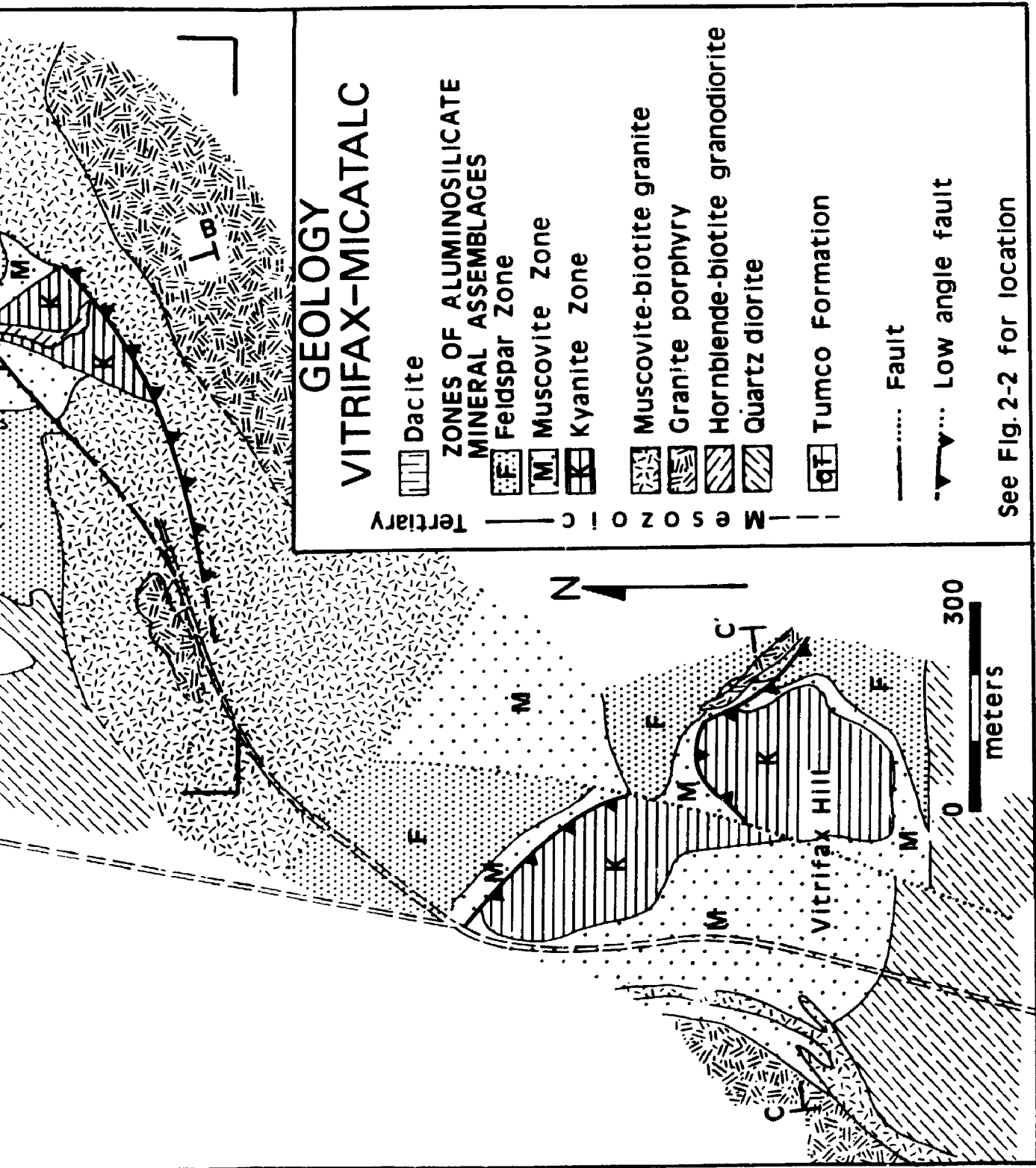
**FIGURE 3-1.** Geology of Micatahc Hill and Vitrifax Hill. A-A', B-B', and C-C' are the traces of cross sections of Figure 3-2. Low angle faults at Micatahc Hill are the western extension of the American Girl Fault; teeth on hanging wall. Area of Figs. 3-6 and 4-10 is within the box defined by the four marked corners.



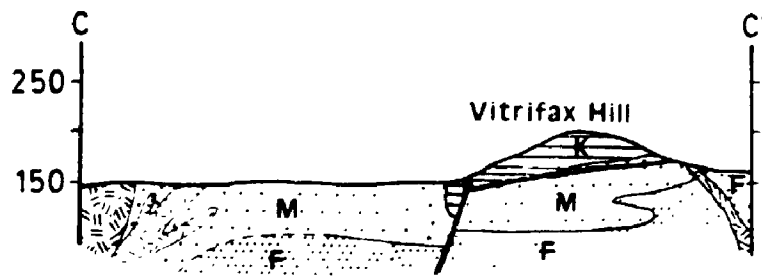
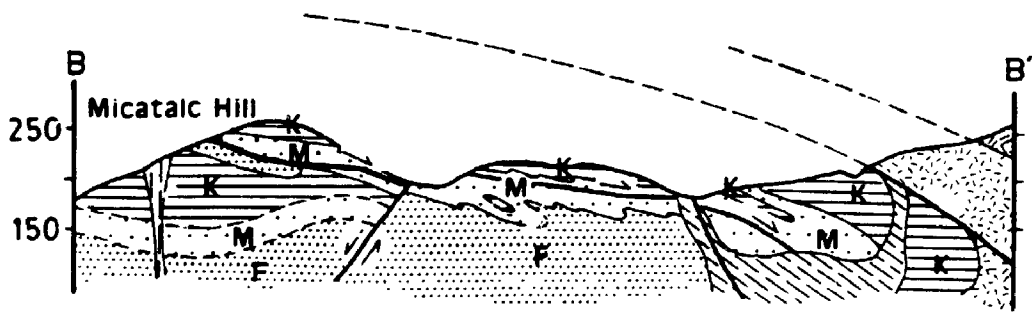
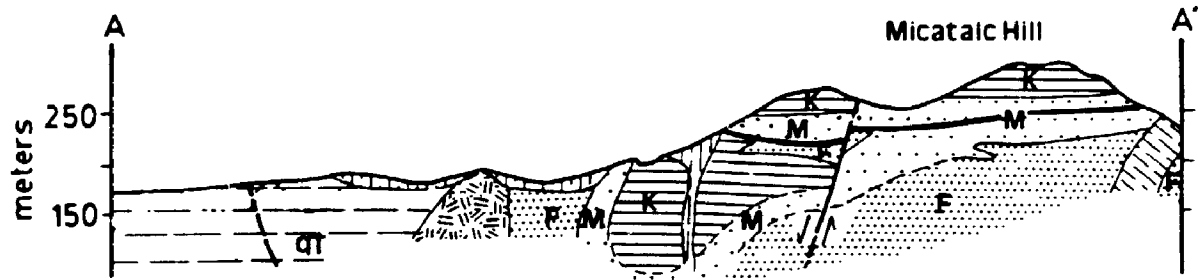
Area of  
Figs. 3-6, 4-10

**GEOLOGY**  
**VITRIFAX-MICATALC**

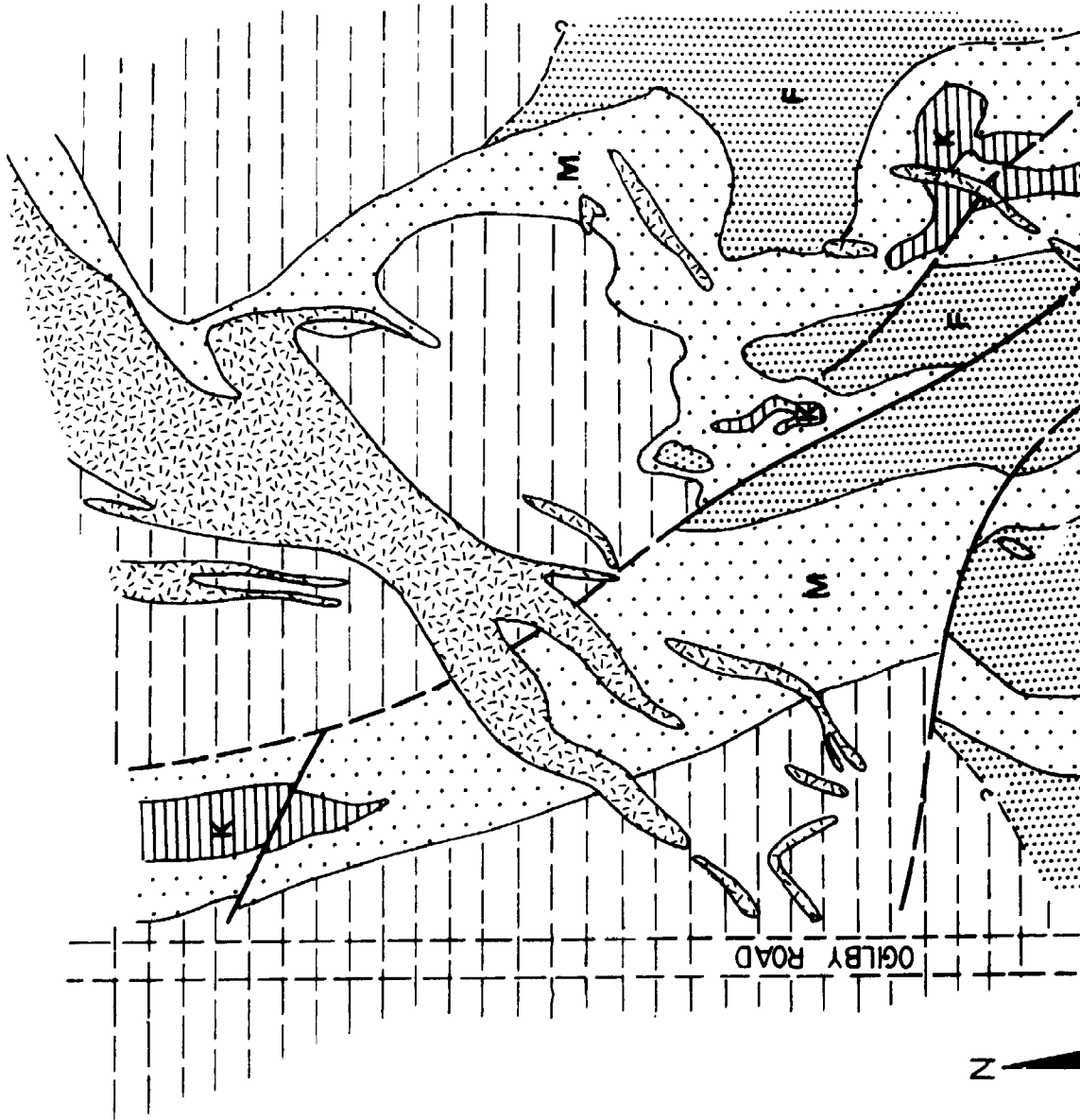
□ Dacite  
□ TONES OF ALUMINOSILICATE  
□ Secondary



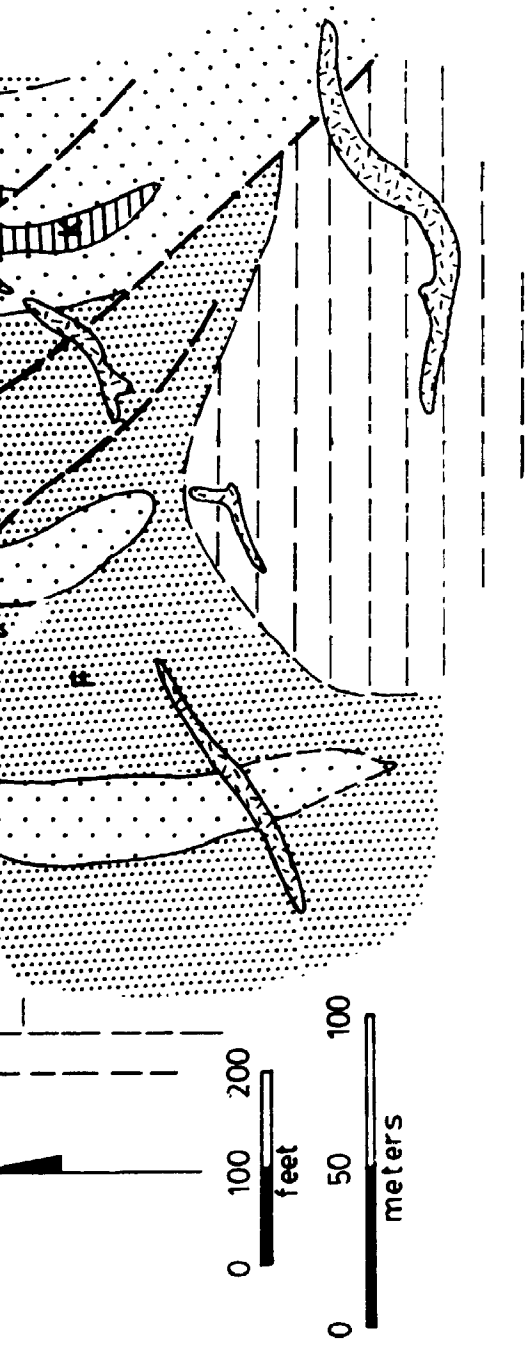
**FIGURE 3-2.** Cross sections of Micatale Hill and Vitrifax Hill. Symbols and scale are the same as in Figure 3-1. No vertical exaggeration.



**FIGURE 3-3.** Geology of the Hedges area.








# GEOLOGY OF HEDGES

SE1/4 NW1/4 SECT 11 T15S R20E

## ZONES OF ALUMINOSILICATE MINERAL ASSEMBLAGES

 Pegmatite

 Feldspar Zone

 Muscovite Zone

 Kyanite Zone

 Tumco Formation

See Fig 2-2 for location

**PLATE 1.** Characteristics of quartzofeldspathic gneiss of the Tumco Formation and quartz diorite. **a.)** Matrix-supported, sub-angular to sub-rounded lithic fragment in quartzofeldspathic gneiss, Tumco Formation, Hedges area. **b.)** Layering in the Muscovite Zone, Micatahc Hill area, interpreted as relict bedding. **c.)** Quartz-muscovite-chlorite-apatite-magnetite-kyanite inclusions (dark) in quartz-muscovite-magnetite-apatite-chlorite granofels interpreted as altered quartz diorite. **d.)** Photomicrograph of quartz diorite, plane light. Aggregate of hornblende and biotite elongate parallel to the foliation; hornblende are the coarser grained, euhedral prisms, biotite is finer grained; groundmass is medium grained quartz and feldspar, dark area at top of slide is coarse plagioclase porphyroblast. Scale bar equals 1 mm. **e.)** Close-up of aggregate shown in (d), showing biotite (B) replacing hornblende (H) and intergrown with magnetite (mt). Scale bar equals 0.1 mm. **f.)** Photomicrograph of host rock in (c): coarse, randomly oriented chlorite (Ch) in a groundmass of quartz, fine, non-oriented muscovite (ms), and apatite (not shown). Scale bar equals 0.5 mm.

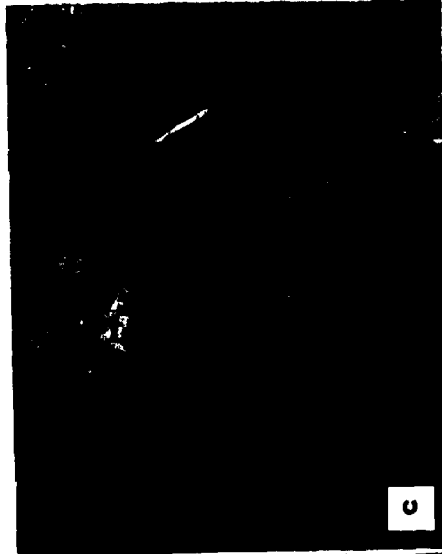
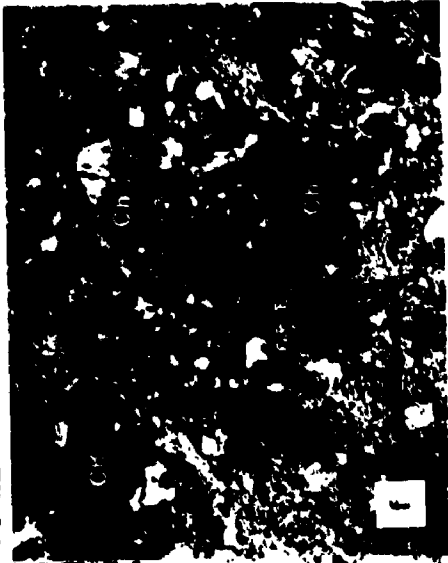


(Plate 7a), and faint cross bedding is locally preserved in quartzite. Numerous thin (less than 5 cm thick), foliation-parallel pegmatitic lenses occur within the gneisses, and may represent metamorphic segregation.

The gneiss is fine grained, 0.2 to 1 mm, roughly equigranular, with 30-35% polygonal quartz, 25-30% microcline and 25-35% plagioclase (Appendix A). Quartz has undulose extinction and small, round subgrains. Feldspar is granoblastic, also with undulose extinction, and irregular grain boundaries. Myrmekitic intergrowths are common. Granoblastic plagioclase composition ranges from 0.03 Ca atoms per formula unit (pfu) to 0.20 atoms pfu, corresponding to An<sub>3</sub> to An<sub>20</sub> (see Fig. 4-3), indicative of the peristerite field, and K-feldspar averages about Or<sub>94</sub> (Fig. 3-4).

Subhedral, lepidoblastic biotite defines the foliation, ranging in size from 0.1 to 0.3 mm. Biotite has about 60% of the phlogopite molecule in the phlogopite-annite solid solution series, and contains less aluminum than most other biotite in the study area (Fig. 3-5). Hornblende has a slight preferred orientation. Together, hornblende and biotite comprise 8 to 12% of the gneiss, although mafic-rich gneiss contains up to 25% hornblende and biotite. Disseminated, equant, angular to rounded magnetite grains lack exsolution lamellae of ilmenite, but is replaced by hematite along grain rims and fractures. Epidote is disseminated within patches, particularly concentrated in and around plagioclase. Late chlorite partly replaces biotite, and occurs in veinlets with

**FIGURE 3-4.** Composition of K-feldspar from the country rocks.  
Symbols: K-feldspar from muscovite-biotite granite, solid circles (gr); K-feldspar from distal granodiorite, solid squares (gd), and K-feldspar from quartzofeldspathic gneiss of the Tumco Formation, solid triangles (qT).

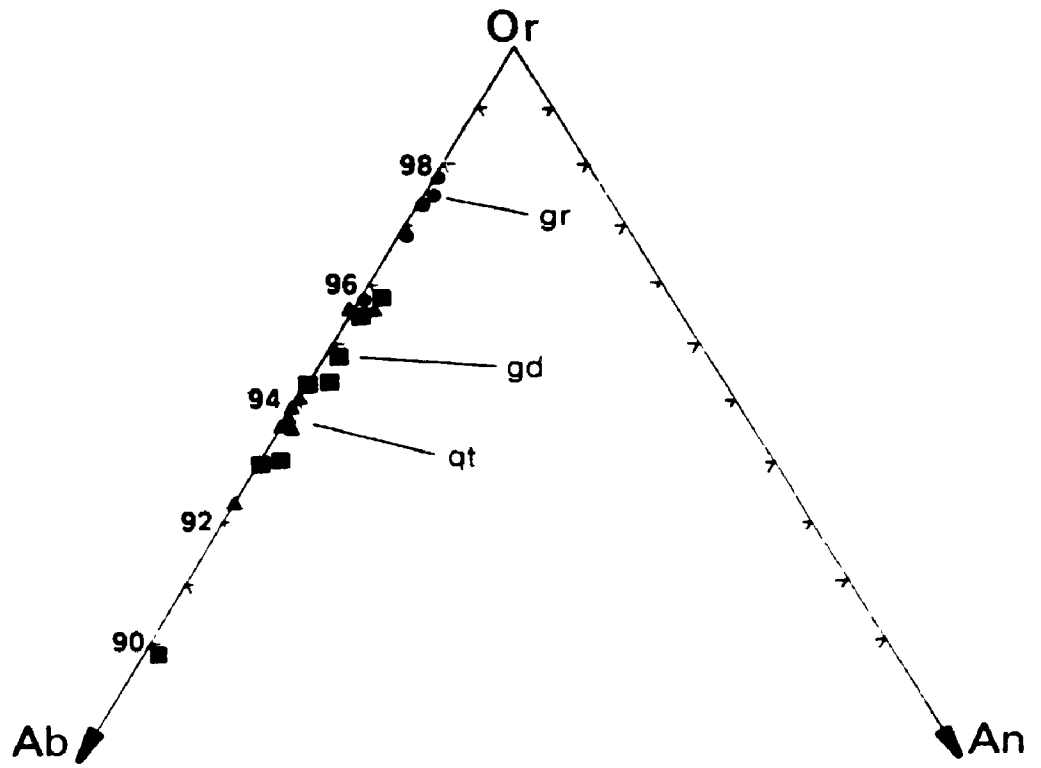
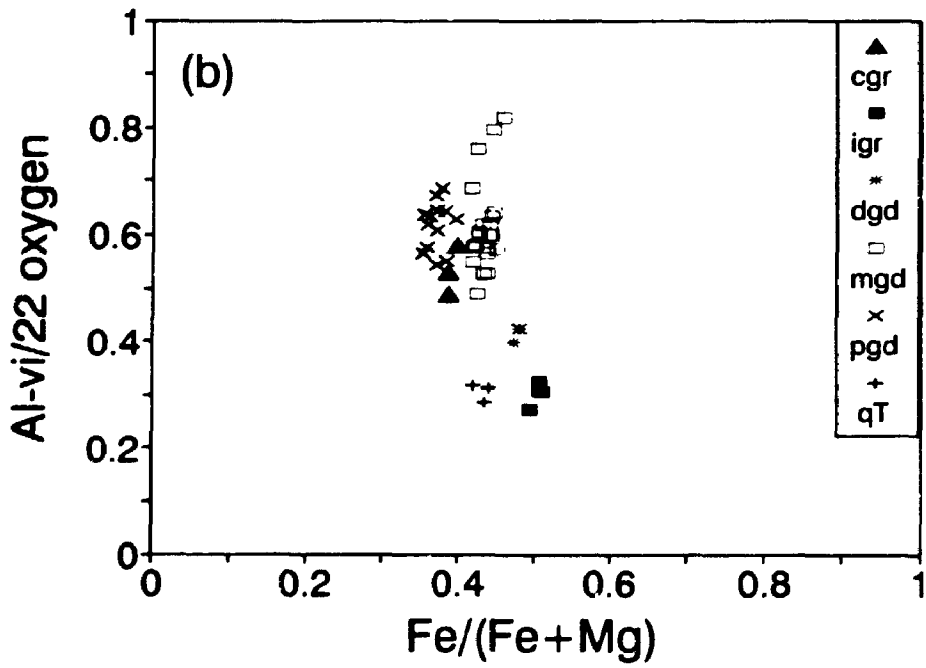
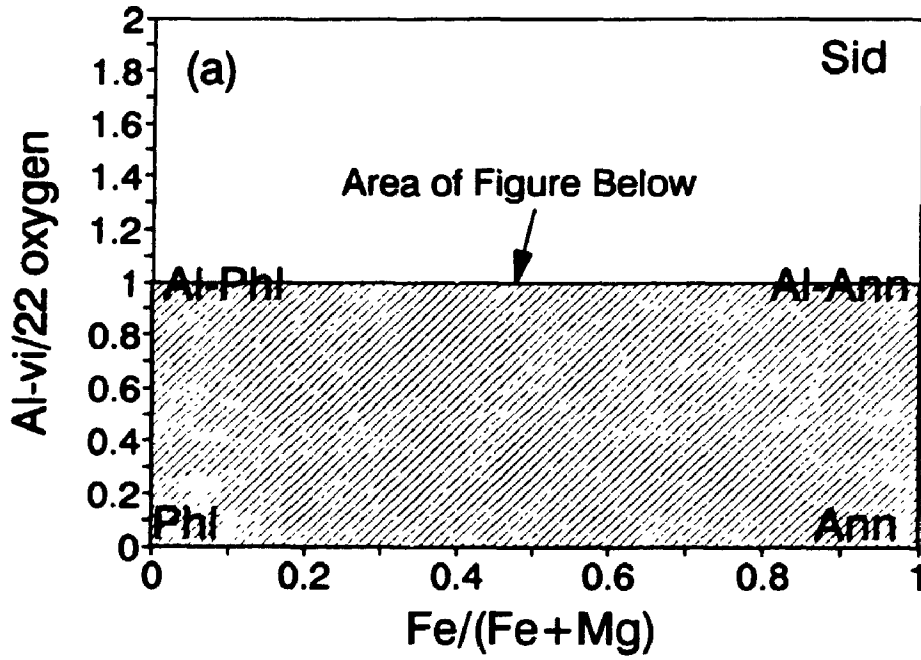


**FIGURE 3-5.** Composition of biotite from the country rocks within the siderophyllite-(eastonite)-phlogopite-annite quadrilateral (after Guidotti, 1984).  $Fe/(Fe+Mg)$  is plotted along the abscissa, octahedral aluminum (Al-vi) per 22 oxygens along the ordinate. a.) End member compositions: Eas = eastonite, Sid = siderophyllite, Al-Phl = aluminum-phlogopite, Al-Ann = aluminum annite, Phl = phlogopite, Ann = annite. b.) Composition of biotite. Symbols: cgr, muscovite biotite granite from the contact zone; igr, interior muscovite biotite granite; dgd, distal granodiorite; mgd, medial granodiorite; pgd, proximal granodiorite; qT, quartzofeldspathic gneiss of the Tumco Formation.





carbonate.

The clasts contrast texturally with the groundmass. They are coarser grained than the foliated matrix, and contain quartz, microcline, plagioclase and biotite. Quartz and feldspar have serrated grain boundaries, undulose extinction, and subgrains. Relict hypidiomorphic granular texture is common.

### **3.3. Intrusive Rocks.**

#### **3.3.1. Regional Correlation.**

The intrusive rocks are subdivided into quartz diorite, hornblende-biotite granodiorite, granite porphyry, muscovite-biotite granite, and pegmatite. All are present in the Micatahc Hill-Vitrifax Hill area (Fig. 3-1), although pegmatite is uncommon, occurring as small dikes. Only pegmatite dikes are exposed at Hedges (Fig. 3-3), and quartz monzonite (Fig. 2-2) is absent at these sites.

Age relationships have been worked out in considerable detail by Dillon (1976), Branham (1988), and Tosdal and Wooden (1991). Quartz diorite is equivalent to Mesozoic(?) quartz diorite of Henshaw (1942), to Proterozoic(?) diorite orthogneiss of Dillon (1976), and is part of the 173 Ma intrusive suite of Tosdal and Wooden (1991). Muscovite-biotite granite and granite porphyry, are equivalent to the central and marginal facies of Jurassic biotite granite of Dillon (1976), with an age of 160-173 Ma. Tosdal and Woodr (1991) have assigned the biotite granite of Dillon (1976) to a regional

160-173 Ma suite of granitic rocks. Pegmatite is equivalent to the northern, leucocratic biotite granite facies of Dillon (1976), although pegmatite may be part of a regional 158-160 Ma leucocratic granite (Tosdal and Wooden, 1991). Granodiorite was originally mapped as part of the diorite by Dillon (1976) and Branham (1988), but the presence of K-feldspar distinguishes it from the quartz diorite, and compositionally it is a granodiorite (Appendix B). Based on contact relationships described below, it is assigned to the 160-173 Ma suite of Tosdal and Wooden (1991).

### 3.3.2. Quartz diorite.

Quartz diorite is a large sill-like body mostly restricted to the area south of Vitrifax Hill, with smaller bodies near Micatalc Hill (Figs. 2-1 and 3-1). Contacts with the Tumco Formation are gradational through a gradual increase in mafic mineral content or an increase in the number of rounded xenoliths toward the diorite. It is inequigranular, with medium to coarse, anhedral plagioclase (10%) and subhedral to skeletal hornblende poikiloblasts (10%) set in a fine grained groundmass of quartz, feldspar and epidote (Appendix A and Plate 1d). Lepidoblastic biotite (15%) defines the foliation, either as singular grains or in aggregates with hornblende where it replaces the latter (Plate 1d and e). Fine rounded epidote is 5% of the rock, occurring as fine, disseminated grains, concentrated in and around plagioclase and hornblende. Carbonate (1%) occurs as fine, disseminated

grains, and in microveinlets, the latter particularly concentrated in plagioclase porphyroblasts.

A schistose rock of quartz-muscovite-chlorite-magnetite-tourmaline-apatite is exposed on top of Vitrifax Hill, interpreted to be altered quartz diorite. It consists of 50% white mica, as fine grained irregular patches and feathery aggregates replacing plagioclase, and 30% undulose groundmass quartz. Chlorite content is high, 12-15%, and occurs as pseudomorphs after hornblende or biotite (Plate 1f). Magnetite, tourmaline, and apatite comprise the remaining constituents. Numerous rounded xenoliths occur in the rock, suggestive of the contact between quartzofeldspathic gneiss of the Tumco Formation and the quartz diorite (Plate 1c). The xenoliths contain 40% quartz, 47% white mica, 10% chlorite, 3% magnetite, and trace kyanite, tourmaline, and apatite. Textures indicate early selective replacement of feldspar by chlorite along cleavage or crystallographic planes, followed by pervasive replacement by muscovite.

### **3.3.3. Hornblende-Biotite Granodiorite.**

#### **3.3.3.1. Field and Textural Relationships.**

Hornblende-biotite granodiorite occurs only at Micatalc Hill. It cross cuts the zones of aluminosilicate mineral assemblages, which are hosted within the gneissic rocks of the Tumco Formation. It is concordant to fabric in the Feldspar Zone but is discordant to fabric in the Muscovite and Kyanite Zones (Fig. 3-1). Muscovite-biotite granite cross cuts horn-

blende-biotite granodiorite, although this relationship is complicated by syn- to post-emplacement faulting. There is sequential variation in mineral assemblage and texture across the granodiorite away from the granite. From granite outward, mineral assemblages and textures vary as follows (Fig. 3-6):

1.) Proximal granodiorite (adjacent to granite to 60m away) has the mineral assemblage quartz-plagioclase(andesine to labradorite)-hornblende-magnetite. Texturally, the rock is granoblastic and coarse grained.

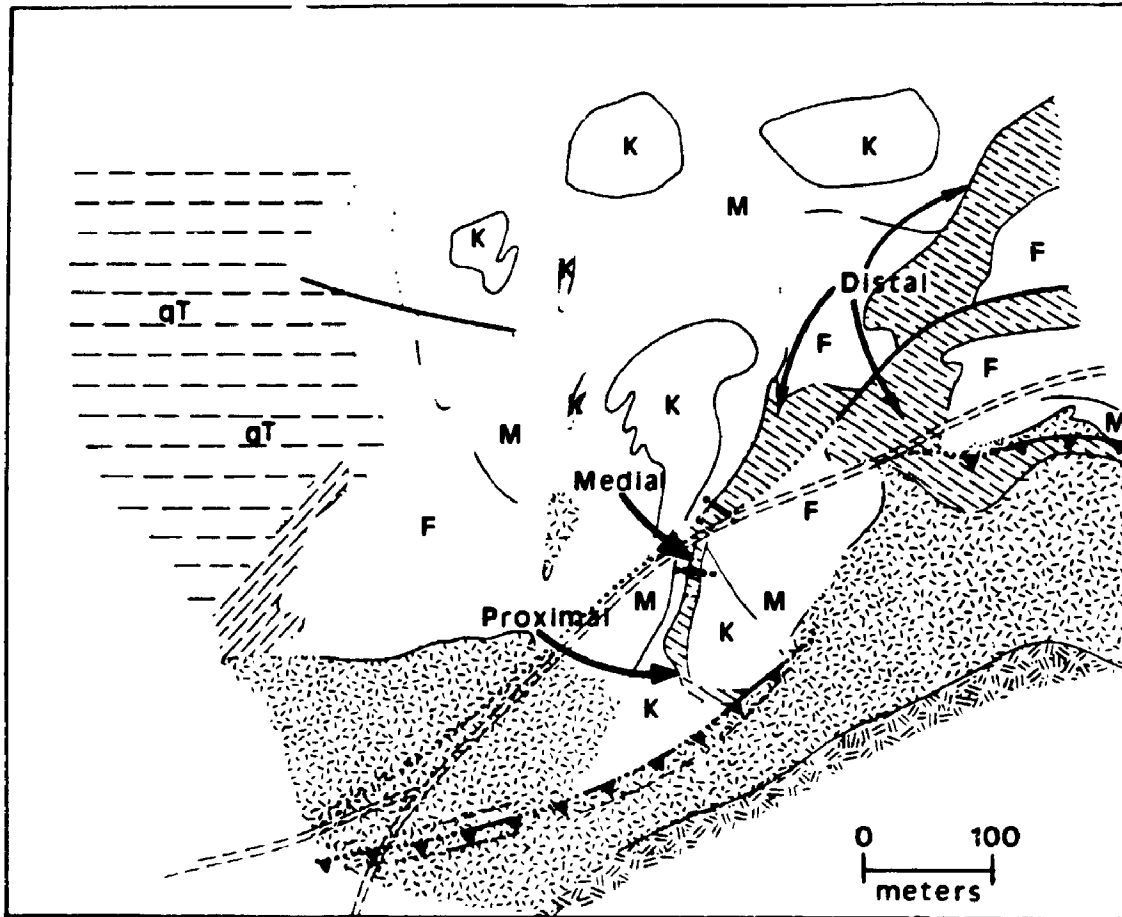
2.) Medial granodiorite (60m to 90m away from the granite) has the mineral assemblage quartz-plagioclase(oligoclase to andesine)-biotite-magnetite-garnet, and is coarse grained and granoblastic.

3.) Distal granodiorite (greater than 90m from the granite) has the mineral assemblage quartz-plagioclase(oligoclase)-K-feldspar-biotite-epidote, and is fine to medium grained and foliated.






This variation in mineral assemblage and fabric in hornblende-biotite granodiorite occurs only where it cross cuts the aluminosilicate mineral assemblage zones. Where granodiorite is in contact with the granite elsewhere, similar mineral and textural variation is absent.


Proximal granodiorite, hosted within the Kyanite Zone of

**FIGURE 3-6.** Detailed geologic relationships between muscovite-biotite granite, hornblende-biotite granodiorite, and low angle fault zones. Short heavy solid lines within the granodiorite represent the contacts between distal, medial, and proximal granodiorite. Mineral and textural variability occurs only where granodiorite cross cuts the Muscovite (M) and Kyanite (K) Zones of the aluminosilicate mineral assemblages. Granodiorite adjacent to fault at far right of map is schistose and mylonitic. Miocene dacite is omitted for simplicity, and symbols for the Feldspar, Muscovite and Kyanite Zones are omitted to emphasize the intrusive rocks. See Fig. 3-1 for location.



**CONTACT RELATIONSHIPS AT MICATALC HILL**

- |   |   |
|---|---|
|  Muscovite-biotite granite       | <b>ZONES OF ALUMINOSILICATE<br/>MINERAL ASSEMBLAGES</b> |
|  Granite porphyry                |   |
|  Hornblende-biotite granodiorite | F Feldspar Zone   |
|  Quartz diorite                  | M Muscovite Zone  |
|  Tumco Formation                 | K Kyanite Zone  |

- Contact (dotted where covered)  
 Fault ( " )

See Fig 3-1 for location

the aluminosilicate mineral assemblages, has a coarse grained granoblastic texture. Biotite is absent, and hornblende is the dominant mafic mineral, comprising 34% of the rock. Hornblende is coarse, subhedral and poikiloblastic, and is intergrown with plagioclase and magnetite (Plate 2c). Simple and lamellar twinning and subgrains are well developed. Kink bands are common, with partial recrystallization to very fine polygonal grains along the kink bands. Recrystallization of plagioclase to fine grains is less extensive than in medial granodiorite. The primary habit is as coarse, anhedral, lath-shaped poikiloblasts up to 3 mm, with pristine albite twinning (Plate 2c). Quartz has weak to moderate undulose extinction, local subgrain development with sutured and irregular grain boundaries. Subhedral, slender elongate magnetite grains are partially to wholly included within hornblende. Epidote, chlorite, and zircon are trace accessories, and chalcedony occurs as late fracture fillings.

Proximal granodiorite within the Kyanite Zone immediately adjacent to shear zone contact with muscovite-biotite granite has a mineral assemblage and fabric similar to medial granodiorite. Hornblende is absent; the Fe-bearing minerals are biotite, garnet, epidote and chlorite. As in medial hornblende-biotite granodiorite, plagioclase commonly occurs as aggregates of fine polygonal grains, and coarse plagioclase poikiloblasts are less abundant and more highly fractured than in proximal granodiorite farther away from muscovite-biotite granite. Very fine white mica occurs disseminated throughout,

**PLATE 2.** Characteristics of hornblende-biotite granodiorite and granite porphyry. a.) Photomicrograph of distal granodiorite. Plagioclase (P) extensively replaced by fine epidote, K-feldspar (K) by very fine white mica or clay. Quartz (Q) is clear. Note myrmekite (M) replacement of K-feldspar. Scale bar is 0.5 mm. b.) Photomicrograph of medial granodiorite. Aggregate of fine, polygonal, zoned plagioclase (P) occupies the central portion of the photo, interpreted as recrystallized porphyroblasts. Note lack of epidote, and sieve-textured myrmekitic grains (m) in groundmass. Arrows point to decussate biotite. Scale bar equals 0.5 mm. c.) Photomicrograph of proximal granodiorite, with intergrown plagioclase (P), hornblende (H), magnetite (m) and quartz (clear). Scale bar equals 1 mm. d.) Electron backscatter image of irregular zoning in plagioclase. Darker patches are calcic ( $An_{60}$ ), lighter patches are less calcic ( $An_{45}$ ). e.) Photomicrograph of granite porphyry. Coarse K-feldspar porphyroblasts (relict phenocrysts), with Carlsbad and Tartan twinning, in a fine grained groundmass of quartz, plagioclase, K-feldspar, biotite, and white mica. Scale bar equals 1 mm. f.) Photomicrograph of altered granite porphyry. Coarse feldspar porphyroblast (F) is aggregate of fine polygonal grains; recrystallized quartz veinlet (Q) in upper right corner. Very fine white mica extensively replaces feldspar in the groundmass.





and is concentrated in small seams, with epidote and chlorite.

Medial granodiorite is granoblastic, and cross cuts both the Muscovite and Kyanite Zones of the aluminosilicate mineral assemblages (Fig. 3-6). Notably absent are K-feldspar and hornblende. Plagioclase comprises 45% of the rock, occurring as coarse myrmekitic grains to 3 mm, containing numerous inclusions of quartz, and as aggregates of fine (0.5 mm) polygonal grains, the latter optically zoned (Plate 2b). It is replaced by epidote and, unlike plagioclase of distal granodiorite, has a dusting of clay or fine white mica. Quartz, at 22%, shows strong undulose extinction, and sutured grain boundaries are much more common than in distal granodiorite. Biotite poiklioblasts (17%) are subhedral and non-oriented (Plate 2b). They are commonly intergrown with irregular, equant magnetite, the latter containing exsolution lamellae and blebs of ilmenite. Apatite and garnet, the latter as euhedral microporphyroblasts, are trace accessories. Minor secondary products include chlorite and carbonate, and muscovite comprises 3% as a replacement of K-feldspar.

Distal granodiorite is hosted within the Feldspar Zone of the aluminosilicate mineral assemblages. It is foliated, fine to medium grained, and roughly equigranular. Lepidoblastic biotite comprises 22% of the rock, as singular grains or in aggregates elongate parallel to the foliation, similar in habit to that in quartz diorite. Plagioclase, at 18%, consists of fine, equant, irregular to polygonal grains and coarse, sieve textured porphyroblasts containing inclusions of

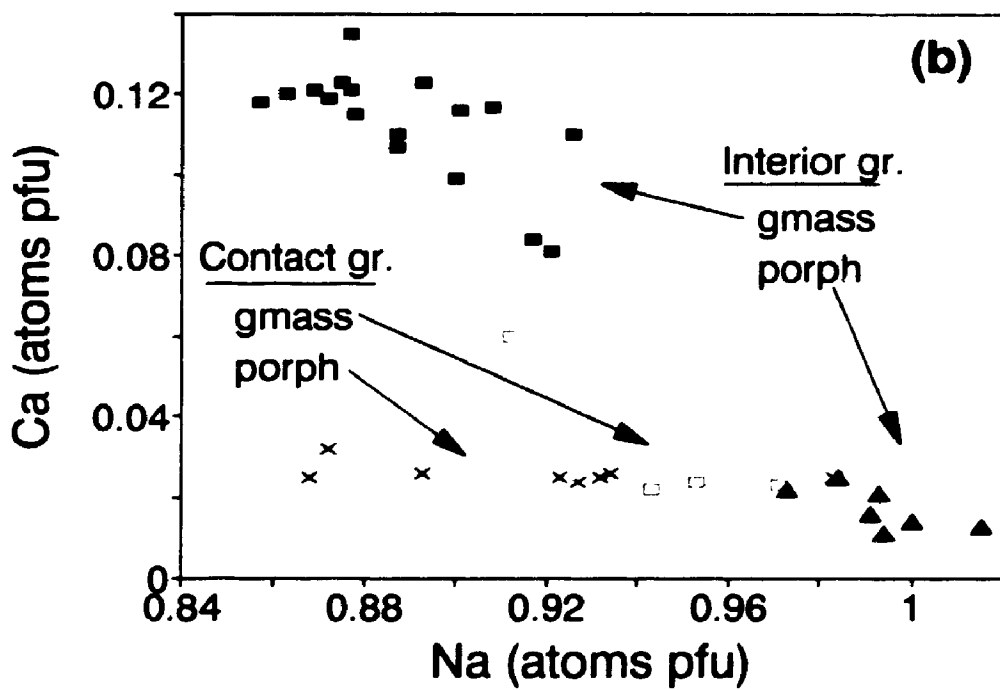
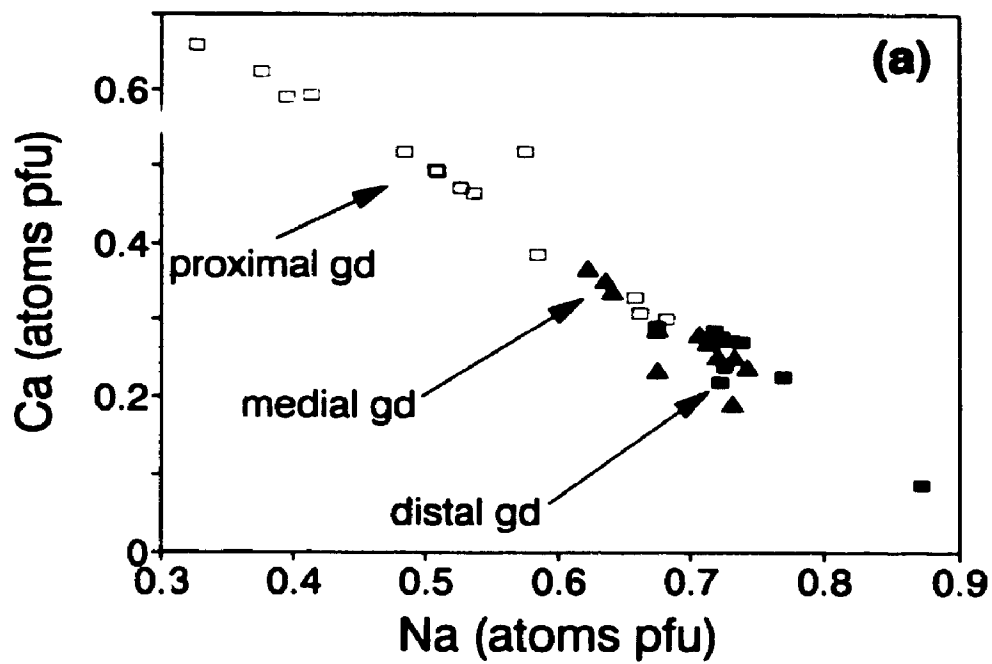
fine non-oriented biotite, quartz and K-feldspar. Albite twin lamellae are commonly diffuse and exhibit pinch-and-swell structures. Equant K-feldspar (16%) usually contains tartan twinning. Rim myrmekite penetrates K-feldspar (Plate 2a), and patch anti-perthite, of K-feldspar in a plagioclase host, also occurs. Interstitial, anhedral quartz has sutured boundaries and undulose extinction. Epidote content is relatively large at 12%, occurring as very fine, rounded disseminated grains, particularly concentrated in plagioclase (Plate 2a). Elongate, anhedral hornblende (5%) is penetrated by biotite and epidote, suggesting replacement by the latter two. Sphene is a trace accessory. This fabric and mineralogy occurs where the granodiorite is not hosted within the Muscovite and Kyanite Zones of the aluminosilicate mineral assemblages, including along the eastern contact zone with muscovite-biotite granite (Fig. 3-6).

### 3.3.3.2. Feldspar Composition.

Plagioclase composition varies from about  $An_{26}$  in distal granodiorite up to  $An_{67}$  in proximal granodiorite (Fig. 3-7a), although composition is in part a function of habit. In distal granodiorite, porphyroblasts and polygonal groundmass grains average about  $An_{26}$  (co-existing K-feldspar has a composition about  $Or_{94.5}$ ). Co-existing K-feldspar averages about  $Or_{94}$  (Fig. 3-4), and BaO averages 0.44 wt.%.

Groundmass and porphyroblastic plagioclase in medial granodiorite are compositionally similar to plagioclase in the

**FIGURE 3-7.** Composition of plagioclase from the intrusive rocks. **a.)** Ca vs. Na, granodiorite, plotted as atoms per formula unit (pfu). Open squares, proximal granodiorite; filled triangles, medial granodiorite; filled squares, distal granodiorite. **b.)** Ca vs. Na, muscovite-biotite granite. Interior granite: filled squares, fine grained plagioclase in the groundmass; filled triangles, coarse plagioclase poikiloblasts. Granite from the contact zone: open squares, groundmass plagioclase; x's, coarse, myrmekitic plagioclase poikiloblasts.



distal granodiorite ( $An_{26}$  to  $An_{28}$ ). Recrystallized porphyroblasts (polycrystalline aggregates) are distinctly more calcic, however, averaging  $An_{35}$ . In proximal hornblende-biotite granodiorite, plagioclase is still more calcic and quite variable: porphyroblasts range from  $An_{45}$  to  $An_{66}$ , and fine polygonal grains range from  $An_{30}$  to  $An_{60}$ . Some of this variability is due to zoning, which varies from simple core-to-rim zonation to highly irregular, worm-like intergrowths or exsolution features (Plate 2d).

#### 3.3.3.3. Biotite Composition.

Biotite from distal granodiorite contains approximately 48% of the phlogopite molecule within the phlogopite-biotite solid solution series (Fig. 3-5). There is a pronounced increase in Al-vi and a decrease in  $Fe/(Fe+Mg)$  from distal to proximal granodiorite, leading toward the Al-phlogopite corner. In addition, from distal granodiorite to medial granodiorite, there are concomitant increases in Mg, Ti, K, Na, and Ba in biotite, and decreases in Ca, Mn and Si. Proximal granodiorite immediately adjacent to muscovite-biotite granite contains biotite with larger contents of Mg and K, and less Fe, Ca, and Si. The net result is a further decrease in the  $Fe/(Fe+Mg)$  ratios (Fig. 3-5).

#### 3.3.3.4. Garnet Composition.

Garnet is a trace mineral in medial granodiorite and in proximal granodiorite adjacent to muscovite-biotite granite.

It is fine grained, and unzoned to slightly zoned. Compositions can be expressed as mole fractions of almandine, spessartine, pyrope and grossularite. Garnet of medial granodiorite average  $\text{Alm}_{45}\text{Sps}_{35}\text{Prp}_{10}\text{Grs}_{10}$ , whereas that from proximal granodiorite is slightly more enriched in Fe and Mg, with a composition of  $\text{Alm}_{53}\text{Sps}_{24}\text{Prp}_{15}\text{Grs}_8$  (see Fig. 4-13).

### 3.3.3.5. Origin of Mineral and Textural Variation.

There is sequential mineral assemblage and fabric variation in hornblende-biotite granodiorite relative to muscovite-biotite granite where granodiorite cross cuts the Muscovite and Kyanite Zones of the aluminosilicate mineral assemblages. Mineral assemblages vary from labradorite-hornblende-magnetite in proximal granodiorite (closest to muscovite-biotite granite) to quartz-oligoclase to andesine-biotite-garnet-magnetite in medial granodiorite to quartz-andesine quartz-oligoclase-microcline-biotite-epidote in distal granodiorite (farthest from muscovite-biotite granite). As indicated, plagioclase compositions range from  $\text{An}_{30}$  to  $\text{An}_{67}$  in proximal granodiorite, from  $\text{An}_{26}$  to  $\text{An}_{35}$  in medial granodiorite, and from  $\text{An}_9$  to  $\text{An}_{30}$  in distal granodiorite. There is also a regular increase in K-bearing minerals in granodiorite away from muscovite-biotite granite. Proximal granodiorite has no K-bearing minerals, medial granodiorite has biotite, and distal granodiorite has K-feldspar and biotite. Rock fabrics vary from granoblastic in proximal and medial granodiorite to a foliated in distal granodiorite. In

addition, there is a reduction in grain size from proximal to distal.

Individual mineral textures are more complex. Plagioclase in proximal granodiorite is as coarse, lath-shaped porphyroblasts, with pristine albite twinning. In medial granodiorite, abundant aggregates of fine, polygonal grains occur with coarse, myrmekitic plagioclase, the former habit similar to that found in granodiorite adjacent to the shear zone contact with muscovite-biotite granite. Pinch-and-swell structures in albite twinning are common. Plagioclase in distal granodiorite is primarily as coarse, anhedral poikiloblasts, with minor fine, polygonal grains.

Quartz in proximal granodiorite, with weak to moderate undulose extinction, contains local subgrains, the latter a feature absent in medial and distal granodiorite. In medial granodiorite, quartz has strong undulose extinction, with well developed sutured grain boundaries. Although quartz in distal granodiorite contains similar textures to that in medial granodiorite, they are less pronounced. Hornblende, abundant in proximal granodiorite and low in abundance in distal granodiorite, has prominent subgrain development in proximal granodiorite, particularly along kink bands.

The overall mineral and fabric variation in hornblende-biotite granodiorite relative to muscovite-biotite granite are indicative of thermal metamorphism of granodiorite by the granite. However, the decrease in K-bearing minerals in granodiorite toward muscovite-biotite granite points to a loss



of  $K^+$  from granodiorite during this event, and suggests considerable mobility of ions out of granodiorite. These mineral variations are observed only where granodiorite cross cuts the Muscovite and Kyanite Zones of the aluminosilicate mineral assemblages, suggesting a relationship between metamorphism of hornblende granodiorite and the location of the zones of aluminosilicate minerals. This will be addressed further in Chapter 7.

In addition, deformation textures in quartz and hornblende, such as undulose extinction, kink bands, and subgrain development are most pronounced in medial and proximal granodiorite, suggesting an increase in strain toward the contact with muscovite-biotite granite. This contrasts with plagioclase, in which the most pronounced deformation textures are in medial granodiorite, in the form of pinch-and-swell structures and abundant aggregates of fine, polygonal grains. These textures are characteristic of plastic behavior in a ductile environment for each of these minerals (Spry, 1969; Brodie and Rutter, 1985), and indicate ductile deformation was syn- to post-contact metamorphism.

#### **3.3.4. Granite Porphyry.**

Granite porphyry underlies the area south of Micatale Hill, and occurs as discordant dikes throughout the Micatale Hill-Vitrifax Hill area (Fig. 3-1). Contacts between this rock and muscovite-biotite granite are sharp, with no thermal overprint. Dillon (1976) noted that the contact between the

two is mutually intrusive, and concluded that although roughly contemporaneous, the granite porphyry was slightly younger than the muscovite-biotite granite. However, granite porphyry is intensely sericitized and cross cut by numerous quartz veinlets where it cross cuts the Muscovite Zone, whereas muscovite-biotite granite lacks such features where it cross cuts the Muscovite Zone west of Vitrifax Hill. In addition, outcrop patterns west of Vitrifax Hill suggest muscovite-biotite granite has intruded along the contact between granite porphyry and quartz diorite. Granite porphyry is therefore considered to be older than muscovite-biotite granite, acknowledging that they are most likely consanguineous.

Granite porphyry has relict porphyritic texture, with phenocrysts of K-feldspar (11%), plagioclase (8%) and quartz (3-4%) set in a fine grained groundmass (55%) of mosaic to sutured quartz and feldspar (Plate 2e). Anhedral to euhedral K-feldspar phenocrysts have sutured and recrystallized grain boundaries. Carlsbad twinning is common, tartan twinning is patchy, and micrographic intergrowths with quartz are common. The phenocrysts host inclusions of quartz, plagioclase, muscovite, and opaques. Coarse, poikiloblastic to sieve plagioclase has embayed, corroded and sutured grain boundaries, with patches of tartan twinned microcline.

Quartz phenocrysts are equant to elongate, with sutured to embayed grain boundaries, and with undulatory extinction. Disseminated biotite occurs as fine anhedral to subhedral grains and, unlike previously discussed rocks, has only a

slight preferred orientation. Muscovite habit is similar to biotite, and coarser grains have well developed 001 faces. Magnetite (2%) is found as fine euhedral, octahedral grains. Secondary products include partial replacement of K-feldspar by fine white mica, plagioclase by epidote, and biotite by chlorite. Carbonate occurs as fine anhedral grains, generally associated with plagioclase and muscovite.

Granite porphyry cross cuts the Muscovite Zone on the east side of Vitrifax Hill (Fig. 3-1), where the primary porphyritic texture is retained, but coarse feldspar porphyroblasts are recrystallized granular aggregates (Plate 2f). Abundant fine, white mica replaces groundmass and porphyroblastic feldspar, and numerous quartz veinlets with recrystallized quartz cross cut the rock.

### **3.3.5. Muscovite-Biotite Granite.**

#### **3.3.5.1. Field and Textural Relationships.**

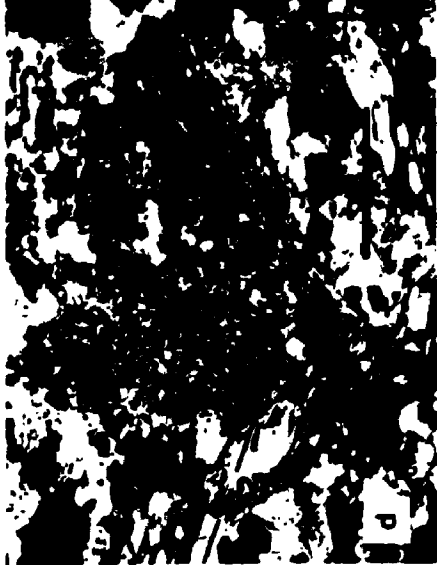
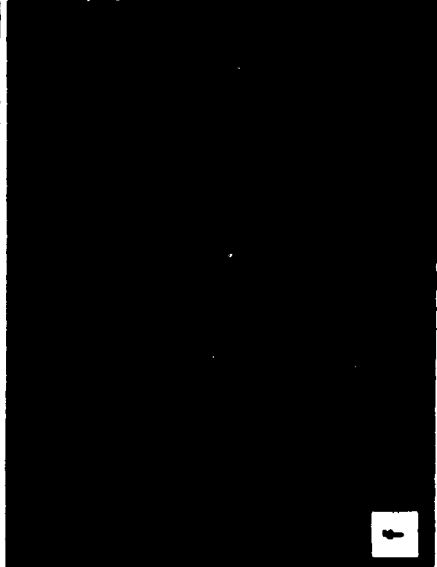
Muscovite-biotite granite is a concordant to discordant intrusion along the south boundary of Micatalc, and west of Vitrifax Hill (Fig. 3-1). Thermal aureoles are small or absent, mostly confined to within 1.5 m of the contact. It has a pronounced foliation and is finer grained adjacent to the Tumco Formation, suggestive of a chilled margin. Mutually cross-cutting relationships between muscovite-biotite granite, hornblende-biotite granodiorite and low angle shear zones indicates partial contemporaneity of intrusion and shearing (Fig. 3-6).

The mineral and fabric characteristics of muscovite-biotite granite vary with proximity to its contact with Tumco Formation, hornblende-biotite granite and the aluminosilicates. The interior of muscovite-biotite granite is seriate inequigranular, with a grain size range of 0.05 to 12 mm. Plagioclase occurs as rectangular to irregular-shaped plagioclase poikiloblasts, up to 8 mm in size, and as polygonal groundmass grains. Equant, blocky microcline poikiloblasts range in size up to 12 mm. The coarse feldspars commonly have embayed grain boundaries and local undulose extinction. Deformation bands in plagioclase commonly contain very fine recrystallized plagioclase and white mica. Irregular-shaped masses of microcline are wholly to partially enclosed within plagioclase (Plate 3a and b), the latter replaced by fine clays and subhedral muscovite whereas the former remains unaltered. However, rim myrmekite penetrates microcline (Plate 3c), and symplectic intergrowths are common.

Quartz ranges from 0.3 mm to 8 mm in diameter, is anhedral, with undulose extinction and sutured to smooth, locally embayed, grain boundaries. Aggregates of subhedral to anhedral, lepidoblastic biotite, 0.05 to 0.3 mm, define the foliation. Muscovite occurs as a very fine replacement of plagioclase, as well as coarser, non-oriented, subhedral grains interstitial to feldspar or intergrown with, and replacing, biotite (Plate 3b). Trace accessory minerals include zircon, sphene, epidote, and late carbonate veinlets.

Muscovite-biotite granite along the contact zone is

**PLATE 3.** Characteristics of muscovite-biotite granite and pegmatite. **a.)** Photomicrograph of muscovite-biotite granite, showing plagioclase-K-feldspar relationships. Plagioclase (P), with albite twinning, is intimately intergrown with K-feldspar (K), which contains tartan twinning. Note the presence of relict Carlsbad twinning in the central porphyroblast, and the quartz inclusions (white). Scale bar equals 1 mm. **b.)** Detail of relationships in (a). K-feldspar (K) is dark, intergrown with light plagioclase (P). Note extensive alteration of plagioclase by clays or fine, white mica (dusty appearance), and replacement by muscovite (M). Subhedral muscovite also in groundmass; elsewhere muscovite cross cuts aggregates of biotite. Scale bar equals 0.2 mm. **c.)** Photomicrograph of muscovite-biotite granite showing penetration of K-feldspar by rim myrmekite. Scale bar equals 0.05 mm. **d.)** Photomicrograph of muscovite-biotite granite from the contact zone. Coarse, poikiloblastic plagioclase deflecting  $S_2$  foliation, defined by intergrown muscovite and biotite. Scale bar equals 1 mm. **e.)** Folded pegmatite dike (P), cross cutting quartzofeldspathic gneiss of the Tumco Formation and an earlier, small aplite dike (A).  $S_1$  is the orientation of the regional foliation. **f.)** Photomicrograph of muscovite-biotite granite showing relationships between muscovite (M) and biotite (B), defining  $S_2$  foliation.



schistose, locally mylonitic, with a marked increase in muscovite and quartz content, and a decrease in K-feldspar content and grain size relative to interior granite (Appendix A). Lepidoblastic muscovite (14%) and biotite define the foliation, commonly occurring in folia which wrap around coarse feldspar porphyroclasts (Plate 3d and f). Microcline comprises 5% of the rock, as compared to 24% in interior granite. Wormy inclusions of quartz in plagioclase are much more abundant than in interior granite, and indicate significant replacement of microcline by myrmekite. Diffuse twin bands and pinch-and-swell structures in twin planes of plagioclase, as well as pseudo-checkerboard twinning are commonplace. White mica replaces plagioclase, and is much coarser grained than in interior granite. Trace accessories include zircon, garnet, epidote and carbonate.

#### 3.3.5.2. Feldspar Composition.

K-feldspar poikiloblasts in the interior of muscovite-biotite granite average  $Or_{97}$ , representing the most potassic K-feldspar in the study area (Fig. 3-4). They contain an average of 0.25 wt.% BaO, considerably less than that of K-feldspar in hornblende granodiorite. These compositional differences probably reflect original magmatic compositions, as Ba is preferentially taken up in K-feldspar of intermediate rocks (Smith and Brown, 1988).

Plagioclase composition varies with crystal habit and rock fabric. Poikiloblasts in the interior of muscovite-

biotite granite average  $An_3$ , whereas groundmass grains from the same rock are distinctly more calcic, at  $An_{11}$  (Fig. 3-7b). In contrast, both myrmekitic poikiloblasts and groundmass grains average  $An_3$  in schistose granite from the contact zone. The intimate intergrowths of coarse K-feldspar and plagioclase in interior granite, the common occurrence of myrmekite and near total absence of K-feldspar in granite of the contact zone, suggest the more sodic compositions of plagioclase in muscovite-biotite granite were formed during replacement of K-feldspar by albite.

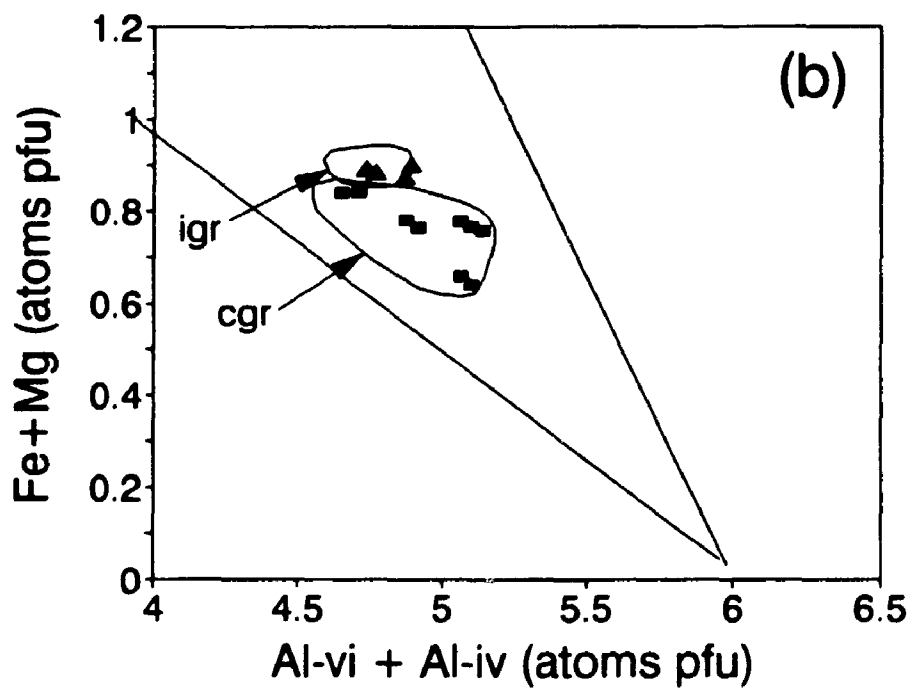
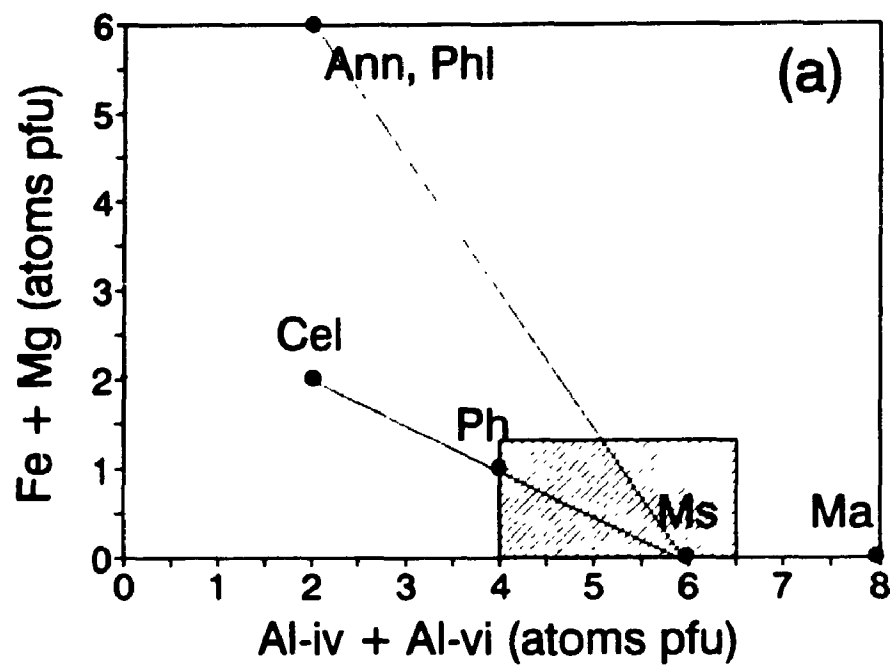
#### 3.3.5.3. Muscovite Composition.

Subhedral muscovite of the interior muscovite-biotite granite is phengitic, with an average of 6.2 atoms pfu Si, almost complete interlayer site occupancy of K, but rather high Fe+Mg (Fig. 3-8). This suggests considerable solid solution between ideal muscovite, phengite and the trioctahedral micas. In addition, the average Ti content is rather high, averaging 0.12 atoms pfu. These characteristics are similar to compositions of primary igneous muscovites from peraluminous granites (Miller, et. al., 1981), and are distinct from the white micas from the aluminosilicate mineral assemblages (see Chapter 4).

Relative to the interior of muscovite-biotite granite, muscovite of the schistose to mylonitic granite at the margins is depleted in K, Fe and Ti, and enriched in Na, Ba and Al (Fig. 3-8). These trends reflect interlayer exchange,  $KNa_1$ ,



**FIGURE 3-8.** Composition of muscovite from muscovite-biotite granite. **a.)** General relationships between end member compositions within Fe+Mg and Al<sub>ox</sub> composition space. Trioctahedral micas are annite (Ann) and phlogopite (Phl), dioctahedral micas are celadonite (Cel), phengite (Ph), muscovite-paragonite (Ms), and margarite (Ma). Tie lines joining muscovite-paragonite with the trioctahedral micas and with phengite and celadonite are shown. Area of (b) is shaded. **b.)** Muscovite compositions from interior of the muscovite-biotite granite (igr) and from the contact zone of the muscovite-biotite granite (cgr).



and  $\text{KBa}_1$ , where the charge imbalance resulting from the substitution of  $\text{Ba}^{2+}$  for  $\text{K}^+$  is compensated for by the removal of Fe and Ti, or addition of Al.

#### 3.3.5.4. Biotite Composition.

Biotite from the interior of muscovite-biotite granite contains 50% of the phlogopite molecule, and Al-vi occupies 0.3 sites per 22 oxygens (Fig. 3-5). As such, it is compositionally similar to biotite of the distal phase of the hornblende granodiorite and biotite of the quartzofeldspathic gneiss. Biotite of the schistose to mylonitic granite from the margin, however, has higher Al and Mg (Fig. 3-5), as well as Na, and lower Fe and Ti than that from the interior. These changes are similar to the changes in the composition of biotite in hornblende granodiorite as the contact is approached. In contrast with biotite variation across hornblende granodiorite, Si increases and K decreases in biotite of granite as the contact is approached.

#### 3.3.5.5. Late to Post-Magmatic Changes.

In the interior of muscovite-biotite granite, rim myrmekite penetrates K-feldspar, and patchy intergrowths of coarse K-feldspar and albite, with composition  $\text{An}_1$ , occur in a groundmass of more calcic albite ( $\text{An}_{11}$ ). Such compositional relationships between coarse and fine phases are opposite to "normal" magmatic cooling trends. Furthermore, replacement of albite by relatively coarse, subhedral muscovite with magmatic

compositions indicates late magmatic or subsolidus processes were involved. The extensive replacement of K-feldspar by myrmekite ( $An_3$ ) in the margin of muscovite-biotite granite indicates albitization went further toward completion here. Intergrowths of muscovite and biotite in mica-rich domains which are deflected by coarse feldspar suggest deformation was late-magmatic, consistent with the conflicting cross cutting relationships at Micatalc Hill (Fig. 3-6).

### 3.3.6. Pegmatite and aplite.

Pegmatite and aplite occur as discordant dikes, sills, and irregular pods throughout the Cargo Muchacho Mountains, but are particularly abundant north of American Girl Canyon. Dikes and sills range from 2 cm to 10 m thick, irregular-shaped to rounded pods may attain sizes up to 3 m. They commonly contain folds axial planar to the regional fabric (Plate 3e). They are the only intrusive rock exposed at Hedges, where they cross cut the zones of aluminosilicate mineral assemblages. At Hedges, the aluminosilicate mineral zones are hosted within mylonites, and pegmatite dikes are deflected across these mylonite zones without being intensely deformed, suggesting intrusion late during shearing: map patterns indicate sinistral shear (Fig 3-3).

Pegmatite has seriate textures with extensive subgrain formation. Plagioclase (50%), microcline (25%), and quartz (20%) are the primary minerals, with accessory muscovite (3-4%) and garnet (1-2%). Plagioclase is seriate, fine to coarse

grained, anhedral, fractured, bent, and kinked. Numerous closely spaced fractures have led to subgrain rotation. Quartz, is also fine to coarse grained, with undulose extinction and well developed subgrain boundaries. Microcline, on the other hand, is generally fine to medium grained, mostly interstitial, and commonly with myrmekitic intergrowths. Anhedral to subhedral muscovite is fine to medium grained, intergrown with feldspar and quartz. Garnet occurs as small rounded, anhedral to euhedral grains, partially enclosed by the other minerals.

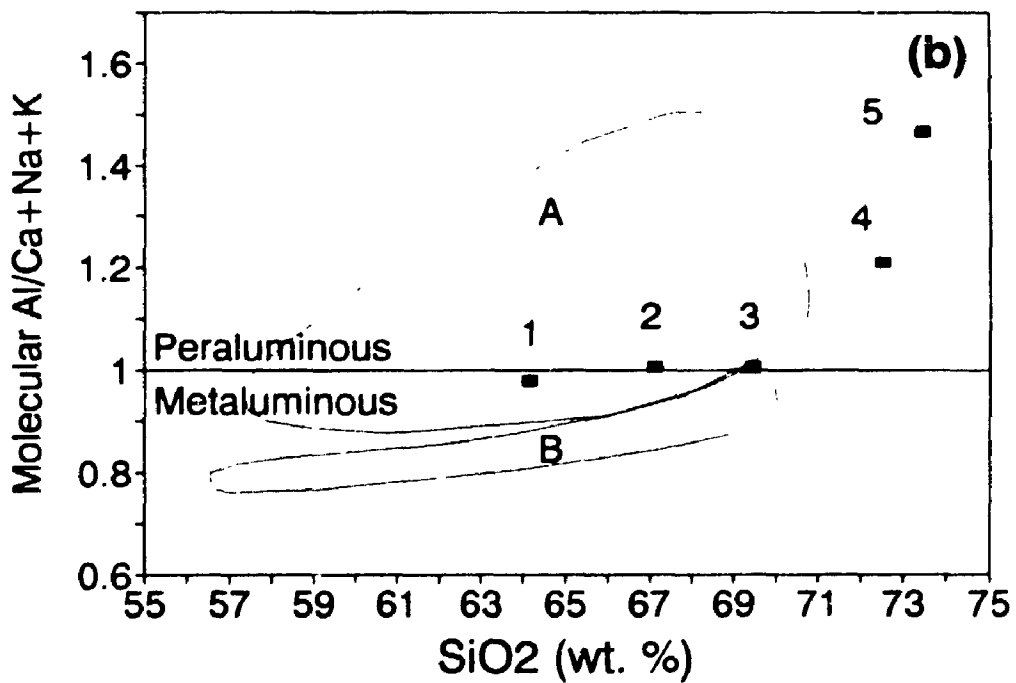
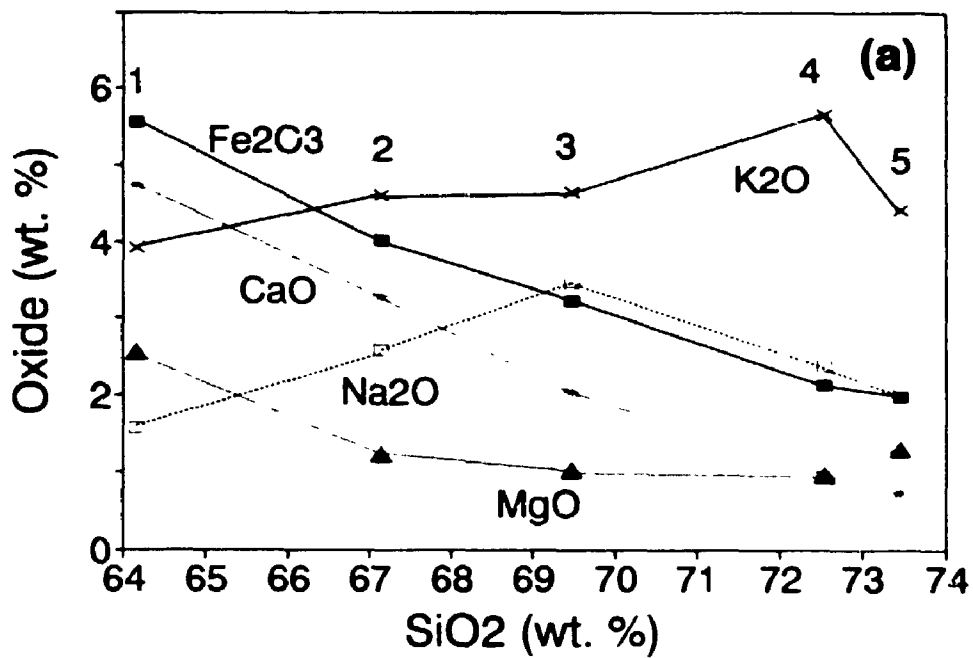
### 3.3.7. Compositional Variation and Magma Type.

Hornblende-biotite granodiorite, granite porphyry and muscovite-biotite granite belong to the 160-173 Ma calc-alkaline suite of Tosdal and Wooden (1991) and Murphy et. al. (1990).  $\text{SiO}_2$  content varies from 64% in granodiorite to 73% in muscovite-biotite granite (Fig. 3-9a). There is progressive decrease of  $\text{Fe}_2\text{O}_3$ , CaO and MgO, and an overall increase in  $\text{Na}_2\text{O}$  and  $\text{K}_2\text{O}$  with  $\text{SiO}_2$  content. Muscovite-biotite granite is heterogeneous, ranging from 67%  $\text{SiO}_2$  to 73%  $\text{SiO}_2$ . The group is metaluminous to peraluminous (Fig 3-9b), consistent with the presence of subhedral muscovite with magmatic compositions.

### 3.4. Miocene Dacite.

Unmetamorphosed dacite occurs as a shallow dike at Micatahc Hill, which cross-cuts metamorphic rocks and alum-

FIGURE 3-9. Whole rock composition of the intrusive rocks from the Micatac Hill area. (a) Harker-type diagram showing variation of major oxides versus  $\text{SiO}_2$ . (b) Molecular  $\text{Al}/(\text{Ca}+\text{Na}+\text{K})$  versus  $\text{SiO}_2$ , showing the peraluminous nature of the intrusive rocks; data for field labelled "A" is from Dillon (1976), data for the field labelled "B" is from Branham (1988). Numbers are: 1, hornblende-biotite granodiorite (B0512-4); 2 and 4, muscovite-biotite granite, interior (GN-1 and B0511-1); 3, granite porphyry (B0511-3); 5, muscovite-biotite granite, contact zone (B0511-2).



inosilicates at a high angle to metamorphic fabric. Dillon (1976) tentatively correlated it with Miocene volcanics elsewhere in the lower Colorado River region. Contacts are sharp with little or no aureole. They vary from nearly flat-lying, where the dacite is unconformable on quartzofeldspathic gneiss and orthogneiss, to very steep, where it cross-cuts gneisses. These features suggest it was emplaced very close to its current position; that is, after uplift and partial erosion of the older metamorphic rocks. It contains xenoliths of quartzofeldspathic gneiss, mafic volcanic rocks and pyroxenite, and xenocrysts of pyroxene. The dacite is porphyritic, with phenocrysts of biotite, quartz and plagioclase in a pilotaxitic to felty groundmass.

### 3.5. Summary.

The pre-Cenozoic rocks in the study area consist of Mesozoic gneiss of the Tumco Formation and Jurassic intrusive rocks. The Tumco Formation, primarily quartzofeldspathic gneiss, with minor quartzite and mafic gneiss, suggests a sedimentary origin, at least in part, for the protolith. Widespread matrix supported, relict lithic fragments, indicates deposition in proximity to a source region comprised of plutonic rocks. The deposition of Tumco sediments thus occurred during a tectonically active time period.

Intrusive rocks are quartz diorite, part of the 173 Ma suite of Tosdal and Wooden (1991), and granite porphyry, hornblende-biotite granodiorite and muscovite-biotite granite,



which are part of the 160-173 Ma suite of Tosdal and Wooden (1991). Field and compositional characteristics of the granodiorite-granite group indicate consanguineous emplacement of these rocks. They evolved from metaluminous to peraluminous types with differentiation, and emplacement accompanied deformation along low angle shear zones. Pegmatite cross cuts these rocks and is most likely equivalent to the 158-160 Ma leucogranite suite of Tosdal and Wooden (1991).

The Tumco Formation contains mineral assemblages characteristic of lower amphibolite facies metamorphism. Fabrics and mineral assemblages in quartz diorite, hornblende granodiorite, and muscovite-biotite granite also point to metamorphism to lower amphibolite facies. Thermal aureoles around the intrusions are small or absent, suggesting mesozonal levels of emplacement (Barton et. al., 1988). Exception to this is the local thermal overprint of hornblende-biotite granodiorite by muscovite-biotite granite.

Although overprinted by regional metamorphism, quartzofeldspathic gneiss and intrusive rocks have mineral compositions related to distinct origins. Granoblastic plagioclase and lepidoblastic biotite of quartzofeldspathic gneiss have compositional characteristics of those in amphibolite-grade metapelites (Smith and Brown, 1988; Guidotti, 1984). The composition and textures of feldspars and muscovite from muscovite-biotite granite indicate significant late magmatic fluid-rock interaction during emplacement. Distinct K-feldspar BaO contents between muscovite-biotite granite and

hornblende-biotite granodiorite are consistent with retention of magmatic compositions, whereas plagioclase composition in hornblende granodiorite reflects metasomatic and dynamic metamorphism.

**CHAPTER 4 -- MINERAL AND TEXTURAL VARIATION IN THE ZONES OF  
ALUMINOSILICATE MINERAL ASSEMBLAGES.**

**4.1. General Statement.**

Kyanite-bearing rocks are part of an asymmetrically-zoned sequence of aluminosilicate assemblages which occur at three sites on the west flank of the Cargo Muchacho Mountains, at Hedges, at Micatalc Hill, and at Vitrifax Hill (Figs. 2-2, 3-1 and 3-3). The aluminosilicate assemblages occur as tabular zones at Micatalc and Vitrifax along strike with the American Girl and Madre-Padre gold deposits, respectively. The mineral zones are concordant to the regional foliation, dipping south at 27°. The kyanite-bearing layers are up to 20 m thick at these sites. In contrast, the aluminosilicate assemblage zones at Hedges are much smaller, the kyanite-bearing rocks being small rod-shaped bodies up to 8 m in diameter.

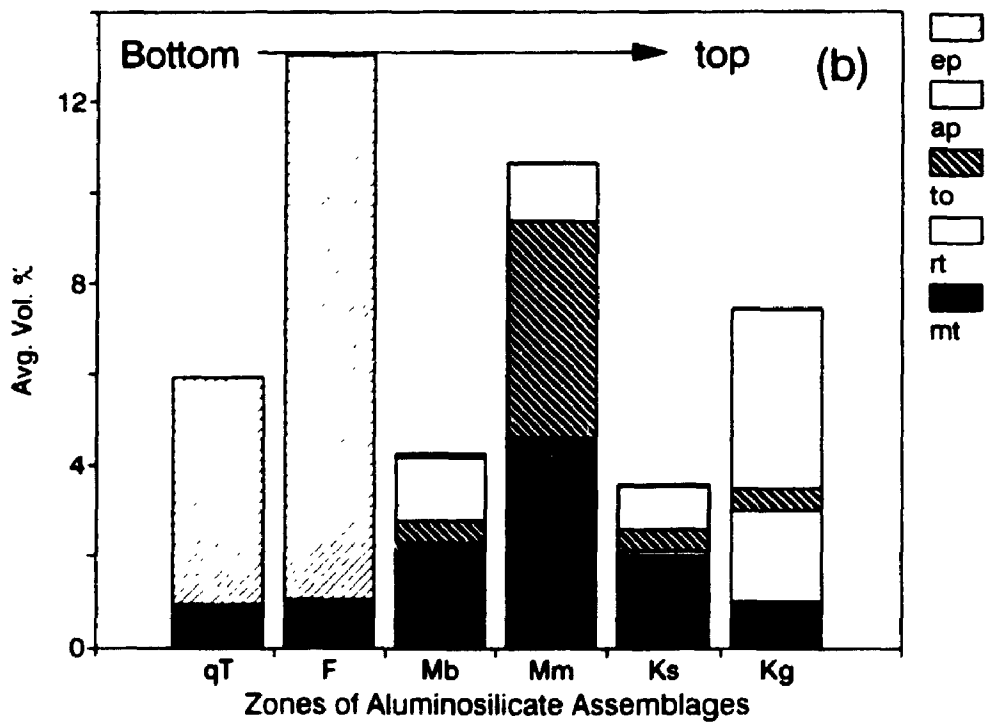
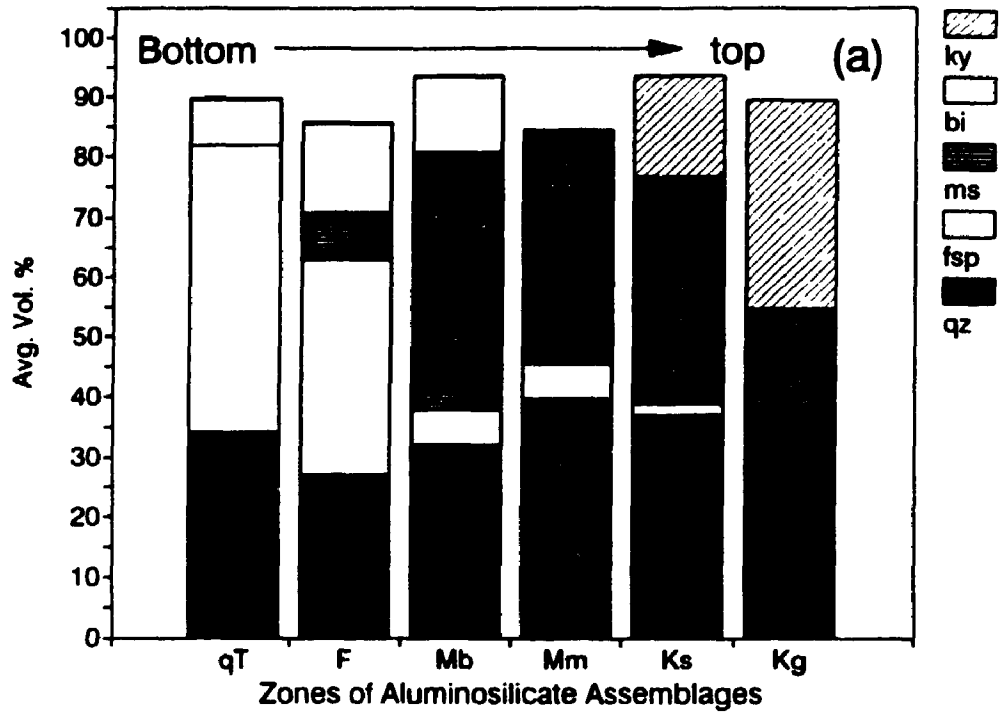
The mineral assemblage zones are named according to the predominant aluminum silicate in each zone, and because the mineral assemblage zones are relatively flat-lying, zoning is in a vertical sense, from bottom to top, the Feldspar Zone, the Muscovite Zone, and the Kyanite Zone (Fig. 3-2). The Feldspar Zone grades down into quartzofeldspathic gneiss of the Tumco Formation. Because the rocks of the Kyanite Zone are resistant to weathering, the upper contact is commonly missing because of erosion of overlying less resistant material, except for a small length south of Micatalc Hill, where it is in fault contact with muscovite-biotite granite. Relationships to structurally higher rocks are therefore obscure.

In addition to variation in the alkali-aluminosilicates, regular changes also occur in the abundance of Fe- and Ti-bearing mineral phases, as well as fabrics (Fig. 4-1). The general characteristics are:

- 1.) The Feldspar Zone has a porphyroblastic, gneissic fabric with the mineral assemblage quartz-plagioclase-biotite-magnetite-epidote (with local garnet, K-feldspar, chlorite, carbonate).
- 2.) The Muscovite Zone has schistose, mylonitic and crenulated fabrics, with the mineral assemblage quartz-muscovite-biotite-magnetite-apatite-tourmaline (with local plagioclase, garnet).
- 3.) The Kyanite Zone has granofelsic fabric, with the mineral assemblage quartz-kyanite-(muscovite)-apatite-tourmaline-magnetite-rutile (with local lazulite, pyrophyllite, andalusite, garnet, hematite, paragonite, margarite); mylonitic fabrics are locally present and are accompanied by an increase in muscovite content.

The Muscovite Zone can be further subdivided into the biotite and magnetite subzones, based on the presence or absence of biotite, as described below.

**FIGURE 4-1.** Variation of modal mineralogy from the quartzofeldspathic gneiss of the Tumco Formation to the Kyanite Zone of the aluminosilicate mineral assemblages. The data are averages of compositions presented in Appendix 1. (a) major minerals, (b) minor and trace accessories. Zones are: **qT**, quartzofeldspathic gneiss of the Tumco Formation; **F**, Feldspar Zone; **Mb**, Muscovite Zone, biotite subzone; **Mm**, Muscovite Zone, magnetite subzone; **Ks**, schistose and mylonitic Kyanite Zone; **Kg**, granoblastic Kyanite Zone. Minerals are: **ky**, kyanite; **bi**, biotite; **ms**, muscovite; **fsp**, feldspar; **qz**, quartz; **ep**, epidote; **ap**, apatite; **to**, tourmaline; **rt**, rutile; **mt**, magnetite.



## 4.2. Gross Characteristics.

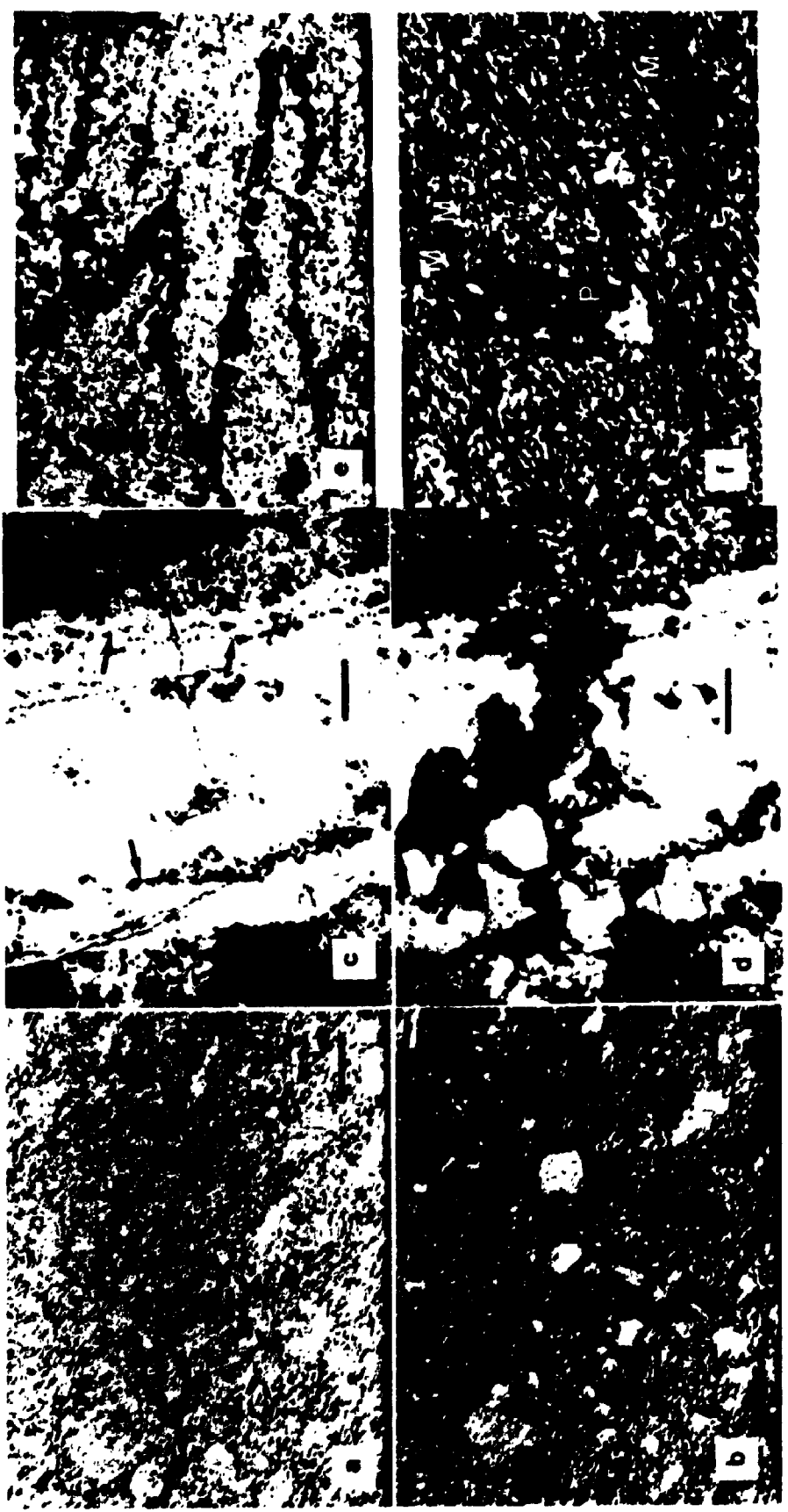
### 4.2.1. Feldspar Zone.

The Feldspar Zone is gneissic, with coarse plagioclase poikiloblasts in a fine grained granoblastic groundmass of quartz, plagioclase, lepidoblastic biotite, epidote and magnetite (Plate 4a and b). Minor accessory minerals are garnet, tourmaline, zircon and relict hornblende (Appendix A). Chlorite and carbonate minerals fill late fractures and replace plagioclase and biotite. The fabric and grain size, with the exception of the porphyroblasts, are similar to quartzofeldspathic gneiss of the Tumco Formation. Biotite defines the foliation, which is deflected by coarse feldspar porphyroblasts (Plate 4a and b). Muscovite occurs in the Feldspar Zone within 5 m of the Muscovite Zone in spaced cleavages (Plate 4f), concentrated along the sides of feldspar poikiloblasts facing the direction of maximum flattening.

Locally, epidote makes up 45% of the Feldspar Zone. Relict plagioclase porphyroblasts are set in a very fine grained groundmass of polygonal quartz and plagioclase. Both groundmass and porphyroblastic and groundmass plagioclase are extensively replaced by epidote. Epidote veinlets are folded (Plate 4e), and are cross cut by later quartz-epidote and quartz veinlets. Quartz-epidote veinlets contain coarse granoblastic quartz with interlocking to sutured grain boundaries, and inclusion bands of epidote (Plate 4c and d), suggesting metamorphic recrystallization of an earlier crack-seal fabric (Ramsay and Huber, 1987).

**PLATE 4.** Characteristic textures of the Feldspar Zone. a.) Photomicrograph, plane polarized light. Biotite defines the foliation ( $S_1$ ), which is deflected by coarse feldspar porphyroblasts (light areas). Scale bar equals 2 mm. b.) Same field of view as (a), crossed polars. Coarse feldspar porphyroblasts, dominantly plagioclase, set in a fine grained groundmass of quartz, feldspar, biotite and epidote. c.) Photomicrograph of epidote-rich granofels, with quartz-epidote veinlet cross cutting fine grained quartz-epidote. Inclusion bands of epidote, parallel to the vein walls (arrows), is a crack-seal texture. Scale bar is 1 mm. d.) Same view as in (c), crossed polars. Quartz in the veinlet is recrystallized to irregular grains with undulose extinction. e.) Photomicrograph of epidote-rich Feldspar Zone, with folded epidote veinlets. Plane light, scale bar equals 2 mm. f.) Photomicrograph of porphyroblastic Feldspar Zone adjacent to the Muscovite Zone. Plagioclase porphyroblast (P) deflects muscovite in spaced cleavages or shear bands (M). Note the abundance of inclusions of quartz in plagioclase. Scale bar equals 1 mm.





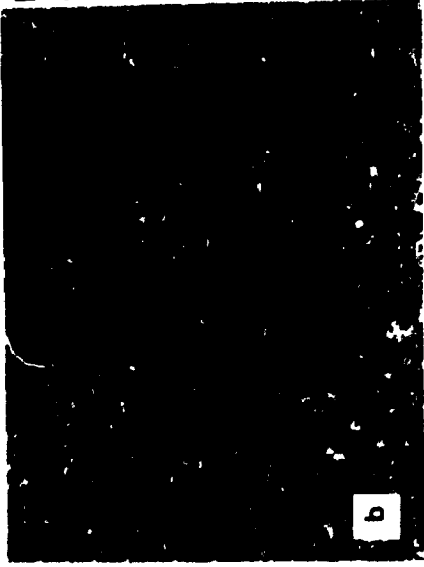
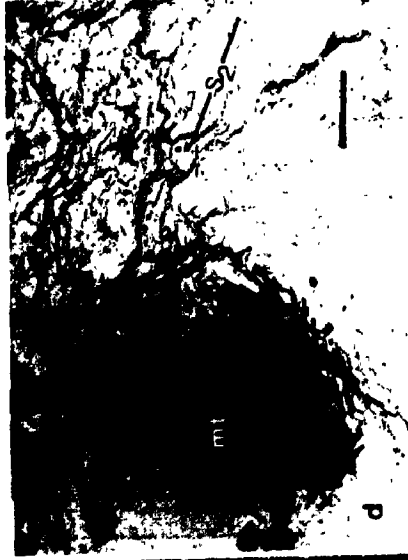
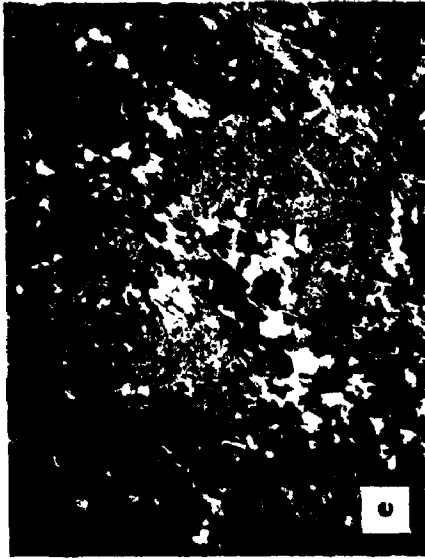
#### 4.2.2. Muscovite Zone.

The Muscovite Zone is schistose and mylonitic, with more than 90% quartz plus muscovite (Plate 5a and b). Biotite and magnetite are characteristic accessories. Tourmaline, apatite, garnet, and zircon occur in variable concentrations (Fig. 4-1 and Appendix A). Epidote is absent, but plagioclase may occur locally as rounded porphyroclasts and polygonal groundmass grains. Overall grain size is much less than that of both the Feldspar and Kyanite Zones. In the Muscovite Zone this is 0.05 to 0.3 mm, compared to 0.2 to 1.0 mm in the Feldspar Zone, and 0.5 mm to 2 cm in the Kyanite Zone.

The presence or absence of biotite defines a biotite subzone and a magnetite subzone. The biotite subzone of the Muscovite Zone is adjacent to the Feldspar Zone, and has coarse, non-oriented biotite porphyroblasts, with fine grained groundmass magnetite (Plate 5c). The magnetite subzone of the Muscovite Zone, next to the Kyanite Zone, has only magnetite as the characterizing accessory (Plate 5d). The contact between the two subzones contains either a high content of tourmaline, very-coarse euhedral tourmaline (up to 8 cm), or quartz-tourmaline veinlets. On the north flank of Micatahc Hill, interlayered, elongate lenses and pods of mylonitic and crenulated biotite and magnetite subzones indicate transposition of these layers, probably due to mylonitization.

**PLATE 5. Characteristics of the Muscovite and Kyanite Zones.**

**a.)** Photomicrograph of schistose Muscovite Zone with muscovite and fine, granoblastic quartz. Scale bar equals 0.5 mm. **b.)** Photomicrograph of mylonitic Muscovite Zone, with anastomosing shear bands of muscovite. Scale bar equals 1 mm. **c.)** Photomicrograph from the biotite subzone, showing randomly oriented biotite poikiloblasts (b) and lepidoblastic muscovite (m) defining foliation. Magnetite occurs as small, equant disseminated grains (black). Scale bar equals 0.5 mm. **d.)** Photomicrograph of the magnetite subzone, with foliation deflected around coarse magnetite porphyroblast (mt). Scale bar equals 1 mm. **e.)** Photomicrograph of the Muscovite Zone with aggregates of fine muscovite and coarser lepidoblastic muscovite, defining foliation. Scale bar equals 0.5 mm. Numbers 2 and 4 represent Type 2 and Type 4 muscovite, respectively (see text, Section 4.3.3). **f.)** Photomicrograph of the Kyanite Zone, showing late cross cutting muscovite (M) in granoblastic quartz(Q) and kyanite(K). Scale bar equals 1 mm.



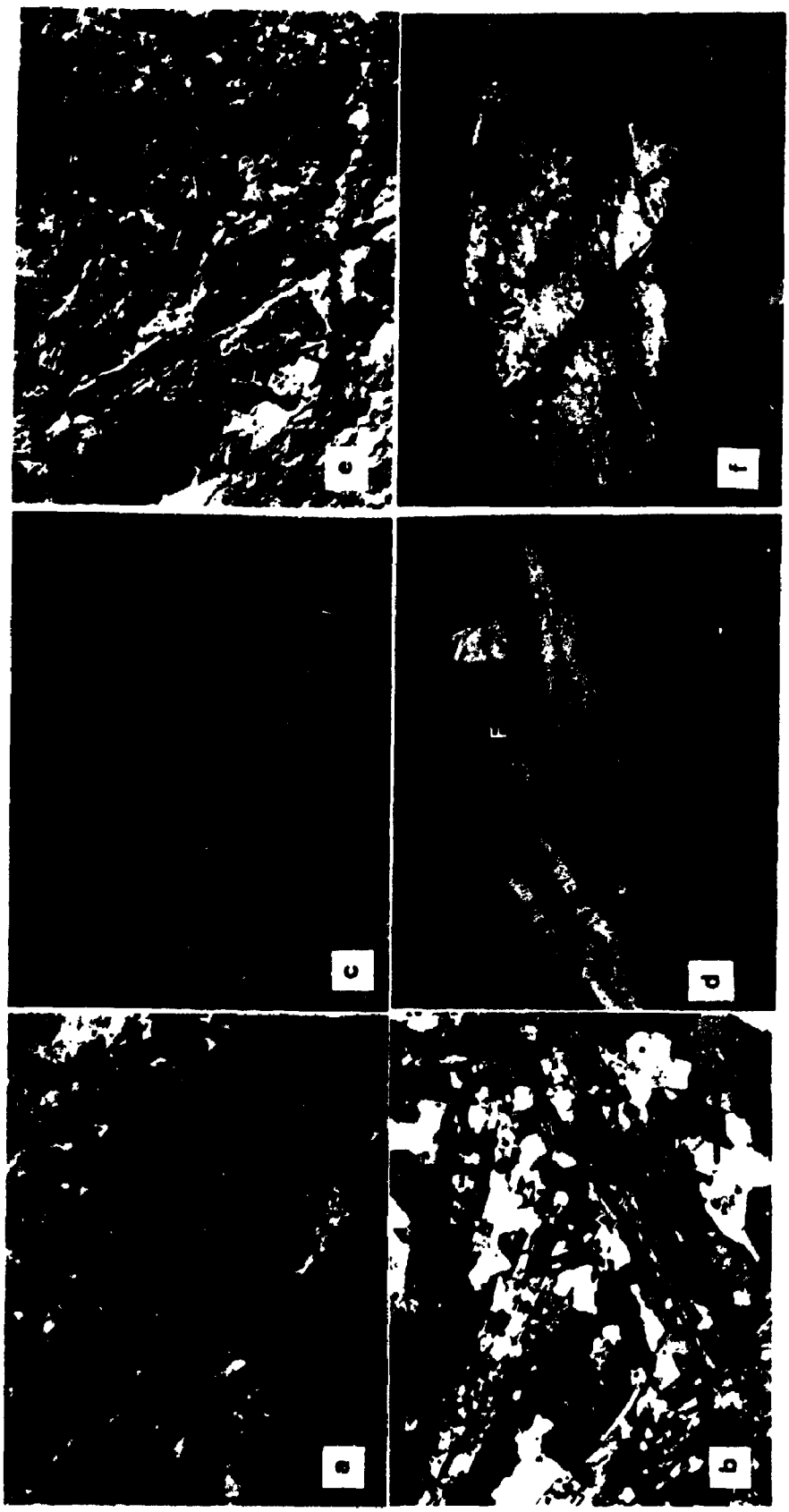
#### 4.2.3. Kyanite Zone.

The Kyanite Zone is primarily granoblastic, with quartz and kyanite as the main minerals. The structure is massive to banded, the latter with alternating kyanite-rich and kyanite-poor bands 2-10 cm thick (Plate 6a). Vugs are common, up to 3% by volume. Muscovite averages 15% by volume, and magnetite, rutile, tourmaline and apatite are minor but ubiquitous (Appendix A). Porphyroblasts of kyanite, tourmaline and apatite are anhedral and sieve textured (Plate 6a). Local, or trace, accessories are andalusite, lazulite, specular hematite, pyrophyllite, zircon, and limonite after pyrite. Chlorite is generally restricted to late veinlets and vugs with carbonate and chalcedony, although it replaces rare biotite.

With increasing muscovite content, foliation becomes more pronounced, with schistose to mylonitic fabrics predominant in muscovite-rich specimens. Muscovite is up to 68% by volume, and kyanite, tourmaline, and apatite porphyroblasts are euhedral and inclusion-poor (Plate 6d). Rods of granoblastic quartz-kyanite are hosted in schistose to mylonitic quartz-muscovite-kyanite, and the latter occurs as thin (less than 6 cm wide) anastomosing layers surrounding lens-shaped pods of granoblastic quartz-kyanite.

On the north flank of Vitrifax Hill there are numerous irregular, angular to rounded and amoeboid pods of granoblastic quartz-kyanite within weakly foliated to schistose quartz-kyanite-muscovite (Plate 6c). These pods of kyanite and

**PLATE 6.** Characteristics of the Kyanite Zone. **a.)** Compositional layering in granoblastic Kyanite Zone. Dark layers are relatively enriched in quartz, magnetite and tourmaline, light colored layers are relatively enriched in kyanite. **b.)** Photomicrograph of granoblastic quartz-kyanite, with randomly-oriented, poikiloblastic to skeletal kyanite. Scale bar equals 0.7 mm. **c.)** Ameboid pod of kyanite (blue) and quartz (white, rim) in foliated quartz, kyanite, and muscovite. **d.)** Photomicrograph of schistose Kyanite Zone, with coarse, euhedral, relatively inclusion-free kyanite in a fine grained muscovite and quartz groundmass. Dark gray porphyroblast at top of photo is relict feldspar (F), replaced by muscovite and kyanite. Scale bar equals 1 mm. **e.)** Stockwork fractures cross cutting massive, granoblastic quartz and kyanite. Quartz is white, kyanite blue. Fractures (arrows) contain kyanite (as at arrow labelled A) which has extremely high length-width ratios along the fractures. **f.)** Cross cutting quartz-kyanite veinlets in foliated quartz, muscovite, and kyanite. Small veinlets (1), oblique to foliation, are cross cut by larger, foliation-parallel veinlet (2).



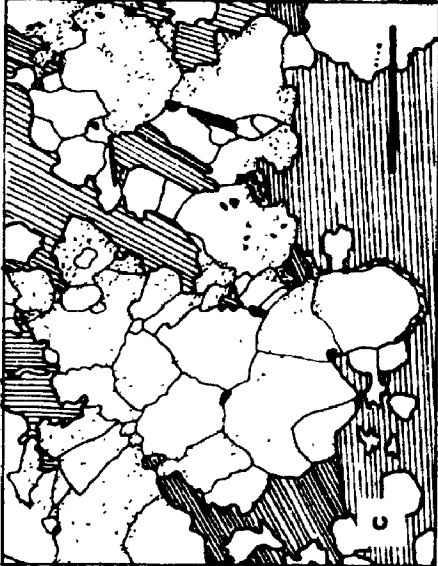
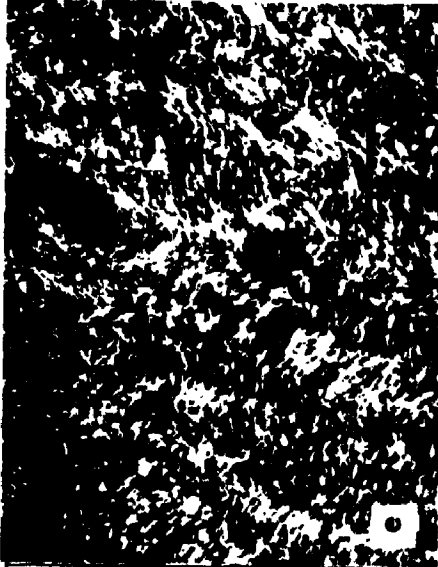
quartz, from 5 cm to 30 cm in diameter, are zoned, with kyanite-rich cores and thin quartz-rich rims. At the same site, stockwork-like fractures and cross cutting veinlets contain quartz, kyanite, magnetite and rutile (Plate 6e and f). The foliated groundmass grades into massive granoblastic quartz-kyanite through a decrease in veining and foliation.

There are thin concordant layers with the assemblage quartz-biotite-muscovite-staurolite-kyanite-garnet at the contact between the Kyanite Zone and Muscovite Zone at Micatahc Hill and within the Kyanite Zone at Vitrifax Hill (Sample B0430-3, Appendix A). These are very coarse grained (up to 10 mm) and granoblastic, with sieve textured staurolite, garnet, and kyanite porphyroblasts and interstitial biotite, muscovite and quartz. Chlorite, tourmaline, and zircon are minor fine grained phases. Magnetite and rutile are the primary oxides, although ulvospinel and ilmenite were identified by microprobe analysis as blebs and lamellae in magnetite. Branham (1988) interpreted these layers as a separate alteration zone. However, they are not continuous, nor present at all three sites, and their variable position relative to the surrounding zones of aluminosilicate minerals suggest these layers formed from metamorphism of a pre-existing layering or unusual fluid-rock reactions.

Massive to banded, granoblastic, quartz-rich layers, up to 1 m in thickness, occur in both the Muscovite and Kyanite Zones. Clear quartz overgrowths on sub-rounded, inclusion-rich quartz grains suggest these layers may be metamorphosed sand-



**PLATE 7.** Characteristics of minerals and textures of the zones of aluminosilicate mineral assemblages. a.) Photomicrograph of quartzite within the Muscovite Zone, plane light. Zoning in quartz is from rounded inclusion-rich cores (dusty appearance) to clear rims. Note fracture containing muscovite (M) and apatite (A). Scale bar equals 1 mm. b.) Same field of view as in (a), crossed polars. c.) Tracing from photomicrograph of granoblastic quartz-kyanite with irregular zoning in quartz. Stippled areas are inclusion-rich zones, clear areas are inclusion-poor zones in quartz. Note that grain boundaries cross cut zone boundaries at high angles. Kyanite represented by lined pattern, magnetite as small black grains. Scale bar equals 1 mm. d.) Photomicrograph of aggregate of magnetite and quartz grains with biotite, in finer grained groundmass of quartz and muscovite, from the Muscovite Zone. Note the rectangular outline of the aggregate indicating replacement of biotite. Scale bar equals 0.5 mm. e.) Photomicrograph of crenulated foliation in the magnetite subzone of the Muscovite Zone. Rectangular magnetite grains are oriented parallel to the folded foliation. Scale bar equals 0.5 mm. f.) Photomicrograph of granoblastic quartz and kyanite, plane light. Microfracture (arrows) containing magnetite and rutile cross cuts aggregate of kyanite grains. Note that kyanite is inclusion-free adjacent to the microfracture, but inclusion-rich away. Scale bar equals 5 mm.



stones (Plate 7a and b). These layers are transposed and attenuated in the mylonitic parts of the zones of aluminosilicate minerals.

#### 4.2.4. Relationships to Intrusive Rocks.

The zones of aluminosilicate mineral assemblages at Micatahc and Vitrifax Hills are structurally below the main bodies of intrusive rocks (Figs. 3-1 and 3-2). At Micatahc Hill, Jurassic hornblende-biotite granodiorite cross cuts the Muscovite and Kyanite Zones of the aluminosilicate assemblages at a high angle, and in turn has been thermally metamorphosed by muscovite-biotite granite. The granodiorite does not, however, contain minerals of the host Muscovite and Kyanite Zones. Muscovite-biotite granite is schistose, muscovite-rich and K-feldspar-poor where it is in fault contact with the Kyanite Zone. Miocene dacite cross cuts the zones of aluminosilicate assemblages at a high angle. At Hedges, pegmatite dikes cross cut the zones of aluminosilicate assemblages at high angles (Fig. 2-3). The dikes contain none of the minerals found in the aluminosilicates.

Where granite porphyry cross cuts the Muscovite Zone at Vitrifax Hill, the granite is muscovite-rich (Figs. 3-1 and Plate 2f). Relict plagioclase still remains, however, and the porphyritic texture is still present. Muscovite-biotite granite also cross cuts the Muscovite Zone at Vitrifax Hill, but does not contain the abundance of muscovite comparable to that of granite porphyry. It does contain abundant myrmekite

with only a small amount of K-feldspar, similar to muscovite-biotite granite adjacent to the Kyanite Zone at Micatalc.

There are quartz-muscovite-apatite-chlorite assemblages with irregular to oval inclusions of quartz-muscovite-kyanite-chlorite-apatite exposed in the Kyanite Zone at the top of Vitrifax Hill (Plate 1c). The shape and size of these inclusions is similar to that of inclusions of quartzofeldspathic gneiss of the Tumco Formation in quartz diorite elsewhere in the range. As the quartz diorite projects to the top of Vitrifax, the assemblage hosting the xenoliths is interpreted to be altered quartz diorite.

#### **4.3. Mineral, Textural and Compositional Variation.**

##### **4.3.1. Quartz.**

In the Feldspar Zone, groundmass quartz is fine grained and polygonal with weak undulose extinction. Rare coarse grains occur, with irregular and embayed boundaries, strong undulose extinction, and well developed subgrains. In the Muscovite Zone, quartz is polygonal, mosaic-textured, with full extinction or weak undulose extinction. Triple junctions are common. Coarse grains and aggregates of coarse grains have strong undulose extinction, sutured grain boundaries and development of subgrains. Pressure shadows of feldspar, biotite and magnetite porphyroblasts contain relatively strain-free quartz.

In the Kyanite Zone, granoblastic quartz is inequigranular, ranging from 0.1 mm to 5 mm. These grains vary from

serrated grains with undulose extinction and with abundant subgrains, to grains with relatively smooth boundaries and weak undulose extinction. Fluid inclusions, some of which contain lazulite, are abundant and occur commonly along microfractures. Zonation in quartz consists of irregular-shaped inclusion-rich patches which are surrounded by, or interfinger with, clear, inclusion-free quartz, bearing no relationship to grain boundaries (Plate 7c). This is distinct from zoning in quartz in quartzite of the Tumco Formation (compare Plate 7a), and indicates recrystallization of previously zoned quartz, the irregular shape of which suggests considerable mobility of  $\text{SiO}_2$ .

#### 4.3.2. Feldspar.

Plagioclase is the main feldspar in the zones of aluminosilicate mineral assemblages, and is common in the Feldspar Zone, but is rare in the Muscovite and Kyanite Zones. K-feldspar is sporadic, as rounded poikiloblasts containing patch myrmekite only in the Feldspar Zone. Plagioclase is coarse, anhedral poikiloblasts in the Feldspar Zone, up to 1 cm long, with rectangular to rounded shapes, sutured grain boundaries, undulose extinction and local development of subgrains (Plate 4b). In contrast, groundmass plagioclase is polygonal and optically zoned. In the Muscovite Zone, plagioclase occurs as optically zoned polygonal groundmass grains with no or weak undulose extinction and rare rounded porphyroblasts in mylonitic rocks. In foliated rocks of the Kyanite

Zone, rare relict plagioclase porphyroblasts are extensively replaced by muscovite, kyanite and tourmaline.

K-feldspar of the Feldspar Zone is  $Or_{90}$  to  $Or_{95}$  (Fig. 4-2), has high BaO contents, up to 0.9 wt. %, and up to 10% of the albite molecule, making them among the most sodic of any of the K-feldspars. As such they are distinctive from K-feldspars in the intrusive rocks and in the Tumco Formation (compare Fig. 3-5).

Plagioclase becomes more calcic from quartzofeldspathic gneiss of the Tumco Formation into the Muscovite Zone (Fig. 4-3a). The charge imbalance of the substitution of  $Ca^{2+}$  for  $Na^+$  results in an accompanying substitution of  $Al^{3+}$  for  $Si^{4+}$  (Fig. 4-3b). Fine grained, granoblastic plagioclase in quartzofeldspathic gneiss of the Tumco Formation averages  $An_{13.7}$ . It ranges from  $An_3$  to  $An_{21}$  in a single specimen, however, which is within the peristerite field. In the Feldspar Zone, plagioclase composition varies from  $An_8$  to  $An_{11}$ , averaging  $An_{10.6}$ , with no compositional distinction between porphyroblasts and groundmass grains. Most of this variability occurs between sample sites, as averages within samples range from  $An_{11}$  to  $An_{31}$ . Polygonal groundmass plagioclase and porphyroclasts from the Muscovite Zone average  $An_{26}$ , and relict plagioclase from the Kyanite Zone averages  $An_{40}$ .

#### 4.3.3. Muscovite.

Muscovite occurs in all zones of aluminosilicate mineral assemblages, but is absent from quartzofeldspathic gneiss of

**FIGURE 4-2.** Composition of K-feldspar from the Feldspar Zone.

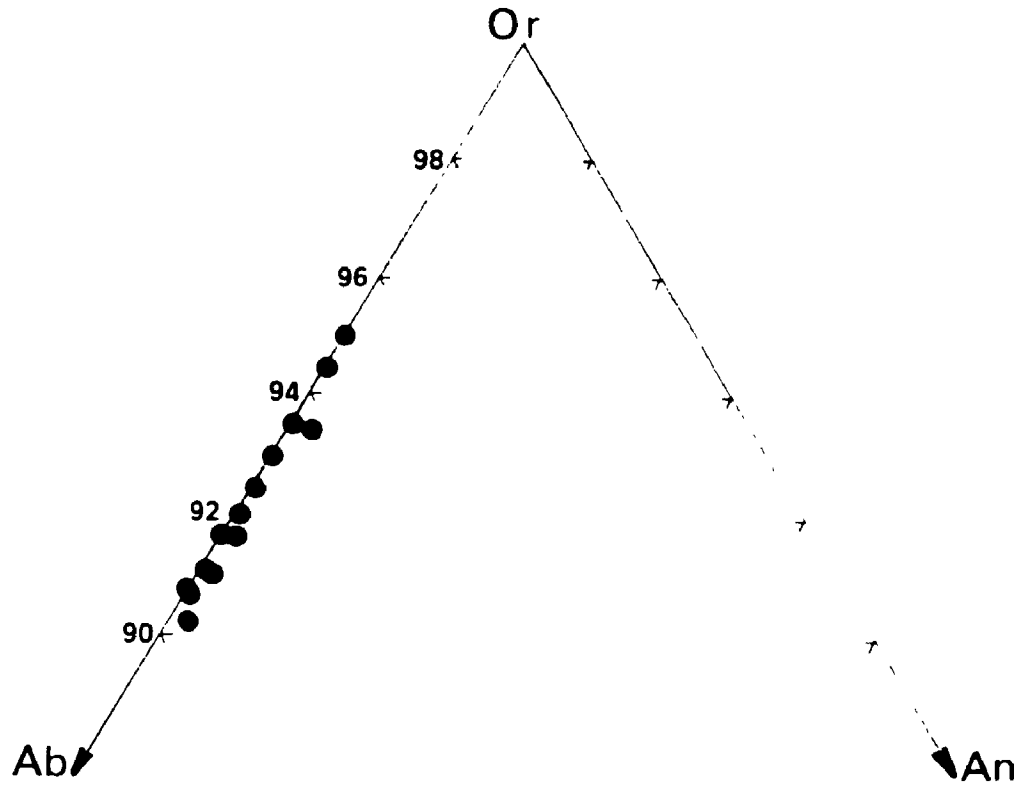
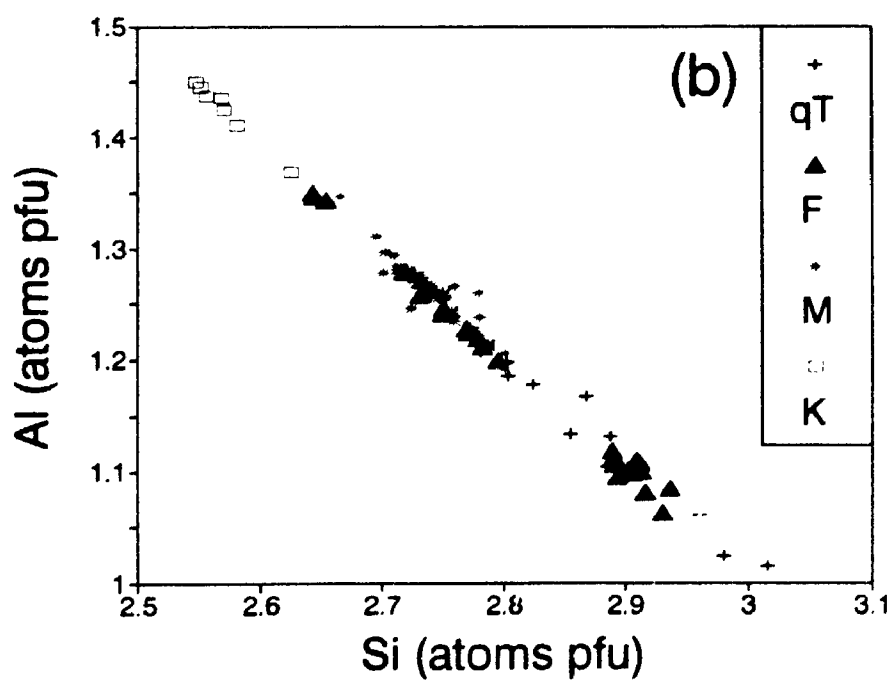
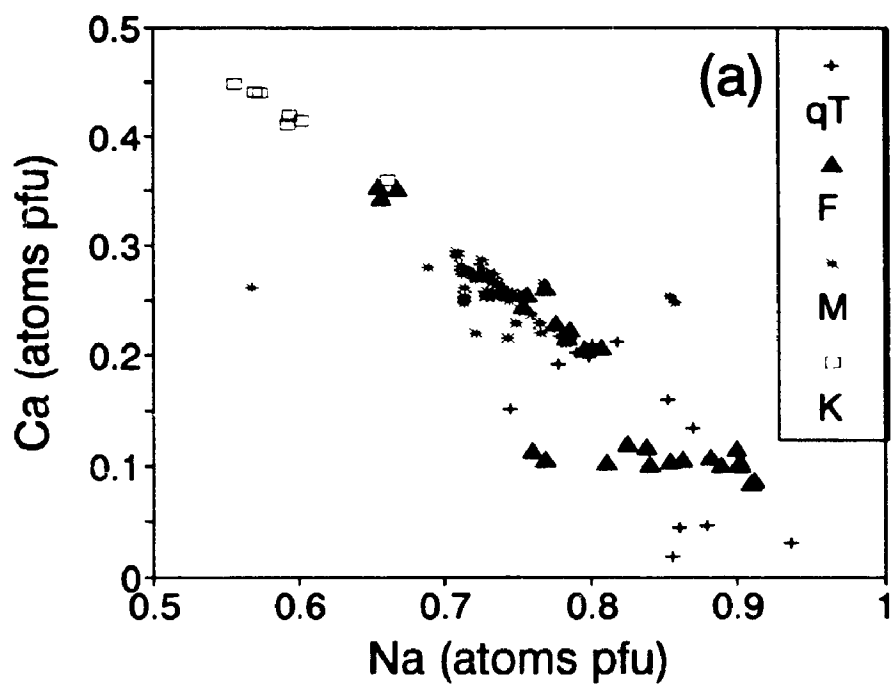




**FIGURE 4-3.** Composition of plagioclase in the zones of aluminosilicate mineral assemblages. **a.)** Ca vs. Na, **b.)** Al vs. Si. Symbols: filled squares, quartzofeldspathic gneiss of the Tumco Formation (qT); filled triangles, Feldspar Zone (F); asterisks, Muscovite Zone (M) open squares, Kyanite Zone (K).



the Tumco Formation. Identified species include muscovite, phengitic muscovite, paragonite, margarite, and pyrophyllite, and solid solutions between these end members. The last three are restricted to the Kyanite Zone: pyrophyllite replaces kyanite and muscovite, and paragonite and margarite replace relict feldspar. Muscovite has four general habits:

Type 1: Fine, non-aligned groundmass grains in quartzose, muscovite-poor layers, and fine to medium grained, non-aligned to lepidoblastic muscovite in muscovite-rich layers from 1 to several cm thick (Plate 5a).

Type 2: Clots, or aggregates, of fine muscovite, some with near-rectangular outlines, suggesting replacement of earlier feldspar or kyanite porphyroblasts (Plate 5e).

Type 3: Fracture-, microfracture-, and vein-fillings (Plate 5f).

Type 4: Fine to medium grained muscovite thin, crenulated, foliation-parallel, mica-rich domains (Plate 5b).

Types 1 and 4 are the dominant habits. Type 1 results in a subtle compositional banding, reflecting either primary compositional layering or metamorphic or metasomatic segregation. Because the Muscovite Zone is very fine grained, Type 1 muscovite may alternatively represent recrystallized foliated mus-

covite. Kyanite, tourmaline and apatite invariably replace Type 1 muscovite. Type 4 muscovite forms S-C fabrics typical of mylonites (Lister and Snoke, 1984), and is also as crenulations. Spaced fractures containing muscovite in the Feldspar Zone may be either Type 1 or Type 4. The foliation of Type 4 muscovite has conflicting relationships to porphyroblasts: it cross cuts, and is deflected by, coarse porphyroblasts of biotite, magnetite, tourmaline, apatite, and kyanite, but is rarely cross cut by them. Type 4 muscovite is therefore in part later than these minerals and overprints Type 1, making distinction between the two difficult.

There appears to be no compositional distinction among the muscovite of different habits. There is, however, progressively more Na and total Al, and less Si, Ti, Fe, Mg, Mn, and K, in muscovite from the Feldspar Zone to the Kyanite Zone (Fig. 4-4). F and Cl contents are very low, mostly below detection limits. Most of the variation in composition of muscovite is by solid solution in the muscovite to paragonite, the muscovite to phengite, and the trioctahedral to dioctahedral mica series.

Muscovite has about 5% of the paragonite molecule in the Feldspar Zone, 15% in the Muscovite Zone, and 20-40% in the Kyanite Zone (Fig. 4-5). In addition, Fe plus Mg is nearly 1 atom pfu in muscovite of the Feldspar Zone, 0.45 atoms pfu in the Muscovite Zone, and 0.1 to 0.3 atoms pfu in the Kyanite Zone (Fig. 4-6). Thus, muscovite from the Feldspar Zone is phengitic, and progression to the Kyanite Zone involves move-

**FIGURE 4-4.** Composition of muscovite in the zones of aluminosilicate mineral assemblages. Compositions are plotted as atoms per formula unit (pfu), and are the result of recalculation of oxide weight percent to structural formula on the basis of 22 O. Mineral zone abbreviations are: F, Feldspar Zone; Mb, biotite subzone, Muscovite Zone; Mm, magnetite subzone, Muscovite Zone; Ks, schistose to mylonitic Kyanite Zone; Kg, granoblastic Kyanite Zones. Error bars represent one standard deviation.

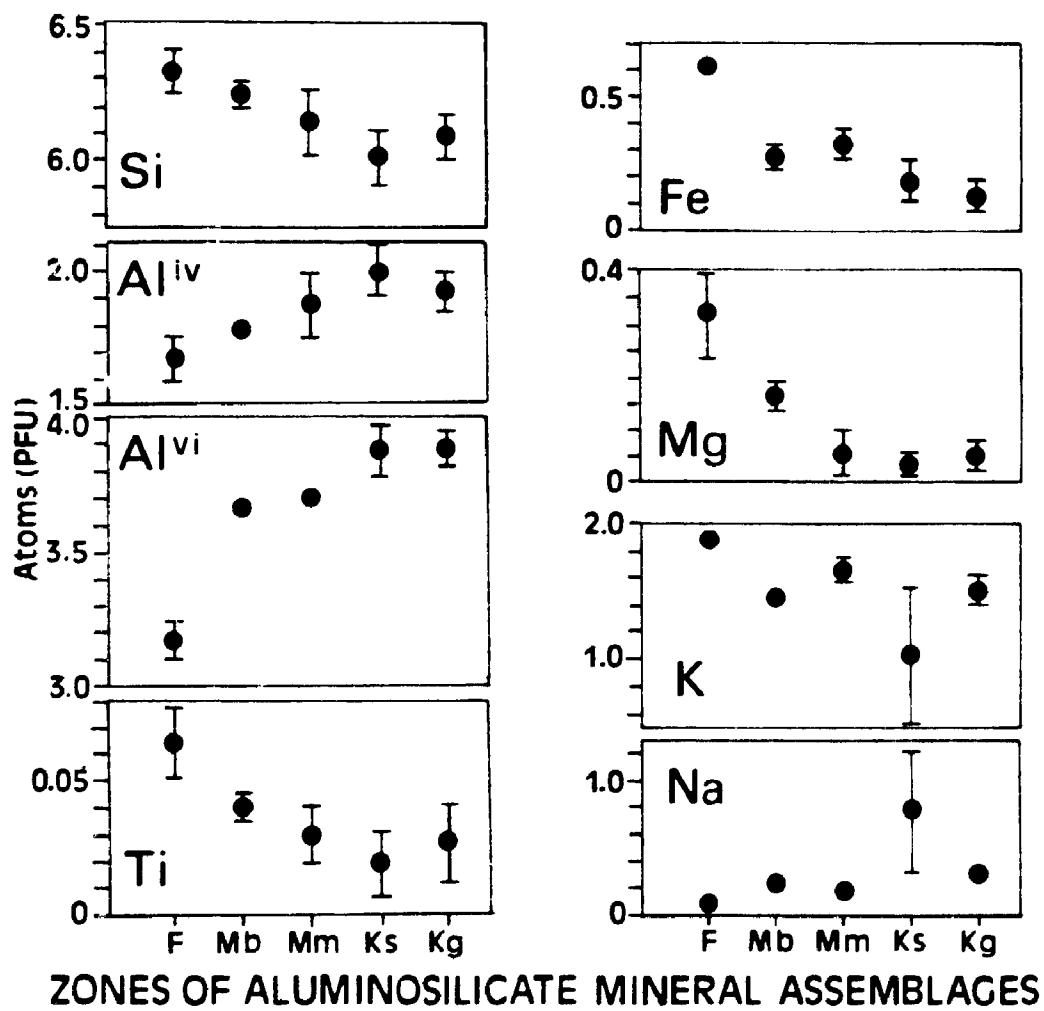


**FIGURE 4-5.** Paragonite content of muscovite from the zones of aluminosilicate mineral assemblages, as a function of  $Al_{16}$ . Filled triangles, Feldspar Zone (F); filled squares, biotite subzone of the Muscovite Zone (Mb); asterisks, magnetite subzone of the Muscovite Zone (Mm); open squares, Kyanite Zone (K). Paragonite-rich analyses (greater than 60%) are from muscovite-rich, mylonitic Kyanite Zone, where paragonite replaces relict feldspar.

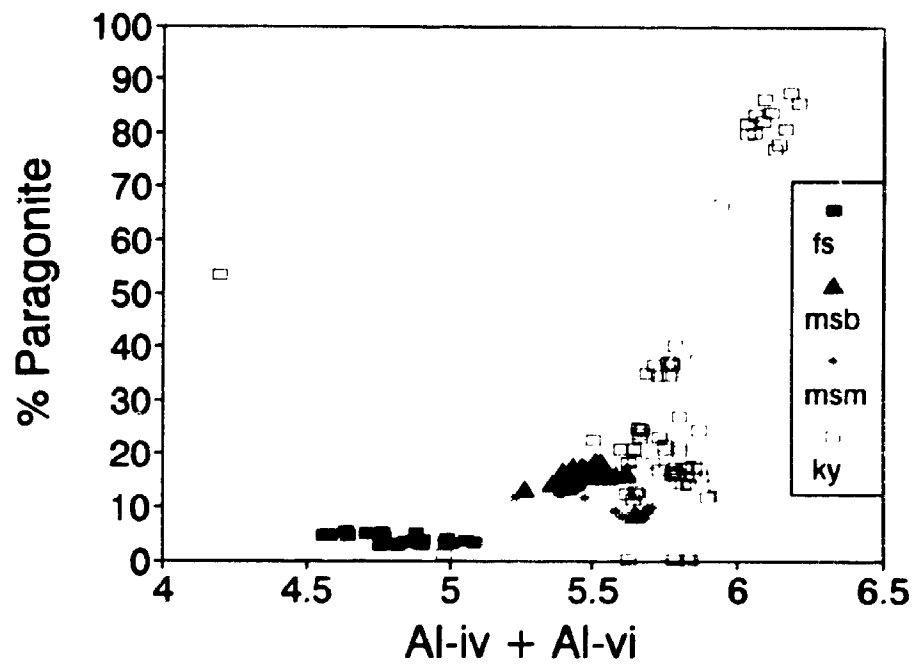
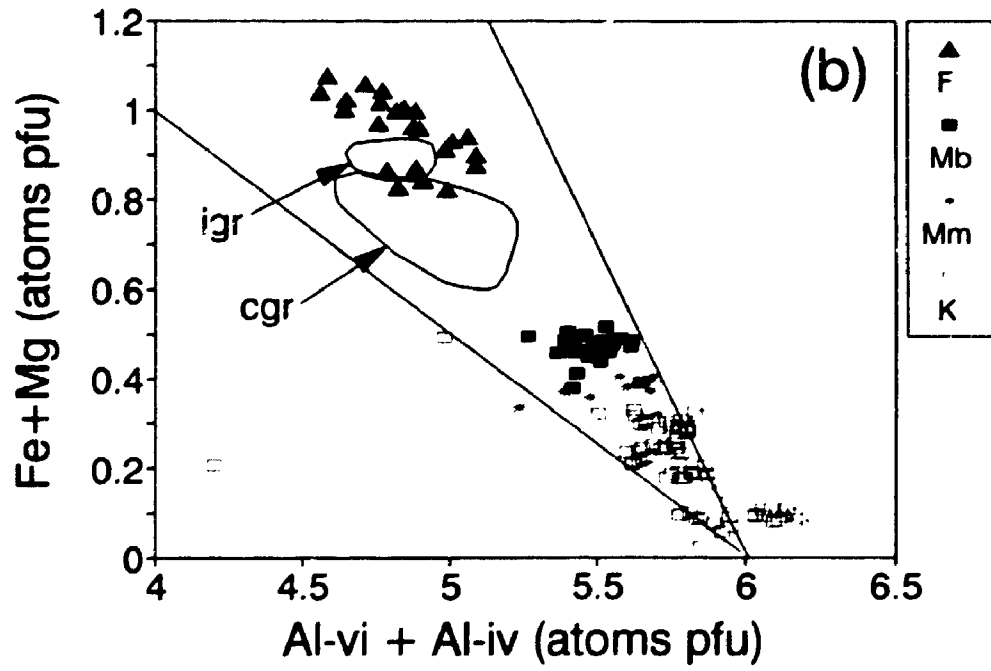
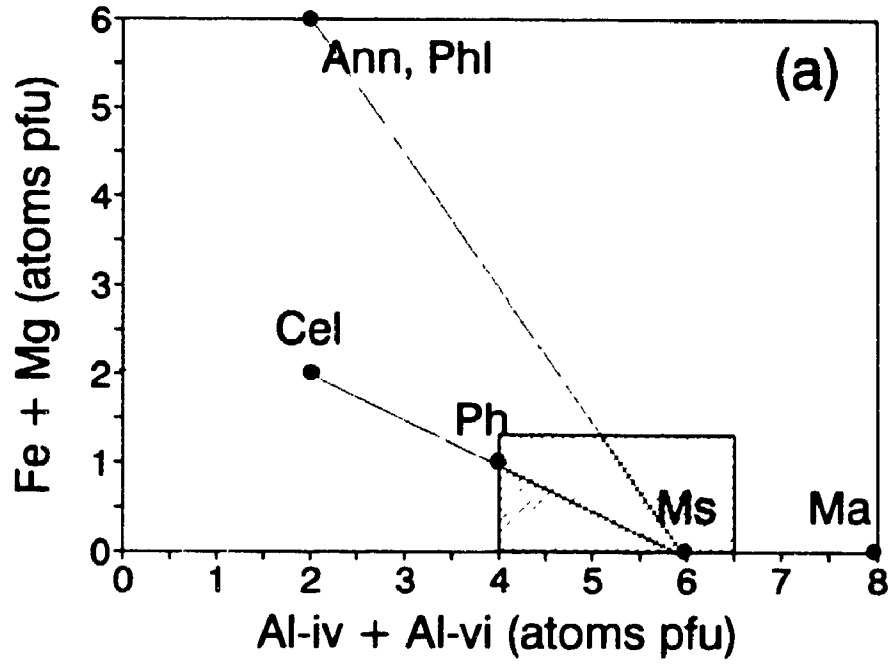




**FIGURE 4-6.** Fe+Mg in muscovite from the zones of aluminosilicate mineral assemblages, as a function of  $Al_{tot}$ . a.) End member compositions; for explanation of abbreviations, see Fig. 3-8. b.) Composition of white micas. Symbols as in Fig. 4-5 and fields as in Fig. 3-8.



ment away from the phengite end member to the muscovite/paragonite end member. Furthermore, the data are between the celadonite-muscovite and biotite-muscovite tie lines indicating considerable solid solution with the trioctahedral micas as well as with phengitic micas. In conjunction with this decrease in Fe+Mg, Fe/(Fe+Mg) increases slightly from the Feldspar Zone to the Kyanite Zone, but there is little covariance with Fe content (Fig. 4-7a).

#### 4.3.4. Biotite.

Biotite is subhedral and lepidoblastic in the Feldspar Zone, and is deflected by coarse feldspar and quartz (Plate 4a and b). Very fine, randomly oriented biotite grains are included in plagioclase porphyroblasts. In the Muscovite Zone (biotite subzone), biotite varies from fine, slightly aligned groundmass grains to coarse, non-oriented (decussate) poikiloblasts, up to 2 mm in size (Plate 5c). In the Kyanite Zone, biotite is restricted to small and unusual concordant layers of staurolite-garnet-bearing rocks, where it is in fractures and is intergrown with, and interstitial to, coarse porphyroblasts of garnet, staurolite, and kyanite.

Considerable variation in biotite composition occurs within and between mineral zones (Fig. 4-8). There is an overall increase of total Al, Mg, and Na with progression from gneiss of the Tumco Formation to the Kyanite Zone, and a decrease in Si, Fe, Mn, K, and Ti. Substitution of F for OH is much greater in biotite than in muscovite, as reflected in

**FIGURE 4-7.** Fe vs. Fe/(Fe+Mg) in a.) muscovite and b.) biotite. Symbols: crosses, quartzofeldspathic gneiss of the Tumco Formation (qT); filled triangles, Feldspar Zone (F); asterisks, Muscovite Zone (M); open squares, Kyanite Zone (K).

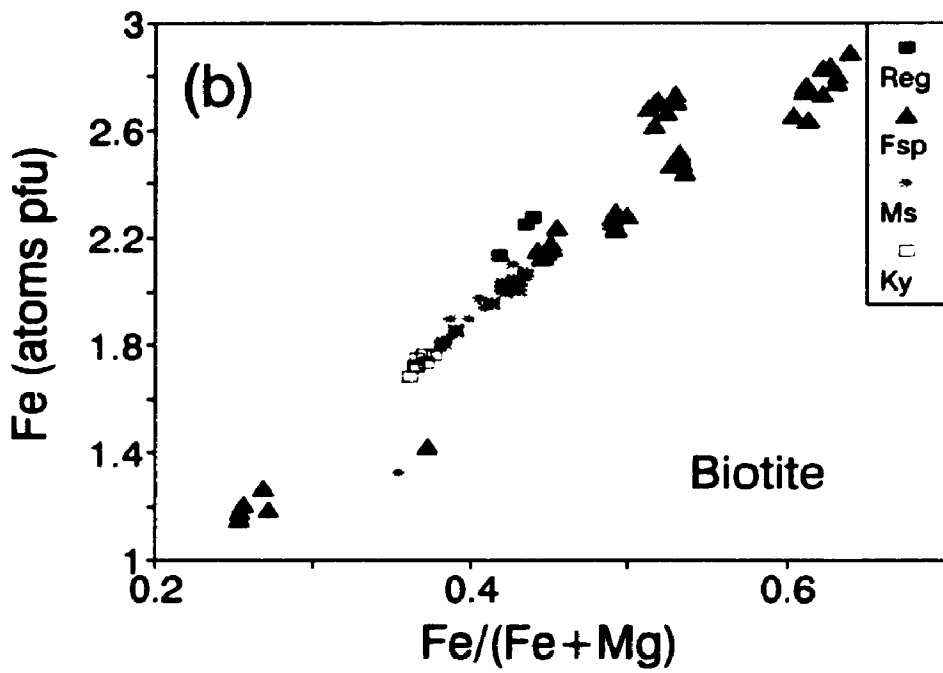
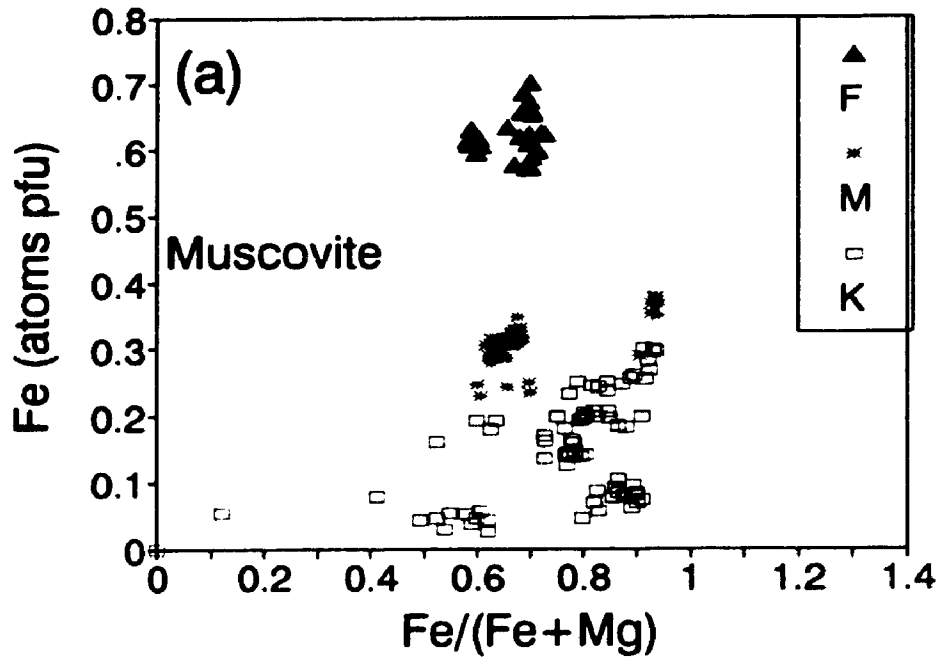
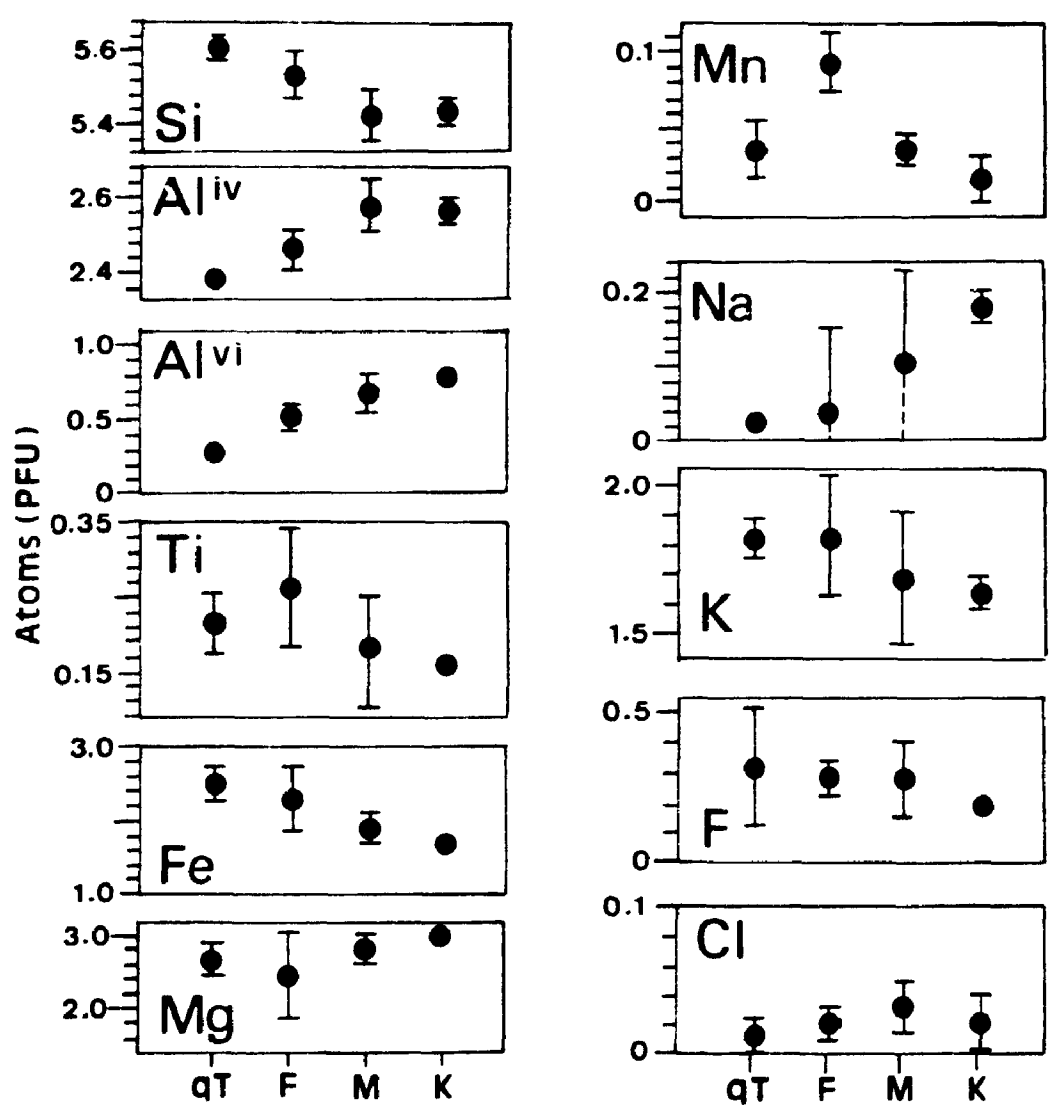


**FIGURE 4-8.** Composition of biotite in the zones of aluminosilicate mineral assemblages. Mineral Zone abbreviations: qT, quartzofeldspathic gneiss of the Tumco Formation; F, Feldspar Zone; M, Muscovite Zone; K, Kyanite Zone.



ZONES OF ALUMINOSILICATE MINERAL ASSEMBLAGES

concentrations of up to 1.65 wt. % F, although there is an overall decrease in F from gneiss of the Tumco Formation into the Kyanite Zone. Mg and Al increase from the gneiss of the Tumco Formation into the Kyanite Zone.

There is an overall decrease in the  $Fe/(Fe+Mg)$  ratios of biotite from the Feldspar Zone to the Kyanite Zone, consistent with the increase in Mg content (Fig. 4-9). Unlike muscovite, in which  $Fe/(Fe+Mg)$  does not vary with Fe content,  $Fe/(Fe+Mg)$  ratios in biotite have a strong correlation with Fe content (Fig. 4-7). Within the Feldspar Zone,  $Fe/(Fe+Mg)$  ratios of biotite are variable, and individual samples have distinct compositional fields (Fig. 4-9). Spatially,  $Fe/(Fe+Mg)$  of biotite decreases regularly from the gneiss of the Tumco Formation into the Kyanite Zone (Fig. 4-10). These characteristics are interpreted to indicate progressive oxidation of biotite, for an increase in the oxidation state of iron leads to the uptake of Fe by magnetite, resulting in a decrease in  $Fe/(Fe+Mg)$  ratios of the remaining biotite (see Chapter 7). In contrast,  $Fe/(Fe+Mg)$  ratios of muscovite increase from the gneiss of the Tumco Formation into the Kyanite Zone (Fig. 4-10). Guidotti (1984) and Baldelli et. al. (1989) suggest that muscovite is sensitive to bulk rock compositional control, and this contrasting behavior of  $Fe/(Fe+Mg)$  in muscovite (Figs. 4-7a and 4-10) is attributed to control by bulk rock compositions.



**FIGURE 4-9.** Fe/(Fe+Mg) vs. Al-vi in biotite from the zones of aluminosilicate mineral assemblages. a.) End-member compositions (see Fig. 3-5 for explanation). b.) Biotite composition. Symbols: crosses, quartzofeldspathic gneiss of the Tumco Formation (qT); filled triangles, Feldspar Zone (F); asterisks, Muscovite Zone (M); open squares, Kyanite Zone (K). Numbers below groups of triangles are samples from the Feldspar Zone (1, B0512-1; 2, B1218-4; 3, B0512-7t; 4, B1218-3; 5, B1219-16; 6, B0512-10); these samples correspond to the groups of triangles plotted immediately above each number. Single triangle located at the bottom of the plot belongs to group 1.

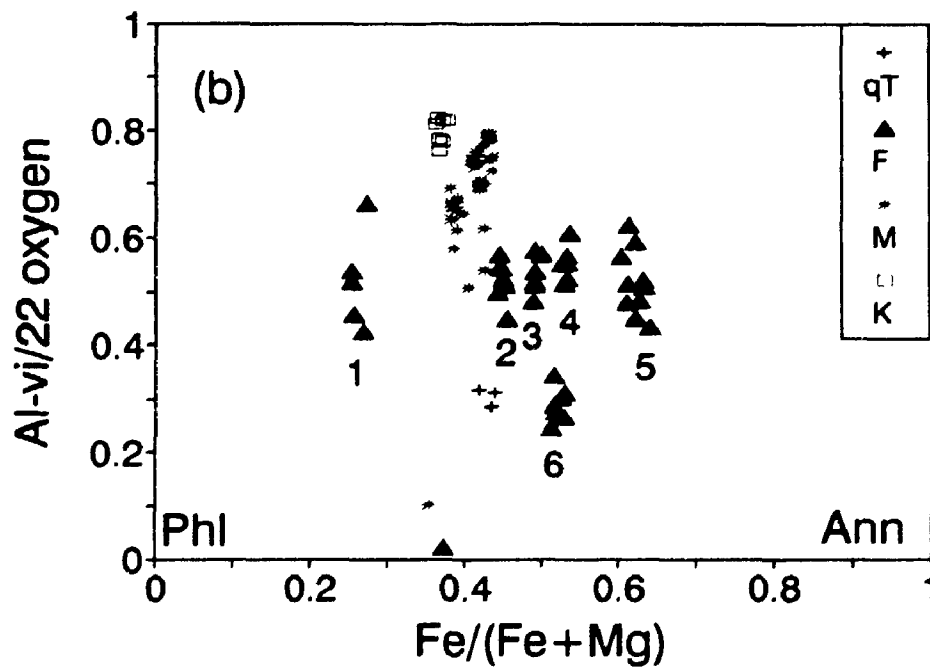
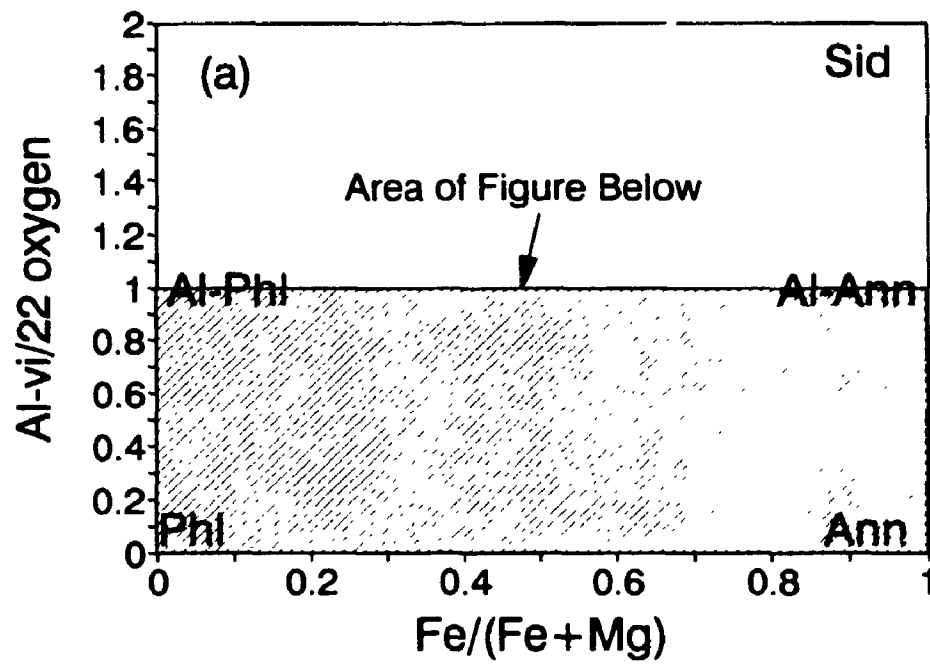
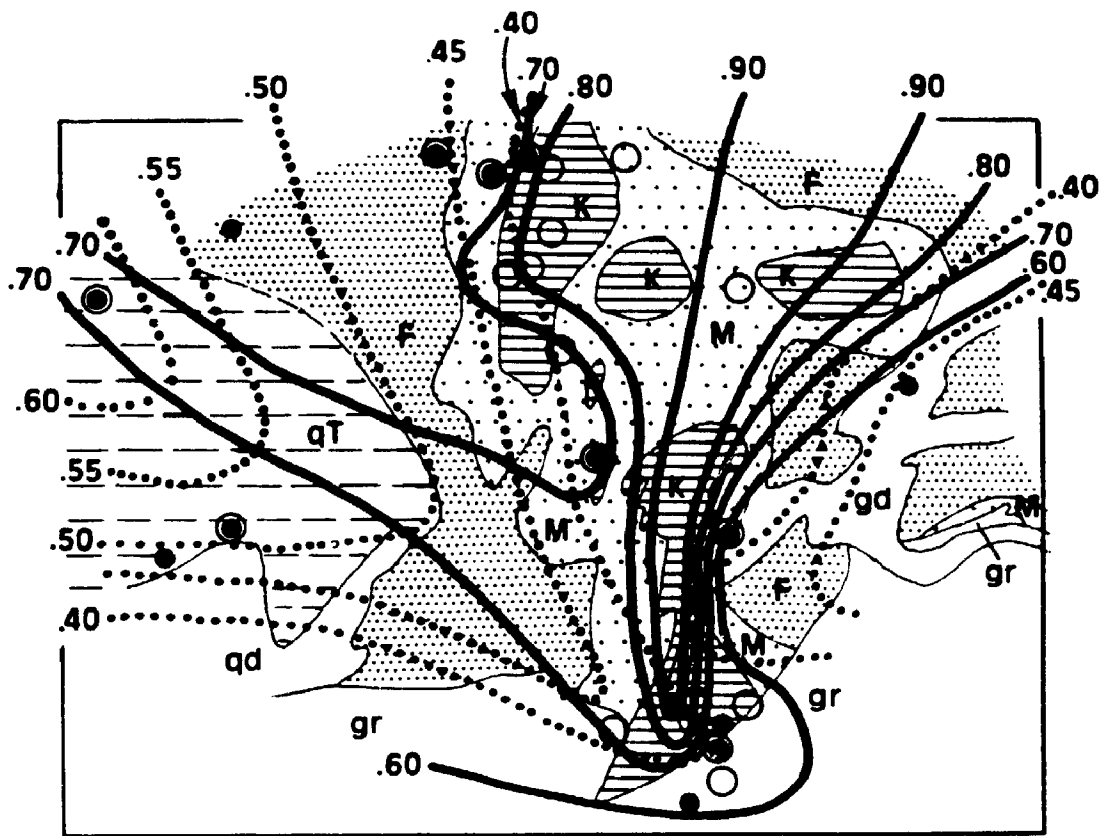


**FIGURE 4-10.** Variation of  $Fe/(Fe+Mg)$  in micas with respect to the zones of aluminosilicate mineral assemblages at Micatale Hill.  $Fe/(Fe+Mg)$  ratio of biotite, dotted contours;  $Fe/(Fe+Mg)$  ratio of muscovite, solid contours. Data points: open circles, muscovite; filled circles, biotite. Lithologic symbols are as in Fig. 3-1. Granite porphyry and Miocene dacite has been omitted for simplicity, and intrusive rocks have been left unpatterned to emphasize the distribution of the aluminosilicate mineral assemblages. Symbols: qd, quartz diorite; gd, hornblende-biotite granodiorite; gr, muscovite-biotite granite. See Fig. 3-1 for location.



Fe/(Fe+Mg) in Muscovite and Biotite, Micatahc Hill

sample location muscovite contour

See Fig. 3-1 for location

#### 4.3.5. Magnetite.

Magnetite in the Feldspar Zone and the biotite subzone of the Muscovite Zone is fine grained, anhedral, and disseminated. Local coarse porphyroblasts, which both deflect and cross cut the foliation, consist of aggregates of fine, recrystallized polygonal grains. In the magnetite subzone, magnetite is coarse grained, up to 5 mm, euhedral, and equant (Plate 5d). Rectangular to rounded aggregates of fine magnetite intergrowths with quartz suggest replacement of earlier biotite porphyroblasts (Plate 7d). In rocks with pronounced crenulation, lath-shaped magnetite is elongate parallel to foliation, suggesting recrystallization during crenulation (Plate 7e).

In the Kyanite Zone magnetite is fine to coarse, anhedral to subhedral, equant porphyroblasts and disseminated rounded granoblasts. These are enclosed by, and intergrown with, kyanite, quartz and tourmaline. Ilmenite lamellae are abundant, and rutile and hematite penetrate magnetite from grain rims. It also occurs in fractures and microfractures, alone or with kyanite and rutile (Plate 7f).

#### 4.3.6. Kyanite.

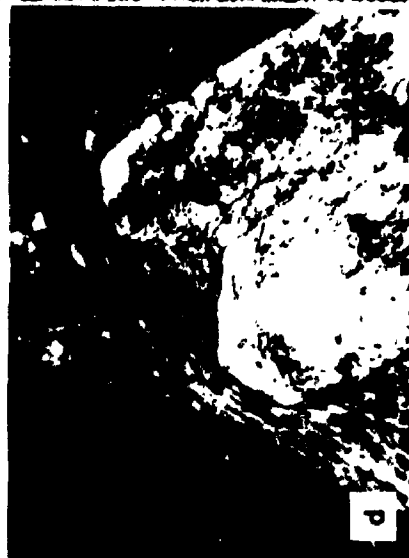
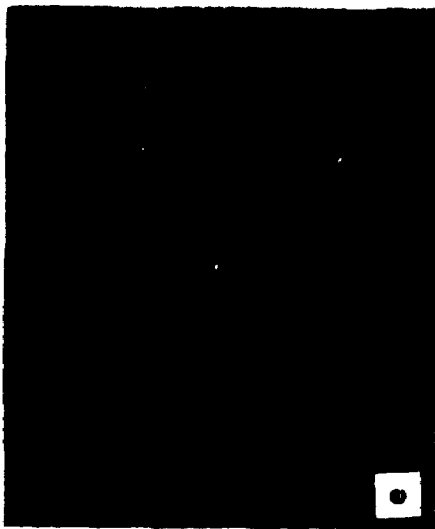
Granoblastic kyanite is anhedral to subhedral, non-oriented poikiloblasts, up to 3 cm long, or as clots of radiating kyanite grains (Plate 6b). With increasing kyanite content, the kyanite is a network of interlocking grains with interstitial quartz. Kyanite is locally skeletal, with

inclusions of fine quartz, magnetite, rutile, and lazulite. Intergrowths with tourmaline, lazulite, apatite and magnetite are common. Core to rim zonation is characterized by both inclusion-rich (sieve) cores surrounded by inclusion-free rims, as well as the reverse. Simple twinning and repetitive twinning occur, and bent and kinked grains indicate pre- to syn-deformation growth (Plate 8a).

In contrast, kyanite porphyroblasts in foliated, muscovite-rich specimens of the Kyanite Zone are euhedral and inclusion-free (Plate 6d). They commonly deflect foliation, but may have pronounced alignment parallel to it. Zonation, where present, is represented by sieve-textured cores and inclusion-free rims (Plate 8b, c, and d). Where foliation is crenulated, zoned kyanite with well developed (100) faces contain ragged (001) ends, cutting across growth zones, which suggests either brittle behavior, in the form of breaking, or dissolution, during crenulation. However, growth during this deformation is indicated by inclusion-free overgrowths on the ragged ends of some grains (Plate 8c). This is supported by the occurrence of inclusion trails which have a regular angular variation with respect to the grain edge (Plate 8d). Fractures in kyanite containing intergrowths of quartz and muscovite, which are oriented parallel and perpendicular to the foliation indicate foliation-parallel extension of kyanite porphyroblasts and movement of ions during this event.

**PLATE 8.** Textural relationships of kyanite and tourmaline.

a.) Photomicrograph of granoblastic Kyanite Zone, with bent, euhedral kyanite grain in groundmass of coarse, inclusion-free quartz. Scale bar equals 0.1 mm. b.) Photomicrograph of zoned, broken kyanite grain from crenulated, mylonitic Kyanite Zone. Note zoning on euhedral grain boundaries. Scale bar equals 0.2 mm. c.) Photomicrograph, plane light, of zoned kyanite with ragged terminations in crenulated Kyanite Zone. Note inclusion free growth zones on euhedral faces as well as on ragged ends. Scale bar equals 1 mm. d.) Photomicrograph of zoned, euhedral kyanite porphyroblast in crenulated Kyanite Zone. Note angular variation of inclusion trails (marked by white lines) with respect to grain boundary.  $S_2$  deflected around porphyroblasts. Scale bar equals 0.5 mm. e.) Photomicrograph of repetetively zoned tourmaline in the Muscovite Zone. Plane light. Scale bar equals 0.5 mm. f.) Photomicrograph of tourmaline in the Muscovite Zone, plane light. Tourmaline is aligned in the plane of  $S_2$ . Scale bar equals 1 mm.





#### 4.3.7. Tourmaline and Apatite.

Tourmaline and apatite have similar habits to one another and to kyanite. Of the two, tourmaline is more widespread, and occurs in greater local abundance. Both are rare in the Feldspar Zone, but common in the Muscovite and Kyanite Zones, although usually less than 2-3%. Where muscovite content is large, they are fine to very coarse, euhedral prisms, up to 1.5 cm long, oriented parallel or sub-parallel to the plane of foliation (Plate 8f), and parallel to the axis of crenulations. By contrast, they are coarse, anhedral, and sieve textured where muscovite is minor or absent. Zoning in tourmaline occurs in two ways: 1.) simple, with sieve textured cores surrounded by inclusion-free rims in a granoblastic texture and 2.) simple and repetitive optical and compositional zonation in foliated texture (Plate 8e). The former are typically coarse, anhedral grains, whereas the latter are fine to coarse, euhedral prisms.

Tourmaline at Micatalec and Hedges is in the schorl-dravite-uvite solid solution series (Fig. 4-11). The Ca content is low in these tourmalines, typically less than 0.06 atoms per formula unit (Fig. 4-12). Optically zoned grains are also compositionally zoned (Figs. 4-11b,c and 4-12). The dominant substitutional scheme is  $\text{FeMg}_1$ , where dravite-rich cores evolve to schorl-rich rims. However, core to rim zonation in individual grains is variable, with a general increase in  $\Sigma\text{Al}$ , Ti, Fe, Ca, and F, and a decrease in Si, Na, and Mg. Reversals in composition from core to rim are common, giving rise

**FIGURE 4-11.** Tourmaline compositions plotted on a molecular Al-Fe-Mg diagram after Henry and Guidotti (1985). Compositional fields are: 1.) Li-rich granitoid pegmatites and aplites, 2.) Li-poor granitoids and their associated pegmatites and aplites, 3.) Ferric iron-rich quartz tourmaline rocks (altered granites), 4.) Metapelites and metapsammities coexisting with an Al-saturating phase, 5.) Metapelites and metapsammities not co-existing with an aluminum saturating phase, 6.) Ferric iron-rich quartz-tourmaline rocks, calc-silicate rocks and metapelites, 7.) Low-Ca metaultramafics and Cr,V-rich metasediments, 8.) metacarbonates and metapyroxenites.

**A.)** Tourmaline compositions from the Muscovite and Kyanite Zones at Micatalc Hill and Hedges. **B.)** Core to rim variation, sample MT4, Muscovite Zone, Micatalc Hill. **C.)** Core to rim variation in tourmalines from the Muscovite and Kyanite Zones at Hedges and Micatalc Hill.

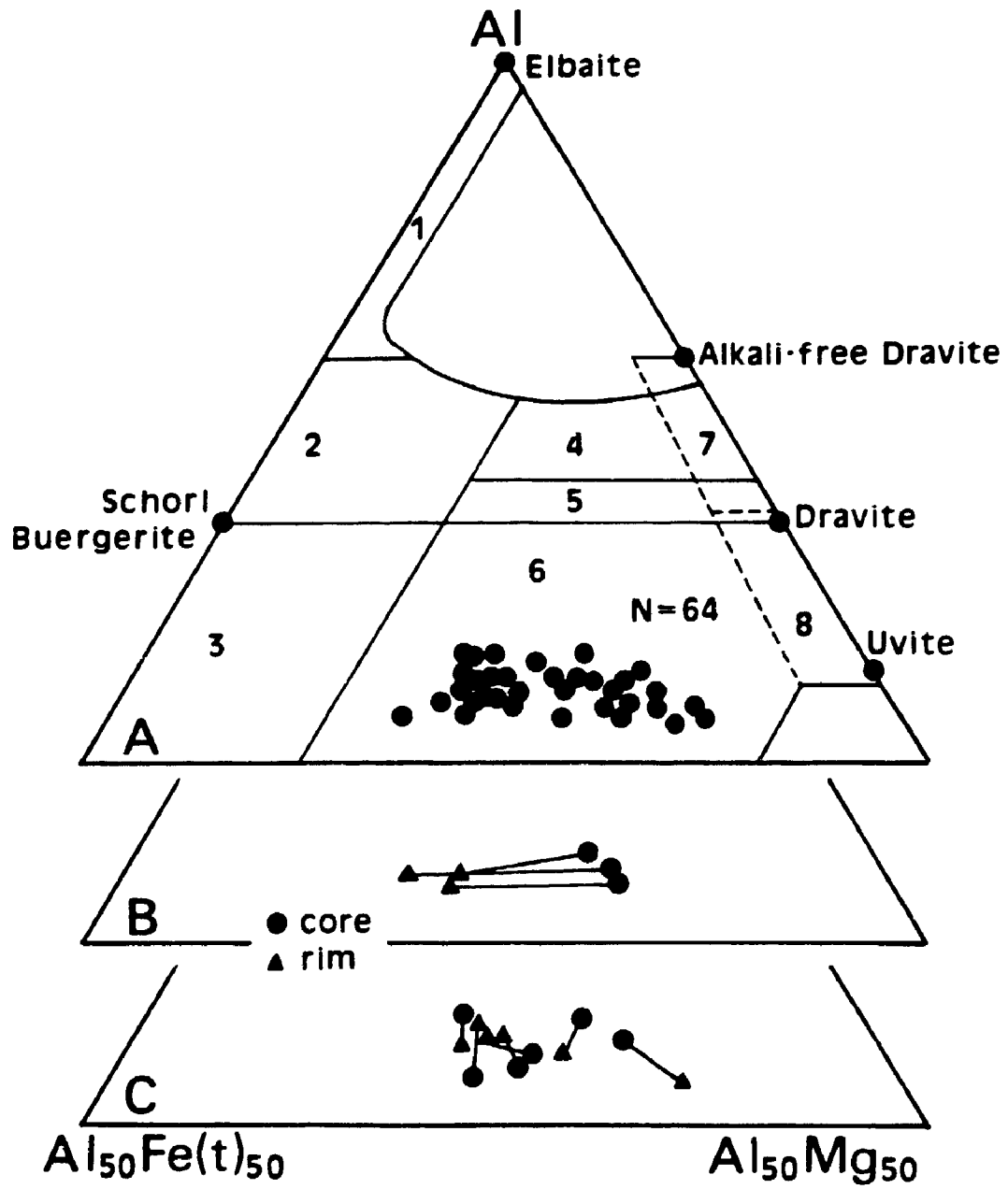
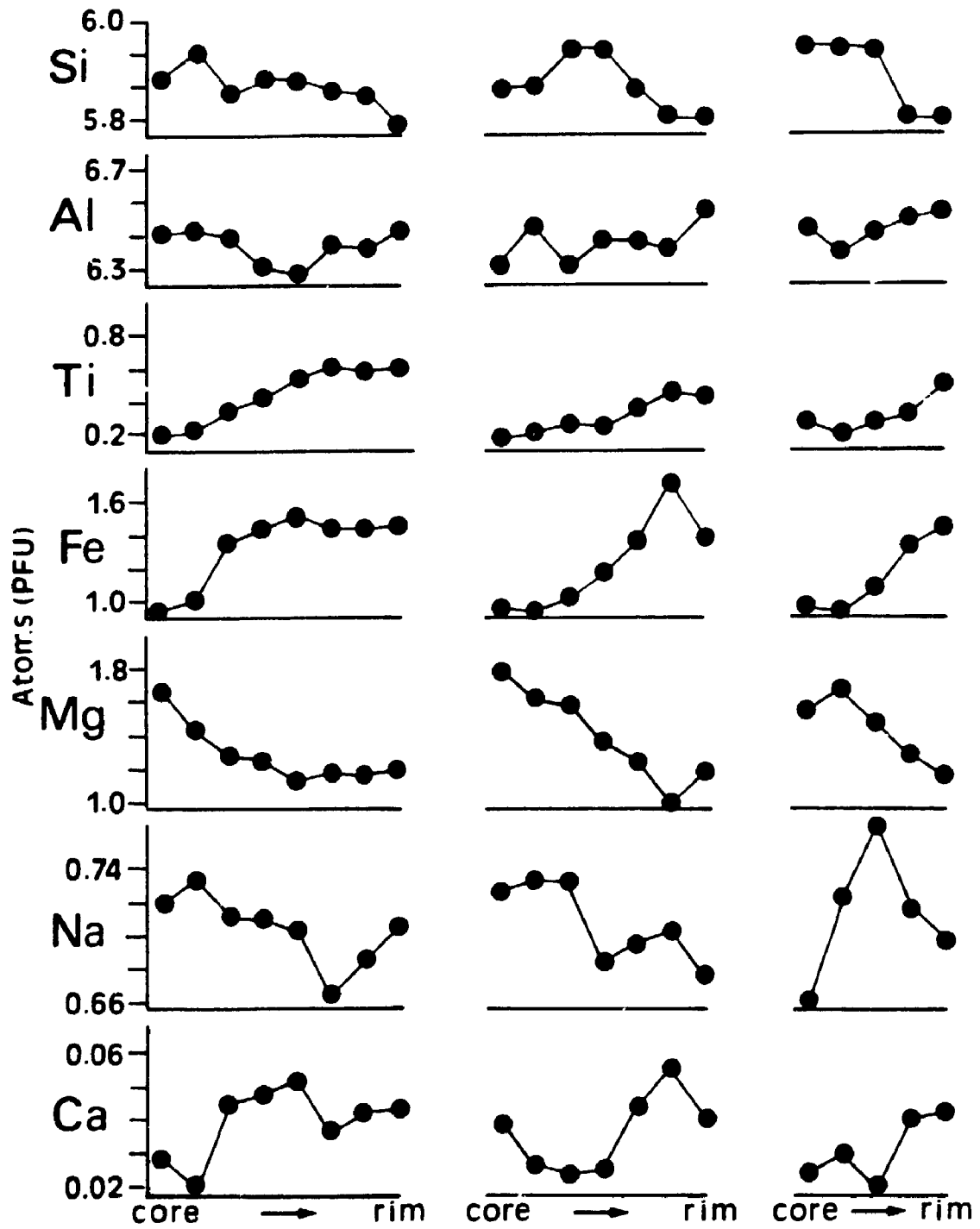


**FIGURE 4-12.** Variation in composition from core to rim in three tourmaline grains from sample MT4, Micatahc Hill.



to the repetitive zonation visible in backscatter images. Such complex zoning is only seen in tourmalines from the foliated portions of the Muscovite and Kyanite Zones.

Tourmaline compositions plotted on molecular Al-Fe(tot)-Mg and Ca-Fe(tot)-Mg ternary diagrams such as Fig. 4-11 allow assessment of the solid solution scheme. The diagram is useful because there is no reliance on a particular method of normalizing structural formula (Henry and Guidotti, 1985). In addition, these cations cover the common substitutions found in natural tourmalines, and inferences can be made about cations not determined by microprobe analyses. A tourmaline which plots in field 1 on Fig. 4-11, for instance, can be assumed to contain significant amounts of Li due to its charge coupling with Al. Similarly, tourmaline compositions which lie below the schorl-dravite line can be inferred to contain significant Fe<sup>3+</sup> if the uvite component is small. The tourmalines from the Micatalec and Hedges areas all plot below this line, and contain less than 0.06 atoms pfu Ca, indicating low uvite contents. This suggests relatively large Fe<sup>1+</sup> abundances in tourmaline, which is consistent with the oxide mineralogy of magnetite and rutile. It is also consistent with the variation in biotite composition, which suggests progressive oxidation from the gneisses of the Tumco Formation into the Kyanite Zone (section 4.3.4).

#### 4.3.8. Garnet.

Garnet occurs in all the zones of aluminosilicate mineral

assemblages, but is uncommon. In both the Feldspar and Muscovite Zones, it is fine grained, subhedral to euhedral, locally poikiloblastic. Relationships to foliation are obscure in most instances, although locally garnet grains deflect, and are cross cut by, the foliation. In the Kyanite Zone, it is restricted to staurolite-bearing rocks, where it is very coarse grained, up to 1 cm.

Fine grained garnet in the Feldspar and Muscovite Zones is unzoned to slightly zoned, whereas the coarse grains in the Kyanite Zone contain a pronounced compositional zonation. Within the almandine-spessartine-pyrope-grossular solid solution series, garnet from the Muscovite Zone is from  $\text{Alm}_{50}\text{-Sps}_{30}\text{Prp}_{11}\text{Grs}_9$  to  $\text{Alm}_{46}\text{Sps}_{38}\text{Prp}_8\text{Grs}_7$  (Fig. 4-13). There is a small core-to-rim decrease in the Ca content, and a small increase in the Mn content (Fig. 4-14). In contrast, the coarse grained garnets from the Kyanite Zone, which overlap compositionally those of the Muscovite Zone, have considerable core to rim zonation in the X-site cations. Fe and Mg increase, and Mn and Ca decrease, from core to rim. Such zonation has been interpreted as normal prograde metamorphic conditions (Tracy, et. al., 1976), where metamorphic reactions progressively liberate Mn. As Mn is preferentially taken up in the early growth of the garnet, it is progressively depleted from the area of growth, resulting in Mn-poor, (Fe+Mg)-rich, rims.

#### 4.3.9. Rutile.

Rutile is minor, but widespread, in the Kyanite Zone, and

**FIGURE 4-13.** Composition of garnet in the zones of aluminosilicate mineral assemblages and hornblende-biotite granodiorite. Diagonal line pattern represents the field of garnet compositions from the Muscovite Zone (M) and Kyanite Zone (K); filled triangles are core to rim zoning in garnet (direction of arrow) from the Kyanite Zone. Gd, undivided granodiorite; Gdm, medial granodiorite; Gdp, proximal granodiorite adjacent to muscovite-biotite granite.



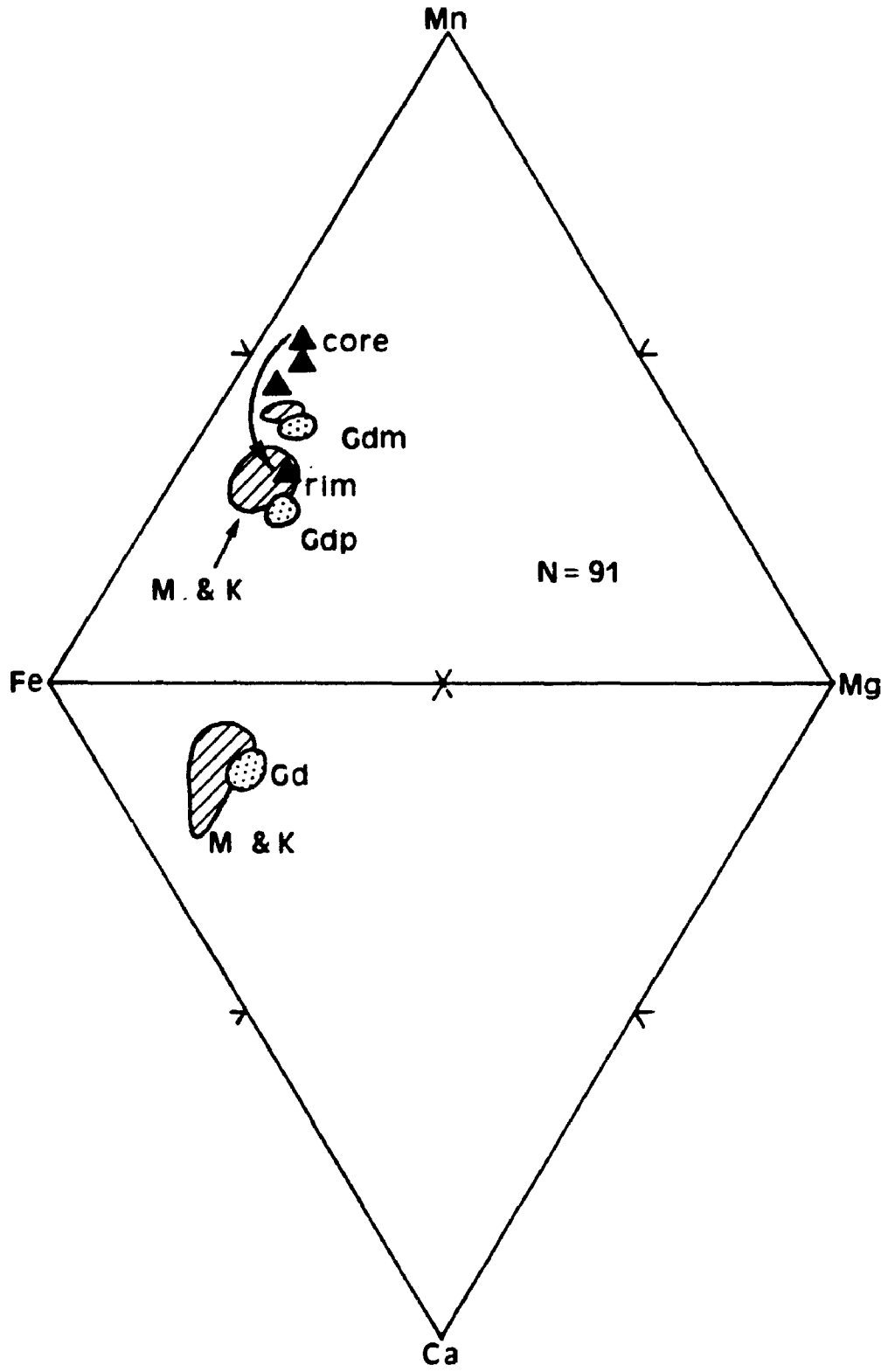
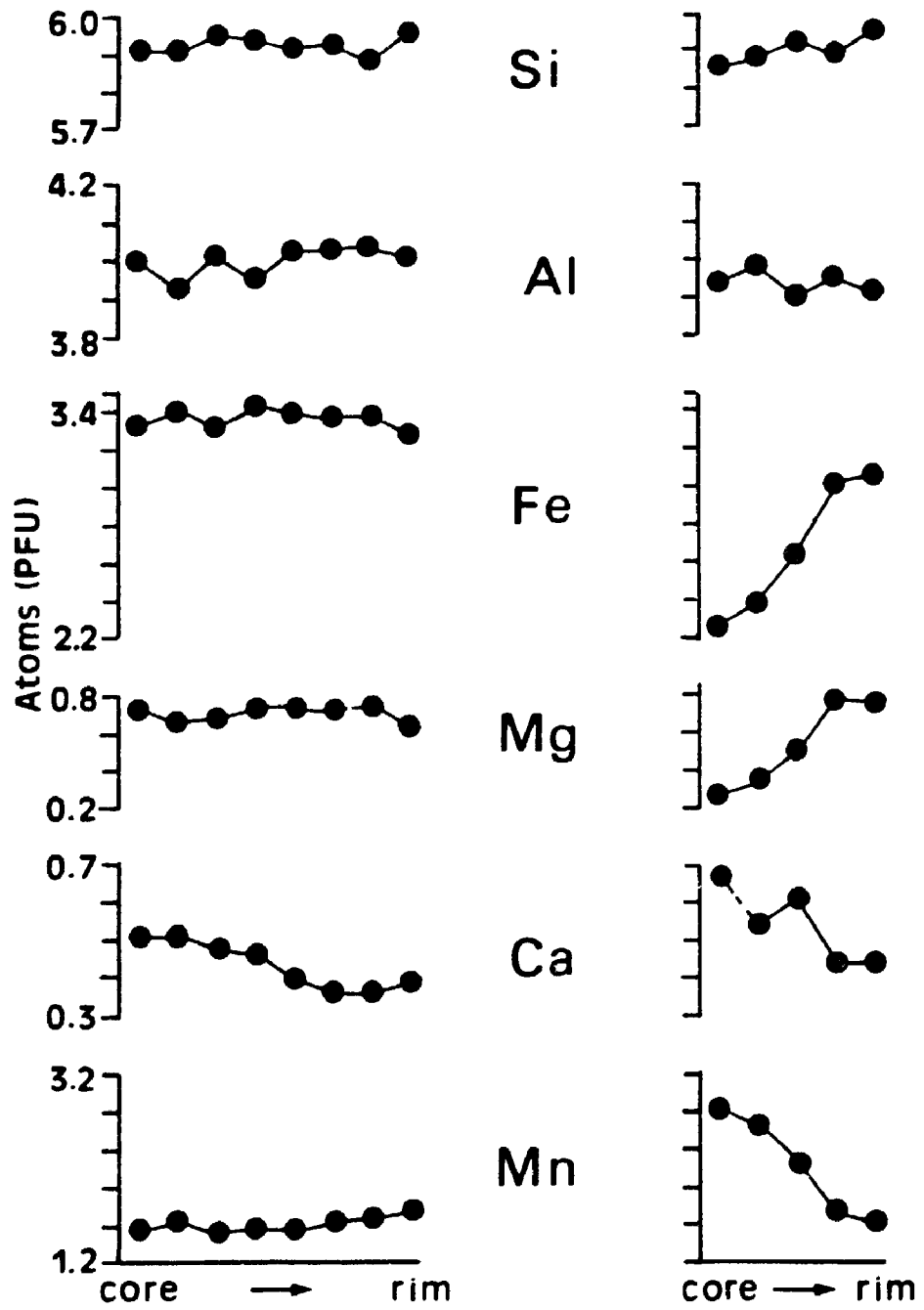


**FIGURE 4-14.** Variation in composition from core to rim in garnet from the Muscovite and Kyanite Zones. Left diagram is sample B0430-4, Muscovite Zone. Right diagram is sample B0430-3, granoblastic staurolite-biotite-garnet-kyanite-quartz-muscovite-chlorite from the Kyanite Zone.



is rare in the Muscovite Zone. It occurs along fractures, as fine disseminated grains or in shotgun-like clots. The latter commonly have a square outline, suggesting replacement of magnetite. This is consistent with reflected light petrography and electron backscatter images, in which rutile penetrates magnetite grains from the rim.

#### **4.3.10. Trace Minerals.**

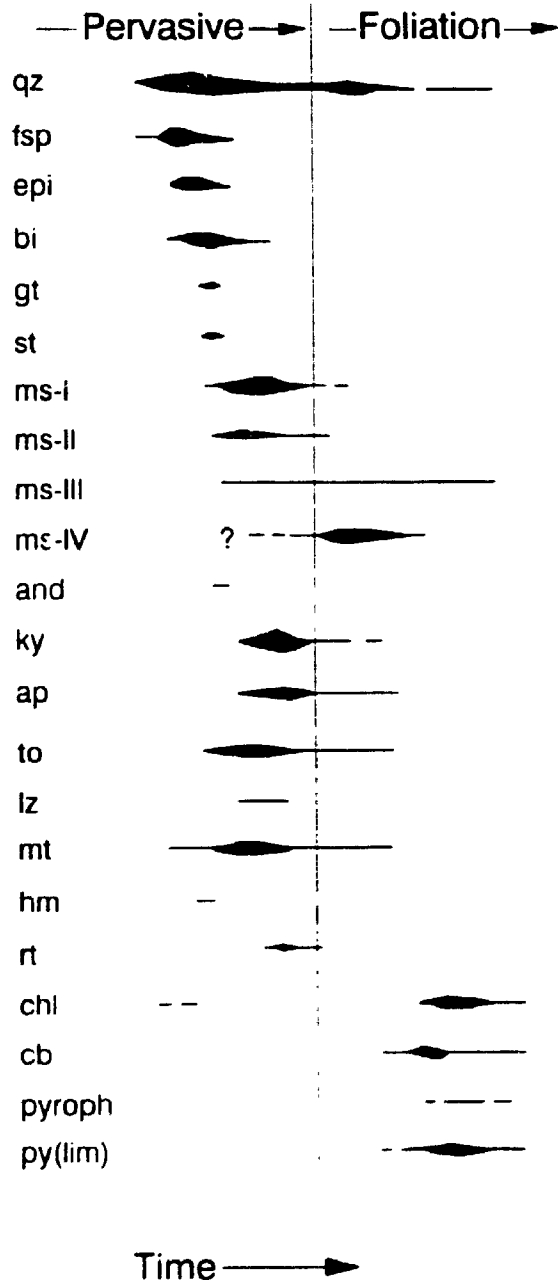
Limonite pseudomorphs of pyrite are disseminated throughout rocks of the Kyanite and Muscovite Zones, but are mostly concentrated within late fractures with chlorite and carbonate minerals. Disseminated grains and fractures cross-cut foliation, and rectangular grains are elongate parallel to the crenulated foliation. Gypsum is also in these fractures in surface exposure where there is an abundance of limonite, and like the limonite is probably a product of weathering.

Lazulite is in the Kyanite Zone, but is rare. It is anhedral, fine to coarse grained, with blue to purple pleochroism, and intergrown with kyanite. Lamellar and sector twinning are well developed. It is locally replaced by muscovite, pyrophyllite, and a fine grained, red opaque mineral, probably hematite. Lazulite also occurs in round fluid inclusions within quartz and kyanite, some of which are necked.

#### **4.4. Mineral Paragenesis.**

The general sequence of mineral growth (Fig. 4-15) is

**FIGURE 4-15.** Paragenetic sequence of minerals in the zones of aluminosilicate mineral assemblages: pervasive replacement and foliation-hosted replacement. Mineral abbreviations: qz, quartz; fsp, plagioclase feldspar; epi, epidote; bi, biotite; gt, garnet; st, staurolite; ms-I, Type 1 muscovite; ms-II, Type 2 muscovite; ms-III, Type 3 muscovite; ms-IV, Type 4 muscovite; and, andalusite; ky, kyanite; ap, apatite; to, tourmaline; lz, lazulite; mt, magnetite; hm, hematite; rt, rutile; chl, chlorite; cb, carbonate minerals; pyroph, pyrophyllite; py(lim), limonite after pyrite.



based on the textural relationships, summarized in the following. In the Feldspar Zone, the main minerals are plagioclase, biotite, epidote and quartz. Anhedral plagioclase poikiloblasts deflect the foliation as defined by biotite in the Feldspar Zone. Plagioclase is replaced by epidote and, in the Feldspar Zone adjacent to the Muscovite Zone, by muscovite (Types 2 and 4). Quartz-epidote veinlets, with crack-seal fabrics, contain recrystallized quartz, and cross cut earlier folded veinlets of epidote. Growth of coarse plagioclase poikiloblasts therefore at least in part predates growth or recrystallization of biotite, epidote and muscovite.

In the Muscovite Zone, the main minerals are quartz, muscovite, biotite, and magnetite, with large local abundances of tourmaline. Plagioclase is minor, as unstrained polygonal groundmass grains intergrown with muscovite. Decussate biotite is cross cut by, or deflects, foliation defined by Type 4 muscovite, and is therefore earlier than Type 4 muscovite. The relationship of biotite to Type 1 muscovite is not as clear, and biotite at oblique angles to this lepidoblastic muscovite may be earlier or later. Rectangular aggregates of magnetite-quartz intergrowths in the Muscovite Zone suggest replacement of biotite, and coarser porphyroblasts of magnetite deflect aligned muscovite (Types 1 and 4). Thus, biotite growth was followed by magnetite growth, and muscovite at least in part post-dates these minerals.

The main minerals of the Kyanite Zone are quartz and

kyanite, but magnetite, rutile, tourmaline, apatite and muscovite are ubiquitous. Minor, local relict plagioclase is extensively replaced by muscovite, kyanite and tourmaline. Magnetite occurs with kyanite and rutile in fractures, and is intergrown with these minerals in the groundmass. In addition, rutile penetrates magnetite along grain rims. In muscovite-rich portions of the Kyanite Zone, kyanite, tourmaline and apatite are euhedral, relatively inclusion-free, whereas in muscovite-poor portions they are sieve-textured, locally skeletal. Such contrasting habits between these grains in muscovite-rich and muscovite-poor parts of the Kyanite Zone indicate a compositional control on the habit of these minerals. Kyanite, tourmaline and apatite replace Type 1 muscovite, and deflect, or are cross cut by, Type 4 muscovite. Kyanite is also replaced by Type 3 muscovite. Relationships are thus complex between kyanite, tourmaline, apatite and muscovite, and indicate much overlapping growth, with kyanite, tourmaline and apatite replacing early muscovite (Type 1), which is in turn followed by growth of Types 3 and 4 muscovite.

In the Muscovite and Kyanite Zones, fracture-fillings of muscovite, with or without pyrite, magnetite, and tourmaline, cross cut all minerals in these zones, and are most common in the most foliated portions of those zones. These fracture fillings are locally aligned parallel to the foliation and crenulation. Chlorite, pyrite and carbonate occur in discordant fracture fillings, and chalcedony locally occurs in the



centers of these fractures.

The general sequence of mineral growth is therefore an early feldspar (plagioclase and K-feldspar)-biotite-epidote assemblage, followed by a muscovite-biotite-magnetite assemblage, which is in turn followed by a kyanite-magnetite-rutile assemblage, all with quartz. This mineral growth was dispersed and pervasive, and was followed by mineral growth along foliation, crenulation and fractures. The growth of Type 4 muscovite in S-C fabrics and crenulations, and Type 3 muscovite, with magnetite and tourmaline, in fractures, succeeded growth of Type 1 muscovite, marking the change from pervasive replacement to foliation and fracture controlled recrystallization, which culminated with development of a mylonitic fabric. In foliated rocks, overgrowths of inclusion-free kyanite on inclusion-rich kyanite, and inclusion trails in rotated kyanite grains, indicate replacement continued during development of the mylonitic foliation. Finally, chlorite, pyrite, and carbonate minerals formed along fractures, post-dating the pervasive and foliation replacement assemblages.

#### 4.5. Summary.

Shallow-dipping, tabular zones of aluminosilicate mineral assemblages in the Cargo Muchacho Mountains are along strike with known gold concentrations. From structural bottom to top, mineral assemblage zonation is quartz-feldspar-biotite-magnetite-epidote, quartz-muscovite-biotite-magnetite, and quartz-kyanite-magnetite-rutile, designated the Feldspar Zone,

the Muscovite Zone, and the Kyanite Zone, respectively. The Feldspar Zone grades down into quartzofeldspathic gneiss of the Tumco Formation.

There is variation in fabric and mineral habit and composition from the gneiss of the Tumco Formation into the Kyanite Zone of the aluminosilicate mineral assemblages. The Tumco Formation is fine grained and gneissic. The Feldspar Zone is also gneissic, but contains coarse poikiloblasts of plagioclase and, locally, microcline. In addition, there is more biotite and epidote in the Feldspar Zone than in the gneiss of the Tumco Formation. The Muscovite Zone is schistose to mylonitic and crenulated, with coarse porphyroblasts of biotite, magnetite, tourmaline and apatite in a very fine grained groundmass of quartz and muscovite. The Kyanite Zone is coarse grained and granoblastic.

The coarse grain size of the minerals in the Kyanite Zone of aluminosilicate mineral assemblages, in conjunction with decussate and poikiloblastic textures in all zones, are characteristic of static growth (Spry, 1969). Such textures are dispersed and pervasive in the zones of aluminosilicate mineral assemblages, and overprint of these textures by mylonitic and crenulation fabrics indicate a relatively early development of this pervasive replacement. Textures such as overgrowths of clear kyanite on broken, inclusion-rich kyanite in foliated and crenulated portions of the Kyanite Zone indicate the replacement process continued during the development of mylonitic and crenulated fabrics. Thus, early

pervasive replacement evolved into later foliation controlled replacement and recrystallization.

Mineral compositions vary across the vertical zonation of the aluminosilicate mineral assemblages. The aluminum content of feldspar, muscovite and biotite increases from the gneiss of the Tumco Formation into the Kyanite Zone. In plagioclase, the coupled substitution of  $\text{CaAlNa}_1\text{Si}_1$ , results in an increase in the Ca content from albite/oligoclase in the Tumco Formation to andesine in the Kyanite Zone.

Muscovite varies from phengitic muscovite in the Feldspar Zone to paragonitic muscovite in the Kyanite Zone, with an increase in Na and  $\text{Fe}/(\text{Fe}+\text{Mg})$  ratios, and a decrease in Si, Ti, Fe, Mg, Mn, and K. There appears, however, to be no variation in composition among muscovite with different habits. Thus Type 3 and Type 4 muscovite have compositions similar to one another in the Kyanite Zone, but are distinct from Type 3 and Type 4 of the Muscovite Zone. Such relationships show that, despite the temporal differences between muscovite habit, composition of muscovite varies as a function of mineral assemblage.

In addition to an increase in  $\text{Al}_{\text{tot}}$ , biotite has an increase in Na and Mg, and a decrease in Si, Fe, Mn, K, Ti, and  $\text{Fe}/(\text{Fe}+\text{Mg})$  ratios from the gneiss of the Tumco Formation into the Kyanite Zone. The decrease in  $\text{Fe}/(\text{Fe}+\text{Mg})$  ratios suggests progressive oxidation of iron from the gneiss of the Tumco Formation into the Kyanite Zone, and is consistent with an increase in the abundance of Fe-Ti oxides as the main Fe-

bearing minerals.

Individual grains of tourmaline and garnet have systematic increase in Fe from core to rim. In garnet, there is also a core to rim decrease in Mn and Ca, and an increase in Mg and Si. In contrast, tourmaline grains have variable core to rim zonation, but there is essentially a decrease in Mg and Si, and an increase in Al, Ti, and Ca. As suggested by Henry and Guidotti (1985), low uvite contents in tourmaline may indicate relatively high ferric iron content.

The widespread occurrence of quartz, epidote, muscovite, kyanite, magnetite, rutile, tourmaline and apatite in veins and fractures, and the presence of fluid inclusions in quartz and kyanite, among others, some of which contain lazulite, are evidence for the presence of fluids during pervasive replacement. Zonation from feldspar-bearing mineral assemblages (Feldspar Zone) to muscovite-bearing assemblages (Muscovite Zone) and kyanite-bearing assemblages (Kyanite Zone) are similar to the results of experiments which show that progressive removal of cations via  $H^+$ -ion metasomatism may form such assemblage variations (Hemley, 1959; Hemley and Jones, 1964; Shade, 1974; Hemley et. al., 1980), and further point to the role of fluids in the formation of these mineral assemblages.

The timing of the formation of aluminosilicate assemblages relative to intrusive rocks is constrained on the older side by the quartz diorite and granite porphyry, which contain aluminosilicate mineral assemblages where they are within the

mineral zones. Hence, development of the aluminosilicate mineral assemblages by pervasive replacement post-dates the intrusion of these rocks. In contrast, muscovite-biotite granite and hornblende granodiorite cross cut the zones of aluminosilicate mineral assemblages and do not contain minerals of the aluminosilicate assemblages, except where they are schistose to mylonitic. Thus, pervasive replacement preceded emplacement of hornblende-biotite granodiorite and muscovite-biotite granite, but foliation and fracture controlled replacement and recrystallization continued during and, perhaps, after their emplacement. Similarly, Jurassic pegmatite and Miocene dacite cross cut the zones, and retain their primary mineralogy.

## CHAPTER FIVE -- STRUCTURE.

### 5.1. General Statement.

All pre-Tertiary rocks contain a south-dipping foliation, striking  $90^{\circ}$  to  $135^{\circ}$ . This foliation is regional in extent, defined essentially by parallelism of biotite. The most common mineral assemblage in the quartzofeldspathic gneiss of the Tumco Formation is quartz-oligoclase-microcline-biotite-epidote-magnetite, consistent with regional metamorphism to epidote-amphibolite facies. Contacts between rock types are generally concordant to the foliation, although locally they may be discordant. Pegmatite dikes are discordant to the foliation, and have folds for which this foliation is axial planar.

Superimposed on this regional foliation are narrow zones, less than 1 m wide to 3 m wide, with S-C and schistose fabrics. These fabrics, in conjunction with the fine grain size, suggests these are mylonitic in origin. These zones are sub-parallel to the regional foliation, striking roughly due east and dipping  $27^{\circ}$  south (Figs. 2-2 and 3-1). High angle North to Northwest striking faults offset all rock types (Dillon, 1976). They contain clay fault gouge and breccia indicative of relatively shallow, brittle conditions. These are covered in the study area, and their location is inferred from contact relationships and from mapping by Dillon (1976).

The focus here is the relationship of fabric and hence deformation to the zones of aluminosilicate mineral assemblages. The rocks are grouped according to their fabric and

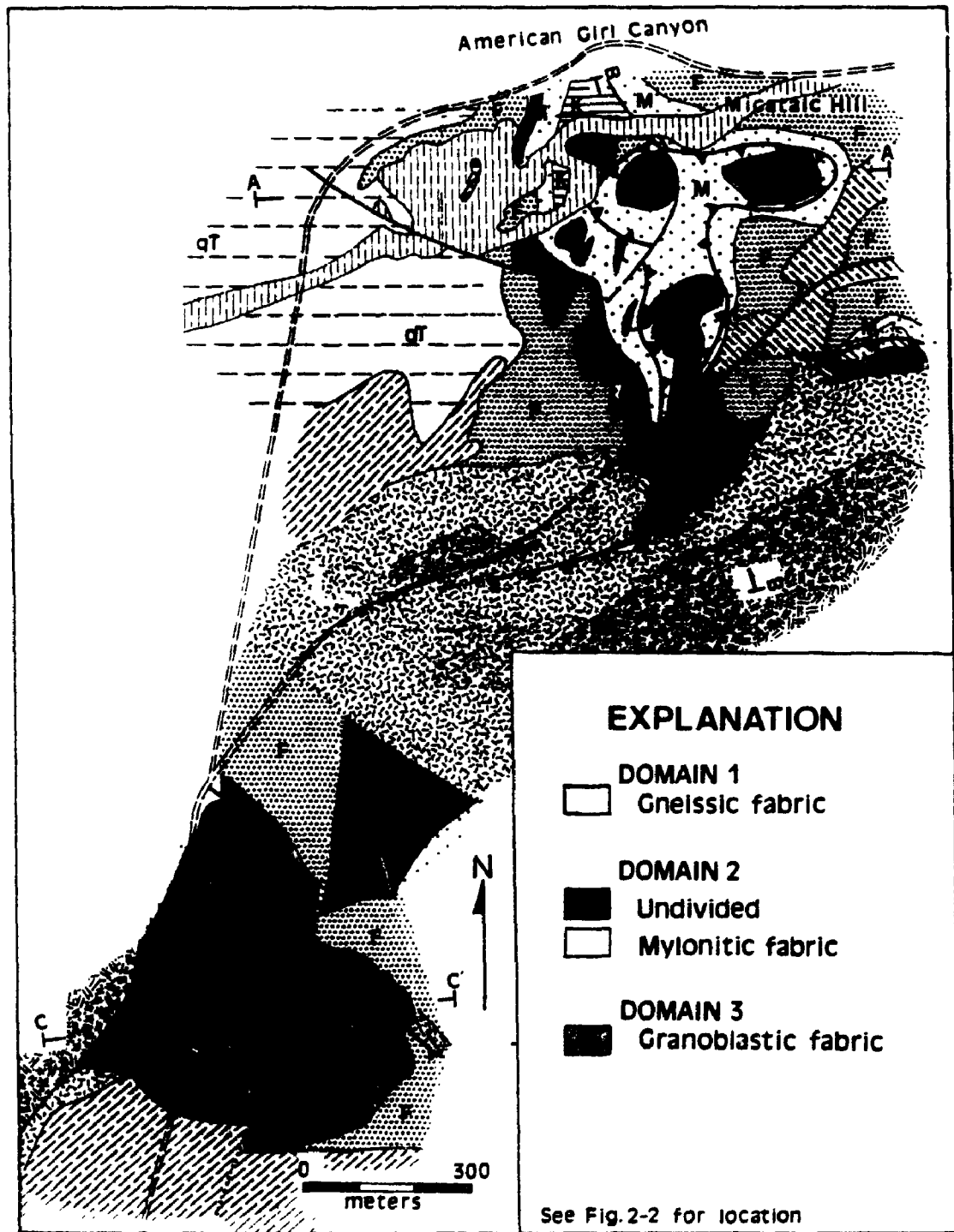
mineralogy, and the events producing these fabrics are evaluated. Standard terminology from Turner and Weiss (1963) is used to distinguish the fabric-generating events. The capital letter M denotes regional metamorphism, D denotes deformation, and planar fabrics, linear features and folds are denoted S, L, and F, respectively. Subscripts attached to these designations represent the relative timing: the greater the number, the later the feature. In this scheme,  $S_0$  represents bedding, and subsequent planar features, such as gneissic banding or schistosity are designated  $S_1$ ,  $S_2$ , etc. There is considerable temporal overlap of the events producing the fabrics; therefore, these designations reflect distinct styles of deformation as much as temporal relationships.

### **5.2. Domainal Analysis: Fabric Characteristics and Orientation.**

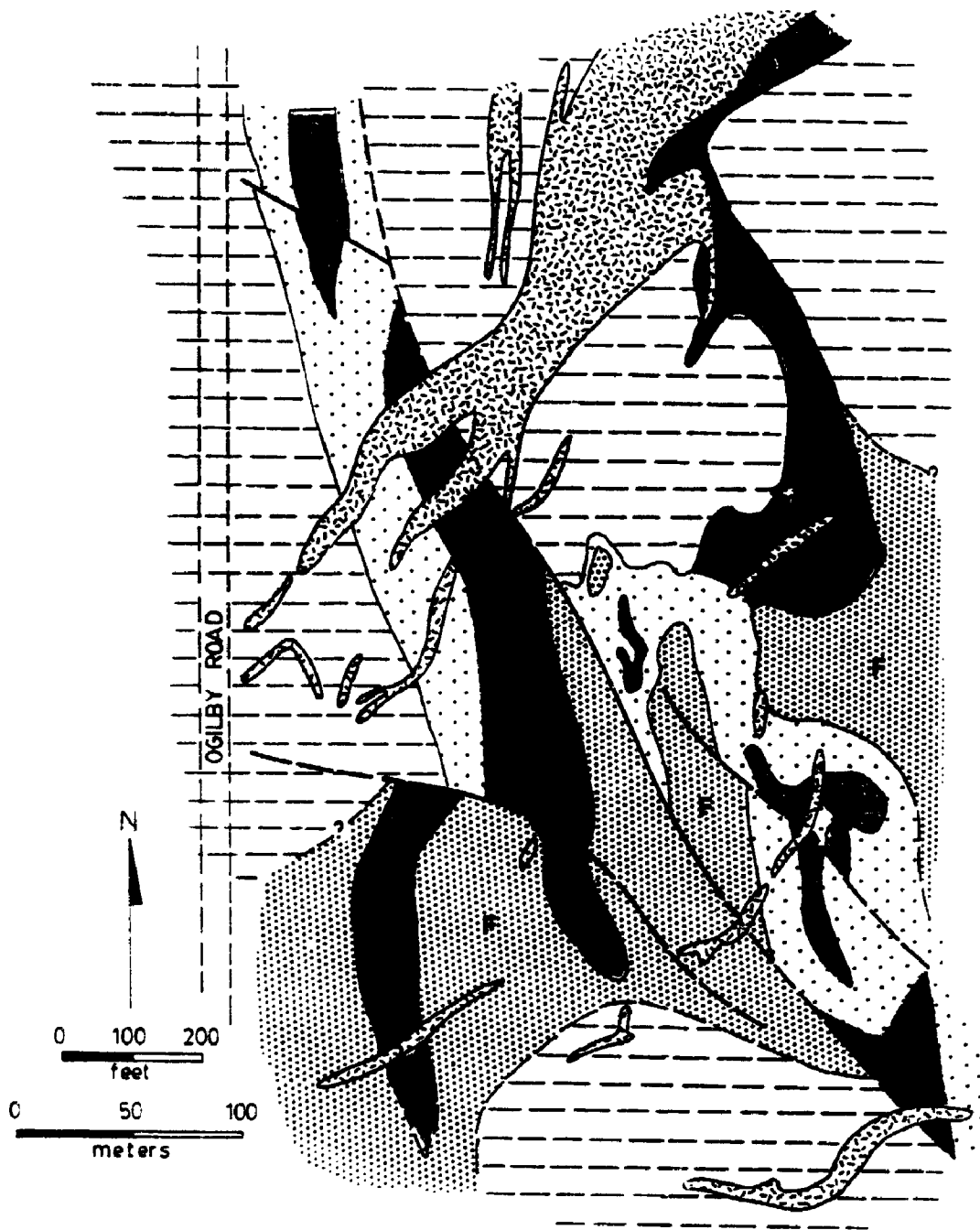
Three distinct fabrics, with a regular distribution in and around the zones of aluminosilicate mineral assemblages, make up three domains (Figs. 5-1 and 5-2). Domain One has a foliated to gneissic fabric, and includes gneiss of the Tumco Formation, intrusive rocks and the Feldspar Zone. Domain Two has schistosity, mylonitic fabric and a crenulation foliation, and is essentially coincident with the Muscovite Zone. Domain Three has a granoblastic fabric, and contains the Kyanite Zone and that portion of hornblende granodiorite where it cross cuts the Kyanite Zone at Micatalc Hill.

**FIGURE 5-1.** Subdivision of foliation into domains of gneissic, schistose to mylonitic, and granoblastic fabrics at Micatahc and Vitrifax Hills. Domain 1 has gneissic fabric; Domain 2 has undivided schistose and mylonitic fabrics and mylonitic fabrics; Domain 3 has granoblastic fabrics. Domains are superimposed on the geology. The low angle faults and mylonite zones at Micatahc Hill are the western extension of the American Girl Fault Zone (see Fig. 2-2).







**FIGURE 5-2.** Subdivision of foliation into domains of gneissic, schistose to mylonitic, and granoblastic fabrics at Hedges, superimposed on the geology. Domain subdivisions as in Fig. 5-1.



### EXPLANATION


**DOMAIN 1**  
 Gneissic  
 fabric


**DOMAIN 2**  
 Undivided  

 Mylonitic  
 fabric


**DOMAIN 3**  
 Granoblastic  
 fabric

### 5.2.1. Domain One: Foliated to Gneissic Fabric.

Domain One has a foliated to gneissic fabric, defined by parallelism of lepidoblastic biotite (Plate 1d and Plate 4a), but there is also lineated hornblende, feldspar, and quartz. Over most of the area, biotite is disseminated, and there is only a slight arrangement of these minerals into discontinuous compositional bands of alternating light and dark minerals, generally a few grains thick and a few cm long. The mineral assemblage is quartz-feldspar-biotite-(hornblende)-epidote-magnetite, consistent with regional metamorphism to epidote-amphibolite facies. Hence, the gneissosity is interpreted as a product of regional metamorphism. Textures indicating replacement of hornblende by biotite and epidote in quartz diorite and hornblende-biotite granodiorite is a retrogression of hornblende (Plate 1e).

The foliation in the Feldspar Zone is deflected by coarse plagioclase poikiloblasts (Plate 4a and b), which indicates growth of the feldspar poikiloblasts occurred prior to final growth and recrystallization of lepidoblastic biotite. By inference, the aluminosilicate assemblages formed before the end of regional metamorphism. Folded epidote veinlets and recrystallized crack-seal fabrics in the Feldspar Zone also point to this timing (Plate 4c, d, and e).

Foliated to gneissic fabric is labelled  $S_1$  (Table 5-1). In quartzofeldspathic gneiss of the Tumco Formation and the Feldspar Zone, average strike and dip for  $S_1$  is  $309^\circ$  and  $27^\circ\text{SW}$ , respectively, at Micatalc, and  $314^\circ$  and  $44^\circ\text{SW}$ , respectively, at

TABLE 5-1. Average fabric orientations, Vitrifax Hill, Micatalc Hill, and Hedges. Foliation and lineation data are plotted on the maps in Appendix D.

Fabric	Designation	Lithology <sup>1</sup>	Orientation <sup>2</sup>
<b>MICATALC</b>			
Gneissosity	S <sub>1</sub>	Paragneiss (52)	309, 27S (42, 11)
Gneissosity	S <sub>1</sub>	Orthogneiss (19)	289, 27S (39, 9)
Schistosity	S <sub>2A</sub>	Ms/Ky Schist (82)	318, 30S (56, 15)
Crenulation Cleavage	S <sub>2B</sub>	Ms/Ky Schist	
Lineation	L <sub>2</sub>	Ms/Ky Schist	205, 24SW (22, 9)
<b>HEDGES</b>			
Gneissosity	S <sub>1</sub>	Paragneiss (42)	314, 44S (27, 12)
Schistosity	S <sub>2A</sub>	Ms/Ky Schist	328, 52S (55, 16)
Crenulation Cleavage	S <sub>2B</sub>	Ms/Ky Schist	
Lineation	L <sub>2</sub>	Ms/Ky Schist	175, 24SE (9, 8)
<b>VITRIFAX</b>			
Gneissosity	S <sub>1</sub>	Qz. Diorite	302, 24S (24, 8)
Gneissosity	S <sub>1</sub>	Granite	268, 48S (15, 6)
Schistosity	S <sub>2A</sub>	Ms/Ky Schist	259, 48S (26, 14)
Gneissosity	S <sub>1</sub>	Ky granofels	259, 56S (26, 14)

<sup>1</sup> Number of measurements in parentheses.

<sup>2</sup> Numbers in parentheses are one standard deviation for strike (trend) and dip (plunge), respectively.

Hedges (Table 5-1; Upper stereonet, Figs. 5-3 and 5-4). This clockwise and steepening rotation at Hedges relative to Micatalc is part of a broad curvature of  $S_1$  along the west side of the Cargo Muchacho Mountains (Dillon, 1976). Hornblende granodiorite and muscovite-biotite granite at Micatalc have fabric orientations distinct from the quartzofeldspathic gneiss of the Tumco Formation, averaging  $289^\circ$ ,  $30^\circ\text{SW}$  (Table 5-1).

Exposure of quartzofeldspathic gneiss of the Tumco Formation is limited at Vitrifax; therefore, all  $S_1$  measurements are from the intrusive rocks, mostly from the 173 Ma quartz diorite. Strike and dip average  $302^\circ$  and  $24^\circ\text{SW}$ , respectively (Upper stereonet, Fig. 5-5), similar to quartzofeldspathic gneiss of the Tumco Formation at Micatalc. In contrast, foliation in muscovite-biotite granite at Vitrifax contains a distinctly different orientation, striking  $268^\circ$  and dipping  $43^\circ\text{S}$  (Table 5-1), which roughly parallels its contacts with the quartz diorite, granite porphyry and the Muscovite Zone along the west side of Vitrifax (see Fig. 3-1).

### **5.2.2. Domain Two: Schistose, Mylonitic and Crenulated Fabrics.**

#### **5.2.2.1. General Characteristics.**

Domain Two is schistose to mylonitic and crenulated, mainly as a tabular layer between Domains One and Three. Mylonitic fabrics of Domain Two occur in bands, or zones, from less than 1 m wide to more than 5 m wide. The smaller bands

**FIGURE 5-3.** Lower hemisphere stereographic projections,  $S_1$  and  $S_2$ , at Micatahc Hill. Upper diagram: contoured poles to planes for  $S_1$  in Domain 1. Lower diagram: contoured poles to planes for  $S_2$  in Domain 2; point A represents the axis (pi-pole) around which the  $S_2$  data are positioned. Contour intervals are 5% points per 1% area.

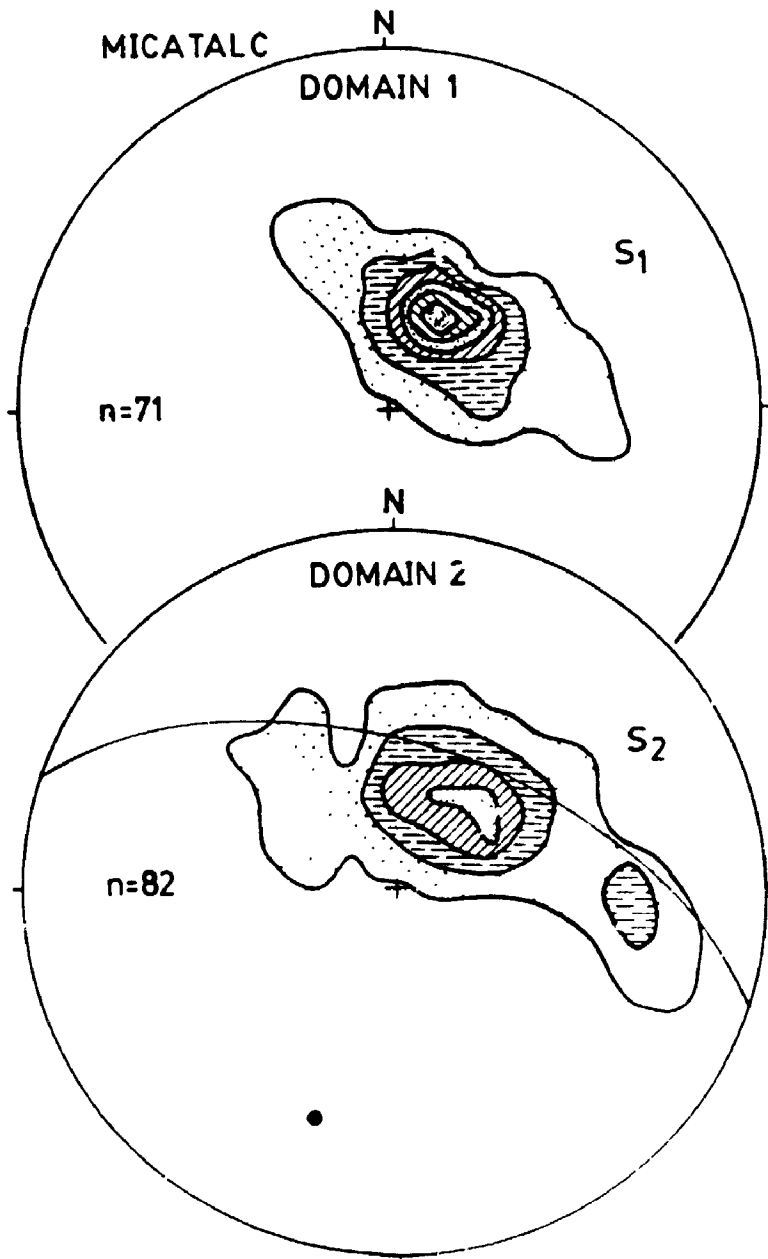




**FIGURE 5-4.** Lower hemisphere stereographic projection,  $S_1$  and  $S_2$ , at Hedges. Upper diagram: contoured poles to planes for  $S_1$ . Lower diagram: contoured poles to planes for  $S_2$ ; point A represents the axis (pi-pole) around which the  $S_2$  data are positioned. Contour intervals are 5% points per 1% area.

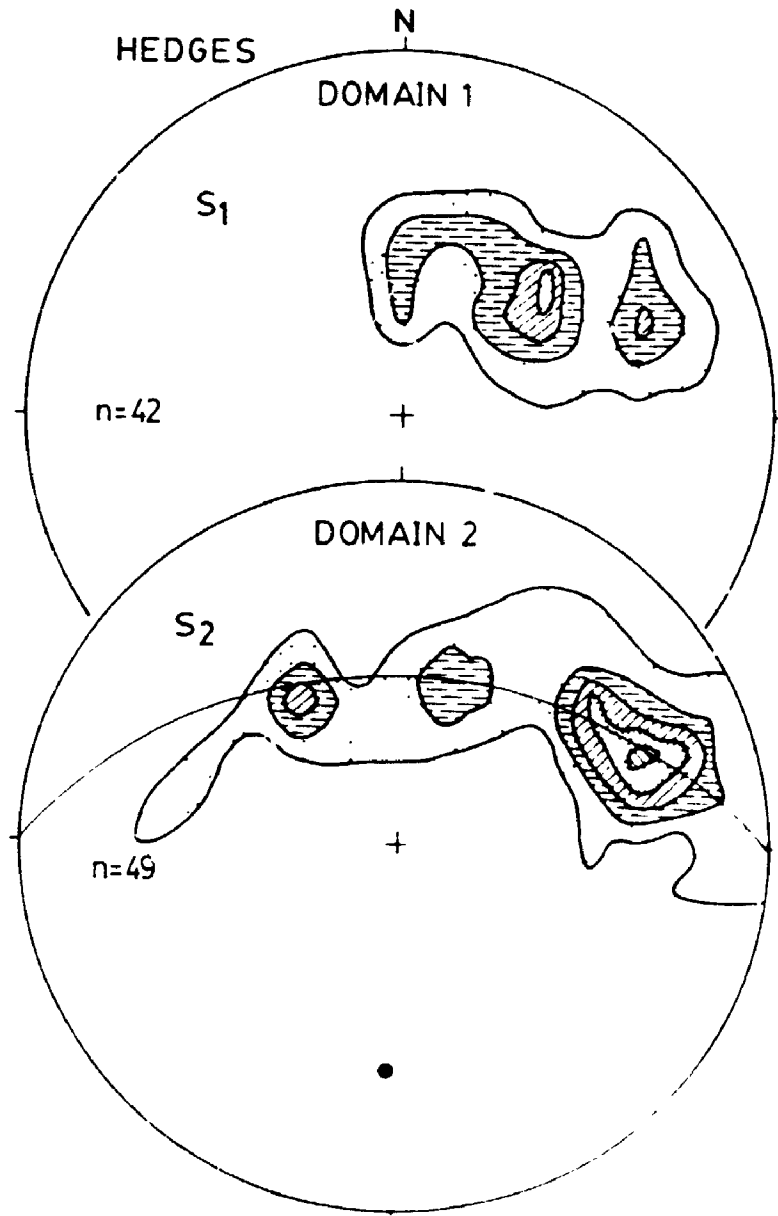
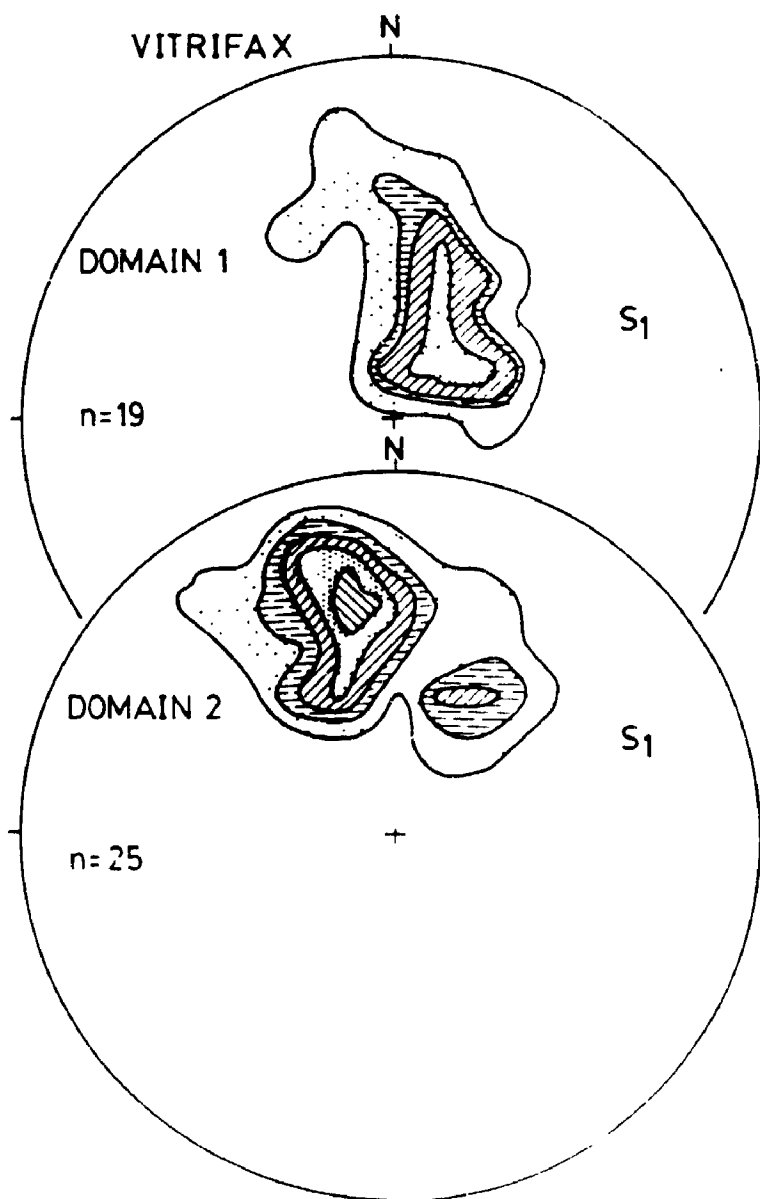


**FIGURE 5-5.** Lower hemisphere stereographic projections for  $S_1$  at Vitrifax Hill. Upper diagram: contoured poles for  $S_1$  within Domain 1. Lower diagram: contoured poles to planes for  $S_1$  in Domain 2. Contour intervals are 5% points per 1% area.



(less than 10 cm wide) form anastomosing layers which separate pods and lenses of granoblastic quartz-kyanite. The larger mylonite bands are relatively linear, hosting rods of granoblastic quartz-kyanite. These features, together with fine grain size and pronounced foliation, indicate the mylonite bands are shear zones (Ramsay and Huber, 1988). On the north flank of Micatahc Hill, irregular-shaped and folded lenses of mylonitic biotite and magnetite subzones of the Muscovite Zone occur within one another, indicating transposition has occurred, consistent with high strain associated with shear zones.

Shear zones are oriented sub-parallel to the regional foliation, striking about  $90^\circ$  and dipping about  $27^\circ\text{S}$  at Micatahc Hill and Vitrifax Hill, and about  $330^\circ$  and  $52^\circ\text{SW}$ , respectively, at Hedges. At Micatahc Hill, shear zones in Domain Two are the western extension of the American Girl Fault Zone (Figs. 2-2, 3-1 and 5-1). Mutually cross-cutting relationships between muscovite-biotite granite, hornblende granodiorite and shear zones here indicate 160-173 Ma magmatism and mylonitization partly overlapped in time (Figs. 5-1 and 3-6).

The mineral assemblages in Domain Two are a function of the zonation within the aluminosilicate mineral assemblages. Quartz-muscovite-biotite-magnetite (with local feldspar, tourmaline, apatite, and garnet) occurs in that part of Domain Two occupied by the biotite subzone of the Muscovite Zone. Quartz-muscovite-magnetite (with local tourmaline and apatite)

occurs in the magnetite subzone of the Muscovite Zone, and quartz-muscovite-kyanite-magnetite (with local tourmaline, apatite, rutile) occurs in the Kyanite Zone. Muscovite-biotite granite has the assemblage quartz-albite-muscovite-biotite in Domain Two. Fracture and vein fillings of muscovite, magnetite, and limonite after pyrite occur throughout Domain Two.

#### 5.2.2.2. Foliation Characteristics and Orientation.

Muscovite is the primary mineral which defines the foliation. As described in Chapter 4, there are four muscovite habits; Type 1 and Type 4 muscovite are predominant in Domain 2. Type 1 muscovite is lepidoblastic, defining schistosity and compositional banding. Type 4 muscovite is confined to thin mica-rich seams and crenulation cleavages, and is the main habit where S-C fabrics occur. It is very fine grained, and the fine grain size of quartz intergrown with this muscovite indicates formation by dynamic recrystallization and polygonization. Quartz, for example, typically has strong undulose extinction and prominent subgrain development in Domains One and Three. In Domain Two, however, it is polygonal, with no or slight undulose extinction, commonly with triple junctions.

Mylonitic fabrics cross cut the foliation of regional metamorphism, and their development is at least in part later than regional metamorphism. In addition, mylonitic fabrics cross cut or are deflected by biotite, feldspar and kyanite

within the zones of aluminosilicate mineral assemblages. Thus, mylonitization also in part post-dates development of the zones of aluminosilicate mineral assemblages. Hence, mylonitization is designated  $D_2$ . However, textures such as clear overgrowths of kyanite on broken, inclusion-rich kyanite grains in Domain Two indicates growth of kyanite continued during  $D_2$ . Therefore, there was overlap in the timing of mylonitization and development of the aluminosilicate mineral assemblages.

Because of the overprint of Type 1 muscovite by Type 4 muscovite, identification of Type 1 is difficult, and its spatial distribution is not well constrained. Thus, the relationship of schistosity to the other fabrics is less clear than that of mylonitic fabrics. Although schistosity and mylonitic fabrics may have different origins, they are included together (Fig. 5-1).

Crenulations are restricted to Domain 2 with mylonitic fabrics, where they offset or fold pre-existing foliation. Crenulations which fold pre-existing foliation have a larger content of muscovite on the limbs of the folds, with aligned magnetite, tourmaline and limonite after pyrite, and a larger content of quartz in the hinges of the folds. Crenulations which offset pre-existing foliation are asymmetric, and produce step-like microfolds or kinks in the foliation, with a larger content of muscovite within the plane of crenulation. Because of these cross-cutting relationships, schistosity and mylonitic fabrics are labelled  $S_{2A}$  and the crenulations are

labelled  $S_{2B}$ .

$S_{2A}$  at Micatalc and Hedges are sub-parallel to  $S_1$  at each site (Lower stereonets, Figs. 5-3 and 5-4). As with  $S_1$ , the foliations at Hedges have a clockwise and steepening rotation relative to that at Micatalc. Average strike and dip of  $S_{2A}$  at Micatalc Hill are  $318^\circ$  and  $30^\circ S$ , respectively. At Hedges, strike and dip are respectively  $328^\circ$  and  $52^\circ S$ . There is considerably more scatter in the attitudes of  $S_{2A}$  than in those of  $S_1$  at both sites. A best-fit girdle and pi-pole are determined (Figs. 5-3 and 5-4), the latter representing the axis around which the foliations have been folded.

$S_{2A}$  at Vitrifax strikes  $259^\circ$  and dips  $48^\circ S$  (Lower stereonet, Fig. 5-5; Table 5-1). This represents a counterclockwise rotation relative to foliation in Domain One, in contrast to that at Micatalc which has a clockwise rotation. There is also much less scatter in the attitudes than at Hedges or Micatalc, suggesting less influence by post- $D_{2A}$  deformation.

#### 5.2.2.3. Lineation Characteristics and Orientation.

The axes of crenulations and the intersection of crenulations with mylonitic and schistose fabrics form a pronounced lineation, named intersection lineation here. Kyanite, quartz, tourmaline, and apatite locally have pronounced alignment parallel to the intersection lineation. In addition, Domain Two has rods of granoblastic quartz-kyanite, up to 3 m in diameter.  $S_{2A}$  wraps around these rods, and parallelism of these rods with mineral lineation and intersection



lineation indicates similar timing of formation. These lineations are designated  $L_2$ .

$L_2$  at Micatahc has a trend and plunge of  $205^\circ$  and  $24^\circ\text{SW}$ , respectively, whereas at Hedges, the trend and plunge are  $175^\circ$  and  $24^\circ\text{SE}$ , respectively (Fig. 5-6).  $L_2$  at both sites is parallel to the determined pi-poles for the  $S_2$  data (compare Fig. 5-6 with Figs. 5-3 and 5-4), and suggests a common origin for these structures. The lineations are in part defined by the intersection between crenulations ( $S_{2B}$ ) and schistosity or mylonitic fabrics ( $S_{2A}$ ). As these planar features are restricted to Domain 2, they are thought to be related to mylonitization, and parallelism of mineral lineations and rod structures suggest a similar origin (Dennis and Secor, 1987).

#### 5.2.2.4. $D_2$ Movement Direction.

Kinematic markers which provide evidence of displacement direction include megascopic features such as drag folds and offset of contacts between rock types, and microscopic features such as S-C fabrics, mica fish, rotated porphyroblasts and asymmetric crenulation cleavages (Simpson and Schmid, 1983; Lister and Snoke, 1984; Dennis and Secor, 1987). The current position of rock types at Micatahc Hill suggest reverse movement along the American Girl Fault. However, microscopic features such as rotated prophyroblasts and S-C fabrics indicate normal displacement along the low angle shear zones at Micatahc Hill (Plate 9). Although equivocal, the fabrics suggest the low angle shear zones at Micatahc Hill had

**FIGURE 5-6.** Lower hemisphere stereographic projection,  $L_2$ , at Micatalc Hill (upper diagram) and Hedges (lower diagram). Contour intervals are 5% points per 1% area.

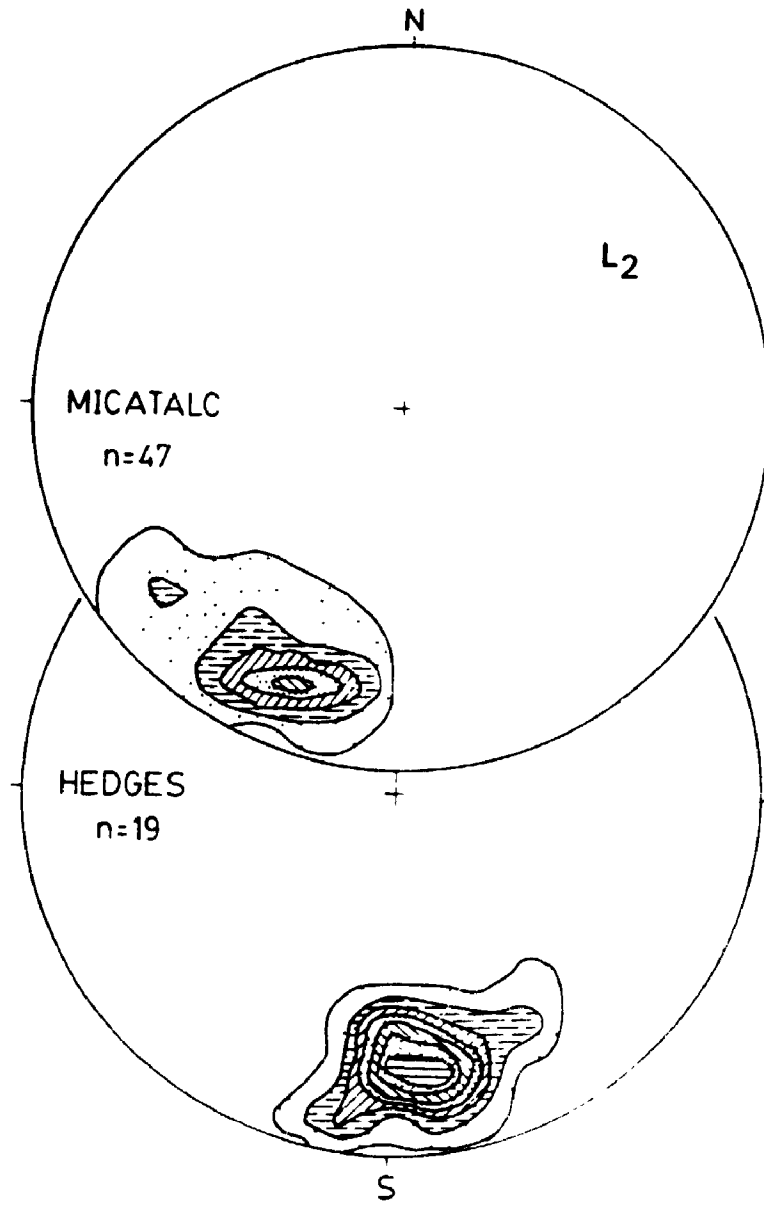


**PLATE 9.** Kinematic indicators, Domain 2, Micatahc Hill. All photomicrographs are oriented so that north-northeast is to the left. Shear sense is dextral in all photographs. **a.)** Asymmetric augen structure containing kyanite. Note concentration of muscovite adjacent to upper left side of kyanite, facing the direction of maximum compression. Plane light, scale bar equals 1 mm. **b.)** Same field of view as (a), crossed polars. **c.)** Rotated muscovite defining S- and C-fabrics. Scale bar equals 0.1 mm. **d.)** Similar relationships as in (c). Scale bar equals 0.1 mm. **e.)** Asymmetric augen structure containing magnetite porphyroblast. Augen is outlined, and mica is concentrated on upper left side of magnetite, identifying maximum compression direction. Clear, unstrained quartz occurs on the right side in pressure shadow. Scale bar equals 1 mm. **f.)** Closer view of porphyroblast in (e). Note strain-free quartz elongate perpendicular to magnetite grain boundary and randomly oriented muscovite in augen structure.



normal, S- to SE-directed movement accompanying emplacement of the 160-173 Ma intrusive rocks. This is consistent with the results of Tosdal and Haxel (1987), Branham (1988) and Tosdal (1990), who proposed pronounced normal movement along the American Girl fault during the Jurassic.

Similar data was not acquired from Hedges or Vitrifax. However, unaltered pegmatite dikes are deflected in a left-lateral sense across the shear zones at Hedges (Fig. 3-3). This deflection may be a direct result of sinistral movement, or may be refraction caused by emplacement into rocks of different competency. In either instance, since the deflection is small, shearing at Hedges was virtually complete by the time of emplacement of these dikes.

### **5.2.3. Domain Three: Granoblastic Fabrics.**

Domain Three is granoblastic with the mineral assemblage is quartz-kyanite-muscovite-magnetite (with tourmaline, apatite, rutile, lazulite, garnet, staurolite, andalusite) in the Kyanite Zone, and quartz-andesine/labradorite-hornblende-biotite-magnetite in hornblende-biotite granodiorite. The Kyanite Zone of Domain Three is massive or coarsely banded, as defined by variation in relative abundance of kyanite, quartz, magnetite and tourmaline.

As described above and in Chapter 4, deflection of biotite ( $S_1$ ) around coarse feldspar poikiloblasts in the Feldspar Zone of Domain One indicates the development of the zones of aluminosilicate mineral assemblages occurred prior to

the end of regional metamorphism. In addition, rods of granoblastic quartz-kyanite hosted within mylonitic Muscovite and Kyanite Zones in Domain Two indicate pre-D<sub>2</sub> development of the aluminosilicate assemblages. Textures in Domain Three such as undulose extinction, bent and kinked grains, and subgrain formation support this, suggesting textural readjustment by aluminosilicate minerals caused by strain. Thus, fabrics in Domain 3, like those of Domain 1, are designated S<sub>1</sub>.

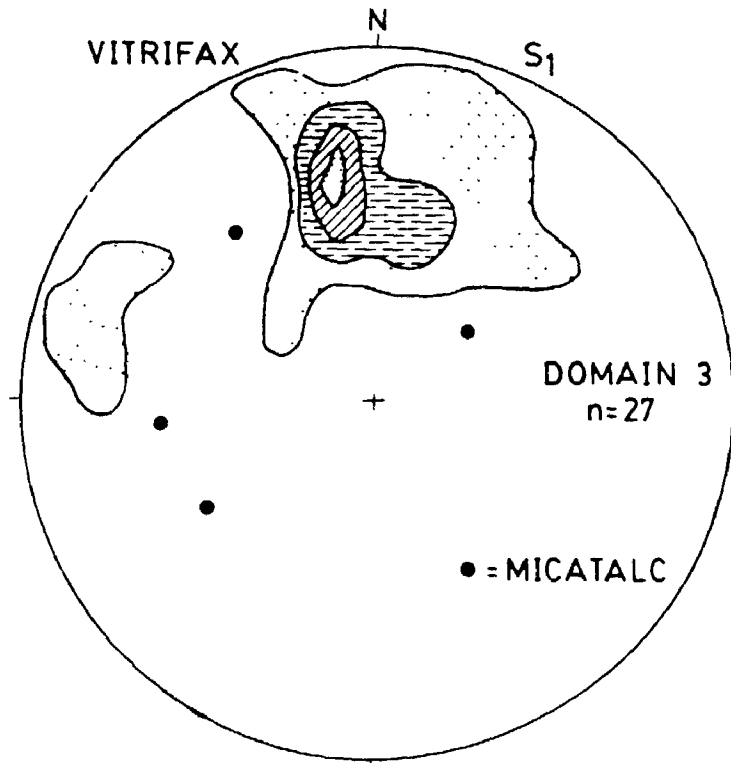
The only data for S<sub>1</sub> from Domain 3 comes from Vitrifax Hill, where gneissic banding is well developed (Fig. 5-7). Average orientation is 259°, 56°S, which represents a considerable counterclockwise rotation and steepening relative to S<sub>1</sub> of Domain 1 (Compare Figs. 5-7 and 5-5). This orientation is sub-parallel to S<sub>2</sub> at Vitrifax, suggesting rotation was caused by D<sub>2</sub> deformation.

### **5.3. Post-D<sub>2</sub> Deformation.**

Post-D<sub>2</sub> faults and shear zones of various orientations offset rock types and D<sub>1</sub> and D<sub>2</sub> structures (Figs. 2-2, 3-1 and 3-3). Although these structures are covered by alluvium in this thesis area, they are inferred from the mapping of Dillon (1976). Post-D<sub>2</sub> fabrics and minerals appear to be restricted to the fault zones, and elsewhere in the range are characterized by breccia and clay fault gouge. In this thesis area, fabrics such as mortar structure in intrusive rocks and granoblastic quartz and quartz-kyanite may be related. In some

**FIGURE 5-7.** Lower hemisphere stereographic projection,  $S_1$ , in Domain 3 at Vitrifax Hill. Contour interval is 5% points per 1% area.





instances veinlets containing limonite after pyrite, muscovite, chlorite, quartz, chalcedony, and carbonate minerals cross cut  $D_1$  and  $D_2$  fabrics, and are thus post- $D_2$ . However, deflection of Type 4 muscovite ( $D_2$ ) by coarse limonite after pyrite indicates at least some of this latest stage of mineral precipitation preceded cessation of  $D_2$ .

#### 5.4. Summary.

The salient points depicting the nature and timing of events are summarized as follows:

1.) Foliated to gneissic fabrics of Domain One occur on a regional scale; this and the common occurrence of the mineral assemblage quartz-oligoclase-microcline-biotite-epidote (with or without hornblende, chlorite, and carbonate minerals) is consistent with regional metamorphism to lower amphibolite facies.

2.) Mylonitic fabrics of Domain Two cross cut the gneissic fabric, and crenulation cleavages cross cut mylonitic fabrics. Thus, regional foliation and gneissic fabrics are labelled  $S_1$ , regional metamorphism  $D_1$ , mylonitic fabrics  $S_{2A}$ , crenulation cleavages  $S_{2B}$ , and mylonitization  $D_2$ .

3.) The mylonitic and crenulation fabrics occur in shear zones which have mutually cross cutting relationships

with the 173-160 Ma hornblende granodiorite and muscovite-biotite granite. Thus mylonitization is partly contemporaneous with these intrusive rocks.

4.) Deflection of  $S_1$  by coarse feldspar poikiloblasts in Domain One indicates only that growth of the feldspar pre-dated the end of regional metamorphism. Recrystallization of quartz-epidote veinlets suggests similar timing.

5.) Textures and structures in the aluminosilicate mineral assemblages of Domains Two and Three, such as rods of granoblastic quartz-kyanite, kink bands, mineral lineations, subgrain formation, and triple junctions, indicate dynamic recrystallization and polygonization occurred as a result of strain, and show that the aluminosilicate mineral assemblages formed prior to development of mylonitic fabrics.

6.) Textures and structures in the aluminosilicate mineral assemblages, such as the growth of inclusion-free kyanite rims on broken, inclusion-rich kyanite grains in Domain 2, and the occurrence of muscovite, magnetite and limonite after pyrite in veinlets, indicate growth of these minerals continued during and after  $D_2$ .

7.) As discussed in Chapters 3 and 4, the 173 Ma quartz

diorite and the 173-160 Ma granite porphyry contain metasomatic minerals of the aluminosilicate mineral assemblages. Fabric development in Domain Three, and formation of the zones of aluminosilicate mineral assemblages, occurred between emplacement of the 173-160 Ma granite porphyry and development of mylonitic fabrics, and is thus designated  $S_1$ .

8.) There is a persistent relationship between fabric orientation and rock type, particularly in the intrusive rocks. The pronounced variations in strike and dip in the muscovite-biotite granite and the quartz diorite at Vitrifax Hill, for instance, parallel the intrusive contacts, suggesting a relationship between foliation orientation and emplacement of the intrusives. Similarly, the clockwise and steepening rotation of  $S_1$  and  $S_2$  to the northwest at Hedges relative to Micatahc may be related to the emplacement of the large body of muscovite-biotite granite in the main part of the range north of American Girl Canyon (see Fig. 2-2).

These characteristics suggest a sequence of events beginning with emplacement of 173 Ma quartz diorite during regional metamorphism ( $D_1$ ). This was followed by emplacement of the 173-160 Ma suite, during which early pervasive metasomatism occurred.  $D_1$  continued through this period, but emplacement of muscovite-biotite granite and hornblende

granodiorite was accompanied by  $D_2$ -style deformation, in the form of shear zones. Previously existing zones of aluminosilicate minerals were deformed during  $D_2$ , although metasomatism continued, located in the shear zones.

## CHAPTER SIX -- MOBILITY OF MAJOR AND TRACE ELEMENTS.

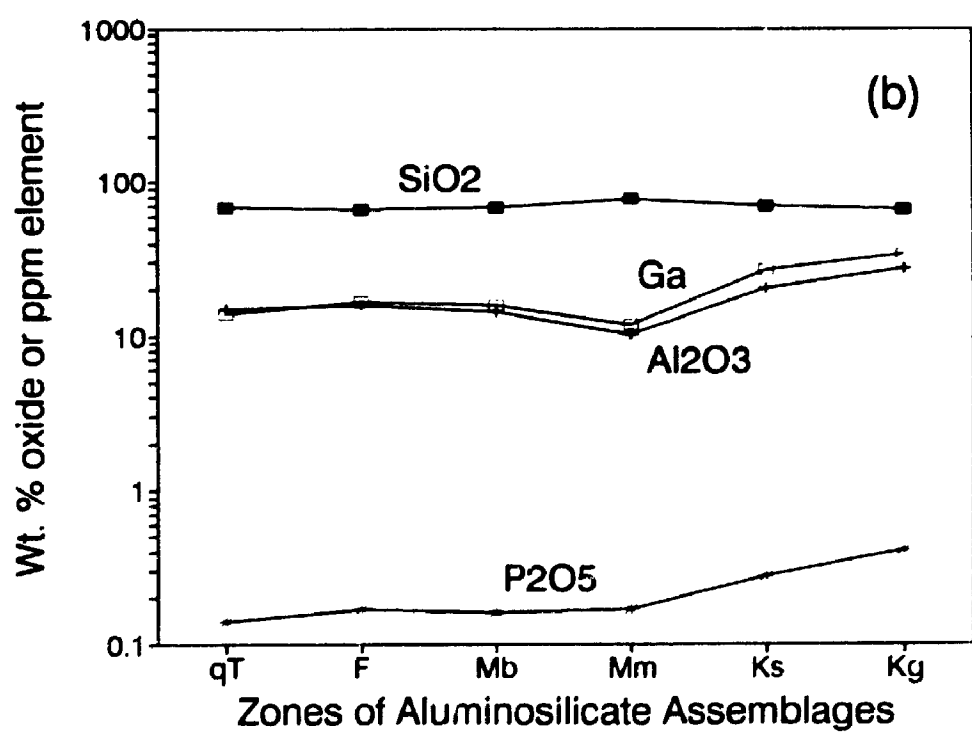
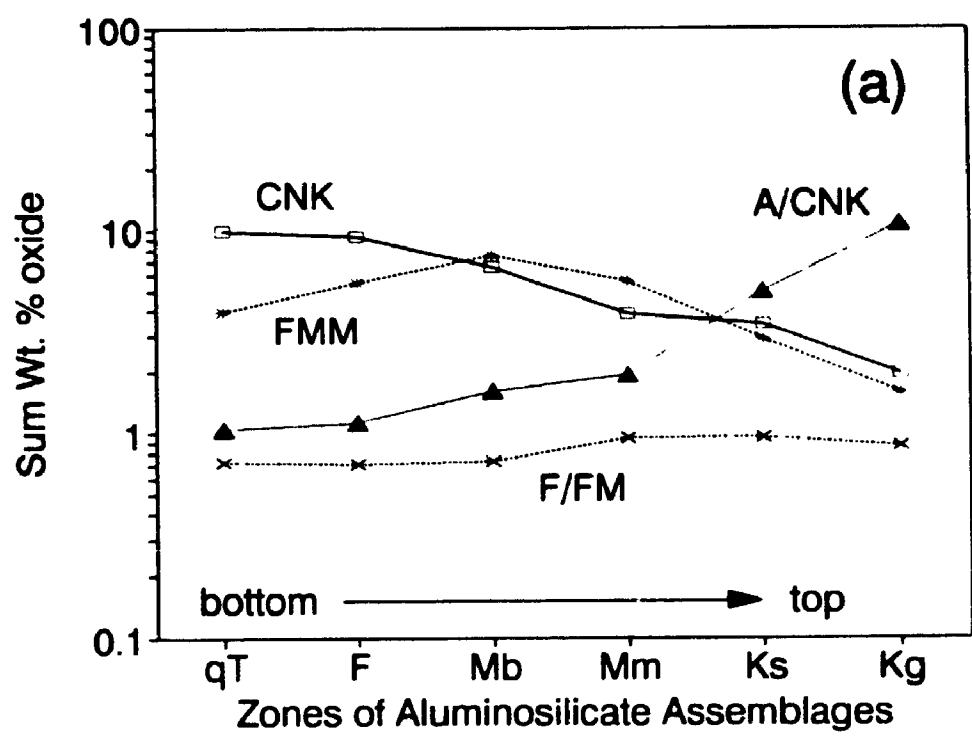
### 6.1 General Statement.

In the zones of aluminosilicate mineral assemblages, the occurrence of aluminosilicate minerals in fractures and veinlets indicate fluids were present during the development of the aluminosilicate mineral assemblages. There are progressive increases of aluminum, titanium and phosphorus, and decreases in most of the remaining elements, from quartzofeldspathic gneiss of the Tumco Formation into the Kyanite Zone of the aluminosilicate mineral assemblages. Variations in composition are reflected in mineral abundance, and can be related to either pervasive replacement or shear zone-hosted replacement.

### 6.2. Distribution of the Elements.

Concentration of the major and trace elements are reflected in the relative abundance and composition of mineral phases. The succession from the quartzofeldspathic gneiss of the Tumco Formation into the Kyanite Zone of the aluminosilicate mineral assemblages has an overall increase in the bulk rock content of  $Al_2O_3$ ,  $TiO_2$ ,  $P_2O_5$ , Ga, and V (Figs. 6-1 and 6-6). In contrast, there is an overall decrease in the abundance of the oxides of Fe, Mg, Mn, Ca, Na, and K, coincident with a decrease in the abundance of feldspar and mica from the Feldspar Zone to the Kyanite Zone (compare Fig. 4-1). The result is an increase in molecular  $Al_2O_3/(CaO+Na_2O+K_2O)$  (Fig. 6-1a).  $Fe_2O_3/(Fe_2O_3+MgO)$  also increases across these zones.

**FIGURE 6-1.** Major element composition of the zones of aluminosilicate mineral assemblages. **(a)**  $CNK = CaO + Na_2O + K_2O$ ;  $FMM = Fe_2O_3 + MgO + MnO$ ;  $A/CNK = \text{molecular } Al_2O_3 / (CaO + Na_2O + K_2O)$ ;  $F/FM = Fe_2O_3 / (Fe_2O_3 + MgO)$ . **(b)**  $SiO_2$ ,  $Al_2O_3$ ,  $P_2O_5$ , and Ga. Abbreviations: qT, quartzofeldspathic gneiss of the Tumco Formation; F, Feldspar Zone; Mb, biotite subzone, Muscovite Zone; Mm, magnetite subzone, Muscovite Zone; Ks, schistose to mylonitic, Kyanite Zone; Kg, granoblastic Kyanite Zone.





### 6.2.1. Silicon.

Compared to the other major oxides,  $\text{SiO}_2$  content is relatively constant from the quartzofeldspathic gneiss of the Tumco Formation into the Kyanite Zone, and reflects the content of quartz (Fig. 6-1b).  $\text{SiO}_2$  ranges from a low of 67% in the Feldspar Zone, where quartz is less than 30%, to a high of 77% in the magnetite subzone of the Muscovite Zone, which has almost 40% quartz. The correlation between quartz and  $\text{SiO}_2$  content indicates the proportion of other silicate minerals plays a minor role in the variability of silicon concentration (eg.  $\text{SiO}_2$  is supersaturated with respect to other silicate minerals).

### 6.2.2. Aluminum, Gallium and Phosphorus.

There is rough parallelism in the variation of  $\text{Al}_2\text{O}_3$ , Ga and  $\text{P}_2\text{O}_5$  contents, with a general increase from quartzofeldspathic gneiss of the Tumco Formation to the Kyanite Zone of the aluminosilicate mineral assemblages (Fig. 6-1b). Aluminum content more than doubles, ranging from less than 15% in the quartzofeldspathic gneiss to as much as 35% in the Kyanite Zone, reflected primarily by the presence of kyanite. Greater abundance of feldspar, biotite and epidote in the Feldspar Zone result in part from slightly more  $\text{Al}_2\text{O}_3$  than in the quartzofeldspathic gneiss of the Tumco Formation. The smaller concentration of aluminum in the Muscovite Zone, particularly sharp in the magnetite subzone, mirrors the abundance of  $\text{SiO}_2$ . This reversal is in part a constant sum

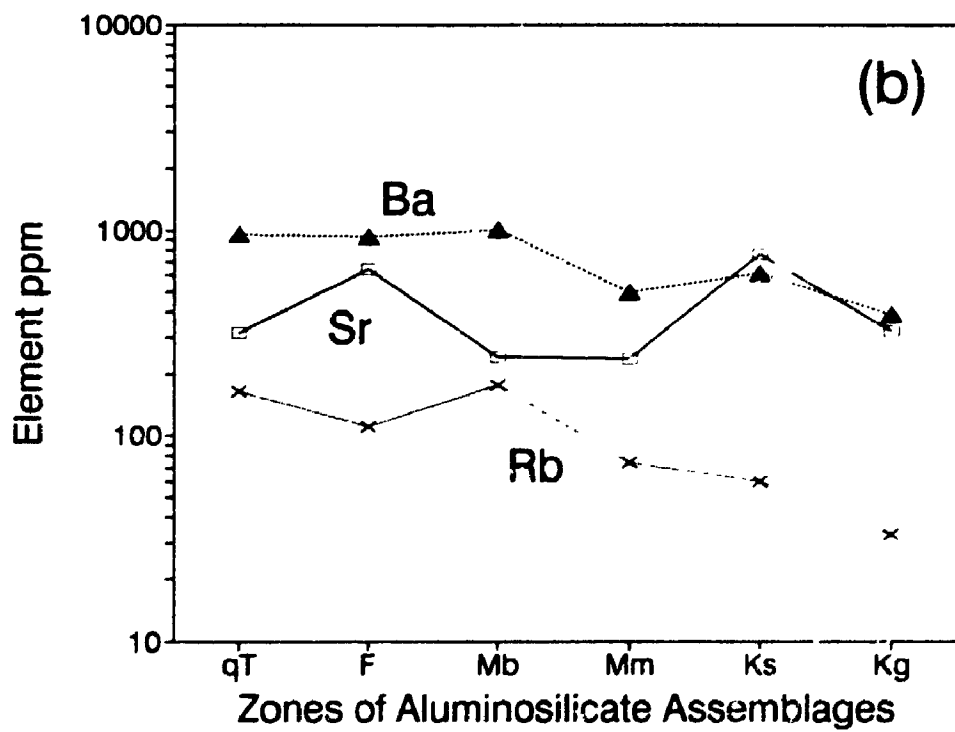
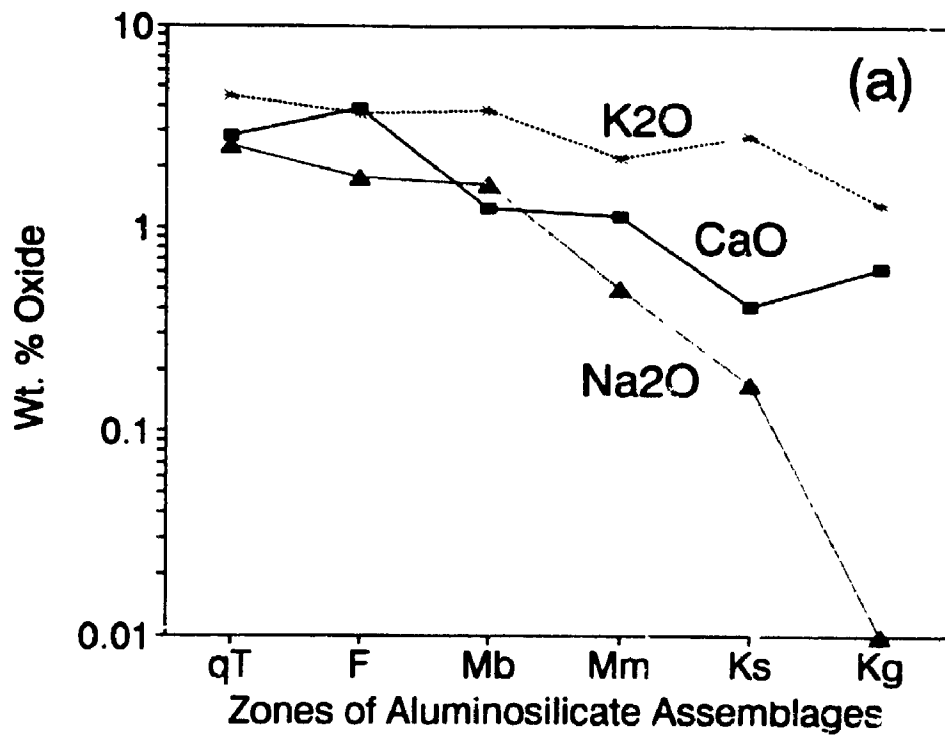
problem, as the main aluminum-bearing phase, muscovite, is more than 40%. Gallium is covariant with aluminum (correlation coefficient,  $r=0.88$ ), reflecting the ready substitution of Ga for Al. Its abundance more than doubles from 14 ppm in quartzofeldspathic gneiss of the Tumco Formation to 34 ppm in granoblastic Kyanite Zone.

$P_2O_5$  has a sharp increase in abundance, tripling from 0.14% in quartzofeldspathic gneiss of the Tumco Formation to 0.41% in the Kyanite Zone (Fig 6-1). This increase is particularly sharp in the Kyanite Zone, where apatite nearly triples in amount. Lazulite is also present, but only in trace amounts because of small amounts of Fe and Mg. Thus it does not contribute greatly to the  $P_2O_5$  content.

### 6.2.3. Alkali and Alkaline Earth Oxides.

There is an overall decrease in the amount of  $CaO$ ,  $Na_2O$ ,  $K_2O$ , Rb, and Ba from quartzofeldspathic gneiss of the Tumco Formation to the Kyanite Zone, a trend parallel to the amount of feldspar in the mineral assemblage zones.  $\Sigma CaO+Na_2O+K_2O$  is greater than 10% in quartzofeldspathic gneiss of the Tumco Formation, with more than 25% feldspar, and diminishes to less than 2% in the Kyanite Zone, with essentially no feldspar (Figs. 6-1 and 6-2a). Larger plagioclase and epidote contents in the Feldspar Zone are due to increased  $CaO$  relative to quartzofeldspathic gneiss of the Tumco Formation. Although biotite content is also greater in the Feldspar Zone, less K-feldspar is a function of less  $K_2O$ . High total mica content

**FIGURE 6-2.** Abundance of alkali and alkaline earth elements in the zones of aluminosilicate mineral assemblages. **a.)**  $K_2O$ ,  $Na_2O$ , and  $CaO$ . **b.)** Sr, Ba, and Rb. Mineral zone abbreviations as in Fig. 6-1.



in the biotite subzone of the Muscovite Zone results from slightly greater  $K_2O$ , but less  $K_2O$  in the magnetite subzone in part explains the lack of biotite. In schistose, muscovite-rich Kyanite Zone, greater  $K_2O$  is reflected in abundant muscovite.

The variation in Rb and Ba parallel that of  $K_2O$  (Fig. 6-2), although Rb deviates from this parallelism in the schistose Kyanite Zone.  $K_2O$  and Rb are covariant, with  $r$  equal to 0.84, and  $K_2O$  and Ba have moderate covariance, with  $r$  equal to 0.76. Strontium has a marked increase in abundance in the Feldspar Zone relative to all other zones (Fig. 6-2b), a characteristic consistent with its tendency to follow calcium, with which it has moderate to strong covariance ( $r=0.81$ ). Exception to this is the schistose, muscovite-rich Kyanite Zone, which is enriched in Sr relative to Ca.

Less alkali and alkaline earth metals and more aluminum leads to a large increase in the molecular  $Al/Ca+Na+K$  (abbreviated A/CNK) from the quartzofeldspathic gneiss of the Tumco Formation to the Kyanite Zone (Fig. 6-1a). This ratio varies from 1.05 in quartzofeldspathic gneiss, to 10.67 in the Kyanite Zone. An A/CNK of 3 or more occurs for very aluminous mineral assemblages, and has been used by Ririe (1990) as an index of alteration.

#### 6.2.4. Transition Metals.

The transition metals are more abundant from quartzofeldspathic gneiss of the Tumco Formation to the Muscovite Zone,

and less abundant in the Kyanite Zone (Fig. 6-1a). The sum  $\text{Fe}_2\text{O}_3 + \text{MgO} + \text{MnO}$  is largest in the biotite subzone, greater than 8%, and diminishes to just over 1% in the Kyanite Zone. In detail, MnO and MgO have maxima in the biotite subzone of the Muscovite Zone, at 0.36% and 2.01%, respectively, and minima of less than 0.01% and 0.10%, respectively, in schistose to mylonitic Kyanite Zone (Fig. 6-3a).  $\text{Fe}_2\text{O}_3$  abundance parallels this, but is greatest in the magnetite subzone, at 5.35%.

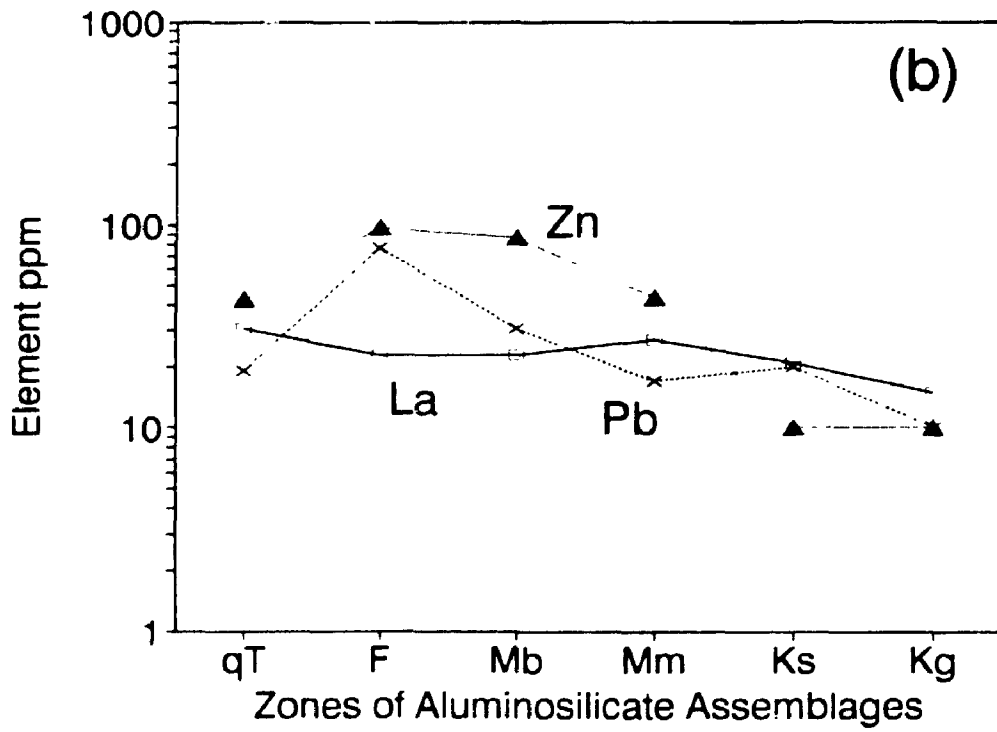
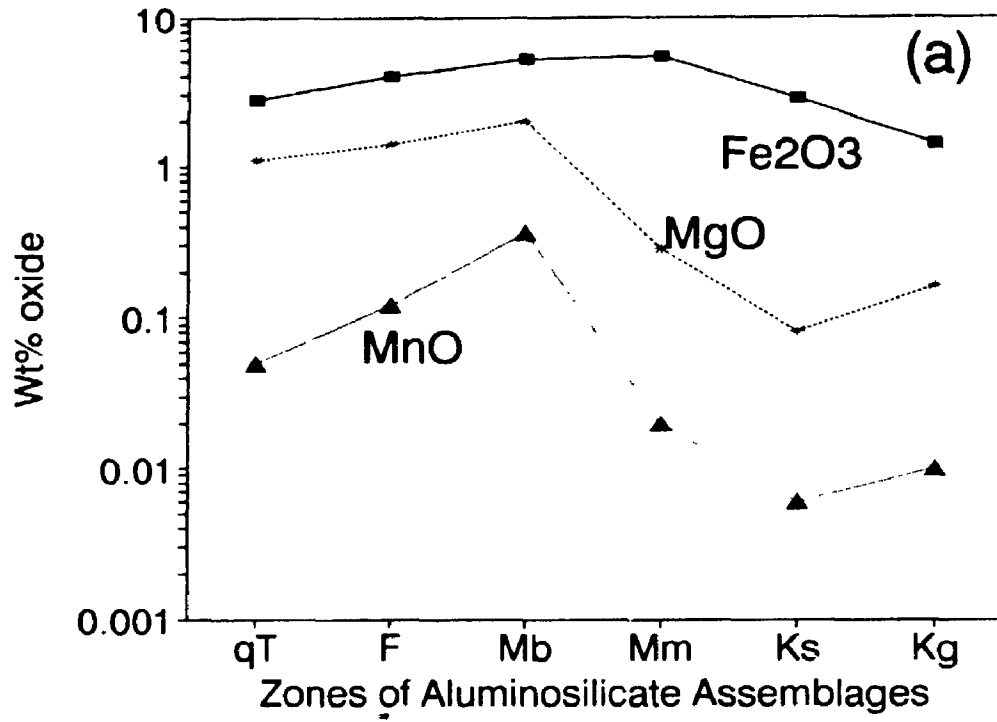
The trends of all three oxides parallel the variation in biotite abundance which is 8% in quartzofeldspathic gneiss of the Tumco Formation, 15% in the Feldspar Zone, and 13% in the biotite subzone of the Muscovite Zone. High  $\text{Fe}_2\text{O}_3$  concentration in the magnetite subzone results in large magnetite and tourmaline contents.  $\text{Fe}_2\text{O}_3 / (\text{Fe}_2\text{O}_3 + \text{MgO})$  increases from 0.718 in quartzofeldspathic gneiss of the Tumco Formation to over 0.9 in the Kyanite Zone (Appendix B), due to the relative variations in iron and magnesium.

Lead and zinc are co-variant, with maxima in the Feldspar Zone and minima in the Kyanite Zone (Fig. 6-3b). Pb, with its large ionic radius, substitutes for  $\text{K}^+$  in biotite, and to a lesser extent in K-feldspar. Zn, on the other hand, probably substitutes for Fe and Mg in biotite.

#### 6.2.5. Ti, Zr, Nb, Y, and V.

$\text{TiO}_2$ , Zr, Nb, Y, and V are considered together because they commonly behave similarly and because they are considered relatively immobile. Nevertheless, their distribution is not

**FIGURE 6-3.** Abundance of transition metals in the zones of aluminosilicate mineral assemblages. **a.)**  $\text{Fe}_2\text{O}_3$ , MgO, and MnO. **b.)** Pb, Zn, La. Mineral Zone abbreviations as in Fig. 6-1.



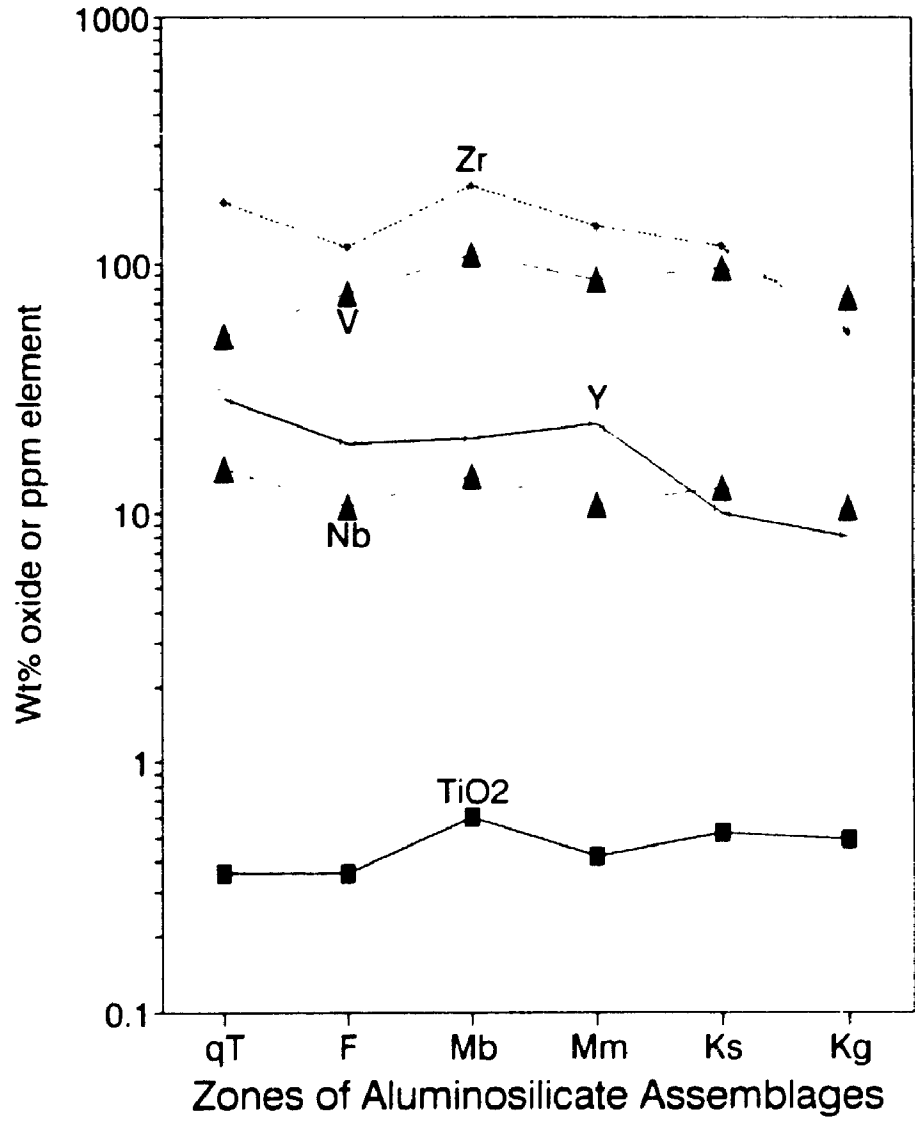


coincident (Fig. 6-4).  $\text{TiO}_2$  and V abundances are roughly parallel, with greater abundance in the Kyanite Zone, with 0.49%  $\text{TiO}_2$  and 73 ppm V, than in quartzofeldspathic gneiss of the Tumco Formation, with 0.36%  $\text{TiO}_2$  and 52 ppm V. Both have maxima in the biotite subzone of the Muscovite Zone, with 0.60%  $\text{TiO}_2$  and 109 ppm V.

The main Ti-bearing phase is magnetite (Appendix C), although both muscovite and biotite have small quantities of  $\text{TiO}_2$ . Ilmenite occurs only in trace amounts, and contributes little to this total. The increase in titanium from the Feldspar Zone through the Muscovite Zone is therefore reflected in the increasing mica and magnetite concentrations. In the Kyanite Zone, magnetite and rutile are the main hosts.

Zirconium also has a maximum in the biotite subzone of the Muscovite Zone, but, unlike Ti and V, is less abundant in the Kyanite Zone than in quartzofeldspathic gneiss of the Tumco Formation. Trace amounts of zircon in all zones account for this abundance. Yttrium decreases in abundance from quartzofeldspathic gneiss of the Tumco Formation to the Kyanite Zone. Niobium also decreases, but less so. Both elements commonly occur in magnetite, apatite, rutile, and zircon. Because the amount of the first three minerals increases from quartzofeldspathic gneiss to the Kyanite Zone, Nb and Y are probably mainly in zircon, a conclusion supported by their general parallelism with Zr.

**FIGURE 6-4.** Ti, Zr, V, Y, and Nb variation in the zones of aluminosilicate mineral assemblage. Mineral zone abbreviations as in Fig. 6-1.



### 6.3. Element Gains and Losses.

#### 6.3.1. Methods.

Attempts to determine the mobility of ions during replacement must consider volume changes. The method followed is the graphical approach of Grant (1986), the basis for which is the mathematical formulation of Gresens (1967). The equation which relates parent rock to product rock:

$$(6-1) \quad C_i^A = (M^0/M^A) (C_i^0 + \Delta C_i)$$

where  $C_i^A$  = the concentration of the  $i^{\text{th}}$  component in the altered rock,  $M^0$  = the mass of the unaltered sample,  $M^A$  = the mass of the altered sample,  $C_i^0$  = the concentration of the  $i^{\text{th}}$  component in the unaltered sample, and  $\Delta C_i$  = the change in concentration of the  $i^{\text{th}}$  component. Volume changes can be related to the above equation via mass:

$$(6-2) \quad M^A/M^0 = (V^A/V^0) (\rho^A/\rho^0)$$

where  $V^A$  = the volume of altered sample,  $V^0$  = the volume of original, unaltered sample,  $\rho^A$  = the specific gravity of the altered sample, and  $\rho^0$  = the specific gravity of the parent sample. From this pair of equations, the relative changes in mass, volume and concentration of elements can be determined. In general,  $M^A/M^0$  is determined graphically, from the isocon ("equal value of concentration") of interest. If several chemically dissimilar elements plot along a line emanating

from the origin, a best-fit isocon can be constructed through these points, generating the mass and volume changes according to similarity of element behavior. This is equivalent to the determination of the volume factor of Gresens (1966) based on the clustering of points at 0% concentration change. On the other hand, if a known volume change occurs, or if a particular element is considered immobile ( $\Delta C_i = 0$ ), the relative concentration changes of the other elements can be determined graphically or calculated according to equation 6-2 above.

The calculations require identification of a parent, against which concentration changes are measured. For the zones of aluminosilicate mineral assemblages in the Cargo Muchacho Mountains, this would be the quartzofeldspathic gneiss of the Tumco Formation (sample #386-1-11, Appendices 1 and 2). No best fit isocon could be determined from the diagrams constructed for the conversion of quartzofeldspathic gneiss to the zones of aluminosilicate mineral assemblages (Figs. 6-5 and 6-6). Thus, assumptions of element immobility or volume change are required to proceed.

The lack of syn-crystallization deformation textures in the Feldspar and Kyanite Zones suggests deformation played a minor role in the growth of these minerals, pointing to fluid-rock interaction as the main control on mineral growth. Volume changes may be quite variable and, considering the wide scatter on the composition-volume plots, a choice of immobile elements is required. Progression into the Kyanite Zone involves the conversion of feldspar to kyanite, and biotite to

**FIGURE 6-5.** Isocon diagrams for the Feldspar and Kyanite Zones (after Grant, 1986). (a) Major element and (b) trace element gains and losses in the Feldspar Zone (squares) and Kyanite Zone (triangles). Parent rock is quartzofeldspathic gneiss of the Tumco Formation. Curves 1 and 2 represent constant aluminum for the Feldspar Zone and Kyanite Zone, respectively. Points above the curves are added to the rock; those below the curves are lost from the rock. For example, in the Feldspar Zone, P, Fe, Na, Ca, Mn, Pb, Zn, Sr, V and Ga are above curve 1 (asterisks), and have been added to quartzofeldspathic gneiss of the Tumco Formation to form rocks of the Feldspar Zone, whereas Si, K, Y, Ba, La, Nb, Rb, and Zr are below curve 1, and have been lost. In contrast, only P and Ga (open squares) are above curve 2 (constant aluminum for the Kyanite Zone); all other elements are below curve 2 and are therefore lost. The amount gained or lost from the rock (%) can be read from the right side of each diagram (scale not shown).

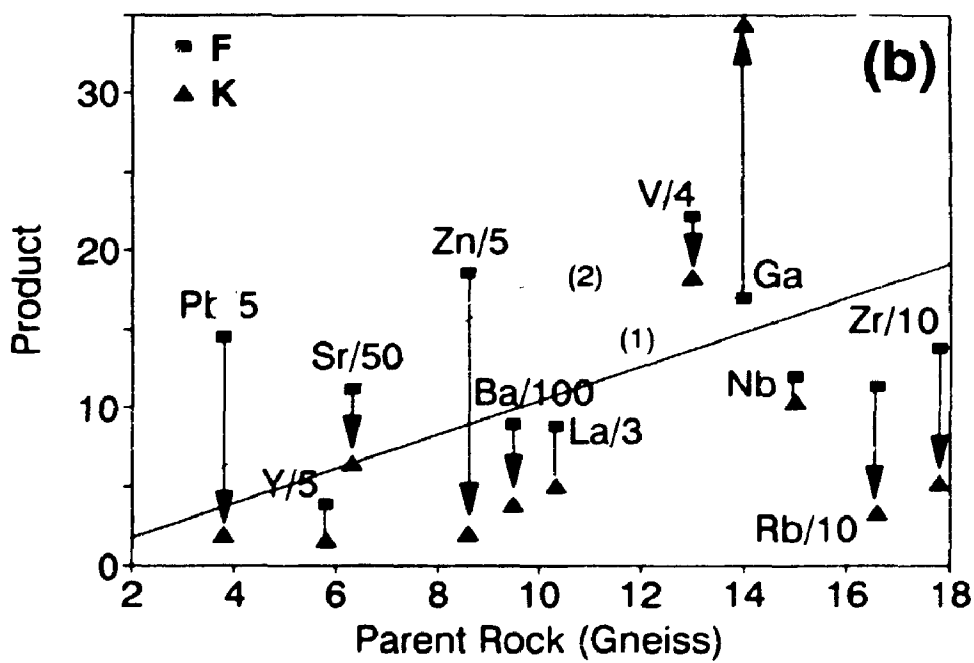
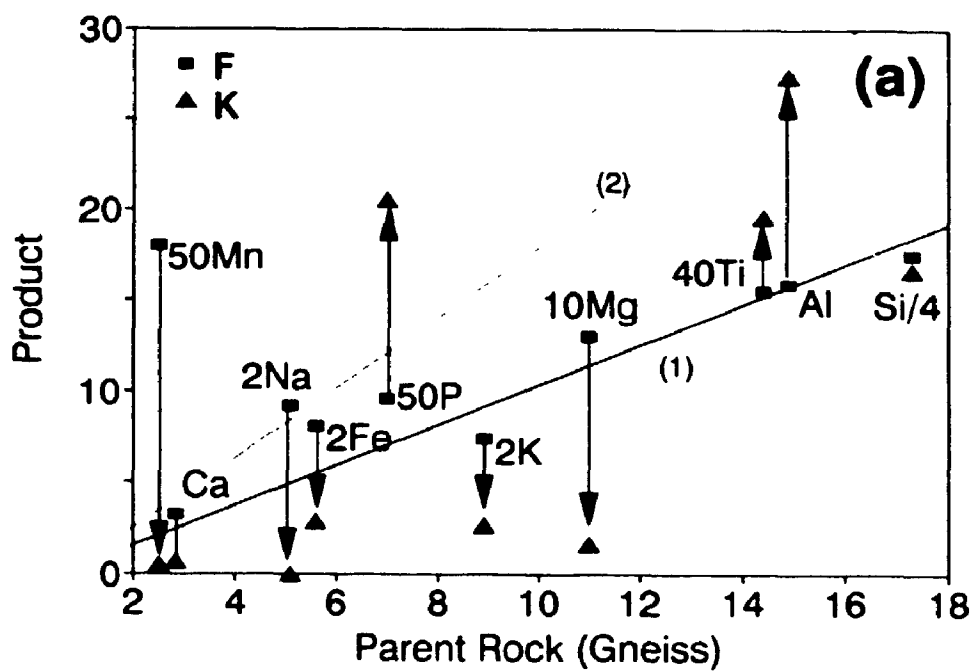
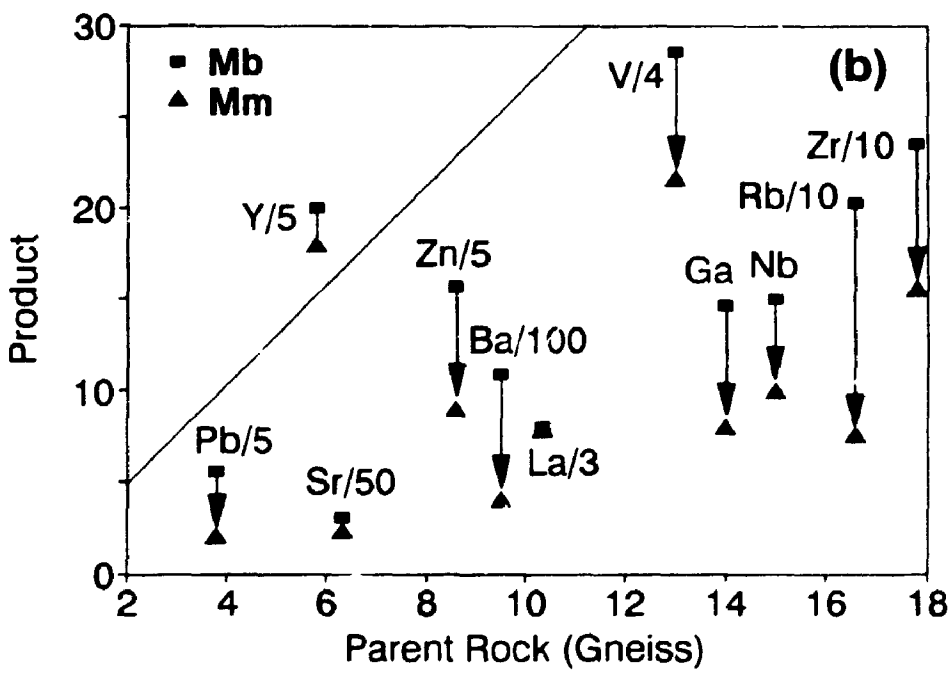
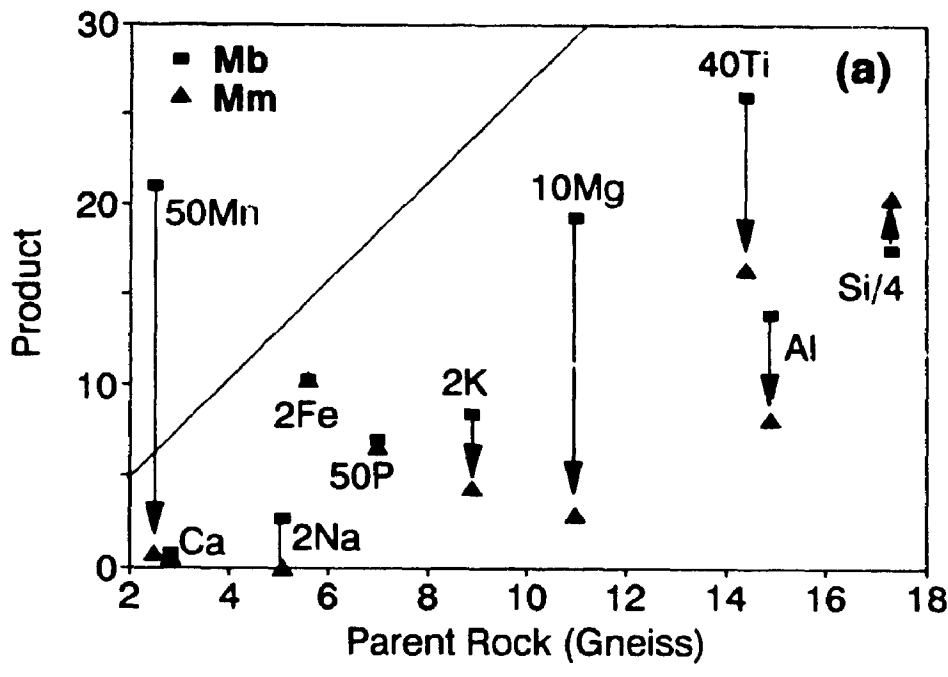


**FIGURE 6-6.** Isocon diagrams for the Muscovite Zone. **(a)** Major element and **(b)** trace element gains and losses in the Muscovite Zone; **Mb**, biotite subzone (filled squares); **Mm**, magnetite subzone (filled triangles). The curves represent volume change of -60%; elements below these curves have been lost, and elements above these curves have been added.





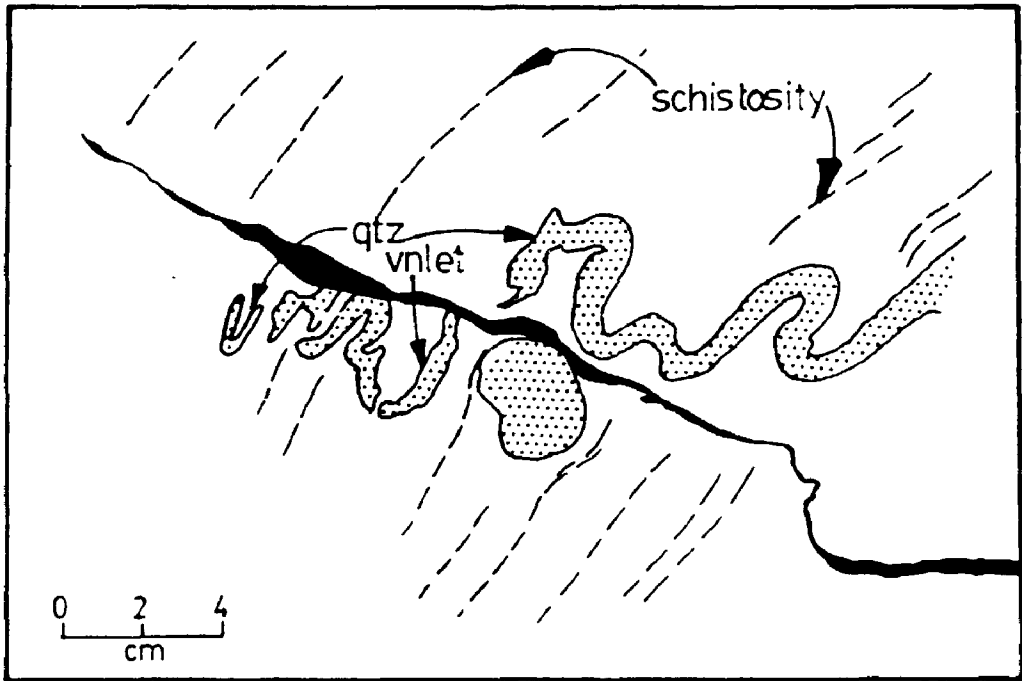
magnetite and, finally, to rutile. Such conversions suggest relative immobility of aluminum and titanium, although the occurrence of kyanite and rutile in fractures and veins suggests at least local movement of  $Al_2O_3$  and  $TiO_2$ . However, on the scale of mineral assemblage variations,  $Al_2O_3$  and  $TiO_2$  can be considered relatively immobile, and calculations were performed assuming constant Ti and constant Al. The calculations assuming constant Ti result in large additions of Al, particularly in the Kyanite Zone. It is difficult to find a source for this aluminum, although the Muscovite Zone is a possible source. The calculations involving constant aluminum are adopted and are discussed below; constant Ti calculations involve slightly less depletion of most elements.

For the mylonitic Muscovite Zone, there is an assumption of a known volume change, based on field evidence. Quartz veinlets are shortened by 60% (Fig. 6-7), which translates to a volume loss of 84%. However, calculations were performed for a volume change of -60%, accepting this as a minimum change. Justification for this comes from Beach (1980) and O'Hara (1988), who suggest a reasonable volume loss of 60% across mylonite zones. A volume loss of 84% results in further depletion of the elements.

### **6.3.2. Compositional changes in the Feldspar and Kyanite Zones.**

The conversion of quartzofeldspathic gneiss of the Tumco Formation to the Feldspar Zone involves a small volume change,

**FIGURE 6-7.** Transposed quartz veinlet in mylonitic Muscovite Zone; tracing from a photograph. Transposition of pre-D<sub>1</sub> quartz veinlet, shows the amount of flattening perpendicular to foliation ( $S_{2A}$ ). Linear shortening of the veinlet is approximately 60%, which translates to a volume decrease of 84%.



at -3%, but significant changes in composition (Fig. 6-8a). Transition metals are uniformly added in large quantities, with increases of 606%, 273%, 111%, 66%, and 37% for MnO, Pb, Zn, V and Fe<sub>2</sub>O<sub>3</sub>, respectively. MgO is approximately constant with a 2% loss. The behavior of the alkali and alkaline earth metals is split along lines of chemical similarity, as Na<sub>2</sub>O, Sr and Ca increase by 76%, 73% and 12%, respectively, whereas Ba, K<sub>2</sub>O, and Rb have respective losses of 12%, 23%, and 36%. Al<sub>2</sub>O<sub>3</sub>, SiO<sub>2</sub>, and TiO<sub>2</sub> have relatively small changes, but the normally "immobile" elements Nb, Zr, and Y have relatively large depletions, at -25%, -27% and -40%, respectively.

In contrast, the conversion of quartzofeldspathic gneiss to granoblastic Kyanite Zone involves a volume reduction of 31%, and losses of all constituents except Al, P, and Ga (Fig. 6-8b). Overall losses of the alkali and alkaline earth metals are slightly greater than those of the transition metals, but both groups have depletions of more than 75%, with 100% of the sodium removed. Zr, Nb, and Y are considerably more depleted than in the Feldspar Zone, with losses of 57%, 62%, and 83%, respectively. P and Ga have increases of 61% and 35%, respectively.

### 6.3.3. Compositional changes in the Muscovite Zone.

In contrast to the Feldspar and Kyanite Zones, conversion of quartzofeldspathic gneiss of the Tumco Formation to the Muscovite Zone involves considerable removal of all elements but MnO and Y (Fig. 6-9). In the biotite subzone of the

**FIGURE 6-8.** Element gains and losses for the Feldspar Zone and Kyanite Zone. (a) Gains and losses during the formation of the Feldspar Zone from the quartzofeldspathic gneiss of the Tumco Formation and (b) Gains and losses during the formation of granoblastic Kyanite Zone from the quartzofeldspathic gneiss of the Tumco Formation.

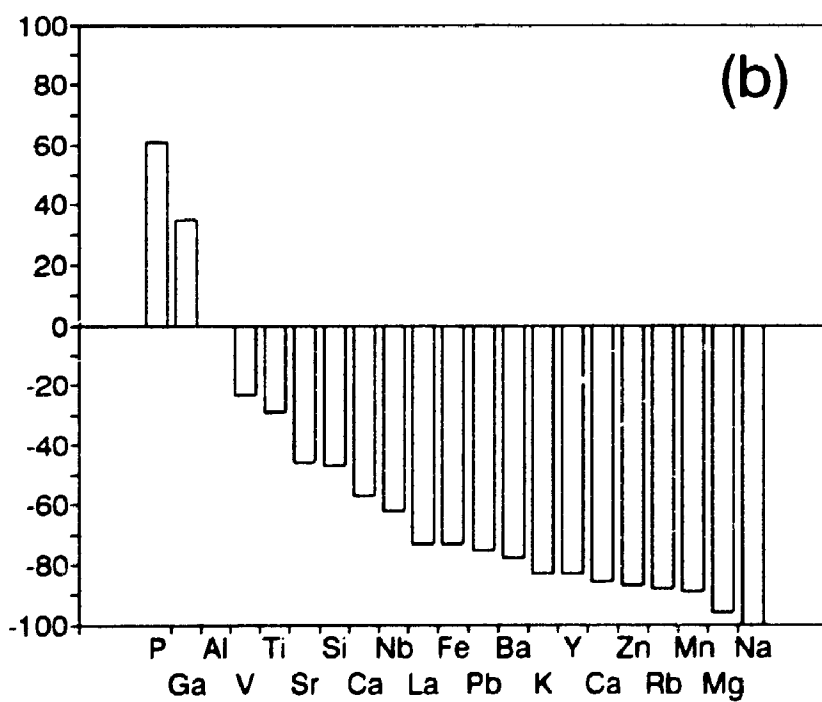
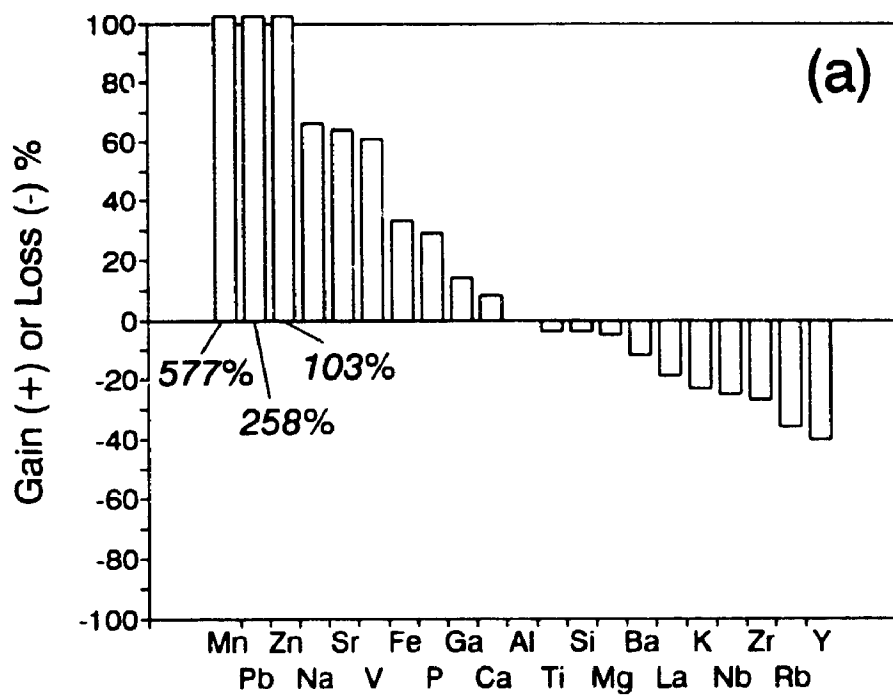
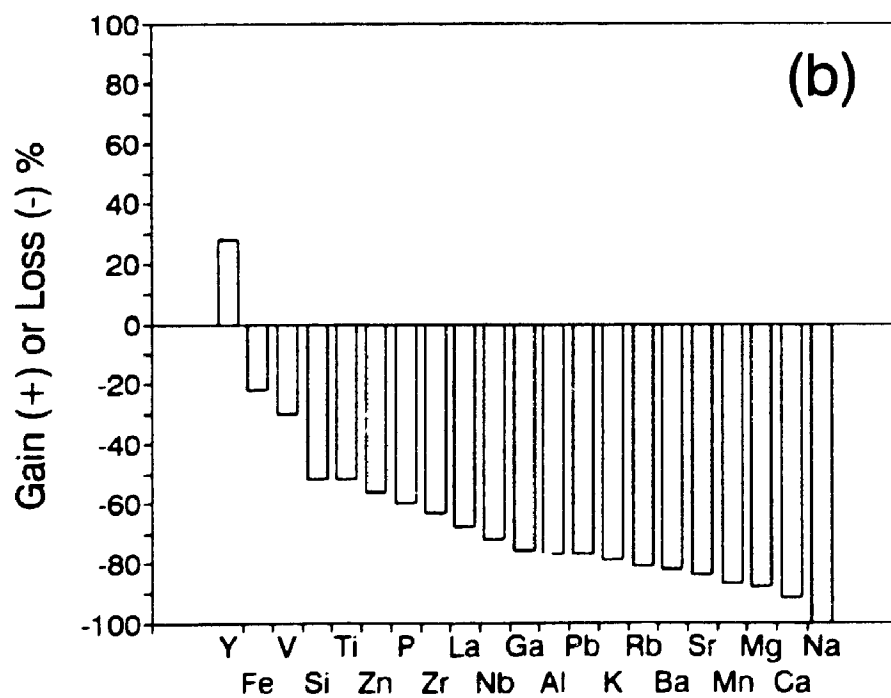
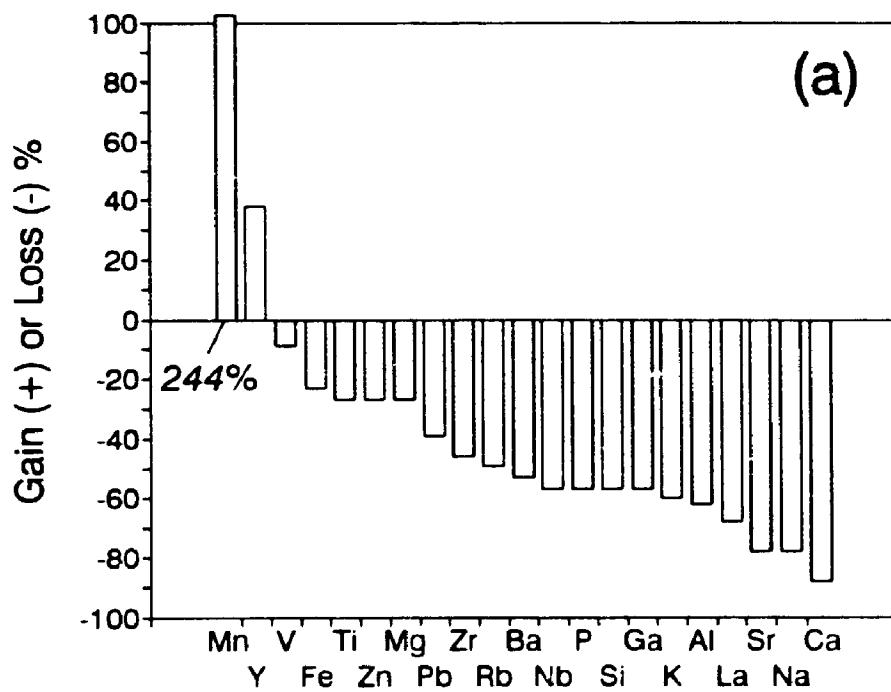


**FIGURE 6-9.** Element gains and losses for the Muscovite Zone.  
**(a)** Gains and losses for the biotite subzone and **(b)** gains and losses for the magnetite subzone.





Muscovite Zone, MnO and Y are enriched, and the transition metals have less overall depletion than the alkali and alkaline earth metals (Fig. 6-9a). Between 30% and 88% of the transition metals have been removed, whereas the alkali and alkaline earth ions have losses between 68% and 100%. Aluminum, phosphorus and gallium are depleted by 62%, 57%, and 57%, respectively. Zr is depleted by 46%, Nb by 57%, TiO<sub>2</sub> by 27%, and SiO<sub>2</sub> by 57%.

With the exception of Fe and Si, depletion of elements is greater in the magnetite subzone than in the biotite subzone of the Muscovite Zone (Fig 6-9b). Mn, which is enriched in the biotite subzone, is depleted by 87% relative to the quartzofeldspathic gneiss of the Tumco Formation. 88% of the MgO, 30% of the V, 77% of the Pb and 56% of the Zn have been removed. Of the alkali and alkaline earth metals, CaO is depleted by 92%, Na<sub>2</sub>O by 100%, K<sub>2</sub>O by 79%, and Sr, Rb, Ba, and La have been depleted by 84%, 81%, 82%, and 68%, respectively. Zr and Nb also have similar depletions, but Y is gained, at 28%, the only element with an increase. Both SiO<sub>2</sub>, at -52%, and Fe<sub>2</sub>O<sub>3</sub>, at -22%, have less depletion than in the biotite subzone.

#### 6.4. Summary.

With some variation, there is an overall decrease in the abundances of most cations from quartzofeldspathic gneiss of the Tumco Formation through the Feldspar and Muscovite Zones to the Kyanite Zone. Al<sub>2</sub>O<sub>3</sub>, TiO<sub>2</sub>, P<sub>2</sub>O<sub>5</sub>, and Ga have large

increases, and  $\text{SiO}_2$  is roughly constant. In general, these variations are reflected in the mineral abundances of the aluminosilicate mineral assemblages. The decrease in alkali and alkaline earth ions is coincident with less feldspar in the Muscovite and Kyanite Zones than in the quartzofeldspathic gneiss of the Tumco Formation and the Feldspar Zone of the aluminosilicate mineral assemblages. Similarly, the greater abundance of aluminum, titanium, and phosphorus in the Muscovite and Kyanite Zones reflect the greater contents of muscovite, kyanite, rutile, and apatite in these zones.

Greater abundances of plagioclase, biotite, and epidote in the Feldspar Zone are mainly the result of the addition of Ca, Na, and Fe, and a minor volume loss. Sr, Mn, Pb, Zn, V, P, and Ga were also added to quartzofeldspathic gneiss of the Tumco Formation to form the Feldspar Zone. In contrast, a significant volume loss occurred in the Kyanite Zone. The assemblage quartz, kyanite, magnetite and rutile is the result of removal of large amounts of alkali, alkaline earth and transition elements. Only  $\text{P}_2\text{O}_5$  and Ga were added, the former resulting in the crystallization of apatite. Although the amount of boron was not determined, the local high contents of tourmaline in the Muscovite and Kyanite Zones, which is absent in the quartzofeldspathic gneiss of the Tumco Formation, indicate boron was added as well. Apatite, lazulite, tourmaline and muscovite locally fixed cations which otherwise would have been removed.

The development of the Muscovite Zone involved a volume

change of at least -60% relative to the quartzofeldspathic gneiss of the Tumco Zone, with removal of all elements except Mn and Y in the biotite subzone, and Y and in the magnetite subzone. Significant quantities of Al, Ga, Ti and P, which were either added to, or relatively immobile in, the Feldspar and Kyanite Zones, were removed from the Muscovite Zone. In addition, there is greater loss of all elements except Si and Fe in the magnetite subzone than in the biotite subzone, indicating the transition from the biotite subzone to the magnetite subzone involved considerable loss of elements. The generally high amounts of tourmaline at this contact suggests the introduction of boron accompanied these changes.

Experimental and theoretical studies show progressive development of aluminous mineral phases and removal of cations may result from reaction between quartz- and feldspar-bearing rocks and hydrous fluids (Hemley, 1959; Hemley and Jones, 1963; Shade, 1974; Helgeson, 1974; Wintsch, 1975b; Wise, 1974; Hemley et. al., 1980), a process known as H<sup>+</sup>-ion metasomatism. Specifically concerned with the Na<sub>2</sub>O-K<sub>2</sub>O-Al<sub>2</sub>O<sub>3</sub>-SiO<sub>2</sub>-H<sub>2</sub>O system, these studies show that a progressive increase in H<sup>+</sup> content, or a decrease in the cation content, of a fluid reacting with a quartz-feldspar rock leads to a shift in mineral stabilities, such that successive stable minerals become enriched in aluminum. At temperatures below 300°C, quartz-feldspar assemblages lead to quartz-muscovite, quartz-pyrophyllite and quartz-kaolinite with progressive cation removal by H<sup>+</sup>-ion metasomatism. Above 300°C, the aluminum-rich end of this

zonation may take the form of other aluminous mineral phases, including andalusite, kyanite, sillimanite and, with less  $\text{SiO}_2$ , corundum (Wise, 1974; Shade, 1974; Wintsch, 1975b; Vernon, 1979 and 1986; Kerrich et. al., 1987). Mineral assemblage zonation in the Cargo Muchacho Mountains, from feldspar-bearing assemblages to muscovite-bearing assemblages to kyanite-bearing assemblages, and the accompanying decrease in most cations, suggests cation-removal was an important process in the development of the zones of aluminosilicate minerals, consistent with an origin by  $\text{H}^+$ -ion metasomatism.

The decussate and poikiloblastic textures in the zones of aluminosilicate mineral assemblages are dispersed and pervasive. Hence,  $\text{H}^+$ -ion metasomatism was pervasive. Rods of granoblastic quartz-kyanite are present in schistose to mylonitic Kyanite Zone, and mylonitic fabrics ( $S_{2A}$ ) cross cut aluminosilicate minerals, indicating pervasive metasomatism was pre- $D_2$ . However, other textures, such as clear kyanite overgrowths on broken, inclusion-rich kyanite in mylonitic Kyanite Zone, and parallelism of elongate minerals, such as tourmaline, to  $S_{2A}$ - $S_{2B}$  intersections, indicate metasomatism continued during  $D_2$ , a conclusion consistent with the large amounts of constituents that were lost from the mylonitic Muscovite Zone. Hence, early pervasive metasomatism and cation removal evolved to later, shear-zone hosted metasomatism and cation removal.

Alkali, alkaline earth and transition elements, which were depleted from the Muscovite Zone and Kyanite Zones during

pervasive metasomatism, were added to the Feldspar Zone. This suggests cation removal from the Muscovite and Kyanite Zones was accompanied by transport of these cations via fluids to, and subsequent precipitation in, the Feldspar Zone, reflected in the relatively high contents of feldspar, biotite and epidote in the Feldspar Zone. Early pervasive metasomatism therefore involved apparent unidirectional fluid flow from the Kyanite Zone to the Feldspar Zone. In contrast, Al, Ga and P, which were either immobile or added to the Kyanite Zone, were lost from the Muscovite Zone, suggesting mylonitization resulted in a change in mineral stability and cation removal. Metasomatism and fluid flow were enhanced in shear zones during D<sub>2</sub>, overprinting the earlier pervasive metasomatism.

**CHAPTER SEVEN -- MINERAL COMPOSITION AND CONDITIONS OF  
ALUMINOSILICATE MINERAL FORMATION.**

**7.1. General Statement.**

Field and textural relationships indicate the zones of aluminosilicate mineral assemblages formed during emplacement of the 173-160 Ma intrusive suite and overlap in time with mylonitization. Bulk rock chemistry, textures and the variation in mineral assemblages indicate hydrous fluids removed major cations from the rocks, resulting in an enrichment of aluminum. Measured mineral composition and theoretical and experimental coexistence of mineral phases provide constraints on the conditions of formation.

**7.2. Pervasive Metasomatism.**

**7.2.1. Bulk Rock Control on Mineral Composition.**

Plagioclase becomes more calcic and aluminous from the quartzofeldspathic gneiss of the Tumco Formation to the Kyanite Zone, a result of coupled substitution of  $Al^{3+}$  for  $Si^{4+}$  and  $Ca^{2+}$  for  $Na^+$  (Fig. 4-3). Similarly, muscovite and biotite also become more aluminous in the same direction (Figs. 4-6 and 4-8). The bulk rock aluminum content of the zones of aluminosilicate mineral assemblages increases from the quartzofeldspathic gneiss to the Kyanite Zone (Fig. 6-1b), suggesting bulk rock control on mineral composition.

Guidotti and Sassi (1976), Guidotti (1984), and Baldelli et al. (1989) have suggested that muscovite composition is particularly sensitive to bulk composition, thus explaining

the trends of aluminum and Fe/(Fe+Mg) in muscovite. However, the Na content of muscovite increases where the bulk rock Na content decreases, from quartzofeldspathic gneiss to the Kyanite Zone. Experimental work in the muscovite-paragonite solid solution series indicates the muscovite-paragonite solvus closes with increasing temperature (Chatterjee and Flux, 1986). Because muscovite becomes less phengitic with an increase in Na, such an interpretation is also consistent with the work of Monier and Robert (1986), which showed that the phengite content of muscovite decreases with increasing temperature. Alternatively, an increase in the Na content of muscovite may be due to an increase in Na activity of the fluid as Na is removed from the bulk rock during metasomatism.

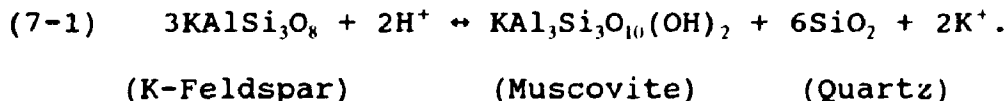
Biotite is also more aluminous and sodic from the quartzofeldspathic gneiss of the Tumco Formation to the Kyanite Zone, suggesting similar controls on composition (Fig. 4-8). However, unlike muscovite, Fe/(Fe+Mg) in biotite decreases from quartzofeldspathic gneiss to the Kyanite Zone (Fig. 4-7 and 4-10). These ratios in biotite suggest increased oxygen fugacity, and is discussed further in section 7.2.3.

#### **7.2.2. Hydrolysis Reactions.**

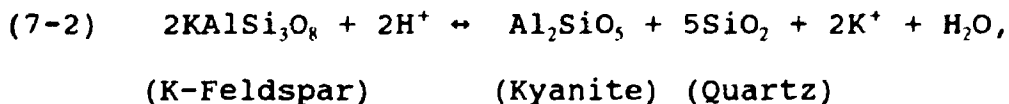
Experimental and theoretical studies of the hydrolysis of silicates are numerous, but the present discussion will be confined to the system  $\text{Na}_2\text{O}-\text{K}_2\text{O}-\text{Al}_2\text{O}_3-\text{SiO}_2-\text{H}_2\text{O}$  (Hemley, 1959; Hemley and Jones, 1963; Shade, 1974; Helgeson, 1974; Wise,



1974; Wintsch, 1975b; Rose and Burt, 1979; Bowers, et. al., 1986). These studies conclude that, given a feldspar-bearing rock in contact with a fluid, progressively lower cation/H<sup>+</sup> in the fluid results in replacement of feldspar by muscovite, which is in turn replaced by a more aluminum-rich phase, either kaolinite, pyrophyllite or one of the polymorphs of Al<sub>2</sub>SiO<sub>5</sub>, depending on temperature (Fig. 7-1). Based on theoretical and experimental data, the K-bearing aluminosilicate minerals in the Cargo Muchacho Mountains, the reactions can be summarized as follows, using end member compositions. Muscovite of the Muscovite Zone may form from K-feldspar of quartzofeldspathic gneiss of the Tumco Formation and of the Feldspar Zone:

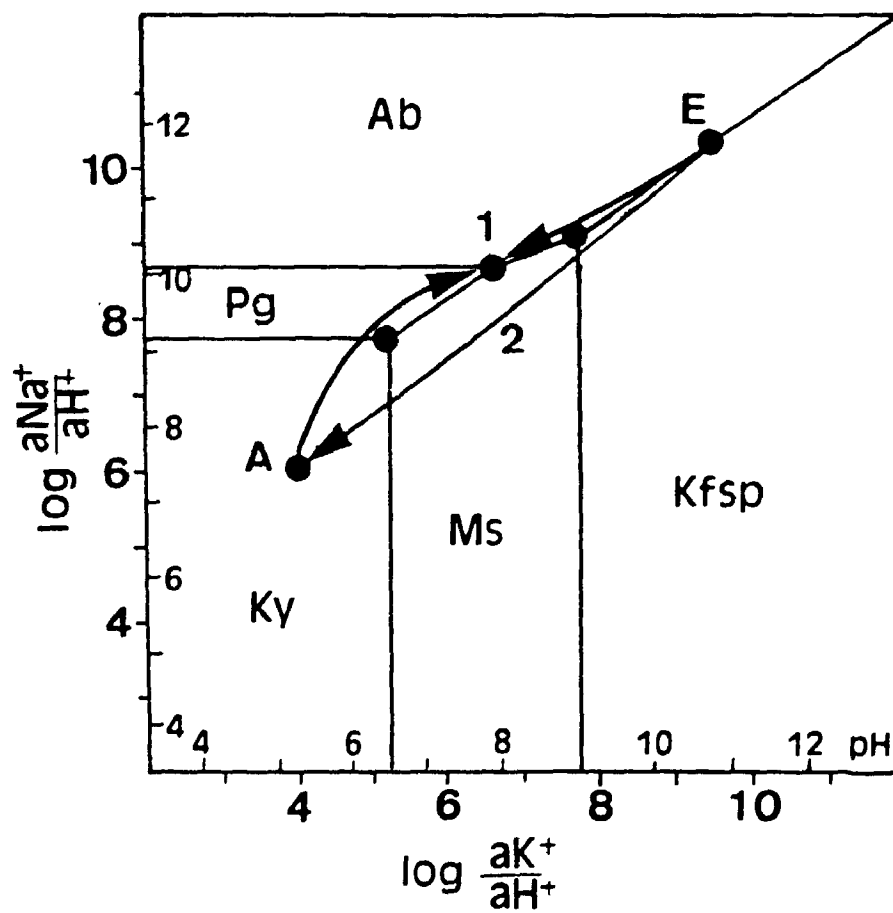


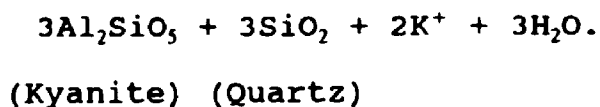
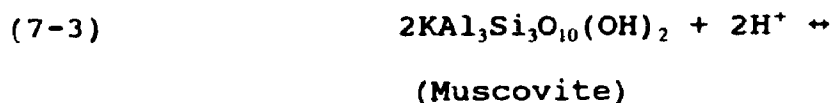
Feldspar of the quartzofeldspathic gneiss and the Feldspar Zone may form kyanite in the Kyanite Zone according to:



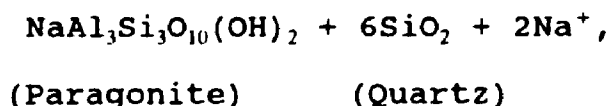
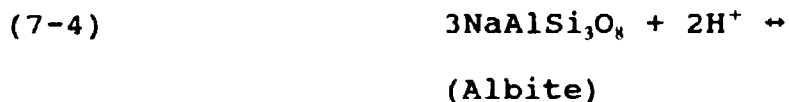
and muscovite of the Muscovite Zone, may form kyanite of the Kyanite Zone according to:

**FIGURE 7-1.** Activity-activity diagram for the system  $K_2O-Na_2O-Al_2O_3-SiO_2-H_2O$ , at  $550^\circ C$  and 5 kb; calculate for an  $H_2O$  activity of 1 using the Supcrt92 program of Johnson et. al. (1992). pH scales on the inside of the diagram along the ordinate and abscissa are calculated as discussed in the text. Mineral abbreviations: **Ab**, albite; **Pg**, paragonite; **Kfsp**, K-feldspar; **Ms**, muscovite; **Ky**, kyanite. The stability of a given mineral phase in contact with an interstitial fluid is governed by cation/ $H^+$  of the fluid. Low ratios indicate either low cation concentration or high  $H^+$  concentration (low pH). A fluid in equilibrium with kyanite (low cation/ $H^+$ ) reacts with a feldspar-bearing rock, removing cations from the rock ( $K^+$  or  $Na^+$  in this instance), and shifting the rock composition toward the muscovite or paragonite stability fields. Transfer of cations from rock to fluid occurs, and if this fluid is static its composition will change toward higher cation/ $H^+$  ratios (Path 1). Convergence of rock and fluid composition may occur at some intermediate point (eg. point 1), and the rock buffers the fluid composition. If there is fluid movement, fluid and dissolved cations are removed from the site of dissolution, and is replaced by new fluid of original (low cation/ $H^+$ ) composition. In this instance, given sufficient fluid, rock compositions will ultimately change to the low cation/ $H^+$  ratios of the fluid (Path 2), and the compositions are fluid buffered.

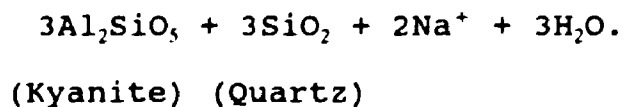
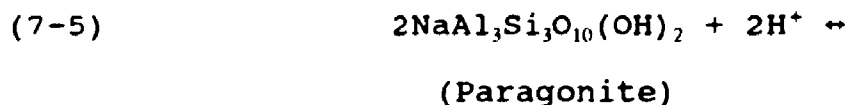




Similar reactions can be written for mineral phases bearing other cations. For Na-bearing phases, the formation of paragonite in the Muscovite Zone from albite of the quartzofeldspathic gneiss and of the Feldspar Zone may occur according to:

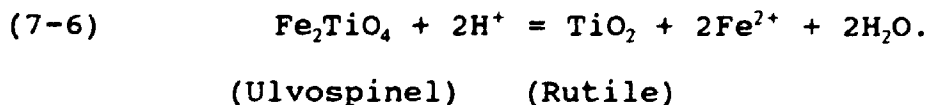


and, for the formation of kyanite of the Kyanite Zone from paragonite of the Muscovite Zone:



The sequence feldspar-mica-kyanite thus represents the forward reactions 7-1 to 7-5, with a progressive liberation of cations,  $\text{SiO}_2$ , and water.  $\text{H}^+$  is consumed in these reactions. In a static fluid this would result in increased cation/ $\text{H}^+$ , leading to stabilization of either muscovite at the expense of kyanite, or feldspar at the expense of muscovite, and the reactions would be buffered by the protolith (Fig. 7-1 and Wintsch, 1975a). Muscovite pseudomorphs feldspar, and foliated muscovite is deflected around feldspar poikiloblasts in pervasive aluminosilicate mineral assemblages. Euhedral kyanite grains cross cut Type 1 muscovite in the Kyanite Zone. The development of the sequence feldspar-muscovite-kyanite requires progressive movement of aqueous fluids with low cation/ $\text{H}^+$  down through the current orientation of the zones of aluminosilicate assemblages at Micatahc and Vitrifax Hills, so that minerals with successively lower ratios overprint earlier ones.

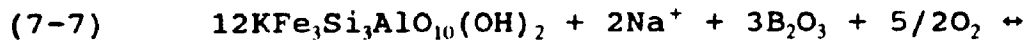
Within the Kyanite Zone, rutile pseudomorphs Ti-magnetite, and this is also an hydrolysis reaction. Taking ulvospinel to represent Ti-magnetite for simplicity, the reaction within the Kyanite Zone may be:



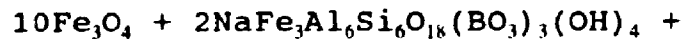
Like the above reactions, water and cations are liberated to the fluids.

### 7.2.3. Oxidation Reactions.

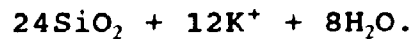
There is a large decrease in biotite across the transition from the biotite subzone to the magnetite subzone in the Muscovite Zone, which represents a change in the oxidation state of iron. The transition from biotite-bearing assemblages to magnetite-bearing assemblages in the Muscovite Zone occurs with an anomalous concentration of tourmaline, suggesting the addition of boron played a role in this process. Using end member compositions, the conversion of biotite to tourmaline and magnetite in the Muscovite Zone may occur according to:



(Annite)



(Magnetite)                      (Tourmaline)

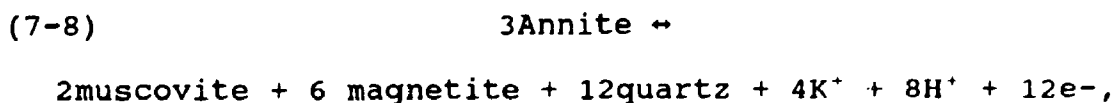


(Quartz)

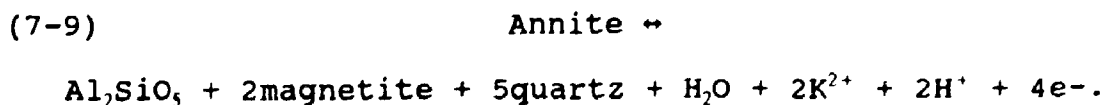
Like the hydrolysis reactions, large amounts of potassium,  $\text{SiO}_2$  and  $\text{H}_2\text{O}$  are liberated from the rocks during oxidation. The reaction fixes iron, however, and involves the uptake of sodium, and to a lesser extent, Ca and Mg, which is observed in analyses of tourmaline.

The pronounced decrease of Fe/(Fe+Mg) in biotite of the quartzofeldspathic gneiss through the Feldspar and Muscovite Zones to the Kyanite Zone also indicates oxidation. Smaller ratios have been noted in biotite of hydrothermal origin relative to biotite of magmatic origin in porphyry copper deposits, and have been interpreted as progressive oxidation (Moore and Czamanske, 1973; Jacobs and Parry, 1979; Bowman, et. al., 1987). There is a decrease in Fe/(Fe+Mg) in ferromagnesian minerals as iron is oxidized during differentiation in magmas, where increasing oxygen fugacity and ferric iron results. Magnetite forms, and biotite is richer in Mg (Czamanske and Wones, 1973; Mason, 1978; Chivas, 1981).

The experimental studies of Wones and Eugster (1965) and Rutherford (1972) show that, in the presence of magnetite and quartz, and either sanidine, muscovite or one of the Al<sub>2</sub>SiO<sub>5</sub> polymorphs, the annite component of biotite decreases with progressive oxidation. Thermodynamic calculations by Wintsch (1980 and 1981), showed similar results:



and



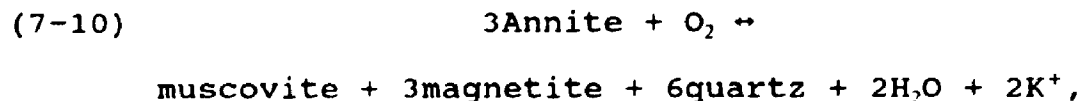
Variation in the annite component of biotite results in the adjustment of proportions of other minerals formed. In general, progressively less annite content is stable in biotite with greater oxidation (Fig. 7-2).

#### 7.2.4. pH of Fluids Affecting Hydrolysis and Oxidation.

Calculated pH for fluids included in the foregoing hydrolysis reactions are in Fig. 7-1 (small numbers on the inside of the axes of the graph). Calculations use the equilibria of reactions 7-1 through 7-5, assuming  $\text{Na}^+$  and  $\text{K}^+$  activities of  $5 \times 10^{-3}$  and  $4 \times 10^{-2}$ , respectively, from fluid inclusion data of Rankin et. al. (1992) and Bennet and Barker (1992). This assumes ideal activity-concentration relationships. Fluids forming the kyanite-bearing rocks were moderately alkaline, with pH less than 8, consistent with the stability of magnetite in the assemblages.

#### 7.2.5. Oxygen Fugacity.

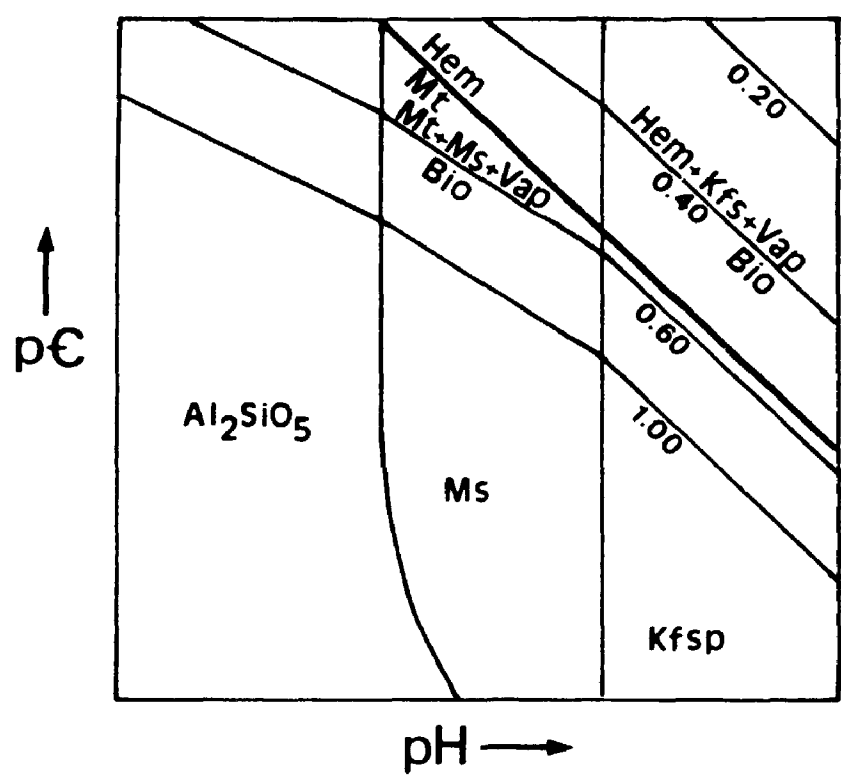
The following reactions set lower and upper limits on oxygen fugacity for the zones of aluminosilicate mineral assemblages:



and



**FIGURE 7-2.** Annite composition as a function of oxidation potential and pH; from Wintsch (1980). Oxidation potential increases toward the top along the ordinate, pH increases toward the right on the abscissa. Mineral abbreviations: Ms, muscovite; Kfsp, K-feldspar; Hem, hematite; Mt, magnetite; Bio, biotite; Vap, water vapor. The bold diagonal line separates the stability field of hematite on the upper right from the stability field of magnetite on the lower left. Finer diagonal lines represent reaction boundaries between the assemblages hematite-K-silicate-water or magnetite-K-silicate-water on the upper right side of the boundaries and biotite on the lower left side. The numbers on the diagonals are the mole fraction of annite in biotite. With increasing oxidation potential, the annite component of biotite decreases.





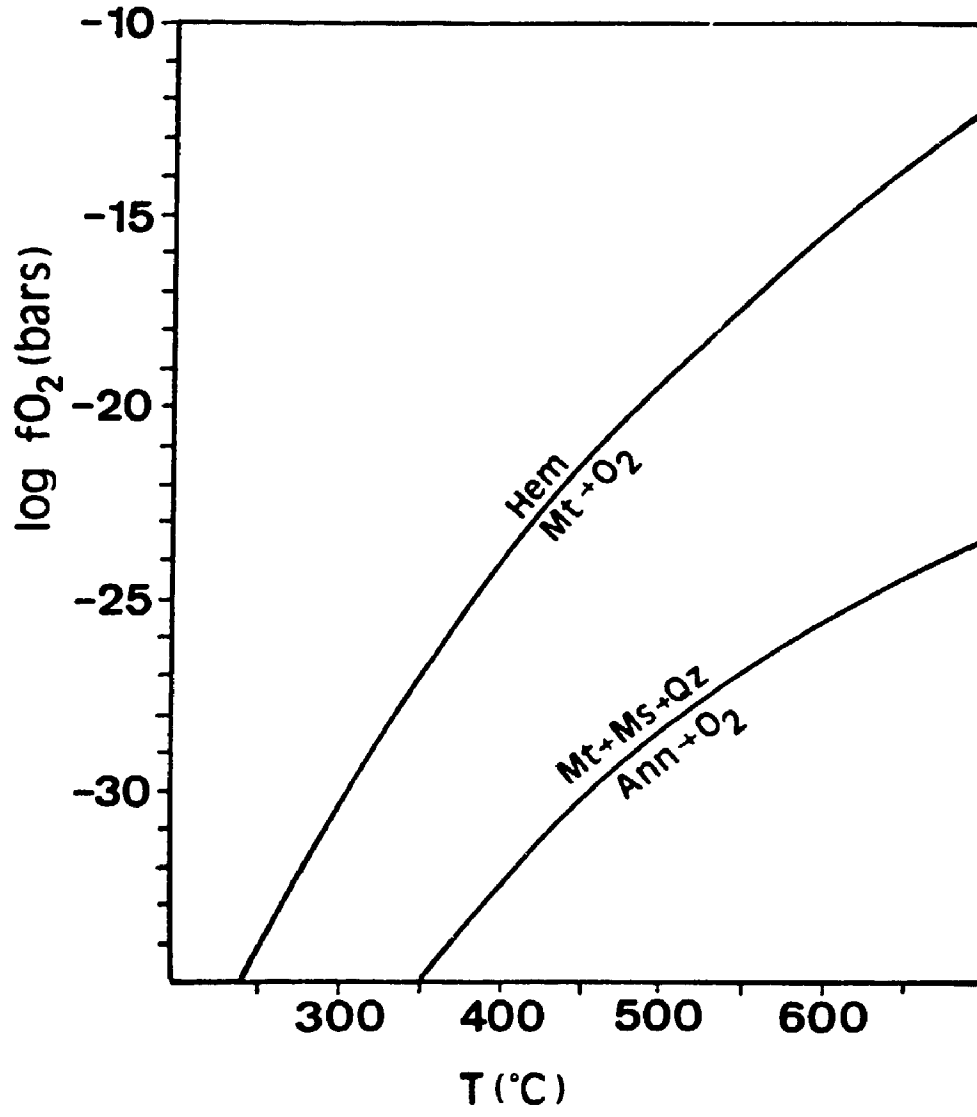
Reaction 7-10 is a modified version of reaction 7-8 (Wintsch, 1980 and 1981). The equilibrium constant for the reaction,  $K_{10} = 25.697$  (calculated according to Johnson et. al., 1992), is defined by:

$$(7-12) \quad \log K_{10} = 2\log(aK^+) + 2\log(fH_2O) - \log(fO_2).$$

This assumes unit activity for water, and reduces the equation to two unknowns. Potassium activity is assumed as in the pH calculations. Accordingly, oxygen fugacity equals approximately  $10^{-27}$  bars at 500°C and 5 Kb, similar to the results of Beane (1974 and 1982) for alteration in porphyry copper deposits. Because pure annite is used in the calculations, which is the most reduced composition, this is inferred to represent a minimum.

Oxygen fugacity calculated according to reaction 7-11 must represent a maximum as magnetite is stable in all mineral zones. For 5 Kb and 500°C, this reaction has  $fO_2 = 10^{19}$  bars. Hematite typically occurs as a replacement of magnetite along rims and fractures. The timing is unknown, and could be very late. Because there is a direct relationship between  $\log(fO_2)$  and temperature (Fig. 7-3), these late hematite rims and fracture fillings do not require a great increase in  $fO_2$ , as a decrease in temperature will suffice. However, the presence of euhedral specularite in schistose Kyanite Zone adjacent to

**FIGURE 7-3.** Temperature- $\log(fO_2)$  diagram for the relationships discussed in the text. Maximum and minimum  $fO_2$  are constrained by the two curves at 550°C. Abbreviations: Hem, hematite; Mt, magnetite; Ms, muscovite; Qz, quartz; Ann, annite.



muscovite-biotite granite suggests that oxygen fugacities were above  $10^{-19}$  bars at least locally.

### **7.3. Mylonite-Hosted Metasomatism.**

#### **7.3.1. Mineral Composition.**

The increase in Ca content of plagioclase has been suggested as a response to bulk rock Al content. However, the presence of unstrained, polygonal grains in schistose to mylonitic Muscovite Zone suggests the increase in Ca content may at least in part be due to deformation along shear zones. Allison et. al. (1979), Brodie (1981), Olsen et. al. (1985) have shown that recrystallized plagioclase in mylonites may be either more sodic or calcic than that in its protolith, depending on the composition of the protolith.

Compositional zoning in tourmaline is thought to be an indicator of changing fluid and rock compositions (Henry and Guidotti, 1985; Slack and Coad, 1989; King, 1987). Tourmaline in the Cargo Muchacho Mountains is repetetively zoned only in schistose to mylonitic Muscovite Zone of Domain 2; such zoning is absent in the coarse tourmaline of granoblastic Kyanite Zone of Domain 3. Repetitive zoning in tourmaline is thus thought to be related to mylonitization in the shear zones of Domain 2. However, compositional zoning in tourmaline in the Cargo Muchacho Mountains includes overall core-to-rim increases in Al, Fe and Ti, and decreases in Mg and Ca (see Figs. 4-11 and 4-12). Such zoning may reflect the increase in bulk rock Al and Ti, and decrease in bulk rock Mg and Ca, as

metasomatism proceeded.

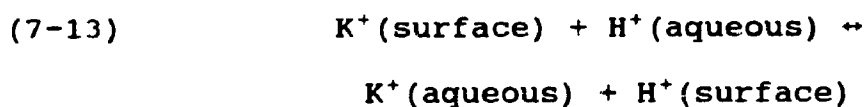
### 7.3.2. Deformation-Induced Mineral Reaction.

The pronounced orientation of prismatic tourmaline and apatite in the plane of  $S_2$ , inclusion-free kyanite overgrowths on poikiloblastic kyanite, and the alignment of rectangular magnetite along the limbs of  $D_2$  microfolds, suggest continued development of aluminosilicate minerals during  $D_2$ . Aluminum and gallium and phosphorus, which were unchanged in or added to granoblastic Kyanite Zone are depleted from mylonitic Muscovite and Kyanite Zones (Chapter 6). Hence, in mylonitic fabrics, there is reverse of reactions 7-2 and 7-5, and continuation of forward reactions 7-1 and 7-4; that is, the production of muscovite at the expense of feldspar and kyanite.

As noted by Spry (1969), Wintsch (1975a), Lister and Snoke (1984), the most significant effect mylonitization has on mineral transformation, apart from the generation of strong preferred crystallographic orientation, is a reduction of grain size. In addition, the number of dislocations and microfractures in strained grains is increased over that of unstrained grains (Wintsch and Dunning, 1985). The surface area available for reaction with interstitial fluids is increased, and the free energy is increased, reducing mineral stability and increasing solubility, promoting reaction (Brodie, 1980; Wintsch 1985).

The effects of decreasing grain size and increasing

available surface area are important for controlling fluid composition (Stevens and Carron, 1948; Wintsch, 1975a and 1981). Most common silicate minerals, when crushed in distilled water, cause an increase in the pH of the fluid (Stevens and Carron, 1948). Wintsch (1975a and 1981) interpreted this as a result of surface exchange of  $H^+$  in the fluid for cations on newly exposed grain surfaces:



As Wintsch (1975a) notes, the equilibrium constant for the exchange of  $H^+$  for  $K^+$  on mineral surfaces (reaction 7-13) at STP is  $10^{9.5}$  for sanidine, and  $10^{7.4}$  for muscovite. The reaction thus goes to completion, unless  $K^+/H^+$  is on the order of 25 million to one. With reduction in grain size there is concomitant increase in surface area and availability of new cationic sites for substitution by  $H^+$ . This reduces the  $H^+$  ion concentration in the fluid, and leads to an increase in the cation/ $H^+$  ratios of the fluid. Feldspar growth is promoted at the expense of mica or mica at the expense of kyanite (see Fig. 7-1).

The depletion of aluminum in the Muscovite Zone may be caused by such a process. Al-oxide is relatively stable at middle pH ranges, but becomes more soluble with a rise or drop from neutral pH (Sokolova and Khodakovskiy, 1977; Stoffregen, 1987). An increase in fluid pH would result from the uptake



of  $H^+$  onto surface sites according to reaction 7-13. The solubility of Al is controlled by the availability of alkali ions not associated with Cl (Anderson and Burnham, 1983; Kerrick, 1988). Low Cl abundance in mica and tourmaline (see Figs. 4-8 and 4-12) suggest low Cl concentrations in the interstitial fluids at Micatahc Hill.

#### **7.4. Evidence for a Magmatic Component to the Fluids.**

Hornblende-biotite granodiorite cross cuts the zones of aluminosilicate mineral assemblages at Micatahc Hill, with distinct mineral assemblage variation (Fig. 3-6). Toward muscovite-biotite granite, mineral assemblages in hornblende-biotite granodiorite are: 1.) oligoclase-microcline-biotite-quartz-epidote, 2.) oligoclase/-andesine-biotite-quartz-magnetite-garnet, and 3.) andesine/labradorite-hornblende-quartz-magnetite. This mineral assemblage variation is consistent with thermal metamorphism of hornblende-biotite granodiorite by muscovite-biotite granite.

However, the decrease in K-bearing mineral phases in hornblende granodiorite toward muscovite-biotite granite implies removal of potassium, suggesting this metamorphism was not isochemical. There is also a concomitant decrease in epidote abundance, an increase in the Ca-content of plagioclase and abundance of plagioclase, and a decrease in biotite  $Fe/(Fe+Mg)$  in hornblende granodiorite toward muscovite-biotite granite. In addition, magnetite becomes stable closer to muscovite-biotite granite. These changes are similar to those

in the zones of aluminosilicate mineral assemblages, and suggest similar hydrolysis and oxidation reactions.

Cameron and Hattori (1987) have suggested that the most likely sources for oxidizing fluids at moderate to deep crustal levels are late stage magmatic fluids. Local large abundances of tourmaline and apatite, the main boron and phosphorus-bearing minerals, in the zones of aluminosilicate mineral assemblages, and the persistent relationship to peraluminous, two-mica granites (granite porphyry and muscovite-biotite granite) suggest a magmatic component to the fluids (Strong, 1989). Furthermore, Whitney (1988) has shown that porphyritic textures may be developed over a small temperature interval in water-rich felsic magmas at high pressure, without a need to rise to shallow depths, thus providing a mechanism for the porphyritic texture of granite porphyry. Although the relationships are less clear at Hedges, the persistent zonation of tourmaline and apatite abundances at these sites suggests similar origins for all three aluminosilicate mineral occurrences.

#### **7.5. Pressure and Temperature.**

Garnet-biotite equilibria are used to estimate temperatures of aluminosilicate mineral formation after Ferry and Spear (1978), Ganguly and Saxena (1984), and Williams and Grambling (1990). The accurate use of such equilibria requires that the phases involved crystallized at the same time, that they were in equilibrium at the time of formation,

and that no post-crystallization structural or chemical changes have occurred. In most instances, however, this is difficult to ascertain, and equilibrium is assumed where there are no textures which dispute the above assumptions. Independent estimates of pressure are required, although this particular geothermometer is relatively insensitive to pressure. For instance, a change in pressure by 1 Kb involves calculated temperature differences of less than  $10^{\circ}$  at  $550^{\circ}\text{C}$  for the garnet-biotite thermometer.

Myrmekitic textures in feldspars in all feldspar-bearing assemblages, and the peristerite composition of plagioclase in quartzofeldspathic gneiss of the Tumco Formation, suggest exsolution has occurred. The use of traditional two-feldspar thermometers are probably not valid considering the presence of these post-crystallization textures (Whitney and Stormer, 1977; Brown and Parsons, 1981; Haselton et. al. 1983; Price, 1985; Fuhrman and Lindsley, 1988). However, the ternary model of Fuhrman and Lindsley (1988) provides a mechanism for determination of equilibrium compositions and temperatures through an iterative procedure, which is briefly described in Appendix C. The model searches for compositions within analytical error (2 mole %) and calculates temperatures for these compositions. If the calculated temperatures and compositions occur outside of accepted limits, they are rejected.

Three garnet-biotite geothermometers are compared here: the original experimentally-derived formulation of Ferry and Spear (1978) and the revised formulations of Ganguly and

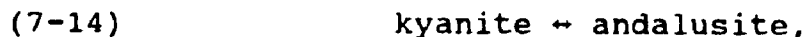
Saxena (1985) and Williams and Grambling (1990). The first considers only the exchange of Fe and Mg between biotite and garnet, whereas the formulation of Ganguly and Saxena (1984) takes into account the added components Ca, Mn and Ti in garnet. Williams and Grambling (1990) add the effects of Ti and ferric iron in biotite. Brief descriptions of these equilibria are given in Appendix C.

Because it cannot be determined by microprobe analysis, estimation of ferric iron content is required for the Williams and Grambling (1990) formulation. Their method for estimating the ferric iron content of biotite in the absence of chemical analyses, is through co-existing ilmenite-hematite solid solutions. In the Cargo Muchacho Mountains, ilmenite only occurs as exsolution lamellae in magnetite, precluding accurate estimation of ferric iron content of biotite via this method. Instead, estimation is based upon previously published Mossbauer spectra of metamorphic biotite, which indicate that the ferric iron content in biotites from metapelites ranges from 5% in graphite-bearing assemblages to well above 20% in hematite-bearing assemblages (Dyar, 1990). Magnetite-bearing rocks contain biotite with ferric iron comprising 20% or less of the total iron, and this is used as a reasonable value. A 10% change in the mole fraction of  $\text{Fe}^{3+}$  leads to a temperature difference of about  $40^\circ$  at  $600^\circ\text{C}$ . It seems unlikely, given the data of Dyar (1990), that ferric iron would deviate more than 20% in the magnetite-bearing assemblages at Micatalc. A change of a few % ferric iron in either direction makes errors

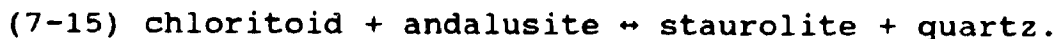
on the order of 15°C in either direction, which is within acceptable limits.

#### 7.5.1. Pressure.

Hayes (1989) concluded that the quartz diorite, 173 Ma and older than the development of the zones of aluminosilicates, crystallized at 6 Kb according to aluminum-in-hornblende geobarometry. The presence of crack-seal fabrics in the Feldspar Zone may indicate lower pressures (Ramsay and Huber, 1988), and 6 Kb is considered a maximum. However, the coexistence of staurolite with kyanite in the Kyanite Zone, indicates minimum pressures of about 4 Kb, constrained by the following reactions:



and



A minimum pressure of 4 Kb is therefore inferred to have prevailed during the formation of the aluminosilicate minerals. For the temperature calculations, an average pressure of 5 Kb is assumed, corresponding to a depth of about 18 Km. The small to absent thermal aureoles around the intrusive rocks suggest mesozonal to catazonal emplacement of the intrusive (Barton et. al., 1988), consistent with the above estimates.

### 7.5.2. Two-Feldspar Geothermometry.

The wide variation in results confirm the feldspars either were not in equilibrium or underwent post-crystallization structural and/or compositional changes (Table 7-1). Failure of the compositions to converge within 2 mole % (the analytical error) resulted in the rejection of 75% of the calculations. In muscovite-biotite granite, this failure is attributed to subsolidus albitization and muscovitization. In the Feldspar Zone, the occurrence of K-feldspar is sporadic, and is thought to represent relict prophyroblasts formed at an earlier stage of metasomatism (Chapter 4).

Only 30% of the calculated temperatures for quartzofeldspathic gneiss of the Tumco Formation gave results that were not rejected, and one of these is relatively low at 294°C. This is considered too low for the ambient conditions. The other two temperatures are higher, at 434°C and 407°C, and probably represent regional metamorphic temperatures. Half of the temperatures from hornblende granodiorite which cross cuts the Feldspar Zone were concordant, and are slightly higher than those from the quartzofeldspathic gneiss of the Tumco Formation, from 465° to 475°C.

### 7.5.3. Garnet-Biotite Thermometry.

Data from the Muscovite Zone, Kyanite Zone and hornblende granodiorite are summarized in Table 7-2, and sample locations shown on Fig. 7-4. Highest temperatures, with a mean of 617°C, are recorded from medial hornblende granodiorite,

TABLE 7-1  
Two-feldspar Geothermometry according to Fuhrman and Lindsley  
(1988).

Lithology	K-fsp, Plag <sup>1</sup>	Temperature <sup>2</sup>
Quartzofeldspathic Gneiss	1,54	434
	3,57	407
	1,55	(714)
	4,58	294
	4,61	(300)
	5,62	(290)
	3,62	(302)
	7,64	(446)
	6,54	(478)
	7,63	(290)
Feldspar Zone	18,20	413
	19,22	(312)
	21,23	(292)
	26,25	(647)
	37,35	(306)
	37,38	(311)
	9,39	(530)
	10,41	(482)
	13,47	(513)
Granite gneiss	15,66	(411)
	16,71	(417)
	17,86	(481)
Granodiorite Gneiss	21,112	466
	20,104	(546)
	19,103	(304)
	26,113	(466)
	23,113	475
	22,112	465

<sup>1</sup> K-feldspar and plagioclase analysis numbers can be referred to Appendix 3.

<sup>2</sup> Calculated temperatures in parentheses are rejected because compositions failed to converge.

**TABLE 7-2.** Calculated temperatures for samples from thermally metamorphosed granodiorite and from the Muscovite Zone and the Kyanite Zone. Inferred pressure is 5 Kb.

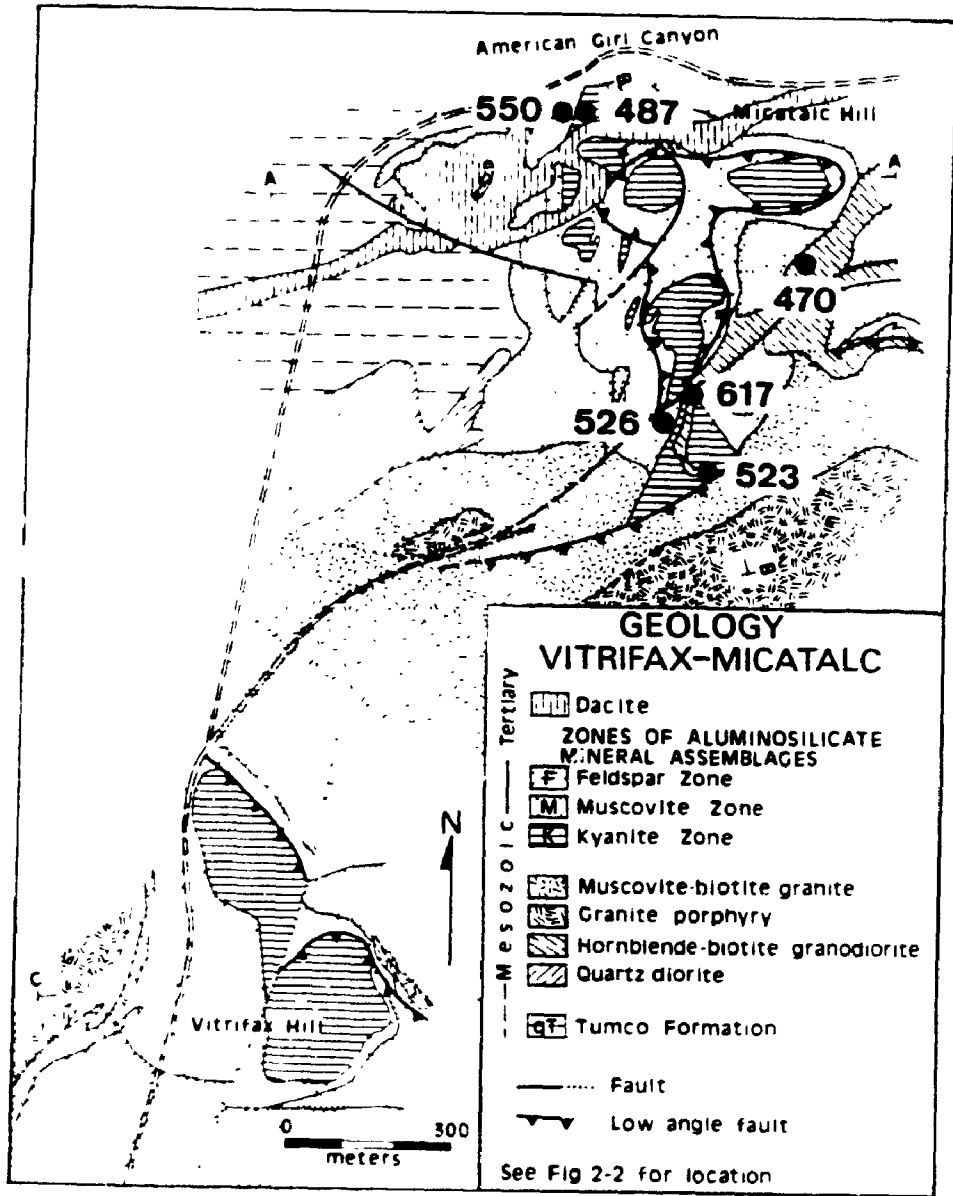
Garnet, <sup>1</sup> Biotite Pair	Temperature(°C) <sup>2</sup>			Garnet, Biotite Pair	Temperature(°C)		
	(1)	(2)	(3)		(1)	(2)	(3)
<u>MT4-3-1286, Granodiorite</u>				<u>B0430-4, Muscovite Zone</u>			
(1;91-1)	589	637	644	(29;91-30)	576	588	596
(3;91-3)	554	602	610	(29;91-31)	569	581	588
(4;91-4)	579	625	632	(31;91-32)	537	559	559
(5;91-5)	581	631	637	(32;91-33)	550	565	569
(6;91-6)	585	629	634	(33;91-34)	550	567	573
(8;91-8)	566	612	617	(34;91-36)	562	570	574
(9;91-9)	571	615	623	(35;91-35)	559	573	578
(9;91-11)	551	601	609	(36;89-68)	531	567	573
(11;91-12)	555	608	611	(37;89-70)	518	540	543
(11;91-14)	543	595	599	(38;89-71)	512	534	539
(14;91-17)	554	605	608	(39;89-75)	519	539	544
(14;91-18)	558	608	611	(40;89-76)	513	531	533
(16;91-19)	561	606	619	(41;89-80)	539	558	561
<u>B0628-1, Granodiorite</u>				(42;89-81)	525	547	551
(18,91-20)	498	507	532	(43;89-83)	533	548	552
(20,91-22)	483	501	521	(44;89-84)	526	546	546
(20,91-23)	525	544	562	(45;91-4)	533	555	557
(22,91-24)	459	499	511	(46;91-5)	547	563	562
(22,91-25)	474	515	525	<u>B0430-3, Kyanite Zone</u>			
(24,91-26)	539	539	567	(47;91-48)	465	500	509
(24,91-27)	531	531	559	(47;91-49)	476	512	520
<u>MT2-3-1286, Muscovite Zone</u>				(49;91-50)	404	474	472
(26;28)	448	513	507	(51;6)	398	478	478
(26;29)	469	535	527	(52,6)	414	479	479
(27;28)	456	520	514	(53,7)	378	464	461
				(54,8)	397	479	476
				(55,9)	413	489	487

<sup>1</sup> Garnet and biotite analyses can be found according to sample number in Appendix C.

<sup>2</sup> Columns represent temperatures calculated according to (1) Ferry and Spear (1978), (2) Ganguly and Saxena (1984) and (3) Williams and Grambling (1990).



**FIGURE 7-4.** Location of samples used in temperature calculations. Temperatures are in degrees centigrade. Map symbols as in Fig. 3-1.



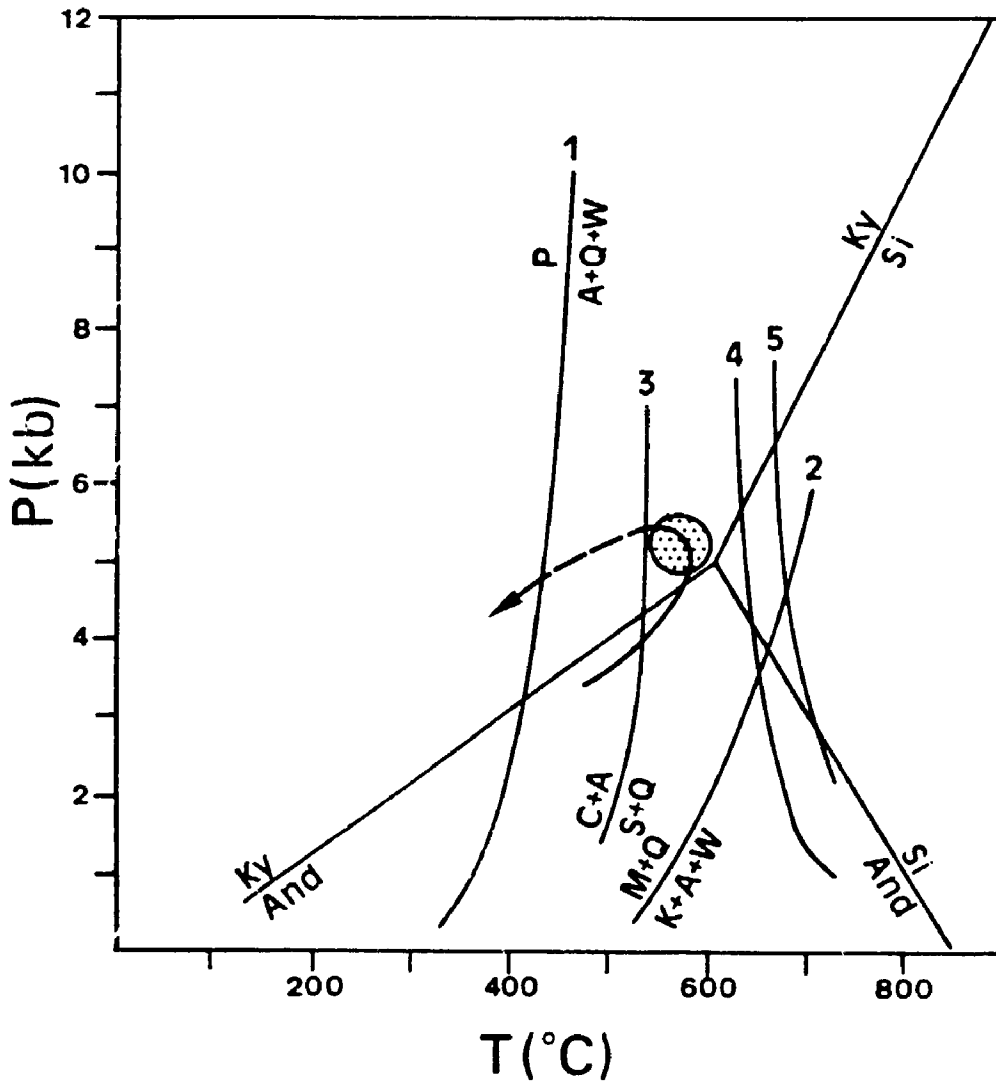
located about 100 m from the contact with muscovite-biotite granite. Those from hornblende granodiorite adjacent to muscovite-biotite granite, however, are considerably lower, averaging 523°C. Temperatures from the Muscovite Zone average 550°C, although lower temperatures, averaging 526°C, occur in the Muscovite Zone closer to muscovite-biotite granite (Fig. 7-4). Temperatures from the Kyanite Zone record the lowest garnet-biotite temperatures, averaging 487°C.

#### 7.5.4. Interpretation of Thermometry.

At Micatalc Hill, the aluminosilicate assemblages formed at temperatures exceeding 500°C, at pressures greater than 4 Kb (Fig. 7-5). However, temperatures are variable within the aluminosilicate mineral assemblages, and the average temperature from the single sample of granoblastic Kyanite Zone, at 487°C, is more than 60°C lower than that calculated for nearby Muscovite Zone, at 550°C. The lower temperatures calculated for the Kyanite Zone are probably the result of the unusual composition: they contain staurolite, biotite and garnet, which are rare in the Kyanite Zone. In addition, the garnets are enriched in Mn, which, because of the definition of  $K_{11}$ , gives lower calculated temperatures.

Lowest temperature in hornblende granodiorite occurs where it cross cuts the Feldspar Zone, at 471°C according to two-feldspar thermometry. Here, hornblende granodiorite contains coarse feldspar poikiloblasts suggestive of thermal or metasomatic overprint. Highest average temperature, 617°C,

**FIGURE 7-5.** Pressure-temperature diagram for the kyanite-bearing rocks in the Cargo Muchacho Mountains. Stippled area represents inferred conditions of formation based on mineral equilibria; arrow represents the inferred progression of P-T conditions based on textural relationships of andalusite, muscovite and pyrophyllite. Mineral abbreviations: P pyrophyllite; A,  $Al_2SiO_5$ ; C, chloritoid; S, staurolite; Q, quartz; M, muscovite; K, K-feldspar; Ky, kyanite; And, andalusite; Si, sillimanite; W, water. Sources are: Aluminum silicate triple point (Richardson et. al., 1969), Reaction 1 (Haas and Holdaway, 1973); Reaction 2 (Kerrick, 1972); Reaction 3 (Richardson, 1968); Reactions 4 and 5 are minimum melting boundaries for hydrous and anhydrous granite, respectively.



occurs in hornblende granodiorite where it contains coarse granoblastic textures, indicative of thermal metamorphism by muscovite-biotite granite. Hornblende granodiorite adjacent to muscovite-biotite granite has lower temperatures, averaging 523°C. The relatively low temperatures are attributed to post-mineral reaction as indicated by the presence of late muscovite-chlorite-pyrite veinlets. In addition, recrystallized, polygonal plagioclase indicate D<sub>2</sub>-style mylonitization has affected the granodiorite here.

The temperatures calculated for the quartzofeldspathic gneiss of the Tumco Formation, although limited in number, suggest temperatures of about 400°C to 430°C. This is consistent with the mineral assemblage quartz-plagioclase-biotite-epidote-magnetite, and is considered a reasonable estimate for regional metamorphic temperatures in the area. Pervasive replacement was therefore a thermal metasomatic event, occurring during emplacement of the 173-160 Ma intrusive suite, at a depth of about 18 Km. Metasomatism continued with D<sub>2</sub> deformation, focussed along shear zones. Reaction with late, lower temperature fluids along shear zones resulted in post-crystallization cation-exchange.

#### **7.6. Summary.**

Measured mineral composition and theoretical and experimental mineral equilibria indicate the zones of aluminosilicate mineral assemblages in the Cargo Muchacho Mountains formed from oxidizing, aqueous fluids. Hydrolysis reactions

account for the gross mineral zonation and depletion of constituents from the rocks, whereas variation in Fe-bearing mineral phases record progressive oxidation. Oxidizing fluids are characteristic of late magmatic fluids, an interpretation consistent with the boron and phosphorus content, as indicated by tourmaline and apatite, in the metasomatic rocks.

The aluminosilicate assemblages formed at temperatures and pressures above 500°C and 4 kb, and accompanied the emplacement of the 173-160 Ma granite porphyry, hornblende granodiorite, and muscovite-biotite granite intrusions. Early pervasive metasomatism closely followed emplacement of granite porphyry, to be cross cut by hornblende granodiorite and muscovite-biotite granite. Temperatures increased as these latter intrusions were emplaced. Metasomatism was restricted by this time to contemporaneous shear zones, which promoted mineral reaction, mineral recrystallization and further removal of constituents.

## CHAPTER EIGHT -- CONCLUSIONS

1.) Zones of aluminosilicate mineral assemblages occur at three sites in the Cargo Muchacho Mountains, southeastern California, in variably deformed, low amphibolite-grade quartzofeldspathic gneiss of the Tumco Formation and Jurassic intrusive rocks. The quartzofeldspathic gneiss is regional in extent and is essentially fine grained quartz-albite/oligo-clase-biotite-epidote-magnetite gneiss. The intrusive rocks are a 173 Ma quartz diorite, and a metaluminous to peraluminous 173-160 Ma suite of hornblende granodiorite, granite porphyry, and muscovite-biotite granite. Pegmatite and aplite cross cut the above rocks. Albitization and muscovitization characterized the later stages of crystallization of muscovite-biotite granite. Emplacement of the 173-160 Ma hornblende-biotite granodiorite and muscovite-biotite granite coincided with deformation along low angle faults (eg. the American Girl Fault), which involved, at least in part, normal movement.

2.) The zones of aluminosilicate mineral assemblages are roughly tabular, shallow dipping layers at Micatalc Hill and Vitrifax Hill. Fabric and mineral assemblage variations in the zones, from structural bottom to top, are: foliated, porphyroblastic quartz-feldspar-biotite-epidote-magnetite in the Feldspar Zone, to schistose and mylonitic quartz-muscovite-biotite-magnetite in the Muscovite Zone, to granoblastic



quartz-kyanite-magnetite-rutile in the Kyanite Zone. The Feldspar Zone grades down into quartzofeldspathic gneiss of the Tumco Formation. The Muscovite Zone is subdivided into a lower biotite subzone, and an upper biotite-free magnetite subzone. All minerals, except feldspar, occur in fractures and veinlets in addition to wall rock.

3.) The compositions of minerals vary regularly from the quartzofeldspathic gneiss of the Tumco Formation through the Feldspar and Muscovite Zones to the Kyanite Zone. Plagioclase varies from  $An_{23}$  in the quartzofeldspathic gneiss to about  $An_4$  in the Kyanite Zone, with a concomitant increase in Al. There is an increase in the Al and Na contents of muscovite and biotite from quartzofeldspathic gneiss into the Kyanite Zone. In addition, Fe, Mg, and K of muscovite and Fe of biotite decrease in this same direction.  $Fe/(Fe+Mg)$  becomes smaller in biotite, but larger in muscovite. Tourmaline is schorl-dravite, and core-to-rim zonation is irregular but has higher Fe, Ti, Al, and Ca, and lower Si, Mg, and Na. Garnet is  $Alm_{50}Sps_{30}Prp_{11}Grs_9$ , with core-to-rim increases in Fe and Mg and decreases in Ca and Mn in the Kyanite Zone.

4.) There is a progressive increase in bulk  $Al_2O_3$ ,  $TiO_2$ ,  $P_2O_5$ , Ga, V, molecular  $Al_2O_3/(CaO+Na_2O+K_2O)$  and  $Fe_2O_3/(Fe_2O_3+MgO)$  from the quartzofeldspathic gneiss of the Tumco Formation to the Kyanite Zone. Mass balance calculations suggest an aluminum enrichment in the Kyanite Zone as a function of removal of

most of the cations, with a volume loss of 39%. Only P, and probably B, are added to this zone. The same elements lost from the Kyanite Zone were added to the Feldspar Zone. In the Muscovite Zone, aluminum as well as the other major cations are lost, with a minimum volume change of -60%.

5.) Measured mineral compositions and theoretical and experimental mineral equilibria indicate the zones of aluminosilicate mineral assemblages formed from oxidizing, aqueous fluids. The fluids progressively removed cations from feldspar-bearing assemblages producing muscovite- and kyanite-bearing assemblages with higher Al, Ti, and P. Mineral textures and bulk composition changes indicate an early pervasive metasomatism followed by a later, shear-zone hosted metasomatism.

6.) Cross cutting relationships indicate that pervasive development of the zones of aluminosilicate assemblages accompanied emplacement of the 173-160 Ma intrusive suite, slightly postdating granite porphyry and predating hornblende granodiorite and muscovite-biotite granite. Theoretical and experimental mineral equilibria indicate mineral growth occurred at pressures exceeding 4 Kb and temperatures greater than 500°C. The metaluminous to peraluminous compositions, the late muscovite and albite formation, and the porphyritic textures, of the 173-160 Ma intrusive suite are consistent with a water-rich magma as a source for the metasomatizing

fluids, which contained high  $fO_2$ , B and P, and low F and Cl. Pegmatites, which cross cut and therefore post date the zones of aluminosilicate mineral assemblages, may also suggest the late magmatic stages were fluid-rich. Focus of fluids along favorable structures, such as shear zones, allowed migration of the fluids to sites within the quartzofeldspathic gneiss of the Tumco Formation distant from the intrusions, as at Hedges.

7.) The zones of aluminosilicate mineral assemblages at Micatalec and Vitrifax Hills lie along strike with gold deposits at American Girl and Madre-Padre, respectively. Branham (1988) suggested that the main-stage gold mineralization post-dated formation of the aluminosilicate mineral assemblages. The contact between alteration related to gold mineralization and the aluminosilicate assemblages is gradational, and no conclusive temporal evidence has yet been ascertained. Alternatively, contemporaneous gold deposition and development of the zones of aluminosilicate mineral assemblages, may have occurred at different locations within the same hydrothermal system. Chlorite and pyrite occur with gold, suggesting reduced conditions. The inferred high oxidation conditions during the development of the zones of aluminosilicate minerals would preclude precipitation of gold (Romberger, 1986).

TABLE A-2 (cont'd) Mineral Modes of the Aluminosilicate Assemblages.

	B0501-5	B0602-7	B0628-4	MT-2	B0430-3	B0430-5	B0501-6	B0501-8
quartz	22	54	14	50	34	37	53	36
plagioclase	12							
K-feldspar								
groundmass plag								
muscovite	32	18	68	42	10	24	8	20
biotite					22			
chlorite					5			
hornblende								
epidote					tr			
garnet		0.1		tr	6			
staurolite					15			
andalusite								
kyanite	23	24	12	6	3	33	31	37
pyrophyllite	1				2			
tourmaline	2	0.1			0.4	0.1	0.1	tr
apatite		3	2	1	tr	2	3	1
lazulite							0.1	0.5
magnetite	3	0.1	3		1	3	2	2
rutile	0.2	0.1		2	1	1	2	2
leucoxene								
limonite (py)								
zircon	0.1		tr		tr	tr	tr	
sphene								
carbonate	0.1				0.4			
monazite								
chalcedony	0.1							
vug								
fluorite	0.2							
clay	4							
#points*	1830	1734	1701	1500	1777	1551	1611	1441

**Notes**

B0501-5. feldspar bearing schistose Kyanite Zone

B0602-7 B0628-4. MT-2 schistose Kyanite Zone

B0430-3 foliated Kyanite Zone

B0430-5 B0501-6 B0501-8 granoblastic Kyanite Zone

Kyanite Zone.

- B0501-4:** mylonitic quartz-muscovite-kyanite-magnetite-tourmaline, Kyanite Zone.
- B0501-5:** crenulated, schistose, porphyroblastic quartz-muscovite-kyanite-tourmaline, Kyanite Zone.
- B0501-6:** granoblastic quartz-kyanite; see B0430-5.
- B0501-7:** schistose muscovite-quartz-kyanite; see B0430-2.
- B0501-8:** granoblastic quartz-kyanite; see B0430-5.
- B0511-1, GN-1:** interior, foliated muscovite-biotite granite.
- B0511-2:** contact zone, schistose muscovite-biotite granite.
- B0511-3:** granite porphyry.
- B0512-1:** foliated to gneissic, porphyroblastic quartz-feldspar-biotite-magnetite-muscovite, Feldspar Zone.
- B0512-4:** (distal granodiorite) foliated hornblende-biotite granodiorite.
- B0512-7t:** gneissic, porphyroblastic quartz-feldspar-biotite-magnetite-epidote, Feldspar Zone.
- B0512-10:** fine grained, gneissic porphyroblastic quartz-feldspar-biotite-hornblende-epidote, Feldspar Zone.
- B0601-1:** porphyroblastic gneiss (Feldspar Zone); see 386-1-10.
- B0602-1A:** porphyroblastic, schistose quartz-muscovite-biotite-tourmaline-magnetite, biotite subzone, Muscovite Zone.
- B0602-7:** porphyroblastic, schistose quartz-kyanite-muscovite-apatite, Kyanite Zone.
- B0628-1:** (proximal granodiorite adjacent to muscovite-biotite granite) see MT4-3-1286.
- B0628-2:** granoblastic quartz-kyanite; see B0430-5.

- B0628-3, B0628-8:** granoblastic quartz from the Kyanite Zone.
- B0628-4:** schistose muscovite-kyanite-quartz-apatite-magnetite, Kyanite Zone.
- B0628-6:** schistose Kyanite Zone; see B0430-2.
- B0628-7:** biotite subzone, Muscovite Zone; see B0430-4.
- B0628-8:** granoblastic quartz; see B0628-3.
- B0628-9:** granoblastic quartz-kyanite; see B0430-5.
- B1218-3:** porphyroblastic, gneissic quartz-feldspar-biotite-epidote-muscovite (Feldspar Zone) adjacent to muscovite-biotite granite.
- B1218-4:** porphyroblastic, gneissic quartz-feldspar-biotite-tourmaline-epidote (Feldspar Zone) adjacent to muscovite-biotite granite.
- B1219-6:** Schistose quartz-muscovite-magnetite, magnetite subzone, Muscovite Zone.
- B1219-16:** porphyroblastic, gneissic quartz-feldspar-biotite-magnetite-epidote (Feldspar Zone).
- DIKE 1B:** (proximal granodiorite) granoblastic hornblende-magnetite granodiorite.
- GN-1:** muscovite-biotite granite; see B0511-1.
- H0319-10:** schistose quartz-muscovite-kyanite-tourmaline-magnetite, Kyanite Zone.
- H0412-4:** crenulated, schistose quartz-muscovite-biotite-magnetite-tourmaline, biotite subzone, Muscovite Zone.
- MT-2:** see B0430-6.
- MT-4:** see B0430-2.
- MT2-3-1286, MT3-3-1286:** schistose quartz-muscovite-biotite-

magnetite, biotite subzone, Muscovite Zone.

MT4-3-128C. (medial granodiorite) granoblastic biotite-  
magnetite-garnet granodiorite.

TOP-1: granoblastic quartz-kyanite-tourmaline, Kyanite Zone.

TABLE A-1. Mineral Modes of the Intrusive Rocks.

	DIKE-1B MT431286	B0512-4	GN-1	B0511-1	B0511-2	B0511-3
quartz	18	22	26	32	29	19
plagioclase	44	45	18	24	31	8
K-feldspar			16	28	24	11
groundmass plag						42
muscovite		3	0.1	2	5	14
biotite	0.1	17	22	10	11	9
chlorite	0.3	4		0.1	0.5	0.1
hornblende	34		5			
epidote	0.5	5	12	2		tr
garnet		0.3	0.1		0.1	
apatite		0.1		0.2		
lazulite						
magnetite	4	3		0.3		
rutile					0.3	
leucoxene						
limonite (py)						
zircon			0.1		0.1	0.1
sphene			1	2		0.5
carbonate		1			0.2	0.1
monazite						
chalcedony						
vug						
fluorite						
clay						
#points*	1500	1349	1645	1606	1550	1543
						1631

## Notes

\*#points = number of points counted per thin section.

DIKE 1B Proximal granodiorite; MT431286: Medial granodiorite.  
 B0512-4: Distal granodiorite; GN-1: Interior muscovite-biotite  
 granite. B0511-1: Interior muscovite-biotite granite; B0511-2:  
 Schistose, contact ms-b; granite; B0511-3: granite porphyry



TABLE A-2. Mineral Modes of the Aluminosilicate Assemblages.

	386-1-11 MT541286	B0601-1	386-1-2	386-1-10	B0430-4	B0628-7	MT231286
quartz	34	27	22	30	28	28	35
plagioclase	23	45		18	7	3	6
K-feldspar	25						
groundmass plag			43		39	37	18
muscovite	0.1	1	7	0.1	14	9	42
biotite	8	19	25	5	10	18	6
chlorite			0.1	1		1	
hornblende	3						
epidote	5	5	1	45		0.1	0.1
garnet		tr				1	
staurolite							
andalusite							
kyanite							
pyrophyllite							
tourmaline							1
apatite		tr	0.1			0.1	2
lazulite							0.1
magnetite	1	2	1	1	1	1	4
rutile							3
leucoxene	1						
limonite (py)							
zircon		tr			0.1		
sphene							
carbonate	1	1	0.1		0.1	1	
monazite					0.1		1
chalcedony							
vug							
fluorite							
clay							
#points*	1612	1424	1543	1512	1581	1596	1600

## Notes:

\*#points = number of points counted per thin section.

386-1-11: quartzofeldspathic gneiss of the Tumco Formation.  
 MT541286, B0601-1, 386-1-2, 386-1-10 porphyroblastic gneiss  
 of the Feldspar Zone B0430-4, B0628-7, feldspar-  
 bearing muscovite schist from the biotite subzone. Musc-  
 ovite Zone MT231286: biotite subzone, Muscovite Zone

TABLE A-2 (cont'd). Mineral Modes of the Aluminosilicate Assemblages.

	MT331286	B0628-3	B0628-8	B0430-2	B0501-7	B0628-6	MT-4	B0430-6
quartz	38	77	92	50	29	40	40	46
plagioclase								
K-feldspar								
groundmass plag					42			
muscovite	45	20	6	38	25	53	40	30
biotite	14							
chlorite	tr	tr	tr	tr				
hornblende								
epidote								
garnet								
staurolite								
andalusite								
kyanite					1			20
pyrophyllite								
tourmaline	tr			5			14	
apatite	tr	2		2		3		1
lazulite								
magnetite	3	1	1	5	3	4	6	3
rutile			1				0.1	tr
leucoxene								
limonite (py)				tr			tr	
zircon	tr	tr	tr		tr		0.1	tr
sphene								
carbonate			0.1	tr		tr	0.5	0.1
monazite								
chalcedony					0.1			
vug		1			1			
fluorite								
clay								
#points*	1029	1596	1555	1503	1450	1554	1509	1585

## Notes:

MT331286: schistose biotite subzone Muscovite Zone

B0628-3 B0628-8: quartzite from the Muscovite Zone

B0430-2, B0501-7 B0628-8, MT-4: schistose magnetite subzone, Muscovite Zone

B0430-6: schistose Kyanite Zone.

TABLE A-2 (cont'd). Mineral Modes of the Aluminosilicate Assemblages.

	B0501-5	B0602-7	B0628-4	MT-2	B0430-3	B0430-5	B0501-6	B0501-8
quartz	22	54	14	50	34	37	53	36
plagioclase	10							
K-feldspar								
groundmass plag								
muscovite	32	18	68	42	10	24	8	20
biotite					22			
chlorite					5			
hornblende								
epidote					tr			
garnet		0.1		tr	6			
staurolite					15			
andalusite								
kyanite	23	24	12	6	3	33	31	37
pyrophyllite	1				2			
tourmaline	2	0.1			0.4	0.1	0.1	tr
apatite		3	2	1	tr	2	3	3
lazulite							0.1	0.5
magnetite	3	0.1	3		1	3	2	2
rutile	0.2	0.1		2	1	1	2	2
leucoxene								
limonite (py)								
zircon	0.1		tr		tr	tr	tr	
sphene								
carbonate	0.2				0.4			
monazite								
chalcedony	0.1							
vug								
fluorite	0.2							
clay	4							
#points*	1830	1734	1701	1521	2072	1551	1611	1441

## Notes

B0501-5. feldspar-bearing schistose Kyanite Zone

B0602-7 B0628-4, MT-2 schistose Kyanite Zone

B0430-3 foliated Kyanite Zone

B0430-5 B0501-6 B0501-8 granoblastic Kyanite Zone

TABLE A-2 (cont'd). Mineral Modes of the Aluminosilicate Assemblies.

	B0628-2	B0628-9
quartz	23	51
plagioclase		
K-feldspar		
groundmass plag		
muscovite	25	8
biotite		
chlorite		
hornblende		
epidote		
garnet		
staurolite		
andalusite		
kyanite	34	39
pyrophi e		
tourmaline		
apatite	10	
lazulite		
magnetite		
rutile	1	2
leucoxene		
limonite (py)		
zircon		
sphene		
carbonate		
monazite		
chalcedony		
vug		
fluorite		
clay		
#points*	1539	1522

## Notes

B0628-2, B0628-9.

granoblastic Kyanite Zone

## APPENDIX B. WHOLE ROCK X-RAY FLUORESCENCE ANALYSIS.

Determination of major and minor elements for whole rock samples was performed by X-Ray Fluorescence on 35 samples from the aluminosilicate assemblages, quartzofeldspathic gneiss, and intrusive rocks. Preparation of samples involved crushing to -250 mesh and drying at 110°C for 2 hours to drive off adsorbed water. Major element analysis was carried out using the heavy absorber fusion technique developed by Norrish and Hutton (1969), in which the sample is fused into a lithium borate glass disk containing lanthanum oxide. Trace element analysis was performed on pressed powdered pellets. Rock samples were analyzed on a Philips 1450 Automated X-Ray Fluorescence Spectrometer in the Geology Department at the University of Western Ontario. The samples were analyzed in three runs which determined separate suites of elements: major oxides, a lithophile element suite (Nb, Zr, Y, Sr, Rb, Ba, Ga, La), and a chalcophile element suite (Pb, Zn, Cu, Ni, Co, Cr, V, S). Accuracy was provided by reference to international and internal standards. Repeated analysis of standards during runs provided precision, allowing correction for short term variation in such factors as voltage supply. Detection limits for all major elements except Na<sub>2</sub>O and MgO is 0.01 wt. %; for Na<sub>2</sub>O and MgO detection limits are 0.05%. Detection limits for the trace elements are 2 ppm for the lithophile elements and 5 ppm for the chalcophile elements.

TABLE B-1 XRF Analyses of Intrusive Rocks

	B0511-1	B0511-2	B0511-3	B0512-4	GN-1
SiO <sub>2</sub>	72.54	73.46	69.47	64.16	67.14
TiO <sub>2</sub>	0.35	0.35	0.44	0.71	0.51
Al <sub>2</sub> O <sub>3</sub>	14.22	13.92	15.05	15.12	15.56
Fe <sub>2</sub> O <sub>3</sub>	2.13	1.99	3.22	5.55	4.01
MnO	0.06	0.06	0.07	0.10	0.07
HgO	0.97	1.29	1.03	2.56	1.23
CaO	0.95	0.74	2.04	4.74	3.28
Na <sub>2</sub> O	2.38	2.04	3.46	1.58	2.58
K <sub>2</sub> O	5.65	4.42	4.64	3.91	4.61
P <sub>2</sub> O <sub>5</sub>	0.07	0.08	0.17	0.21	0.16
LOI(1)	0.70	1.40	0.80	1.10	1.10
	-----	-----	-----	-----	-----
	100.01	99.76	100.39	99.74	100.26
Nb	20	19	15	17	16
Zr	260	246	222	246	200
Y	26	27	23	25	27
Sr	113	72	208	412	279
Rb	206	189	161	190	172
Ba	561	579	718	675	846
Ga	12	11	17	17	14
La	39	38	45	25	38
Pb	22	36	27	41	18
Zn	59	58	56	59	46
Cu	*	10	8	10	17
Ni	6	*	6	14	8
Co	*	*	*	21	8
Cr	*	*	*	13	*
V	40	40	51	136	102
S	*	*	116	117	*
K/Sr	500	614	223	95	165
K/Rb	274	234	288	205	268
K/Ba	101	76	65	58	54
Rb/Sr	1.82	2.63	0.77	0.46	0.61

## Notes

(1)LOI = Loss on ignition

\* = below detection limits

Oxides in weight % elements in ppm

Rock samples are described in Appendix 1

TABLE B-2. XRF Analyses. Aluminosilicate Assemblages.

	386-1-11	B0601-1	386-1-2	386-1-10	B0430-4	B0628-7	MT231286	MT331286	B0430-2
SiO <sub>2</sub>	69.29	62.12	65.80	73.49	66.25	66.98	71.88	71.09	84.12
TiO <sub>2</sub>	0.36	0.50	0.41	0.18	0.47	0.46	0.75	0.72	0.40
Al <sub>2</sub> O <sub>3</sub>	14.90	17.84	15.12	14.49	16.21	16.22	13.00	12.58	7.70
Fe <sub>2</sub> O <sub>3</sub>	2.80	5.52	5.03	1.50	5.27	4.15	5.48	5.82	3.87
MnO	0.05	0.12	0.14	0.09	0.18	1.09	0.10	0.07	0.01
MgO	1.10	2.12	0.61	1.52	2.25	0.94	2.38	2.45	0.28
CaO	2.83	3.37	7.29	0.96	2.60	1.43	0.35	0.58	0.37
Na <sub>2</sub> O	2.54	2.09	1.30	1.97	2.44	3.84	0.21	0.00	0.00
K <sub>2</sub> O	4.46	3.77	3.37	3.89	2.46	3.76	4.29	4.59	1.85
P <sub>2</sub> O <sub>5</sub>	0.14	0.33	0.13	0.07	0.22	0.24	0.09	0.09	0.15
LOI(1)	1.20	1.79	1.00	1.50	1.30	1.10	1.90	1.99	1.10
	-----	-----	-----	-----	-----	-----	-----	-----	-----
	99.66	99.58	100.20	99.66	99.64	100.20	100.44	99.97	99.86
Nb	15	10	12	10	11	16	15	14	9
Zr	178	109	103	139	131	204	258	243	211
Y	29	18	21	18	19	21	20	19	18
Sr	316	674	1160	106	504	306	102	58	171
Rb	166	142	74	118	106	121	242	247	42
Ba	950	1185	744	877	767	782	1165	1333	447
Ga	14	16	15	19	19	18	14	12	7
La	31	20	18	30	19	38	18	16	17
Pb	19	47	58	176	39	59	13	12	13
Zn	43	88	135	66	112	80	72	83	25
Cu	*	*	23	*	11	*	*	*	*
Ni	9	12	7	*	*	6	19	23	*
Co	*	nd	nd	nd	nd	8	11	15	*
Cr	*	*	*	*	*	*	41	52	23
V	52	100	112	*	94	142	105	96	97
S	*	*	*	*	*	*	*	237	*
K/Sr	141	56	29	367	49	123	421	791	108
K/Rb	265	265	455	330	232	311	177	186	440
K/Ba	47	32	45	44	32	48	37	34	41
Rb/Sr	0.52	0.21	0.00	1.11	0.21	0.4	2.37	4.25	0.25

## Notes:

(1)LOI = Loss on ignition

\* = below detection limits

Oxides in weight %, elements in ppm

Rock samples are described in Appendix 1

TABLE B-2 (cont'd). XRF Analyses, Aluminosilicate Assemblages

	B0430-2	B0501-7	B0628-6	MT-4	B0430-6	B0501-5	B0602-7	B0628-4	MT-2
SiO <sub>2</sub>	84.28	67.54	85.49	72.45	75.26	67.59	73.67	61.81	72.27
TiO <sub>2</sub>	0.39	0.46	0.22	0.63	0.36	0.56	0.53	0.62	0.57
Al <sub>2</sub> O <sub>3</sub>	7.72	16.01	6.71	10.56	16.41	22.08	20.69	23.28	19.48
Fe <sub>2</sub> O <sub>3</sub>	3.94	4.74	2.48	10.34	3.78	3.41	1.48	4.53	0.98
MnO	0.01	0.03	0.02	0.02	0.00	0.02	0.00	0.01	0.00
MgO	0.08	0.17	0.28	0.41	0.01	0.17	0.00	0.18	0.05
CaO	0.36	2.80	0.67	0.68	0.24	0.53	0.34	0.47	0.49
Na <sub>2</sub> O	0.00	2.00	0.00	0.00	0.00	0.86	0.00	0.00	0.00
K <sub>2</sub> O	1.89	2.00	2.30	2.70	2.16	1.57	1.54	5.47	3.47
P <sub>2</sub> O <sub>5</sub>	0.14	0.29	0.17	0.07	0.18	0.16	0.31	0.37	0.37
LOI(1)	1.10	4.00	1.60	1.70	1.50	2.90	1.20	2.90	1.90
	-----	-----	-----	-----	-----	-----	-----	-----	-----
	99.91	100.05	99.94	99.57	99.91	99.84	99.76	99.65	99.58
Nb	0	13	6	15	10	15	9	12	17
Zr	0	104	58	200	87	140	17	208	141
Y	*	37	14	22	8	13	8	10	9
Sr	171	604	35	146	652	917	688	526	1021
Rb	42	66	81	106	52	33	29	125	59
Ba	*	788	241	533	802	221	314	775	960
Ga	*	18		17	22	23	25	28	38
La	*	35	23	31	21	28	*	22	35
Pb	13	38	7	11	12	36	10	25	16
Zn	nd	41	57	54	24	27	*	*	*
Cu	nd	10	*	*	*	*	*	*	*
Ni	nd	*	*	17	*	*	*	*	*
Co	nd	*	*	14	*	*	*	*	*
Cr	nd	*	*	38	*	*	*	*	9
V	nd	85	58	105	84	110	76	92	120
S	nd	13113	*	*	*	4909	*	369	*
K/Sr	nd	33	657	185	33	17	22	104	34
K/Rb	nd	303	284	255	415	476	531	438	588
K/Ba	nd	25	95	51	27	71	49	71	36
Rb/Sr	nd	0.11	2.31	0.72	0.08	0.04	0.04	0.24	0.06

## Notes

(1)LOI = Loss on ignition

\* = below detection limits; nd = not determined.

Oxides in weight %, elements in ppm.

Rock samples are described in Appendix 1.



TABLE B-2 (cont'd). XRF Analyses. Aluminosilicate Assemblages

	B0430-3	B0430-5	B0501-6	B0501-8	B0628-2	B0628-9	B0628-3	B0628-8
SiO <sub>2</sub>	65.68	59.60	72.90	68.25	59.00	73.53	93.41	97.76
TiO <sub>2</sub>	0.51	0.68	0.51	0.41	0.52	0.35	0.13	0.58
Al <sub>2</sub> O <sub>3</sub>	16.19	27.93	22.88	26.82	34.64	24.53	3.27	0.52
Fe <sub>2</sub> O <sub>3</sub>	6.63	4.07	1.03	1.41	0.36	0.26	0.78	0.24
MnO	0.09	0.01	0.01	0.01	0.01	0.01	0.01	0.02
HgO	4.31	0.31	0.23	0.08	0.18	0.00	0.10	0.00
CaO	0.43	0.67	0.74	0.90	0.69	0.17	0.41	0.09
Na <sub>2</sub> O	0.00	0.00	0.00	0.00	0.00	0.00	0.00	0.00
K <sub>2</sub> O	3.41	2.72	0.62	0.72	2.11	0.37	1.08	0.28
P <sub>2</sub> O <sub>5</sub>	0.27	0.41	0.33	0.62	0.52	0.17	0.18	0.06
LOI(1)	2.50	3.21	1.00	1.20	2.10	0.70	0.60	0.40
	-----	-----	-----	-----	-----	-----	-----	-----
	100.01	99.61	100.19	100.43	100.13	100.10	99.96	99.95
Nb	12	16	10	7	8	11	4	13
Zr	211	169	42	34	18	0	45	130
Y	21	11	9	12		9	10	15
Sr	122	882	177	331	152	67	29	14
Rb	159	70	13	16	57	11	48	6
Ba	516	1054	356	391	58	88	117	13
Ga	20	37	29	25	41	40	*	*
La	19	53	11	12	*	*	14	*
Pb	14	17	6	6	14	5	7	15
Zn	65	*	*	25	25	*	25	25
Cu	*	*	*	*	*	*	9	7
Ni	7	*	*	*	*	*	*	*
Co	*	*	*	*	*	*	*	*
Cr	7	*	*	13	9	8	*	*
V	94	120	92	81	46	27	10	46
S	*	479	*	261	*	*	82	*
K/Sr	280	31	35	22	139	55	372	200
K/Rb	214	389	477	450	370	336	225	467
K/Ba	66	26	17	16	364	41	92	215
Rb/Sr	1.3	0.08	0.07	0.05	0.37	0.16	1.66	0.43

## Notes.

(1)LOI = Loss on ignition.

\* = below detection limits.

Oxides in weight %, elements in ppm

Rock samples are described in Appendix 1

**APPENDIX C. ELECTRON MICROPROBE ANALYSIS, MINERAL FORMULA  
RECALCULATION AND GEOTHERMOMETER DERIVATIONS.**

**C.1. Method of Analysis.**

Determination of feldspar, mica, tourmaline and garnet compositions were performed by electron microprobe analysis on a JEOL JXA/8600 Superprobe with automated wavelength dispersion spectrometry in the Geology Department at the University of Western Ontario. For silicate analysis a power rating of 15 kV and 10 nA was used. To minimize contamination of analyses by intergrowths or inclusions, a beam diameter of 2 to 5  $\mu\text{m}$  was used. Matrix corrections were made on-line using the ZAF program of Tracor Northern. Periodic repetitive spot analysis was performed to determine whether or not loss by volatilization of the lighter elements occurred. For major element analysis in silicates, error is  $\pm 3$  wt. % relative. Where compositional variation within a given thin section was small, three to six spot analyses of mineral grains were performed. Where greater compositional variability occurred, or where compositional zonation was indicated by backscatter images, more analyses were run, on individual grains and within whole thin sections. The data are presented in Tables C-1 to C-6.

**C.2. Formula Recalculation.**

Recalculation of analyses to structural formula for micas and garnet, based on 22 O and 24 O, respectively, were

performed by the SUPER RECAL program (John Rutledge, University of Toronto). Feldspar formulae were recalculated on the basis of 8 oxygens. Tourmaline formulae were recalculated according to the methods of Henry and Guidotti (1985) and Gallagher (1988). Because B and OH cannot be determined via electron microprobe, these calculations assume maximum filling by B (3 sites) and OH+F+Cl (4 sites). The weight %  $B_2O_3$  necessary to fill the 3 trigonal sites was calculated accordingly. The assumption of filled hydroxyl sites results in calculations based on 29 O atoms per formula unit. Six aluminums are then placed in the Z-site, and all Si are used in the tetrahedral site. Where Si is less than 6, excess aluminum is used to fill that site. Any remaining aluminum goes to the Y-site, accompanying the transition metals, and alkali metals are placed in the X-site.

### C.3. Two-Feldspar Geothermometry: Methods and Derivation.

Spot analyses of alkali and plagioclase feldspars from quartzofeldspathic gneiss, orthogneiss, and aluminosilicate assemblages were carried out. Temperature of formation may be estimated provided the feldspars were in equilibrium at the time of crystallization and they were not subjected to post-crystallization structural and chemical changes. The widespread replacement of K-feldspar by myrmekite indicates that post-crystallization changes were commonplace in these rocks. In addition, the abundance of plagioclase in the Feldspar Zone, as compared to the relative scarcity of K-feldspar,

suggests the two may not have formed at the same time. As a result, most of the traditional two-feldspar geothermometer formulations are probably not of practical use with these rocks (Whitney and Stormer, 1977; Brown and Parsons, 1981; Haselton et. al., 1983). The existence of two feldspars in the unaltered orthogneisses and quartzofeldspathic gneiss, however, leads to the possibility that at least some equilibrium compositions have been retained.

The thermometer employed here is that devised by Fuhrman and Lindsley (1988) because it not only calculates potential equilibrium temperatures, but it also gives a qualitative measure of disequilibrium conditions where they exist. Most two-feldspar thermometer formulations deal with two binaries in the feldspar system, albite-anorthite and albite-orthoclase, and are based solely on the distribution of the albite component between plagioclase and alkali-feldspar (Whitney and Stormer, 1977; Brown and Parsons, 1981; Haselton et. al., 1983). The two-feldspar thermometer developed by Fuhrman and Lindsley (1988) is derived from a ternary solution model which corrects for excess volume, excess free energy and configurational entropy. A detailed derivation of this model is beyond the scope of this work, and the reader is directed to Fuhrman and Lindsley (1988), Ghiorso (1984) and Green and Urdansky (1986) for more detailed explanations. However, in brief, the free energy of mixing is given by:

$$\begin{aligned}
 \text{(C-1)} \quad G^{\text{mix}} = & RT\{X_{ab}\ln[X_{ab}(1-X_{ab}^2)] + \\
 & X_{or}\ln[X_{or}(1-X_{or}^2)] + X_{an}\ln[X_{an}(1-X_{an})^2/4]\} + \\
 & W_{orab}(X_{or}X_{ab})(X_{ab}+X_{or}/2) + W_{abor}(X_{or}X_{ab})(X_{or}+X_{ab}/2) + \\
 & W_{oran}(X_{or}X_{an})(X_{an}+X_{or}/2) + W_{anor}(X_{or}X_{an})(X_{or}+X_{an}/2) + \\
 & W_{aban}(X_{ab}X_{an})(X_{an}+X_{ab}/2) + W_{nab}(X_{ab}X_{an})(X_{ab}+X_{an}/2) + \\
 & W_{oranab}(X_{or}X_{ab}X_{an}),
 \end{aligned}$$

where  $X_i$  is the mole fraction of component  $i$  and the  $W_{i,j,k}$  terms are experimentally determined Margules Parameters which incorporate excess free energy. At equilibrium, the activity relationships in the ternary system are given by:

$$\text{(C-2)} \quad a_{Ab}K\text{-feldspar} = a_{Ab}\text{Plagioclase},$$

$$\text{(C-3)} \quad a_{Or}K\text{-feldspar} = a_{Or}\text{Plagioclase},$$

and

$$\text{(C-4)} \quad a_{An}K\text{-feldspar} = a_{An}\text{Plagioclase}.$$

These are related to equation C-1 by:

$$\text{(C-5)} \quad RT\ln a_i = G^{\text{mix}} + (1-X_i)(\partial G/\partial X_i)_{T,P,X_j,X_k}.$$

Appropriate substitution of equations C-2 to C-4 into equation C-5 gives activity-temperature relationships for each of the

three components, or, ab and an.

The program MTHERM3 uses an iterative procedure whereby equilibrium temperatures are initially calculated for the given feldspar compositions. It then searches in systematically larger compositional increments up to 2 mol % away from the given compositions (within the error of most microprobe analyses) and calculates the temperatures for the three components in each step, according to the sum of differences function:

$$(C-6) \quad f(X_{\alpha}, X_{ab}, X_m \text{ in 2 feldspars}) = \\ ||T_{ab}|-|T_{\alpha}|| + ||T_{\alpha}|-|T_m| + ||T_m| + |T_{ab}||.$$

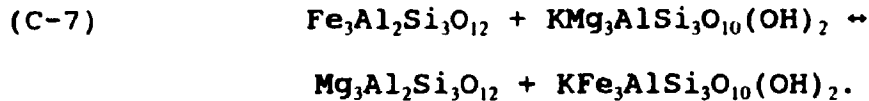
The composition of each phase is adjusted within the margin of analytical error to bring this function to a minimum where, at equilibrium, the temperatures calculated for the three activity relationships should be concordant. Fuhrman and Lindsley (1988) suggest congruent temperatures occur when the highest and lowest temperatures differ by 40°C or less. If the calculated temperature differences are greater than this, the given feldspar compositions are probably not equilibrium compositions.

#### C.4. Garnet-Biotite Thermometry: Methods and Derivation.

Although garnet is comparatively rare in the study area, it occurs with biotite in the aluminosilicate assemblages, in granodiorite and in muscovite-biotite granite. As with the

feldspars, the use of the geothermometer requires that the phases are in equilibrium and that post-crystallization changes are absent or can be accounted for. In most samples, garnets are unzoned. However, where zoned garnets occur, as in sample B0430-3, cores and rims were analyzed. Core analyses were chosen for temperature calculations in such cases, although calculations were also performed for rim compositions. The effect of Mn, enriched in the core, on the calculations is to lower the temperature. Selection of biotite grains for analysis was easier, and grains close to, and further removed from, analyzed garnet were used in the calculations. Spot analyses of biotite showed no core-to-rim compositional zonation. Replacement of biotite by chlorite is common, but posed few problems. The majority of samples lacks any evidence of disequilibrium (eg. replacement by other minerals, resorption textures), although sample B0628-1 contains evidence of later fluid-rock interaction in the form of cross-cutting muscovite-chlorite-magnetite veinlets. The temperatures calculated according to the methods described below were slightly lower.

Garnet-biotite geothermometers derived by Ferry and Spear (1978), Ganguly and Saxena (1984) and Williams and Grambling (1990) were used and compared. These are based on Fe-Mg partitioning between garnet and biotite according to the exchange reaction:



For this reaction, the distribution coefficient,  $K_D$ , is:

$$(C-8) \quad K_D = (\text{Mg/Fe})_{\text{garnet}} / (\text{Mg/Fe})_{\text{biotite}}.$$

Ferry and Spear (1978) experimentally determined this relationship at temperatures between 550°C and 800°C and pressures of 2.07 Kb, which gave:

$$(C-9) \quad \ln K_D = -2109/T(^{\circ}\text{K}) + 0.782.$$

By incorporating necessary enthalpy, entropy and volume changes using data from Robie et. al. (1967), Ferry and Spear derived the following polybaric expression:

$$(C-10) \ln K_D = [4.662T(^{\circ}\text{K}) - 0.057P(\text{bars}) + 12,454]/3RT,$$

which is the relationship used here to calculate temperatures.

Ganguly and Saxena (1984) evaluated the effect of Ca and Mn on the distribution of Fe-Mg between garnet and biotite determined by Ferry and Spear (1978). For reaction C-7 above,

$$(C-11) \quad K_a = [(X_{\text{Fe}}/X_{\text{Mg}})^{\text{gr}} / (X_{\text{Fe}}/X_{\text{Mg}})^{\text{bt}}] * \\ [(\gamma_{\text{Fe}}/\gamma_{\text{Mg}})^{\text{gr}} / (\gamma_{\text{Fe}}/\gamma_{\text{Mg}})^{\text{bt}}],$$



TABLE C-2 (cont'd). Microprobe analyses. Plagioclase.

	34	35	36	37	38	91-2	91-3	91-4	91-5
	cs sieve	same	in core	same	rim	gmass	gmass	core	rim
	B0430-4	B0430-4	B0430-4	B0430-4	B0430-4	B0430-4	B0430-4	B0430-4	B0430-4
SiO <sub>2</sub>	63.43	63.06	62.40	61.76	62.51	60.54	61.81	60.57	60.53
Al <sub>2</sub> O <sub>3</sub>	23.74	24.40	24.62	25.02	24.79	22.87	23.04	23.72	24.01
Na <sub>2</sub> O	8.59	8.43	8.42	8.47	8.41	8.11	8.97	8.61	8.42
K <sub>2</sub> O	0.00	0.00	0.04	0.03	0.01	0.04	0.05	0.04	0.03
CaO	5.40	5.40	5.89	5.85	5.86	4.46	4.36	5.27	5.49
BaO	0.00	0.00	0.00	0.00	0.00				
Total	101.16	101.29	101.37	101.12	101.58	96.02	98.23	98.21	98.48
Structural Formulae (Based on 8 O)									
Si	2.774	2.753	2.731	2.711	2.728	2.781	2.781	2.736	2.727
Al	1.224	1.256	1.270	1.294	1.275	1.238	1.222	1.263	1.275
Na	0.728	0.714	0.714	0.721	0.712	0.722	0.783	0.754	0.736
K	0.000	0.000	0.000	0.002	0.001	0.002	0.002	0.002	0.002
Ca	0.253	0.253	0.276	0.275	0.274	0.220	0.210	0.255	0.265
Ba	0.000	0.000	0.000	0.000	0.000	nd	nd	nd	nd

## Notes

B0430-4 biotite subzone, Muscovite Zone

	91-6	91-7	91-8	91-11	91-12	91-13	91-14	91-15	91-16
	gmass	core	rim	core	polygms	polygms	gmass	polygon	polygon
	B0430-4	B0430-4	B0430-4	B0501-7	B0501-7	B0501-7	B0501-7	B0501-7	B0501-7
SiO <sub>2</sub>	60.61	60.87	61.05	56.97	57.27	56.43	58.2	56.39	56.76
Al <sub>2</sub> O <sub>3</sub>	24.15	23.84	23.98	26.41	27.15	26.91	25.75	27.23	27.27
Na <sub>2</sub> O	8.30	8.47	8.53	6.85	6.81	6.53	7.55	6.51	6.38
K <sub>2</sub> O	0.03	0.06	0.02	0.07	0.11	0.13	0.12	0.14	0.11
CaO	5.72	5.45	5.29	8.56	8.54	9.07	7.45	9.1	9.3
BaO	nd	nd	nd	nd	nd	nd	nd	nd	nd
Total	98.89	98.69	98.87	98.86	99.88	99.07	99.07	99.37	99.62
Structural Formulae (Based on 8 O)									
Si	2.721	2.736	2.737	2.582	2.569	2.557	2.626	2.548	2.552
Al	1.278	1.263	1.267	1.411	1.435	1.437	1.369	1.450	1.445
Na	0.730	0.738	0.742	0.602	0.592	0.574	0.661	0.570	0.556
K	0.002	0.004	0.001	0.004	0.006	0.008	0.007	0.008	0.006
Ca	0.275	0.263	0.254	0.415	0.411	0.440	0.360	0.441	0.448
Ba	nd	nd	nd	nd	nd	nd	nd	nd	nd

## Notes:

nd = not determined

B0430-4: biotite subzone, Muscovite Zone; B0501-7: Kyanite Zone

Williams and Grambling (1990) further modify equations C-8 and C-12 in order to evaluate the effects of ferric iron, manganese, and titanium in biotite on the exchange reaction C-7. With the addition of these components, equation C-12 becomes:

$$(C-15) \quad -RT \ln K_D = -RT \ln K_s + \\ [W_{MgFe}(X_{Fe} - X_{Mg}) + \Delta W_{Ca}(X_{Ca}) + \Delta W_{Mn}(X_{Mn})]^{g1} - \\ [W_{MgFe}(X_{Fe} - X_{Mg}) - \Delta W_{Mn}(X_{Mn}) - \Delta W_{Ti}(X_{Ti}) - \\ \Delta W_{Al}(X_{Al}) - \Delta W_{Fe^{3+}}(X_{Fe^{3+}})]^{b1}.$$

Incorporating interaction parameters for excess terms from previous studies and Fe, Mg non-ideality, equation C-15 leads to the general geothermometer:

$$(C-16) \quad T(K) = [-17042 - 79.5P(\text{bars}) + 0.8(W_{MgFe})^{g1} - \\ W_{MgFe}(X_{Fe} - X_{Mg}) - (\Delta W_{Ca})^{g1}(X_{Ca})^{g1} - \\ (\Delta W_{Mn})^{g1}(X_{Mn})^{g1} + (\Delta W_{Ti})^{b1}(X_{Ti})^{b1} - \\ (\Delta W_{Al})^{b1}(X_{Al})^{b1}] \div \\ R[\ln K_D - 0.782 + \ln(Fe^{2+b1}/Fe^{Tot.b1})].$$

The appropriate K-T relationships used to calculate temperatures are equations C-10, C-13, and C-16.

TABLE C-1. Microprobe Analyses. K-feldspar.

	1	2	3	4	5	6	7	8	9
	Ca.untun	estartan	same	same	ovrgwth	same	dfuntun	ame	fn.gblst
	386-1-11	386-1-11	386-1-11	386-1-11	386-1-11	386-1-11	386-1-11	386-1-11	B0512-1
SiO <sub>2</sub>	65.27	65.99	65.63	65.36	65.31	65.24	66.08	65.93	66.52
Al <sub>2</sub> O <sub>3</sub>	18.58	18.63	18.69	18.24	18.77	18.81	18.62	18.41	18.85
Na <sub>2</sub> O	0.67	0.68	0.66	0.64	0.51	0.40	0.71	0.83	0.92
K <sub>2</sub> O	16.00	16.01	15.36	15.91	16.32	14.77	15.87	15.20	14.58
CaO	0.00	0.00	0.01	0.00	0.00	0.05	0.01	0.00	0.04
BaO	0.36	0.36	0.35	0.41	0.50	0.58	0.36	0.42	0.67
Total	100.89	101.67	100.69	100.55	101.41	99.85	101.64	100.79	101.58
Structural Formulae (Based on 8 Oxygens)									
Si	2.994	3.001	3.002	3.007	2.987	3.003	3.003	3.013	3.009
Al	1.005	0.998	1.008	0.989	1.012	1.02	0.997	0.992	1.005
Na	0.06	0.06	0.059	0.057	0.045	0.036	0.063	0.074	0.081
K	0.936	0.929	0.896	0.934	0.952	0.867	0.92	0.886	0.841
Ca	0	0	0	0	0	0.002	0	0	0.002
Ba	0.006	0.006	0.006	0.007	0.009	0.01	0.006	0.008	0.012

## Notes

386-1-11: quartzofeldspathic gneiss of the Tumco Formation  
 B0512-1 Feldspar Zone

	10	11	12	13	91-18	91-19	91-21	91-24	91-26
	same	fn.gblst	fn.gblst	ovrgwth	ca porph	same	nd porph	microporph	porph
	B0512-1	B0512-1	B0512-1	B0512-1	B1218-4	B1218-4	B1218-4	B1218-4	B1218-4
SiO <sub>2</sub>	65.86	65.20	65.75	65.68	63.17	62.94	63.33	62.71	62.68
Al <sub>2</sub> O <sub>3</sub>	18.49	18.55	18.47	18.81	18.45	18.23	18.18	18.39	18.4
Na <sub>2</sub> O	0.95	1.01	0.87	0.66	1	0.85	0.8	0.88	1
K <sub>2</sub> O	15.11	14.65	14.73	15.06	14.92	14.89	14.93	14.78	14.76
CaO	0.02	0.06	0.03	0.06	0.02	0	0	0	0
BaO	0.68	0.64	0.63	0.90	nd	nd	nd	nd	nd
Total	101.11	100.11	100.48	101.17	97.56	96.91	97.24	96.76	96.84
Si	3.006	3.001	3.011	2.998	2.98	2.989	2.995	2.982	2.97975
Al	0.995	1.006	0.997	1.012	1.026	1.02	1.012	1.031	1.03075
Na	0.084	0.09	0.077	0.058	0.092	0.078	0.073	0.081	0.09225
K	0.88	0.86	0.861	0.877	0.898	0.902	0.901	0.897	0.895
Ca	0.001	0.003	0.001	0.003	0.001	0	0	0	0
Ba	0.012	0.012	0.011	0.016	nd	nd	nd	nd	nd

## Notes:

B0512-1. Feldspar Zone  
 B1218-4. Feldspar Zone adj. to ms-b1 granite.

TABLE C-1 (cont'd.). Microprobe Analyses, K-feldspar.

	91-31	91-32	91-33	91-37	14	15	16	17	18
	In plag	cs porph	gnass	microporps	untun	same	cs untun	same rim	cs porph
	B0512 7t	B1218-10	B1218-10	B1219-16	B0511 1	B0511-1	B0511-1	B0511-1	B0511-1
SiO <sub>2</sub>	63.97	63.65	63.04	63.39	64.56	65.12	64.70	65.05	64.44
Al <sub>2</sub> O <sub>3</sub>	18.45	18.26	18.12	18.4	18.53	18.69	18.52	18.60	18.23
Na <sub>2</sub> O	0.76	0.53	0.81	0.72	0.26	0.24	0.28	0.46	0.32
K <sub>2</sub> O	15.34	15.67	15.09	15.55	16.02	15.76	15.96	15.68	16.06
CaO	0	0	0	0	0.05	0.05	0.03	0.03	0.05
BaO	nd	nd	nd	nd	0.28	0.30	0.19	0.23	0.25
Total	98.52	98.11	97.06	98.06	99.70	100.13	99.69	100.05	99.35
Si	2.99125	2.9935	2.9925	2.96425	2.994	2.999	2.997	2.999	3
Al	1.0165	1.012	1.0135	1.02075	1.013	1.014	1.011	1.011	1
Na	0.069	0.04325	0.298	0.06575	0.023	0.021	0.025	0.041	0.029
K	0.915	0.94	0.9135	0.93375	0.948	0.926	0.943	0.922	0.954
Ca	0	0	0	0	0.002	0.001	0.001	0.001	0.002
Ba	nd	nd	nd	nd	0.005	0.005	0.003	0.004	0.005

## Notes

B0512 7t, B1218 10, B1219-16: Feldspar Zone.

B0511-1 muscovite-biotite granite

	19	20	21	22	23	24	25	26
	fn untun	cs tartan	same	same rim	fn gr	strnuntun	same	
	B0512 4	B0512-4	B0512-4	B0512-4	B0512-4	B0512-4	B0512-4	B0512-4
SiO <sub>2</sub>	65.42	66.78	65.21	65.41	65.90	66.20	65.64	65.42
Al <sub>2</sub> O <sub>3</sub>	18.54	18.41	18.70	18.47	18.38	18.47	18.49	18.54
Na <sub>2</sub> O	0.77	0.42	0.55	0.74	1.12	0.62	0.50	0.58
K <sub>2</sub> O	15.40	15.57	15.91	15.63	15.27	15.64	16.19	15.86
CaO	0.01	0.05	0.04	0.04	0.04	0.01	0.03	0.07
BaO	0.51	0.39	0.40	0.38	0.47	0.43	0.39	0.52
Total	100.65	101.62	100.80	100.68	101.18	101.37	101.22	101.00

## Structural Formulae (Based on 8 Oxygens)

Si	3.001	3.024	2.992	3.001	3.007	3.012	3.001	2.998
Al	1.002	0.983	1.011	0.999	0.988	0.991	0.996	1.001
Na	0.068	0.037	0.049	0.066	0.099	0.055	0.044	0.052
K	0.901	0.9	0.931	0.915	0.889	0.908	0.944	0.927
Ca	0	0.002	0.002	0.002	0.002	0	0.001	0.003
Ba	0.009	0.007	0.007	0.007	0.008	0.008	0.007	0.009

## Notes

B0512 4 hornblende-biotite granodiorite

TABLE C-2. Microprobe Analyses. Plagioclase.

	54	55	56	57	58	59	60	61	62
	fn gr	fn gmass	same			altd	same		same
	386-1-11	386-1-11	386-1-11	386-1-11	386-1-11	386-1-11	386-1-11	386-1-11	386-1-11
SiO <sub>2</sub>	64.66	69.41	69.10	66.29	64.81	65.07	67.66	63.83	63.28
Al <sub>2</sub> O <sub>3</sub>	22.89	20.23	19.71	21.53	21.85	22.46	20.58	22.88	22.96
Na <sub>2</sub> O	9.19	11.25	10.12	10.31	9.99	10.08	10.36	9.40	9.20
K <sub>2</sub> O	0.08	0.08	0.04	0.04	0.08	1.42	0.01	0.19	0.09
CaO	4.11	0.66	0.36	2.90	3.40	0.93	0.99	4.44	4.26
BaO	0.00	0.00	0.00	0.00	0.00	0.00	0.00	0.00	0.00
Total	100.92	101.63	99.35	101.07	100.12	99.96	99.61	100.72	99.79
Structural Formulae (Based on 8 O)									
Si	2.824	2.981	3.016	2.886	2.855	2.868	2.961	2.804	2.802
Al	1.178	1.024	1.014	1.105	1.134	1.167	1.061	1.185	1.198
Na	0.778	0.937	0.856	0.870	0.853	0.861	0.879	0.801	0.790
K	0.004	0.004	0.002	0.002	0.004	0.080	0.001	0.011	0.005
Ca	0.192	0.030	0.016	0.135	0.160	0.044	0.046	0.209	0.202
Ba	0.000	0.000	0.000	0.000	0.000	0.000	0.000	0.000	0.000

## Notes:

386-1-11: quartzofeldspathic gneiss of the Tumco Formation

	63	64	65	91-20	91-22	91-23	91-25	91-27	91-28
	same			polygon	polygon	polygon	gmass	gmass	gmass
	386-1-11	386-1-11	386-1-11	B1218-4	B1218-4	B1218-4	B1218-4	B0512-7t	B0512-7t
SiO <sub>2</sub>	63.96	65.15	61.84	60.57	61.97	61.91	62.15	60.96	61.24
Al <sub>2</sub> O <sub>3</sub>	23.18	21.67	22.79	23.2	23.07	22.85	22.63	24.34	23.55
Na <sub>2</sub> O	9.40	8.67	9.38	8.6	9.01	9.26	9.13	8.39	8.66
K <sub>2</sub> O	0.06	0.03	0.14	0.16	0.26	0.22	0.21	0.26	0.26
CaO	4.22	3.20	4.37	5.24	4.49	4.3	4.27	5.75	5.08
BaO	0.00	0.00	0.00						
Total	100.82	98.71	98.51	97.77	98.7	98.54	98.39	99.7	98.74
Structural Formulae (Based on 8 O)									
Si	2.803	2.888	2.782	2.750	2.779	2.783	2.795	2.718	2.751
Al	1.197	1.132	1.108	1.241	1.219	1.211	1.199	1.279	1.246
Na	0.799	0.745	0.818	0.757	0.784	0.807	0.796	0.725	0.754
K	0.003	0.002	0.008	0.009	0.009	0.013	0.012	0.015	0.015
Ca	0.198	0.152	0.211	0.255	0.216	0.207	0.206	0.275	0.245
Ba	0.000	0.000	0.000	nd	nd	nd	nd	nd	nd

## Notes:

386-1-11 quartzofeldspathic gneiss of the Tumco Formation

B1218-4 B0512-7t: Feldspar Zone

TABLE C-2 (cont'd). Microprobe analyses. Plagioclase.

	91-29 porph B0512-7t	91-30 porph B0512-7t	91-34 polygon B1219-16	91-35 polygon B1219-16	91-36 mass B1219-16	91-38 mass B1219-16	39 fn gr B0512-1	40 same B0512-1	41 same B0512-1
SiO <sub>2</sub>	60.91	62.47	59.02	58.55	58.53	62.06	67.53	67.09	67.26
Al <sub>2</sub> O <sub>3</sub>	23.81	23.49	25.35	25.3	25.37	23.27	21.63	21.86	21.65
Na <sub>2</sub> O	8.84	9.02	7.53	7.63	7.48	9.09	10.06	10.63	9.13
K <sub>2</sub> O	0.08	0.06	0.13	0.15	0.16	0.19	0.12	0.11	0.11
CaO	5.46	4.81	7.13	7.27	7.32	4.67	2.20	2.19	2.31
BaO							0.00	0.00	0.00
Total	99.1	99.85	99.16	98.9	98.86	99.28	101.52	101.87	100.46
Structural Formulae (Based on 8 O)									
Si	2.732	2.770	2.654	2.645	2.644	2.771	2.913	2.893	2.912
Al	1.258	1.228	1.344	1.347	1.350	1.224	1.100	1.111	1.108
Na	0.769	0.776	0.657	0.668	0.655	0.786	0.841	0.889	0.769
K	0.005	0.003	0.008	0.009	0.009	0.011	0.007	0.006	0.006
Ca	0.262	0.229	0.344	0.352	0.354	0.223	0.102	0.101	0.107
Ba	nd	nd	nd	nd	nd	nd	0.000	0.000	0.000

## Notes

B0512-7t, B1219-16, B0512-1: Feldspar Zone

	42 same B0512-1	43 cs ab tw B0512-1	44 same B0512-1	45 fn grano B0512-1	46 same B0512-1	47 fn grano B0512-1	48 cs strain B0512-1	49 same B0512-1	50 same B0512-1
SiO <sub>2</sub>	67.04	67.16	67.07	67.01	66.63	68.16	67.66	66.37	67.59
Al <sub>2</sub> O <sub>3</sub>	21.51	21.60	21.11	21.49	21.89	21.36	21.92	21.56	20.81
Na <sub>2</sub> O	10.15	10.30	10.79	9.81	9.98	9.10	9.73	10.68	10.85
K <sub>2</sub> O	0.07	0.11	0.12	0.20	0.21	0.15	0.13	0.10	0.08
CaO	2.26	2.32	1.82	2.61	2.54	2.46	2.26	2.25	1.88
BaO	0.01	0.00	0.00	0.00	0.02	0.00	0.00	0.70	0.00
Total	101.05	101.46	100.91	101.10	101.28	101.24	101.69	100.95	101.21
Structural Formulae (Based on 8 O)									
Si	2.908	2.903	2.917	2.906	2.889	2.937	2.910	2.891	2.930
Al	1.100	1.101	1.082	1.099	1.119	1.085	1.111	1.107	1.063
Na	0.854	0.863	0.910	0.825	0.839	0.760	0.811	0.902	0.912
K	0.004	0.006	0.007	0.011	0.012	0.008	0.007	0.006	0.004
Ca	0.105	0.107	0.085	0.121	0.118	0.114	0.104	0.105	0.087
Ba	0.000	0.000	0.000	0.000	0.000	0.000	0.000	0.000	0.000

## Notes:

B0512-1: Feldspar Zone

TABLE C-2 (cont'd.). Microprobe Analyses. Plagioclase.

	51	52	53	1	2	3	4	5	6
	fn grano	cs untn	fn gblst	Core of	fn gr	rim	fn.dkcore	lt rim	
	B0512-1	B0512-1	B0512-1	B0430-4	B0430-4	B0430-4	B0430-4	B0430-4	B0430-4
SiO <sub>2</sub>	66.31	66.43	66.68	62.19	61.56	61.57	62.63	62.59	61.48
Al <sub>2</sub> O <sub>3</sub>	21.64	21.34	21.43	24.84	23.90	24.72	24.07	24.52	24.64
Na <sub>2</sub> O	10.44	10.67	10.69	9.07	10.00	10.04	8.77	8.95	8.57
K <sub>2</sub> O	0.18	0.08	0.09	0.07	0.08	0.04	0.07	0.04	0.08
CaO	2.33	2.16	2.49	5.67	5.22	5.38	4.86	5.06	5.79
BaO	0.01	0.03	0.00	0.00	0.00	0.00	0.00	0.00	0.00
Total	100.91	100.72	101.38	101.83	100.76	101.76	101.07	101.16	100.60
Si	2.884	2.894	2.894	2.716	2.725	2.701	2.760	2.741	2.716
Al	1.111	1.098	1.096	1.278	1.247	1.278	1.266	1.266	1.283
Na	0.861	0.903	0.900	0.768	0.858	0.854	0.749	0.760	0.734
K	0.010	0.004	0.005	0.004	0.005	0.002	0.004	0.002	0.005
Ca	0.109	0.101	0.116	0.265	0.248	0.253	0.229	0.237	0.274
Ba	0.000	0.001	0.000	0.000	0.000	0.000	0.000	0.000	0.000

## Notes

B0512-1: Feldspar Zone

B0430-4: biotite subzone Muscovite Zone

	7	8	9	10	11	12	13	14	15
							core	rim	core
	B0430-4	B0430-4	B0430-4	B0430-4	B0430-4	B0430-4	B0430-4	B0430-4	B0430-4
SiO <sub>2</sub>	62.47	61.77	61.17	60.53	61.70	61.30	63.44	62.06	61.74
Al <sub>2</sub> O <sub>3</sub>	24.72	25.49	24.47	25.95	24.61	24.06	23.17	24.63	24.50
Na <sub>2</sub> O	8.57	8.52	8.42	8.29	8.05	8.51	8.68	8.37	8.51
K <sub>2</sub> O	0.06	0.09	0.07	0.06	0.08	0.08	0.06	0.08	0.07
CaO	5.78	5.93	5.87	6.17	5.92	5.62	4.55	5.50	5.37
BaO	0.00	0.00	0.00	0.00	0.00	0.02	0.00	0.00	0.06
Total	101.60	101.80	99.99	100.02	100.36	99.60	99.91	100.70	100.25

## Structural Formulae (Based on 8 O)

Si	2.726	2.696	2.717	2.666	2.725	2.733	2.801	2.731	2.731
Al	1.272	1.311	1.281	1.347	1.281	1.264	1.206	1.277	1.277
Na	0.726	0.721	0.725	0.708	0.689	0.736	0.743	0.714	0.730
K	0.003	0.005	0.004	0.003	0.005	0.005	0.003	0.004	0.004
Ca	0.270	0.277	0.279	0.291	0.280	2.680	0.215	0.262	0.254
Ba	0.000	0.000	0.000	0.000	0.000	0.000	0.000	0.000	0.001

## Notes

B0430-4: biotite subzone Muscovite Zone.

TABLE C-2. Microprobe Analyses, Plagioclase

	16	17	18	19	20	21	22	23	24
	rim	same rim	in grano	in grano	same	cs porph	cs porph	cs porph	cs porph
	B0430-4	B0430-4	B0430-4	B0430-4	B0430-4	B0430-4	B0430-4	B0430-4	B0430-4
SiO <sub>2</sub>	62.52	63.74	62.05	61.37	61.17	62.98	62.85	63.50	62.80
Al <sub>2</sub> O <sub>3</sub>	24.07	23.52	24.48	24.98	24.51	24.51	24.44	24.30	24.01
Na <sub>2</sub> O	6.59	9.03	8.59	8.30	8.44	8.44	8.40	8.96	8.74
K <sub>2</sub> O	0.07	0.09	0.09	0.05	0.08	0.02	0.03	0.00	0.00
CaO	5.50	4.69	5.65	6.24	6.03	5.19	5.28	5.16	5.31
BaO	0.04	0.03	0.00	0.00	0.00	0.00	0.04	0.00	0.00
Total	98.79	101.10	100.86	100.93	100.23	102.04	101.04	101.92	100.86

Structural Formulae (Based on 8 O)

Si	2.780	2.788	2.730	2.703	2.713	2.738	2.751	2.758	2.757
Al	1.261	1.212	1.270	1.297	1.281	1.256	1.261	1.244	1.242
Na	0.568	0.766	0.733	0.709	0.726	0.712	0.713	0.755	0.744
K	0.004	0.005	0.005	0.003	0.005	0.004	0.002	0.000	0.000
Ca	0.262	0.220	0.266	0.294	0.287	0.281	0.248	0.240	0.250
Ba	0.001	0.001	0.000	0.000	0.000	0.000	0.000	0.000	0.000

Notes:

B0430-4: biotite subzone, Muscovite Zone

	25	26	27	28	29	30	31	32	33
	cs porph	ab twi	same	same	cs porph	core in	cs porph	same	same
	B0430-4	B0430-4	B0430-4	B0430-4	B0430-4	B0430-4	B0430-4	B0430-4	B0430-4
SiO <sub>2</sub>	62.18	63.04	61.74	63.40	63.72	63.65	62.45	61.84	62.30
Al <sub>2</sub> O <sub>3</sub>	24.29	24.37	23.45	23.43	23.96	22.99	24.27	24.37	24.30
Na <sub>2</sub> O	8.73	8.71	8.58	9.14	9.07	9.22	8.56	8.73	8.59
K <sub>2</sub> O	0.00	0.00	0.00	0.01	0.01	0.04	0.00	0.00	0.00
CaO	5.42	5.45	5.38	4.60	4.91	4.53	5.48	5.35	5.37
BaO	0.00	0.00	0.00	0.00	0.00	0.00	0.00	0.00	0.00
Total	100.64	101.57	99.14	100.59	101.68	100.43	100.75	100.29	100.56

Structural Formulae (Based on 8 O)

Si	2.739	2.749	2.759	2.787	2.773	2.801	2.745	2.734	2.744
Al	1.261	1.253	1.235	1.214	1.229	1.193	1.258	1.270	1.261
Na	0.746	0.736	0.743	0.779	0.765	0.787	0.730	0.748	0.734
K	0.000	0.000	0.000	0.001	0.001	0.002	0.000	0.000	0.000
Ca	0.256	0.255	0.258	0.217	0.229	0.214	0.258	0.253	0.253
Ba	0.000	0.000	0.000	0.000	0.000	0.000	0.000	0.000	0.000

Notes:

B0430-4: biotite subzone, Muscovite Zone.



TABLE C-2 (cont'd). Microprobe analyses, Plagioclase.

	34	35	36	37	38	91-2	91-3	91-4	91-5
	cs sieve	same	in core	same	rim	gmass	gmass	core	rim
	B0430-4	B0430-4	B0430-4	B0430-4	B0430-4	B0430-4	B0430-4	B0430-4	B0430-4
SiO <sub>2</sub>	63.43	63.06	62.40	61.76	62.51	60.54	61.81	60.57	60.53
Al <sub>2</sub> O <sub>3</sub>	23.74	24.40	24.62	25.02	24.79	22.87	23.04	23.72	24.01
Na <sub>2</sub> O	8.59	8.43	8.42	8.47	8.41	8.11	8.97	8.61	8.42
K <sub>2</sub> O	0.00	0.00	0.04	0.03	0.01	0.04	0.05	0.04	0.03
CaO	5.40	5.40	5.89	5.85	5.86	4.46	4.36	5.27	5.49
BaO	0.00	0.00	0.00	0.00	0.00				
Total	101.16	101.29	101.37	101.12	101.58	96.02	98.23	98.21	98.48
Structural Formulae (Based on 8 O)									
Si	2.774	2.753	2.731	2.711	2.728	2.781	2.781	2.736	2.727
Al	1.224	1.256	1.270	1.294	1.275	1.238	1.222	1.263	1.275
Na	0.728	0.714	0.714	0.721	0.712	0.722	0.783	0.754	0.736
K	0.000	0.000	0.000	0.002	0.001	0.002	0.002	0.002	0.002
Ca	0.253	0.253	0.276	0.275	0.274	0.220	0.210	0.255	0.265
Ba	0.000	0.000	0.000	0.000	0.000	nd	nd	nd	nd

## Notes

B0430-4 biotite subzone, Muscovite Zone.

	91-6	91-7	91-8	91-11	91-12	91-13	91-14	91-15	91-16
	gmass	core	rim	core	polygms	polygms	gmass	polygon	polygon
	B0430-4	B0430-4	B0430-4	B0501-7	B0501-7	B0501-7	B0501-7	B0501-7	B0501-7
SiO <sub>2</sub>	60.61	60.87	61.05	56.97	57.27	56.43	58.2	56.39	56.76
Al <sub>2</sub> O <sub>3</sub>	24.15	23.84	23.98	26.41	27.15	26.91	25.75	27.23	27.27
Na <sub>2</sub> O	8.38	8.47	8.53	6.85	6.81	6.53	7.55	6.51	6.38
K <sub>2</sub> O	0.03	0.06	0.02	0.07	0.11	0.13	0.12	0.14	0.11
CaO	5.72	5.45	5.29	8.56	8.54	9.07	7.45	9.1	9.3
BaO	nd	nd	nd	nd	nd	nd	nd	nd	nd
Total	98.89	98.69	98.87	98.86	99.88	99.07	99.07	99.37	99.82
Structural Formulae (Based on 8 O)									
Si	2.721	2.736	2.737	2.582	2.569	2.557	2.626	2.548	2.552
Al	1.278	1.263	1.267	1.411	1.435	1.437	1.369	1.450	1.445
Na	0.730	0.738	0.742	0.602	0.592	0.574	0.661	0.570	0.556
K	0.002	0.004	0.001	0.004	0.006	0.008	0.007	0.008	0.006
Ca	0.275	0.263	0.254	0.415	0.411	0.440	0.360	0.441	0.448
Ba	nd	nd	nd	nd	nd	nd	nd	nd	nd

## Notes

nd = not determined

B0430-4. biotite subzone, Muscovite Zone; B0501-7 Kyanite Zone

TABLE C-2 (cont'd). Microprobe Analyses, Plagioclase

	91 17	66	67	68	69	70	71	72	73
	polygon	fn gr	same	same	same	fn, core	same	fn.gblast	
	B0501-7	B0511-1	B0511-1	B0511-1	B0511-1	B0511-1	B0511-1	B0511-1	B0511-1
SiO <sub>2</sub>	56.88	66.34	66.52	65.43	65.04	65.14	65.57	66.37	68.44
Al <sub>2</sub> O <sub>3</sub>	26.76	21.90	21.78	22.05	21.76	21.86	22.28	21.50	19.84
Na <sub>2</sub> O	6.78	10.36	10.34	10.53	10.23	10.25	10.40	10.39	12.04
K <sub>2</sub> O	0.13	0.19	0.23	0.18	0.24	0.22	0.23	0.18	0.05
CaO	8.64	2.56	2.60	2.62	2.61	2.61	2.90	2.59	0.27
BaO	nd	0.00	0.00	0.05	0.00	0.00	0.01	0.01	0.00
Total	99.19	101.35	101.52	100.86	99.88	100.08	101.39	101.04	100.65
Structural Formulae (Based on 8 O)									
Si	2.571	2.880	2.884	2.860	2.868	2.866	2.853	2.890	2.976
Al	1.425	1.120	1.113	1.136	1.131	1.134	1.143	1.103	1.017
Na	0.594	0.872	0.869	0.893	0.875	0.875	0.877	0.877	1.015
K	0.008	0.011	0.013	0.010	0.014	0.012	0.013	0.010	0.003
Ca	0.419	0.119	0.121	0.123	0.123	0.123	0.135	0.121	0.013
Ba	nd	0.000	0.000	0.001	0.000	0.000	0.000	0.000	0.000

## Notes.

nd = not determined

B0501-7: Kyanite Zone; B0511-1 muscovite-biotite granite

	74	75	76	77	78	79	80	81	82
	fn.inter	fn.gblast	fn.gblast	same	same	same	fn.subh	fn.inter	fn.inter
	B0511-1	B0511-1	B0511-1	B0511-1	B0511-1	B0511-1	B0511-1	B0511-1	B0511-1
SiO <sub>2</sub>	64.85	65.80	66.13	66.72	66.50	66.68	65.48	66.01	66.58
Al <sub>2</sub> O <sub>3</sub>	21.38	21.38	21.75	21.42	20.76	20.96	21.22	21.61	22.23
Na <sub>2</sub> O	10.57	10.41	10.39	10.68	10.77	10.86	10.84	10.47	10.23
K <sub>2</sub> O	0.20	0.23	0.14	0.10	0.13	0.06	0.05	0.16	0.21
CaO	2.47	2.28	2.47	2.12	1.78	1.72	2.34	2.35	2.55
BaO	0.05	0.01	0.00	0.00	0.04	0.00	0.00	0.00	0.00
Total	99.52	100.10	100.88	101.05	99.97	100.28	99.92	100.59	101.80
Structural Formulae (Based on 8 O)									
Si	2.874	2.891	2.883	2.901	2.921	2.918	2.886	2.886	2.875
Al	1.117	1.107	1.117	1.098	1.075	1.081	1.102	1.113	1.131
Na	0.908	0.887	0.878	0.900	0.917	0.921	0.926	0.887	0.857
K	0.011	0.013	0.008	0.006	0.007	0.003	0.003	0.009	0.012
Ca	0.117	0.107	0.115	0.099	0.084	0.081	0.110	0.110	0.118
Ba	0.001	0.000	0.000	0.000	0.001	0.000	0.000	0.000	0.000

## Notes

B0511-1 interior of muscovite biotite granite

TABLE C-2 (cont'd) Microprobe Analyses, Plagioclase.

	83	84	85	86	87	88	89	90	92
	same	dfnd	kep	cs	porph	same	same	same	fn.dfd
	B0511-1	B0511-1	B0511-1	B0511-1	B0511-1	B0511-1	B0511-1	B0511-1	B0511-2
SiO <sub>2</sub>	65.04	65.96	68.95	69.13	68.05	69.21	68.84	67.90	68.46
Al <sub>2</sub> O <sub>3</sub>	21.37	21.53	19.82	19.70	19.82	19.93	19.86	19.94	20.11
Na <sub>2</sub> O	10.50	10.17	11.92	11.60	11.72	11.89	11.80	11.60	11.31
K <sub>2</sub> O	0.12	0.21	0.11	0.07	0.11	0.09	0.13	0.06	0.07
CaO	2.44	2.56	0.30	0.47	0.44	0.23	0.34	0.53	0.52
BaO	0.01	0.00	0.00	0.00	0.00	0.03	0.00	0.01	0.00
Total	99.47	100.43	101.10	100.97	100.14	101.39	100.97	100.04	100.46
Structural Formulae (Based on 8 O)									
Si	2.879	2.888	2.983	2.991	2.974	2.985	2.982	2.970	2.976
Al	1.115	1.111	1.011	1.005	1.021	1.013	1.014	1.028	1.030
Na	0.901	0.863	1.000	0.973	0.993	0.994	0.991	0.984	0.953
K	0.007	0.012	0.006	0.004	0.006	0.005	0.007	0.003	0.004
Ca	0.116	0.120	0.014	0.022	0.021	0.011	0.016	0.025	0.024
Ba	0.000	0.000	0.000	0.000	0.000	0.001	0.000	0.000	0.000

## Notes:

B0511-1: interior of muscovite-biotite granite

B0511-2: contact zone, muscovite-biotite granite

	93	94	102	91	95	96	97	98	99
	fn.gbist	fn.gbist	fn.gr	cs.porph	cs.untwn	cs	same	same	same
	B0511-2	B0511-2	B0511-2	B0511-2	B0511-2	B0511-2	B0511-2	B0511-2	B0511-2
SiO <sub>2</sub>	68.64	66.29	67.92	68.29	68.32	69.09	69.44	68.62	68.70
Al <sub>2</sub> O <sub>3</sub>	20.24	20.35	20.40	19.76	19.87	19.69	19.72	20.05	19.78
Na <sub>2</sub> O	11.57	10.94	10.81	11.62	10.51	11.01	11.01	11.09	10.24
K <sub>2</sub> O	0.08	0.36	0.07	0.06	0.08	0.08	0.06	0.06	0.08
CaO	0.49	0.47	1.28	0.54	0.55	0.52	0.54	0.56	0.53
BaO	0.01	0.00	0.00	0.00	0.00	0.00	0.00	0.03	0.00
Total	101.03	98.41	100.47	100.27	99.33	100.39	100.77	100.41	99.33
Structural Formulae (Based on 8 O)									
Si	2.971	2.940	2.956	2.979	2.993	2.999	3.007	2.982	2.995
Al	1.032	1.067	1.046	1.016	1.026	1.007	1.005	1.027	1.020
Na	0.971	0.943	0.912	0.983	0.893	0.927	0.923	0.934	0.868
K	0.004	0.020	0.004	0.003	0.004	0.004	0.003	0.003	0.004
Ca	0.023	0.022	0.060	0.025	0.026	0.024	0.025	0.026	0.025
Ba	0.000	0.000	0.000	0.000	0.000	0.000	0.000	0.001	0.000

## Notes:

B0511-2: contact zone, muscovite-biotite granite

TABLE C-2 (cont'd). Microprobe Analyses, Plagioclase.

	100	101	103	104	105	106	107	108	109
	same	same	fn.untwn	fn grphc	wormy	cs porph	coresame	rxtporph	rxtporph
	B0511-2	B0511-2	B0512-4	B0514-2	B0514-2	B0514-2	B0514-2	B0514-2	B0514-2
SiO <sub>2</sub>	69.11	68.93	63.68	62.38	67.22	62.44	62.79	62.16	61.27
Al <sub>2</sub> O <sub>3</sub>	20.09	20.28	22.74	24.41	21.23	24.01	23.60	24.81	25.09
Na <sub>2</sub> O	11.12	10.37	8.42	8.37	10.35	8.52	8.56	7.94	8.41
K <sub>2</sub> O	0.07	0.06	0.32	0.09	0.13	0.10	0.16	0.24	0.20
CaO	0.53	0.68	4.62	5.70	1.84	5.78	5.78	6.21	6.06
BaO	0.00	0.00	0.00	0.02	0.05	0.03	0.00	0.00	0.00
Total	100.91	100.32	99.79	100.96	100.83	100.88	100.89	101.36	101.03
Structural Formulae (Based on 8 O)									
Si	2.986	2.988	2.816	2.739	2.921	2.727	2.762	2.722	2.698
Al	1.023	1.036	1.185	1.263	1.087	1.245	1.223	1.280	1.302
Na	0.932	0.872	0.722	0.713	0.872	0.727	0.730	0.674	0.718
K	0.004	0.003	0.018	0.005	0.007	0.006	0.009	0.013	0.011
Ca	0.025	0.032	0.219	0.268	0.086	0.272	0.272	0.291	0.286
Ba	0.000	0.000	0.000	0.000	0.001	0.001	0.000	0.000	0.000

## Notes:

B0511-2: contact zone, muscovite-biotite granite

B0514-2: distal hornblende-biotite granodiorite

	110	111	112	113	114	115	116	117	118
	rxtporph	cs porph	fn gblst	fn gr	cs porph	fn.dk	same. lt	rimfrxt	coresame
	B0514-2	B0514-2	B0514-2	B0514-2	B0514-2	MT431286	MT431286	MT431286	MT431286
SiO <sub>2</sub>	63.09	63.79	62.11	61.17	62.61	64.55	61.91	60.17	62.12
Al <sub>2</sub> O <sub>3</sub>	23.33	23.46	24.15	24.28	24.49	22.60	24.17	25.91	24.01
Na <sub>2</sub> O	8.99	8.55	8.65	8.38	8.41	8.57	8.24	7.44	8.54
K <sub>2</sub> O	0.23	0.15	0.23	0.17	0.09	0.09	0.09	0.11	0.10
CaO	4.79	5.07	5.73	5.83	5.90	4.08	5.93	7.45	5.32
BaO	0.00	0.00	0.00	0.06	0.03	0.00	0.00	0.00	0.00
Total	100.41	101.02	100.87	99.88	101.54	99.89	100.33	101.09	100.10
Structural Formulae (Based on 8 O)									
Si	2.782	2.791	2.736	2.722	2.736	2.841	2.737	2.653	2.750
Al	1.213	1.210	1.254	1.273	1.261	1.172	1.259	1.347	1.253
Na	0.769	0.725	0.739	0.723	0.713	0.731	0.706	0.636	0.733
K	0.013	0.008	0.013	0.010	0.005	0.005	0.005	0.006	0.006
Ca	0.226	0.238	0.270	0.278	0.276	0.192	0.281	0.352	0.252
Ba	0.000	0.000	0.000	0.001	0.001	0.000	0.000	0.000	0.000

## Notes:

B0514-2: distal hornblende-biotite granodiorite.

MT431286: medial hornblende-biotite granodiorite

TABLE C-2 (cont'd). Microprobe Analyses. Plagioclase.

	119	120	121	122	123	124	125	126	127	
	frndkcore	sameItrm	samerim	ca	sive	lessincl	rxtporph	same	fnngblst	camttidk
	MT431286	MT431286	MT431286	MT431286	MT431286	MT431286	MT431286	MT431286	MT431286	DIKE-1A
SiO <sub>2</sub>	63.07	63.43	63.31	62.50	62.55	59.94	59.36	62.31	60.53	
Al <sub>2</sub> O <sub>3</sub>	23.21	23.93	23.28	23.81	24.07	25.66	26.13	24.07	25.15	
Na <sub>2</sub> O	8.67	8.51	7.87	7.89	8.37	7.44	7.23	8.34	7.65	
K <sub>2</sub> O	0.07	0.12	0.12	0.07	0.09	0.08	0.12	0.11	0.09	
CaO	5.03	5.42	4.93	6.07	5.77	7.08	7.72	5.74	6.93	
BaO	0.00	0.02	0.00	0.00	0.00	0.00	0.03	0.02	0.00	
Total	100.06	101.42	99.51	100.34	100.84	100.20	100.59	100.59	100.34	
Structural Formulae (Based on 8 O)										
Si	2.787	2.768	2.802	2.758	2.749	2.663	2.634	2.747	2.684	
Al	1.209	1.231	1.214	1.238	1.247	1.343	1.367	1.251	1.314	
Na	0.743	0.720	0.675	0.675	0.713	0.641	0.622	0.713	0.658	
K	0.004	0.007	0.007	0.004	0.005	0.005	0.007	0.006	0.005	
Ca	0.238	0.253	0.234	0.287	0.272	0.337	0.367	0.271	0.329	
Ba	0.000	0.000	0.000	0.000	0.000	0.000	0.001	0.000	0.000	

## Notes:

MT431286: medial hornblende-biotite granodiorite

DIKE-1A: proximal hornblende-biotite granodiorite.

	128	129	130	131	132	133	134	135	136	
	sameItrmfrndkcore	samerim	dkcore	samerim	caltmntl	sameckcr	csdknttl	sameIt		
	DIKE-1A	DIKE-1A	DIKE-1A	DIKE-1A	DIKE-1A	DIKE-1A	DIKE-1A	DIKE-1A	DIKE-1A	
SiO <sub>2</sub>	53.64	61.66	52.94	56.02	54.13	51.70	60.35	58.69	56.02	
Al <sub>2</sub> O <sub>3</sub>	29.99	24.62	30.26	27.72	29.96	30.91	26.66	26.36	28.28	
Na <sub>2</sub> O	4.74	7.73	4.30	5.83	4.55	3.71	6.91	6.67	5.59	
K <sub>2</sub> O	0.05	0.08	0.08	0.05	0.07	0.05	0.08	0.05	0.05	
CaO	12.33	6.51	12.89	10.20	12.33	13.52	8.23	8.72	10.80	
BaO	0.05	0.00	0.00	0.02	0.00	0.00	0.00	0.04	0.06	
Total	100.80	100.61	100.47	99.85	101.04	99.90	102.22	100.53	100.82	
Structural Formulae (Based on 8 O)										
Si	2.409	2.720	2.387	2.512	2.421	2.348	2.632	2.611	2.503	
Al	1.587	1.280	1.608	1.471	1.579	1.654	1.371	1.382	1.489	
Na	0.413	0.661	0.376	0.509	0.395	0.327	0.584	0.575	0.494	
K	0.003	0.005	0.005	0.003	0.004	0.003	0.004	0.003	0.003	
Ca	0.593	0.308	0.623	0.492	0.591	0.658	0.385	0.517	0.517	
Ba	1.000	0.000	0.000	0.000	0.000	0.000	0.000	0.001	0.001	

## Notes:

DIKE-1A: proximal hornblende-biotite granodiorite.

TABLE C-2 (cont'd) Microprobe Analyses, Plagioclase

	137	138	139	140
	fnckmttl	sanelttam	sanelt	csporph
	DIKE-1A	DIKE-1A	DIKE-1A	DIKE-1A
SiO <sub>2</sub>	61.54	57.31	57.12	57.07
Al <sub>2</sub> O <sub>3</sub>	25.09	28.13	27.44	27.57
Na <sub>2</sub> O	8.00	5.94	6.08	6.20
K <sub>2</sub> O	0.09	0.04	0.07	0.04
CaO	6.40	10.46	9.82	9.68
BaO	0.00	0.03	0.01	0.00
	-----	-----	-----	-----
Total	101.13	101.91	100.54	100.56

## Structural Formulae (Based on 8 O)

Si	2.703	2.528	2.550	2.547
Al	1.299	1.463	1.444	1.450
Na	0.681	0.508	0.526	0.536
K	0.005	0.002	0.004	0.002
Ca	0.301	0.494	0.470	0.463
Ba	0.000	0.001	0.000	0.000

## Notes

DIKE-1A proximal hornblende-biotite granodiorite

TABLE C-3. Microprobe analyses, Muscovite.

	22	24	27	28	32	35	40	42	43
	B0512-7t	B0512-7t	B0512-7t	B0512-7t	B0512-7t	B1219-16	B1219-16	B1219-16	B1219-16
SiO <sub>2</sub>	47.46	46.21	47.42	46.00	45.97	46.26	45.65	45.55	45.52
TiO <sub>2</sub>	0.71	0.79	0.72	0.49	0.67	0.78	0.34	0.73	0.62
Al <sub>2</sub> O <sub>3</sub>	30.92	29.38	30.59	30.31	30.20	31.15	28.83	29.99	29.79
Cr <sub>2</sub> O <sub>3</sub>	0.00	0.00	0.02	0.00	0.00	0.03	0.00	0.00	0.02
MnO	0.10	0.08	0.04	0.03	0.03	0.09	0.11	0.05	0.04
FeO	6.31	5.86	6.14	5.72	5.53	5.04	4.89	5.15	5.37
HgO	1.54	1.45	1.57	1.49	1.62	1.23	1.38	1.17	1.18
BaO	0.10	0.09	0.09	0.09	0.17	0.10	0.14	0.09	0.10
CaO	0.01	0.01	0.01	0.02	0.01	0.06	0.02	0.01	0.01
K <sub>2</sub> O	10.82	11.12	10.60	10.77	10.75	10.14	10.77	10.58	10.64
Na <sub>2</sub> O	0.25	0.21	0.21	0.24	0.26	0.28	0.22	0.27	0.26
F	0.00	0.00	0.00	0.00	0.00	0.00	0.00	0.00	0.00
Cl	0.01	0.01	0.00	0.02	0.00	0.01	0.00	0.00	0.01
Sum	98.23	95.21	97.41	95.18	95.21	95.17	92.35	93.59	93.56
O=F+Cl	0.00	0.00	0.00	0.00	0.00	0.00	0.00	0.00	0.00
Total	98.23	95.21	97.41	95.18	95.21	95.17	92.35	93.59	93.56
Structural Formulae (Based on 22 O)									
Si	6.308	6.352	6.34	6.304	6.297	6.291	6.43	6.327	6.336
Al <sub>iv</sub>	1.692	1.648	1.66	1.696	1.703	1.709	1.57	1.673	1.664
Al <sub>vi</sub>	3.151	3.111	3.159	3.198	3.172	3.282	3.215	3.236	3.222
Ti	0.071	0.082	0.072	0.05	0.069	0.08	0.036	0.076	0.065
Cr	0	0	0.002	0	0	0.003	0	0	0.002
Fe	0.701	0.674	0.686	0.656	0.634	0.573	0.576	0.598	0.625
Mg	0.305	0.297	0.313	0.304	0.331	0.249	0.29	0.242	0.245
Mn	0.011	0.009	0.005	0.003	0.003	0.01	0.013	0.006	0.005
Ba	0.005	0.005	0.005	0.005	0.009	0.005	0.008	0.005	0.005
Ca	0.001	0.001	0.001	0.002	0.001	0.004	0.002	0.001	0.001
Na	0.064	0.058	0.054	0.064	0.069	0.074	0.06	0.073	0.07
K	1.834	1.95	1.908	1.882	1.870	1.759	1.935	1.875	1.884
F	0	0	0	0	0	0	0	0	0
Cl	0.001	0.001	0	0.001	0	0.002	0	0	0.001
O	22	22	22	22	22	22	22	22	22
Para	3.37	2.79	2.9	3.28	3.54	4.02	3	3.75	3.57
Musc	96.57	97.16	97.04	96.56	96.41	95.49	96.85	96.1	96.33
Marg	0.05	0.05	0.05	0.15	0.05	0.49	0.15	0.05	0.05
Fe/Mg	2.336	2.299	2.209	2.165	1.926	2.341	2.033	2.494	2.572
Fe/Fe+Mg	0.7	0.697	0.688	0.684	0.658	0.701	0.67	0.714	0.72

## Notes

B0512-7t B1219-16. Feldspar Zone

TABLE C-3 (cont'd). Microprobe Analyses. Muscovite.

	44	50	51	90-97	90-98	90-99	90-103	90-104	52
	B1219-16	B1219-16	B1219-16	B1218-3	B1218-3	B1218-3	B1218-3	B1218-3	B0512-1
SiO <sub>2</sub>	45.29	46.08	45.02	45.06	44.77	44.25	44.48	44.64	46.19
TiO <sub>2</sub>	0.73	0.84	0.77	0.69	0.47	0.62	0.45	0.46	0.54
Al <sub>2</sub> O <sub>3</sub>	29.83	29.60	29.51	30.62	31.26	30.32	30.85	31.09	27.53
Cr <sub>2</sub> O <sub>3</sub>	0.00	0.00	0.00	0.00	0.03	0.02	0.00	0.00	0.00
MnO	0.05	0.08	0.05	0.06	0.06	0.05	0.05	0.02	0.03
FeO	5.04	4.94	5.31	5.36	5.40	5.58	5.66	5.24	5.18
MgO	1.21	1.24	1.17	1.43	1.33	1.33	1.36	1.29	2.05
BaO	0.12	0.02	0.04	0.00	0.00	0.00	0.00	0.00	0.15
CaO	0.02	0.04	0.04	0.12	0.08	0.08	0.17	0.13	0.05
K <sub>2</sub> O	10.75	11.02	10.78	10.95	10.87	10.80	10.75	10.79	10.65
Na <sub>2</sub> O	0.22	0.23	0.26	0.25	0.25	0.24	0.27	0.25	0.34
F	0.00	0.00	0.00	0.00	0.00	0.00	0.00	0.00	0.00
Cl	0.00	0.00	0.02	0.01	0.01	0.01	0.00	0.01	0.00
Sum	93.26	94.09	92.92	94.55	94.53	93.30	93.99	93.92	92.71
O=F+Cl	0.00	0.00	0.00	0.00	0.00	0.00	0.00	0.00	0.00
Total	93.26	94.09	92.92	94.55	94.53	93.30	93.99	93.92	92.71
Structural Formulae (Based on 22 O)									
Si	6.321	6.371	6.319	6.225	6.182	6.204	6.187	6.198	6.492
Al-iv	1.679	1.629	1.681	1.775	1.818	1.796	1.810	1.807	1.508
Al-vi	3.227	3.194	3.2	3.21	3.268	3.210	3.244	3.284	3.052
Ti	0.077	0.087	0.081	0.072	0.049	0.065	0.047	0.048	0.057
Cr	0	0	0	0	0.003	0.002	0	0	0
Fe	0.588	0.571	0.620	0.619	0.624	0.654	0.650	0.608	0.609
Mg	0.252	0.256	0.234	0.294	0.274	0.272	0.282	0.267	0.429
Mn	0.006	0.009	0.006	0.007	0.007	0.006	0.006	0.002	0.004
Ba	0.007	0.001	0.002	0.006	0.004	0.004	0.007	0.007	0.008
Ca	0.003	0.006	0.006	0	0	0	0	0	0.008
Na	0.06	0.062	0.071	0.067	0.067	0.065	0.072	0.067	0.091
K	1.914	1.943	1.93	1.929	1.914	1.911	1.907	1.911	1.909
F	0	0	0	0	0	0	0	0	0
Cl	0	0	0.005	0.002	0.002	0.002	0	0.002	0
O	22	22	22	22	22	22	22	22	22
Parg	3.03	3.08	3.54	3.35	3.38	3.27	3.68	3.4	4.63
Musc	96.81	96.62	96.16	96.65	96.62	96.70	96.37	96.6	94.96
Marg	0.15	0.3	0.3	0	0	0	0	0	0.4
Fe/Mg	2.361	2.272	2.685	2.127	2.304	2.375	2.356	2.266	1.426
Fe/Fe+Mg	0.702	0.694	0.729	0.68	0.697	0.704	0.702	0.696	0.588

## Notes:

B1219-16 B1218-3. B0512-1. Feldspar Zone



TABLE C-3 (cont'd). Microprobe Analyses, Muscovite.

	53	55	59	61	62	63	64	67	69
	B0512-1	B0512-1	B0512-1	B0512-1	B0512-1	B0512-1	B0512-1	B0430-4	B0430-4
SiO <sub>2</sub>	45.92	45.93	45.98	46.06	46.17	45.53	46.26	45.03	44.34
TiO <sub>2</sub>	0.59	0.60	0.55	0.54	0.50	0.59	0.54	0.44	0.36
Al <sub>2</sub> O <sub>3</sub>	28.09	28.17	27.74	29.27	28.93	30.01	29.53	35.01	33.62
Cr <sub>2</sub> O <sub>3</sub>	0.00	0.04	0.03	0.00	0.03	0.05	0.05	0.04	0.02
MnO	0.12	0.01	0.07	0.05	0.06	0.04	0.07	0.00	0.00
FeO	5.07	5.26	5.37	5.25	5.30	5.24	5.29	2.74	2.71
MgO	1.95	1.95	2.13	1.99	2.15	1.92	2.17	0.84	0.90
BaO	0.13	0.19	0.16	0.11	0.11	0.08	0.06	0.52	0.53
CaO	0.04	0.00	0.00	0.00	0.00	0.00	0.01	0.00	0.11
K <sub>2</sub> O	10.63	10.59	10.78	10.53	10.69	10.41	10.73	9.36	9.29
Na <sub>2</sub> O	0.39	0.33	0.35	0.37	0.36	0.35	0.32	1.13	1.18
F	0.00	0.00	0.00	0.00	0.00	0.00	0.00	0.00	0.00
Cl	0.01	0.00	0.00	0.01	0.00	0.00	0.01	0.00	0.01
Sum	92.94	93.07	93.16	94.18	94.30	94.22	95.00	95.11	93.07
O=F+Cl	0.00	0.00	0.00	0.00	0.00	0.00	0.00	0.00	0.00
Total	92.94	93.07	93.16	94.18	94.30	94.22	95.00	95.11	93.07
Structural Formulae (Based on 22 O)									
Si	6.430	6.431	6.443	6.364	6.381	6.285	6.342	6.059	6.108
Al-iv	1.562	1.567	1.552	1.636	1.619	1.715	1.658	1.941	1.892
Al-vi	3.079	3.081	3.032	3.10	3.092	3.167	3.113	3.611	3.565
Ti	0.062	0.063	0.058	0.056	0.052	0.061	0.056	0.045	0.037
Cr	0	0.004	0.003	0	0.002	0.005	0.005	0.004	0.002
Fe	0.594	0.616	0.62	0.607	0.613	0.605	0.607	0.308	0.312
Mg	0.408	0.407	0.445	0.41	0.443	0.395	0.435	0.168	0.185
Mn	0.014	0.001	0.008	0.006	0.007	0.005	0.008	0	0
Ba	0.007	0.01	0.009	0.006	0.006	0.004	0.003	0.027	0.029
Ca	0.004	0	0	0	0	0	0.001	0	0.016
Na	0.106	0.09	0.095	0.099	0.096	0.094	0.085	0.295	0.315
K	1.901	1.892	1.928	1.856	1.884	1.833	1.876	1.607	1.632
F	0	0	0	0	0	0	0	0	0
Cl	0.002	0	0	0.002	0	0	0.001	0	0.002
O	22	22	22	22	22	22	22	22	22
Para	5.27	4.5	4.7	5.07	4.87	4.86	4.32	15.51	16.05
Musc	94.44	95.48	95.2	94.93	95.12	95.14	95.62	84.49	83.14
Marg	0.2	0	0	0	0	0	0.05	0	0.82
Fe/Mg	1.444	1.516	1.433	1.495	1.399	1.542	1.412	1.83	1.689
Fe/Fe+Mg	0.599	0.603	0.589	0.599	0.583	0.607	0.585	0.647	0.628

## Notes

B0512-1 Feldspar Zone B0430-4 Muscovite Zone

TABLE C-3 (cont'd). Microprobe Analyses. Muscovite.

	72	73	74	77	85	86	89-1	89-2	2
	B0430-4	B0430-4	B0430-4	B0430-4	B0430-4	B0430-4	B0430-4	B0430-4	B0602-1A
SiO <sub>2</sub>	44.95	44.93	44.75	44.86	43.54	44.43	49.62	48.41	47.99
TiO <sub>2</sub>	0.40	0.43	0.45	0.46	0.37	0.34	0.40	0.47	0.37
Al <sub>2</sub> O <sub>3</sub>	35.25	35.63	34.89	34.92	33.72	35.05	36.41	35.47	35.71
Cr <sub>2</sub> O <sub>3</sub>	0.01	0.01	0.03	0.05	0.08	0.02	0.00	0.00	0.06
MnO	0.00	0.01	0.00	0.03	0.02	0.04	0.00	0.00	0.00
FeO	2.92	2.89	2.95	2.80	2.99	2.78	2.33	2.11	2.88
MgO	0.81	0.81	0.77	0.81	0.81	0.76	0.87	0.77	0.95
BaO	0.47	0.56	0.56	0.47	0.48	0.54	0.00	0.00	0.29
CaO	0.00	0.00	0.00	0.00	0.01	0.00	0.71	0.63	0.01
K <sub>2</sub> O	9.40	9.37	9.32	9.35	8.99	8.92	8.30	8.74	8.81
Na <sub>2</sub> O	1.18	1.18	1.22	1.22	1.15	1.17	0.92	0.92	0.99
F	0.00	0.00	0.00	0.00	0.00	0.00	0.00	0.00	0.00
Cl	0.01	0.01	0.00	0.00	0.00	0.00	0.00	0.00	0.00
Sum	95.40	95.77	94.94	94.97	92.16	94.05	99.56	97.52	98.06
O=F+Cl	0.00	0.00	0.00	0.00	0.00	0.00	0.00	0.00	0.00
Total	95.40	95.77	94.94	94.97	92.16	94.05	99.56	97.52	98.06
Structural Formulae (Based on 22 O)									
Si	6.036	6.01	6.045	6.05	6.058	6.037	6.276	6.27	6.2
Al-iv	1.964	1.99	1.955	1.95	1.94	1.963	1.724	1.71	1.8
Al-vi	3.614	3.625	3.590	3.6	3.586	3.65	2.703	3.683	3.637
Ti	0.04	0.043	0.046	0.047	0.039	0.035	0.038	0.046	0.036
Cr	0.001	0.001	0.003	0.005	0.009	0.002	0	0	0.006
Fe	0.328	0.323	0.333	0.316	0.346	0.316	0.246	0.229	0.311
Mg	0.162	0.161	0.155	0.163	0.168	0.154	0.164	0.149	0.193
Mn	0	0.001	0	0.003	0.002	0.005	0	0	0
Ba	0.025	0.021	0.02	0.025	0.026	0.029	0.035	0.032	0.015
Ca	0	0	0	0	0.001	0	0	0	0.001
Na	0.307	0.306	0.31	0.319	0.31	0.308	0.226	0.231	0.247
K	1.61	1.599	1.606	1.608	1.595	1.546	1.39000	1.444	1.452
F	0	0	0	0	0	0	0	0	0
Cl	0.002	0.002	0	0	0	0	0	0	0
O	22	22	22	22	22	22	22	22	22
Parg	16.02	16.07	16.6	16.55	16.26	16.62	14.42	13.79	14.58
Musc	83.98	83.93	83.4	83.45	83.68	83.38	85.58	86.21	85.36
Marg	0	0	0	0	0.05	0	0	0	0.05
Fe/Mg	2.023	2.009	2.15	1.961	2.025	2.082	1.503	1.537	1.791
Fe/Fe+Mg	0.669	0.668	0.682	0.662	0.676	0.676	0.6	0.606	0.63

## Notes.

B0430-4, B0602-1a: biotite subzone, Muscovite Zone

TABLE C-3 (cont'd) Microprobe Analyses, Muscovite

	3	5	6	8	9	10	11	12	13
	B0602-1A	B0602-1A	B0602-1A	B0602-1A	B0602-1A	B0602-1A	B0602-1A	B0602-1A	B0602-1A
SiO <sub>2</sub>	45.69	48.49	45.86	46.64	46.07	46.13	45.44	45.98	46.07
TiO <sub>2</sub>	0.33	0.29	0.32	0.33	0.30	0.30	0.42	0.32	0.23
Al <sub>2</sub> O <sub>3</sub>	35.27	34.25	35.31	35.20	35.22	35.20	34.36	35.15	35.20
Cr <sub>2</sub> O <sub>3</sub>	0.00	0.05	0.00	0.04	0.00	0.00	0.00	0.00	0.00
MnO	0.03	0.00	0.01	0.05	0.02	0.00	0.02	0.03	0.04
FeO	2.75	2.80	2.84	2.52	2.68	2.82	2.70	2.58	2.79
MgO	0.75	0.98	0.78	0.86	0.84	0.76	0.76	0.80	0.74
BaO	0.31	0.31	0.34	0.23	0.26	0.22	0.27	0.30	0.26
CaO	0.01	0.03	0.02	0.07	0.00	0.00	0.00	0.03	0.02
K <sub>2</sub> O	9.21	9.17	9.34	9.50	9.52	9.71	9.34	9.39	9.35
Na <sub>2</sub> O	1.32	0.93	1.40	1.20	1.31	1.20	1.32	1.39	1.41
F	0.00	0.00	0.00	0.00	0.00	0.00	0.00	0.00	0.00
Cl	0.00	0.01	0.01	0.01	0.00	0.00	0.00	0.00	0.01
Sum	95.77	97.31	96.23	96.65	96.22	96.34	94.63	95.97	96.12
O=F+Cl	0.00	0.00	0.00	0.00	0.00	0.00	0.00	0.00	0.00
Total	95.77	97.31	96.23	96.65	96.22	96.34	94.63	95.97	96.12
Structural Formulae (Based on 22 O)									
Si	6.091	6.322	6.09	6.148	6.112	6.118	6.132	6.114	6.118
Al <sub>iv</sub>	1.909	1.678	1.91	1.852	1.888	1.882	1.868	1.886	1.882
Al <sub>vi</sub>	3.631	3.583	3.616	3.616	3.618	3.619	3.596	3.621	3.627
Ti	0.033	0.028	0.032	0.033	0.03	0.03	0.042	0.032	0.023
Cr	0	0.005	0	0.004	0	0	0	0	0
Fe	0.307	0.205	0.215	0.278	0.297	0.313	0.305	0.287	0.31
Mg	0.149	0.19	0.154	0.169	0.166	0.15	0.153	0.159	0.146
Mn	0.002	0	0.001	0.006	0.002	0	0.002	0.003	0.004
Ba	0.016	0.016	0.018	0.012	0.014	0.011	0.014	0.016	0.014
Ca	0.001	0.004	0.003	0.01	0	0	0	0.004	0.003
Na	0.341	0.235	0.36	0.307	0.337	0.309	0.342	0.358	0.363
F	1.587	1.525	1.582	1.597	1.612	1.642	1.606	1.592	1.584
F	0	0	0	0	0	0	0	0	0
Cl	0	0.001	0.001	0.002	0	0	0	0	0.002
O	22	22	22	22	22	22	22	22	22
Par <sub>9</sub>	17.71	18.31	18.51	18.04	17.28	15.81	17.68	18.32	18.62
Musc	82.23	86.45	81.34	83.44	82.72	84.19	82.32	81.47	81.23
Mar <sub>9</sub>	0.05	0.23	0.15	0.52	0	0	0	0.2	0.15
Fe/Mg	2.08	1.602	2.05	1.677	1.804	2.082	2.002	1.831	2.146
Fe/(Fe+Mg)	0.675	0.616	0.672	0.626	0.643	0.676	0.668	0.647	0.682

## Notes

B0602-1A biotite subzone Muscovite Zone

TABLE C-3 (cont'd). Microprobe Analyses, Muscovite.

	89-41	89-42	89-43
	B0511-1	B0511-1	B0511-1
SiO <sub>2</sub>	45.72	45.91	47.38
TiO <sub>2</sub>	0.99	1.27	1.53
Al <sub>2</sub> O <sub>3</sub>	30.02	30.54	29.93
Cr <sub>2</sub> O <sub>3</sub>	0.00	0.00	0.00
MnO	0.00	0.00	0.00
FeO	4.71	4.97	4.84
MgO	1.63	1.67	1.75
BaO	0.00	0.00	0.00
CaO	0.04	0.08	0.09
K <sub>2</sub> O	11.09	11.10	10.65
Na <sub>2</sub> O	0.32	0.32	0.25
F	0.00	0.00	0.04
Cl	0.00	0.00	0.00
Sum	94.53	95.86	96.46
O=F+Cl	0.00	0.00	0.02
Total	94.53	95.86	96.44
Structural Formulae (Based on 22 O)			
Si	6.294	6.242	6.365
Al-iv	1.706	1.758	1.635
Al-vi	3.166	3.136	3.102
Ti	0.102	0.13	0.155
Cr	0	0	0
Fe	0.542	0.565	0.544
Mg	0.334	0.338	0.35
Mn	0	0	0
Ba	0.002	0.004	0.005
Ca	0	0	0
Na	0.085	0.084	0.065
K	1.947	1.925	1.825
F	0	0	0.017
Cl	0	0	0
O	22	22	22
Parg	4.2	4.2	3.45
Musc	95.8	95.8	96.55
Marg	0	0	0
Fe/Mg	1.621	1.67	1.552
Fe/Fe+Mg	0.619	0.625	0.608

## Notes.

B0511-1 interior, muscovite-biotite granite

TABLE C-3 (cont'd). Microprobe Analyses, Muscovite.

	90-11	90-12	90-13	90-14	90-15	90-19	90-20	89-3	89-4
	B0602-1A	B0602-1A	B0602-1A	B0602-1A	B0602-1A	B0602-1A	B0602-1A	MT-4	MT-4
SiO <sub>2</sub>	46.77	47.07	46.47	46.80	46.86	47.06	45.56	47.49	47.71
TiO <sub>2</sub>	0.37	0.33	0.45	0.30	0.25	0.40	0.17	0.44	0.48
Al <sub>2</sub> O <sub>3</sub>	34.54	34.71	33.94	34.47	34.56	35.24	35.89	35.46	34.86
Cr <sub>2</sub> O <sub>3</sub>	0.00	0.00	0.00	0.01	0.00	0.00	0.00	0.00	0.00
MnO	0.08	0.07	0.00	0.02	0.04	0.07	0.00	0.00	0.00
FeO	2.80	2.69	2.71	2.60	2.84	2.88	3.27	2.27	2.22
MgO	0.87	0.88	0.77	0.89	0.92	0.75	0.12	0.55	0.65
BaO	0.00	0.05	0.13	0.00	0.00	0.00	0.00	0.00	0.00
CaO	0.21	0.26	0.25	0.26	0.20	0.31	0.53	0.22	0.22
K <sub>2</sub> O	9.39	9.12	9.21	9.24	9.24	9.35	9.89	9.16	9.49
Na <sub>2</sub> O	0.99	1.09	1.04	1.08	1.12	1.09	0.61	0.80	0.86
F	0.00	0.00	0.00	0.00	0.00	0.00	0.00	0.11	0.12
Cl	0.01	0.00	0.00	0.00	0.00	0.00	0.00	0.00	0.00
Sum	96.03	96.27	94.97	95.67	96.03	97.15	96.04	96.50	96.61
O=F+Cl	0.00	0.00	0.00	0.00	0.00	0.00	0.00	0.05	0.05
Total	96.03	96.27	94.97	95.67	96.03	97.15	96.04	96.45	96.56
Structural Formulae (Based on 22 O)									
Si	6.201	6.210	6.227	6.218	6.209	6.171	6.08	6.221	6.256
Al <sub>iv</sub>	1.764	1.787	1.773	1.782	1.791	1.829	1.92	1.779	1.744
Al <sub>vi</sub>	3.596	3.612	3.587	3.615	3.604	3.617	3.724	3.695	3.642
Ti	0.037	0.033	0.045	0.03	0.025	0.039	0.017	0.043	0.047
Cr	0	0	0	0.001	0	0	0	0	0
Fe	0.31	0.297	0.304	0.289	0.315	0.316	0.365	0.249	0.243
Mg	0.172	0.172	0.154	0.176	0.182	0.147	0.024	0.107	0.127
Mn	0.009	0.008	0	0.002	0.004	0.008	0	0	0
Ba	0.011	0.013	0.010	0.014	0.01	0.016	0.028	0.011	0.011
Ca	0	0.007	0.014	0	0	0	0	0	0
Na	0.256	0.279	0.27	0.278	0.288	0.277	0.150	0.201	0.219
K	1.588	1.536	1.574	1.566	1.561	1.564	1.683	1.531	1.587
F	0	0	0	0	0	0	0	0.046	0.05
Cl	0.001	0	0	0	0	0	0	0	0
O	22	22	22	22	22	22	22	22	22
Pat 4	15.81	15.21	14.5	15.09	15.56	15.05	8.57	11.72	12.11
Musc	86.19	84.7	84.49	84.91	84.44	84.95	91.43	88.28	87.89
Marg	0	0.39	1	0	0	0	0	0	0
Fe/Mg	1.858	1.76	1.975	1.652	1.757	2.208	15.286	2.316	1.916
Fe/Fe+Mg	0.65	0.638	0.664	0.623	0.637	0.688	0.939	0.698	0.657

## Notes

B0602-1A biotite subzone Muscovite Zone

MT-4 schistose to mylonitic Kyanite Zone

TABLE C-3 (cont'd). Microprobe Analyses, Muscovite.

	89-5	90-22	90-23	90-24	90-25	90-26	90-27	96	97
	MT-4	B1219-6	B1219-6	B1219-6	B1219-6	B1219-6	B1219-6	B0431-1	B0431-1
SiO <sub>2</sub>	49.47	45.65	45.42	44.91	44.58	43.66	45.92	44.49	46.08
TiO <sub>2</sub>	0.46	0.31	0.17	0.19	0.20	0.25	0.25	0.28	0.47
Al <sub>2</sub> O <sub>3</sub>	34.30	35.38	36.04	35.80	35.59	35.01	35.74	37.30	37.30
Cr <sub>2</sub> O <sub>3</sub>	0.00	0.01	0.02	0.00	0.04	0.00	0.02	0.01	0.04
MnO	0.00	0.03	0.04	0.02	0.00	0.02	0.04	0.00	0.02
FeO	2.16	3.37	3.12	2.56	3.24	3.26	3.17	2.12	2.22
MgO	0.52	0.13	0.11	0.15	0.14	0.13	0.14	0.22	0.26
BaO	0.00	0.00	0.02	0.00	0.00	0.00	0.00	0.24	0.23
CaO	0.15	0.32	0.31	0.29	0.34	0.35	0.38	0.01	0.00
K <sub>2</sub> O	9.50	9.85	9.73	9.60	10.10	9.75	9.93	8.56	8.69
Na <sub>2</sub> O	0.85	0.66	0.54	0.69	0.65	0.69	0.58	1.84	1.51
F	0.13	0.00	0.00	0.00	0.00	0.00	0.00	0.00	0.00
Cl	0.00	0.01	0.00	0.01	0.00	0.00	0.00	0.01	0.00
Sum	97.49	95.72	95.52	94.22	94.88	93.12	96.17	95.08	96.82
O=F+Cl	0.05	0.00	0.00	0.00	0.00	0.00	0.00	0.00	0.00
Total	97.44	95.72	95.52	94.22	94.88	93.12	96.17	95.08	96.82
Structural Formulae (Based on 22 O)									
Si	6.399	6.108	6.073	6.072	6.033	6.02	6.109	5.938	6.028
Al <sub>iv</sub>	1.601	1.892	1.927	1.928	1.967	1.98	1.891	2.062	1.974
Al <sub>vi</sub>	3.632	3.686	3.751	3.777	3.709	3.708	3.711	3.805	3.774
Ti	0.045	0.031	0.017	0.019	0.02	0.026	0.025	0.028	0.046
Cr	0	0.001	0.002	0	0.004	0	0.002	0.001	0.004
Fe	0.234	0.377	0.349	0.289	0.367	0.376	0.353	0.237	0.243
Mg	0.1	0.026	0.022	0.03	0.028	0.027	0.028	0.044	0.051
Mn	0	0.003	0.005	0.002	0	0.002	0.005	0	0.002
Ba	0.008	0.017	0.016	0.015	0.018	0.019	0.02	0.013	0.012
Ca	0	0	0.003	0	0	0	0	0.001	0
Na	0.213	0.171	0.14	0.181	0.171	0.184	0.15	0.476	0.382
K	1.569	1.681	1.659	1.656	1.742	1.715	1.685	1.457	1.444
F	0.053	0	0	0	0	0	0	0	0
Cl	0	0.002	0	0.002	0	0	0	0.002	0
O	22	22	22	22	22	22	22	22	22
Para	11.97	9.14	7.77	9.85	8.91	9.71	8.15	24.61	20.89
Musc	88.03	90.76	92.06	90.15	91.09	90.19	91.85	75.34	79.11
Marg	0	0	0.17	0	0	0	0	0.05	0
Fe/Mg	2.331	14.676	16.121	9.651	12.985	14.157	12.867	5.407	4.834
Fe/Fe+Mg	0.7	0.936	0.942	0.906	0.928	0.934	0.928	0.844	0.829

## Notes

MT-4, B0431-1, schistose to mylonitic Kyanite Zone

B1219-6, magnetite subzone, Muscovite Zone

TABLE C-3 (cont'd). Microprobe Analyses, Muscovite.

	100	103	89-14	89-15	89-16	89-17	89-18	89-19	89-20
	B0431-1	B0431-1	B0602-7	B0602-7	B0602-7	B0602-7	B0602-7	F 502-7	B0602-7
SiO <sub>2</sub>	44.09	44.22	45.49	44.18	45.32	44.95	44.86	48.39	44.65
TiO <sub>2</sub>	0.32	0.26	0.11	0.13	0.13	0.55	0.35	0.14	0.43
Al <sub>2</sub> O <sub>3</sub>	35.66	34.97	37.26	36.30	35.34	35.72	36.03	37.45	36.46
Cr <sub>2</sub> O <sub>3</sub>	0.07	0.02	0.03	0.00	0.00	0.00	0.00	0.00	0.00
MnO	0.07	0.00	0.00	0.04	0.00	0.00	0.00	0.00	0.00
FeO	2.14	2.02	2.30	2.17	2.21	2.25	1.29	2.34	2.30
MgO	0.28	0.33	0.12	0.18	0.33	0.16	0.20	0.24	0.15
BaO	0.16	0.18	0.00	0.00	0.00	0.00	0.00	0.00	0.00
CaO	0.00	0.03	0.17	0.10	0.12	0.19	0.13	0.12	0.31
K <sub>2</sub> O	8.58	8.52	8.95	8.92	9.18	7.91	8.65	8.18	7.89
Na <sub>2</sub> O	1.71	1.74	1.57	1.56	1.36	1.17	1.57	1.24	1.33
F	0.00	0.00	0.00	0.00	0.00	0.00	0.00	0.00	0.00
Cl	0.00	0.01	0.00	0.00	0.00	0.00	0.00	0.00	0.00
Sum	93.08	92.30	96.00	93.58	93.99	92.90	93.08	98.10	93.52
O=F+Cl	0.00	0.00	0.00	0.00	0.00	0.00	0.00	0.00	0.00
Total	93.08	92.30	96.00	93.58	93.99	92.90	93.08	98.10	93.52
Structural Formulae (Based on 22 O)									
Si	6.015	6.076	6.012	5.996	6.121	6.094	6.076	6.19	6.026
Al <sub>iv</sub>	1.985	1.924	1.988	2.004	1.879	1.906	1.924	1.81	1.974
Al <sub>vi</sub>	3.748	3.739	3.815	3.801	3.746	3.801	3.827	3.834	3.825
Ti	0.033	0.027	0.011	0.013	0.013	0.056	0.036	0.013	0.044
Cr	0.008	0.002	0.002	0	0	0	0	0	0
Fe	0.244	0.232	0.254	0.246	0.25	0.255	0.146	0.25	0.26
Mg	0.057	0.068	0.024	0.036	0.066	0.032	0.04	0.046	0.03
Mn	0.008	0	0	0.005	0	0	0	0	0
Ba	0.009	0.01	0.009	0.005	0.006	0.01	0.007	0.006	0.016
Ca	0	0.004	0	0	0	0	0	0	0
Na	0.45	0.464	0.401	0.41	0.356	0.308	0.412	0.308	0.340
K	1.493	1.493	1.509	1.544	1.581	1.368	1.494	1.335	1.358
F	0	0	0	0	0	0	0	0	0
Cl	0	0.002	0	0	0	0	0	0	0
O	22	22	22	22	22	22	22	22	22
Furg	23.24	23.66	21.85	21	18.38	18.36	21.62	18.73	20.4
Musc	76.76	76.11	78.95	79	81.62	81.64	78.38	81.27	79.6
Marg	0	0.2	0	0	0	0	0	0	0
Fe/Mg	4.43	3.434	10.754	6.89	3.758	7.89	3.619	5.47	8.603
Fe/Fe+Mg	0.816	0.774	0.915	0.873	0.79	0.888	0.783	0.845	0.896

## Notes

B0431-1 B0602-7. schistose to mylonitic Kyanite Zone

TABLE C-3 (cont'd). Microprobe Analyses. Muscovite.

	89-28	89-29	89-30	90-28	90-29	90-30	90-31	90-32	90-33
	B0501-4	B0501-4	B0501-4	B0501-5	B0501-5	B0501-5	B0501-5	B0501-5	B0501-5
SiO <sub>2</sub>	45.35	48.40	48.06	47.32	46.00	46.41	46.27	30.68	46.34
TiO <sub>2</sub>	0.28	0.29	0.35	0.07	0.29	0.15	0.06	0.00	0.05
Al <sub>2</sub> O <sub>3</sub>	35.79	37.31	36.59	39.61	37.20	38.22	40.14	51.78	41.09
Cr <sub>2</sub> O <sub>3</sub>	0.00	0.00	0.00	0.00	0.00	0.01	0.00	0.00	0.03
MnO	0.00	0.00	0.00	0.04	0.02	0.01	0.01	0.06	0.01
FeO	1.44	1.68	1.56	0.99	1.76	1.46	0.89	0.23	0.83
MgO	0.30	0.29	0.33	0.09	0.25	0.23	0.06	0.10	0.10
BaO	0.00	0.00	0.00	0.00	0.00	0.00	0.00	0.00	0.00
CaO	0.13	0.15	0.14	0.21	0.00	0.01	0.39	12.95	0.66
K <sub>2</sub> O	8.85	7.90	7.78	3.39	7.32	6.68	1.93	0.00	1.80
Na <sub>2</sub> O	1.89	1.36	1.35	4.72	2.54	2.63	5.90	0.80	5.43
F	0.00	0.00	0.00	0.00	0.00	0.00	0.00	0.00	0.00
Cl	0.00	0.00	0.00	0.00	0.01	0.01	0.00	0.00	0.00
Sum	94.03	97.38	96.16	96.44	95.39	95.82	95.65	96.60	96.34
O=F+Cl	0.00	0.00	0.00	0.00	0.00	0.00	0.00	0.00	0.00
Total	94.03	97.38	96.16	96.44	95.39	95.82	95.65	96.60	96.34
Structural Formulae (Based on 22 O)									
Si	6.099	6.21	6.239	6.027	6.052	6.04	5.925	4.019	5.879
Al-iv	1.901	1.79	1.761	1.973	1.948	1.96	2.075	3.981	2.121
Al-vi	3.771	3.851	3.836	3.971	3.819	3.901	3.981	4.011	4.011
Ti	0.028	0.028	0.034	0.007	0.029	0.015	0.006	0	0.005
Cr	0	0	0	0	0	0.001	0	0	0.001
Fe	0.162	0.18	0.169	0.105	0.194	0.159	0.095	0.025	0.088
Mg	0.06	0.055	0.064	0.017	0.049	0.045	0.011	0.02	0.019
Mn	0	0	0	0.004	0.002	0.001	0.001	0.007	0.001
Ba	0.007	0.008	0.007	0	0	0	0	0	0
Ca	0	0	0	0.029	0	0.001	0.054	1.817	0.09
Na	0.493	0.338	0.34	1.165	0.648	0.664	1.465	0.203	1.336
K	1.518	1.293	1.288	0.551	1.228	1.109	0.315	0	0.291
F	0	0	0	0	0	0	0	0	0
Cl	0	0	0	0	0.002	0.002	0	0	0
O	22	22	22	22	22	22	22	22	22
Parg	24.51	20.74	20.87	66.74	34.52	37.41	79.89	16.05	77.81
Musc	75.49	79.26	79.13	31.55	65.47	62.51	17.19	0	16.97
Marg	0	0	0	1.66	0	0.08	2.92	89.95	5.23
Fe/Mg	2.693	3.25	2.652	6.424	3.975	2.586	8.417	1.631	4.714
Fe/Fe+Mg	0.729	0.765	0.726	0.865	0.8	0.781	0.894	0.62	0.825

## Notes

B0501 4.5. schistose to mylonitic Kyanite Zone



TABLE C-3 (cont'd) Microprobe Analyses, Muscovite.

	90-34	90-35	90-36	90-37	90-38	90-39	90-40	90-41	90-42
	B0501-5	B0501-5	B0501-5	B0501-5	B0501-5	B0501-5	B0501-5	B0501-5	B0501-5
SiO <sub>2</sub>	46.35	45.20	30.62	45.51	30.60	46.27	47.49	46.83	46.32
TiO <sub>2</sub>	0.12	0.03	0.00	0.00	0.00	0.05	0.07	0.09	0.01
Al <sub>2</sub> O <sub>3</sub>	37.54	41.07	51.56	40.86	52.25	41.22	40.60	40.87	40.99
Cr <sub>2</sub> O <sub>3</sub>	0.01	0.01	0.03	0.00	0.01	0.01	0.01	0.01	0.00
MnO	0.02	0.01	0.00	0.02	0.08	0.00	0.00	0.03	0.00
FeO	1.81	0.57	0.25	0.78	0.33	0.65	0.78	0.85	0.73
MgO	0.34	0.04	0.12	0.07	0.16	0.08	0.05	0.08	0.07
BaO	0.05	0.00	0.00	0.00	0.00	0.00	0.00	0.00	0.00
CaO	0.08	0.80	12.50	0.76	12.54	0.66	0.35	0.52	1.06
K <sub>2</sub> O	7.06	1.00	0.00	1.60	0.00	0.68	1.84	1.48	1.62
Na <sub>2</sub> O	2.77	6.47	0.93	6.13	1.04	5.66	5.54	5.83	5.56
F	0.00	0.00	0.00	0.00	0.00	0.00	0.00	0.00	0.00
Cl	0.00	0.00	0.00	0.00	0.00	0.00	0.00	0.00	0.00
Sum	96.15	95.20	96.01	95.73	97.01	95.28	96.73	96.59	96.36
O=F+Cl	0.00	0.00	0.00	0.00	0.00	0.00	0.00	0.00	0.00
Total	96.15	95.20	96.01	95.73	97.01	95.28	96.73	96.59	96.36
Structural Formulae (Based on 22 O)									
Si	6.046	5.802	4.031	5.827	3.992	5.891	5.986	5.918	5.877
Al <sup>iv</sup>	1.951	2.198	3.969	2.173	4.308	2.109	2.014	2.082	2.123
Al <sup>vi</sup>	3.82	4.014	4.029	3.992	4.025	4.075	4.017	4.005	4.005
Ti	0.012	0.003	0	0	0	0.005	0.007	0.009	0.001
Cr	0.001	0.001	0.003	0	0.001	0.001	0.001	0.001	0
Fe	0.198	0.061	0.028	0.084	0.036	0.069	0.082	0.09	0.077
Mg	0.064	0.000	0.024	0.013	0.031	0.015	0.009	0.015	0.013
Mn	0.002	0.001	0	0.002	0.009	0	0	0.003	0
Ba	0.003	0	0	0	0	0	0	0	0
Ca	0.011	0.11	1.763	0.104	1.753	0.09	0.047	0.07	0.144
Na	0.701	1.61	0.237	1.511	0.263	1.397	1.354	1.428	1.360
K	1.175	0.164	0	0.261	0	0.11	0.296	0.239	0.162
F	0	0	0	0	0	0	0	0	0
Cl	0	0	0	0	0	0	0	0	0
O	22	22	22	22	22	22	22	22	22
Parg	37.14	85.47	11.87	80.63	13.05	87.45	79.78	82.22	77.1
Musc	62.27	8.69	0	13.85	0	6.91	17.42	13.73	14.78
Marg	0.59	5.84	88.13	5.52	86.95	5.64	2.79	4.05	8.12
Fe/Mg	3.02	8.137	1.169	6.414	1.441	4.559	8.753	6.175	5.851
Fe/Fe+Mg	0.751	0.891	0.539	0.865	0.59	0.82	0.897	0.861	0.854

## Notes

B0501 : schistose to mylonitic Kyanite Zone

TABLE C-3 (cont'd). Microprobe Analyses. Muscovite.

	90-43	90-44	90-45	90-46	90-47	90-48	90-49	90-51	90-52
	B0501-5	B0501-5	B0501-5	B0501-5	B0501-5	B0501-5	B0501-5	B0501-5	B0501-5
SiO <sub>2</sub>	46.18	46.14	46.83	46.19	30.55	45.71	46.27	47.57	46.54
TiO <sub>2</sub>	0.33	0.34	0.28	0.06	0.00	0.05	0.29	0.31	0.18
Al <sub>2</sub> O <sub>3</sub>	36.57	37.34	37.96	40.49	51.98	40.40	36.87	37.89	37.58
Cr <sub>2</sub> O <sub>3</sub>	0.03	0.00	0.01	0.00	0.00	0.02	0.03	0.00	0.00
MnO	0.00	0.03	0.00	0.00	0.00	0.04	0.02	0.01	0.01
FeO	1.86	1.76	1.81	0.65	0.38	0.68	1.80	1.84	1.49
MgO	0.23	0.26	0.18	0.04	0.13	0.04	0.22	0.25	0.24
BaO	0.17	0.06	0.01	0.00	0.00	0.00	0.08	0.13	0.00
CaO	0.00	0.03	0.02	0.46	12.66	0.52	0.00	0.01	0.02
K <sub>2</sub> O	7.20	7.36	6.63	1.18	0.01	1.44	7.15	7.09	7.19
Na <sub>2</sub> O	2.58	2.58	2.95	6.50	1.00	6.37	2.70	2.47	2.74
F	0.00	0.00	0.00	0.00	0.00	0.00	0.00	0.00	0.00
Cl	0.00	0.00	0.00	0.00	0.01	0.00	0.00	0.00	0.01
Sum	95.15	95.90	96.68	95.57	96.73	95.27	95.43	97.57	96.00
O=F+Cl	0.00	0.00	0.00	0.00	0.00	0.00	0.00	0.00	0.00
Total	95.15	95.90	96.68	95.57	96.73	95.27	95.43	97.57	96.00
Structural Formulae (Based on 22 O)									
Si	6.098	6.044	6.056	5.901	4	5.872	6.086	6.102	6.07
Al-iv	1.902	1.956	1.944	2.099	4	2.128	1.914	1.898	1.93
Al-vi	3.788	3.807	3.641	3.996	4.017	3.987	3.8	3.83	3.845
Ti	0.033	0.033	0.027	0.006	0	0.005	0.029	0.03	0.018
Cr	0.003	0	0.001	0	0	0.002	0.003	0	0
Fe	0.205	0.193	0.196	0.069	0.042	0.073	0.198	0.197	0.163
Mg	0.045	0.051	0.035	0.008	0.025	0.006	0.042	0.048	0.047
Mn	0	0.003	0	0	0	0.004	0.002	0.001	0.001
Ba	0.009	0.003	0.001	0	0	0	0.004	0.007	0
Ca	0	0.004	0.003	0.063	1.775	0.072	0	0.001	0.003
Na	0.66	0.655	0.74	1.61	0.254	1.584	0.689	0.614	0.693
K	1.210	1.22	1.094	0.191	0.002	0.236	1.199	1.16	1.196
F	0	0	0	0	0	0	0	0	0
Cl	0	0	0	0	0.001	0	0	0	0.002
O	22	22	22	22	22	22	22	22	22
Parg	35.26	34.68	40.29	86.32	12.5	83.76	36.47	34.59	36.63
Musc	64.74	65.09	59.56	10.31	0.06	12.46	63.53	65.33	65.23
Marg	0	0.22	0.15	3.38	87.42	3.78	0	0.08	0.15
Fe/Mg	4.537	3.864	5.642	9.117	1.64	10.197	4.642	4.152	3.507
Fe/Fe+Mg	0.819	0.794	0.849	0.901	0.621	0.91	0.823	0.804	0.778

## Notes:

B0501-5, schistose to mylonitic Kyanite Zone

TABLE C-3 (cont'd). Microprobe Analyses, Muscovite.

	90-53	90-54	90-55	90-77	90-78	90-79	90-80	90-81	90-82
	B0501-5	B0501-5	B0501-5	B0628-4	B0628-4	B0628-4	B0628-4	B0628-4	B0628-4
SiO <sub>2</sub>	46.06	46.08	47.52	44.15	44.37	44.54	44.86	44.64	50.51
TiO <sub>2</sub>	0.06	0.28	0.07	0.11	0.17	0.26	0.13	0.15	0.00
Al <sub>2</sub> O <sub>3</sub>	39.77	37.26	40.94	36.69	36.79	34.88	36.67	36.36	32.46
Cr <sub>2</sub> O <sub>3</sub>	0.09	0.90	0.00	0.01	0.01	0.00	0.00	0.04	0.00
MnO	0.00	0.02	0.00	0.00	0.00	0.00	0.02	0.00	0.06
FeO	0.79	1.84	0.76	2.61	2.66	2.62	2.51	2.37	0.49
MgO	0.05	0.26	0.06	0.10	0.11	0.14	0.12	0.11	2.27
BaO	0.00	0.05	0.00	0.00	0.00	0.00	0.00	0.00	0.03
CaO	0.34	0.00	0.44	0.04	0.13	0.11	0.12	0.05	0.00
K <sub>2</sub> O	1.82	7.16	1.34	9.57	9.38	9.57	9.63	9.48	10.39
Na <sub>2</sub> O	6.19	2.77	5.66	1.15	1.17	1.15	1.19	1.18	0.07
F	0.00	0.00	0.00	0.00	0.00	0.00	0.00	0.00	0.00
Cl	0.01	0.00	0.00	0.00	0.00	0.00	0.00	0.00	0.00
Sum	95.18	95.72	96.79	94.43	94.79	93.27	95.25	94.38	96.28
O=F+Cl	0.00	0.00	0.00	0.00	0.00	0.00	0.00	0.00	0.00
Total	95.18	95.72	96.79	94.43	94.79	93.27	95.25	94.38	96.28
Structural Formulae (Based on 22 O)									
Si	5.929	6.046	5.971	5.962	5.966	6.093	6.003	6.018	6.576
Al <sub>iv</sub>	2.071	1.954	2.029	2.038	2.034	1.907	1.997	1.982	1.424
Al <sub>vi</sub>	3.962	3.806	4.034	3.8	3.795	3.716	3.786	3.793	3.555
Ti	0.006	0.028	0.007	0.011	0.017	0.027	0.013	0.015	0
Cr	0.009	0	0	0.001	0.001	0	0	0.004	0
Fe	0.085	0.202	0.08	0.295	0.299	0.3	0.281	0.267	0.053
Mg	0.01	0.051	0.011	0.02	0.022	0.029	0.024	0.022	0.44
Mn	0	0.002	0	0	0	0	0.002	0	0.007
Ba	0	0.003	0	0.002	0.007	0.006	0.006	0.003	0
Ca	0.047	0	0.054	0	0	0	0	0	0.004
Na	1.545	0.705	1.379	0.301	0.305	0.305	0.309	0.308	0.018
K	0.294	1.198	0.215	1.648	1.609	1.67	1.644	1.63	1.725
F	0	0	0	0	0	0	0	0	0
Cl	0.002	0	0	0	0	0	0	0	0
O	22	22	22	22	22	22	22	22	22
Parq	81.71	37.03	83.42	0.3	0.31	0.31	0.31	15.91	1.01
Musc	15.81	62.97	12.99	1.65	1.61	1.67	1.64	84.09	98.75
Marg	2.48	0	3.58	0	0	0	0	0	0.24
Fe/Mg	8.865	4.014	7.107	14.644	13.568	10.5	11.831	12.089	0.136
Fe/Fe+Mg	0.899	0.801	0.877	0.936	0.931	0.913	0.922	0.924	0.12

## Notes

B0501-5 B0628-4: schistose to mylonitic Kyanite Zone

TABLE C-3 (cont'd). Microprobe Analyses, Muscovite.

	90-83	89-6	89-7	89-8	89-9	89-10	89-11	89-12	89-13
	B0628-4	B0430-3	B0430-3	B0430-3	B0430-3	B0501-8	B0501-8	B0501-8	B0501-8
SiO <sub>2</sub>	55.86	47.88	45.28	47.23	43.61	47.45	47.19	48.19	48.34
TiO <sub>2</sub>	0.00	0.50	0.44	0.45	0.35	0.12	0.29	0.47	0.51
Al <sub>2</sub> O <sub>3</sub>	27.91	35.77	35.93	36.96	36.04	36.77	36.55	37.18	37.15
Cr <sub>2</sub> O <sub>3</sub>	0.02	0.00	0.00	0.00	0.00	0.00	0.00	0.00	0.00
MnO	0.08	0.00	0.00	0.00	0.00	0.00	0.00	0.00	0.00
FeO	0.74	1.76	1.43	1.77	1.57	1.88	1.79	1.70	1.70
MgO	0.66	0.66	0.73	0.57	0.53	0.19	0.10	0.15	0.13
BaO	0.67	0.00	0.00	0.04	0.00	0.00	0.00	0.00	0.00
CaO	0.00	0.24	0.32	0.26	0.19	0.53	0.42	0.48	0.41
K <sub>2</sub> O	6.09	7.54	8.70	7.54	8.50	8.79	8.61	8.65	8.73
Na <sub>2</sub> O	5.03	1.44	1.87	1.49	2.08	0.86	0.79	0.73	0.81
F	0.00	0.00	0.00	0.00	0.00	0.07	0.00	0.00	0.10
Cl	0.00	0.00	0.00	0.00	0.00	0.00	0.00	0.00	0.00
-----	-----	-----	-----	-----	-----	-----	-----	-----	-----
Sum	97.06	95.79	94.70	96.31	92.87	96.66	95.74	97.55	97.88
O=F+Cl	0.00	0.00	0.00	0.00	0.00	0.03	0.00	0.00	0.04
-----	-----	-----	-----	-----	-----	-----	-----	-----	-----
Total	97.06	95.79	94.70	96.31	92.87	96.63	95.74	97.55	97.84
Structural Formulae (Based on 22 O)									
Si	7.135	6.251	6.055	6.14	5.956	6.187	6.198	6.204	6.204
Al-iv	0.865	1.749	1.945	1.86	2.044	1.813	1.802	1.796	1.796
Al-vi	3.335	3.753	3.716	3.803	3.756	3.837	3.854	3.844	3.822
Ti	0	0.049	0.044	0.044	0.036	0.012	0.029	0.046	0.049
Cr	0.002	0	0	0	0	0	0	0	0
Fe	0.079	0.192	0.16	0.192	0.179	0.205	0.197	0.183	0.182
Mg	0.126	0.128	0.145	0.11	0.108	0.037	0.02	0.029	0.025
Mn	0.009	0	0	0	0	0	0	0	0
Ba	0	0.012	0.017	0.013	0.01	0.027	0.022	0.024	0.021
Ca	0.002	0	0	0.006	0	0	0	0	0
Na	1.246	0.364	0.485	0.376	0.551	0.217	0.201	0.182	0.202
K	0.992	1.256	1.404	1.25	1.481	1.462	1.442	1.42	1.429
F	0	0	0	0	0	0.029	0	0	0.041
Cl	0	0	0	0	0	0	0	0	0
O	22	22	22	22	22	22	22	22	22
Parq	53.47	22.5	24.63	23.04	27.11	12.95	12.24	11.37	12.36
Musc	42.59	77.5	75.37	76.59	72.55	87.05	87.76	88.63	87.64
Marg	3.94	0	0	0.36	0	0	0	0	0
Fe/Mg	0.698	1.496	1.099	1.742	1.662	5.55	10.043	6.359	7.327
Fe/Fe+Mg	0.411	0.599	0.524	0.635	0.624	0.847	0.909	0.864	0.88

## Notes

B0430-3 foliated to granuloblastic staurolite-garnet kyanite zone

B0501-8 granuloblastic kyanite zone

TABLE C-3 (cont'd) Microprobe Analyses, Muscovite.

	89-21	89-22	89-23	89-24	89-25	89-26	89-27	90-56	90-57
	B0628-2	B0628-2	B0628-2	B0628-2	B0628-2	B0628-2	B0628-2	B0628-2	B0628-2
SiO <sub>2</sub>	45.39	45.31	44.95	46.91	47.17	47.39	46.78	46.49	47.04
TiO <sub>2</sub>	0.29	0.35	0.16	0.22	0.15	0.13	0.14	0.00	0.42
Al <sub>2</sub> O <sub>3</sub>	36.78	37.53	37.87	37.73	38.15	38.47	37.26	38.54	37.43
Cr <sub>2</sub> O <sub>3</sub>	0.00	0.00	0.00	0.00	0.00	0.00	0.00	0.00	0.03
MnO	0.00	0.00	0.00	0.00	0.00	0.00	0.00	0.00	0.00
FeO	0.48	0.40	0.47	0.38	0.00	0.43	0.52	0.42	1.29
MgO	0.22	0.15	0.19	0.22	0.12	0.22	0.19	0.06	0.20
BaO	0.00	0.00	0.00	0.00	0.00	0.00	0.00	0.00	0.00
CaO	0.00	0.06	0.05	0.08	0.00	0.02	0.01	0.00	0.00
K <sub>2</sub> O	9.39	9.60	9.28	8.28	8.87	9.09	8.86	9.56	9.08
Na <sub>2</sub> O	1.04	0.85	1.37	0.90	1.25	1.12	1.15	1.03	1.22
F	0.00	0.00	0.00	0.00	0.00	0.00	0.00	0.00	0.00
Cl	0.00	0.00	0.00	0.00	0.00	0.00	0.00	0.00	0.01
-----	-----	-----	-----	-----	-----	-----	-----	-----	-----
Sum	93.59	94.25	94.34	94.72	95.71	96.87	94.91	96.10	96.72
O=F+Cl	0.00	0.00	0.00	0.00	0.00	0.00	0.00	0.00	0.00
-----	-----	-----	-----	-----	-----	-----	-----	-----	-----
Total	93.59	94.25	94.34	94.72	95.71	96.87	94.91	96.10	96.72
Structural Formulae (Based on 22 O)									
Si	6.09	6.04	5.992	6.154	6.138	6.112	6.157	6.064	6.113
Al-iv	1.91	1.96	2.008	1.846	1.862	1.888	1.843	1.936	1.887
Al-vi	3.904	3.935	3.94	3.987	3.987	3.959	3.936	3.988	3.845
Ti	0.029	0.035	0.016	0.022	0.015	0.013	0.014	0	0.041
Cr	0	0	0	0	0	0	0	0	0.003
Fe	0.054	0.045	0.052	0.042	0	0.046	0.057	0.046	0.14
Mg	0.044	0.03	0.038	0.043	0.023	0.042	0.037	0.012	0.039
Mn	0	0	0	0	0	0	0	0	0
Ba	0	0.003	0.003	0.004	0	0.001	0.001	0	0
Ca	0	0	0	0	0	0	0	0	0
Na	0.171	0.22	0.354	0.229	0.315	0.28	0.293	0.26	0.307
K	1.607	1.622	1.578	1.385	1.472	1.495	1.487	1.59	1.505
F	0	0	0	0	0	0	0	0	0
Cl	0	0	0	0	0	0	0	0	0.002
O	22	22	22	22	22	22	22	22	22
Parg	14.41	11.86	18.33	14.18	17.64	15.77	16.48	14.07	16.96
Musc	85.59	88.14	81.67	85.82	82.36	84.23	83.52	85.93	83.04
Marg	0	0	0	0	0	0	0	0	0
Fe/Mg	1.224	1.496	1.388	0.969	0	1.097	1.536	3.928	3.619
Fe/Fe+Mg	0.55	0.599	0.581	0.492	0	0.523	0.606	0.797	0.783

## Notes.

B028-2, granoblastic Kyanite Zone

TABLE C-3 (cont'd). Microprobe Analyses, Muscovite.

	90-58	90-59	90-70	90-71	90-72	90-73	90-74	90-75	89-31
	B0628-2	B0628-2	B0628-2	B0628-2	B0628-2	B0628-2	B0628-2	B0628-2	B0511-2
SiO <sub>2</sub>	46.96	45.45	45.72	46.03	46.97	45.72	45.31	45.21	48.21
TiO <sub>2</sub>	0.12	0.35	0.05	0.45	0.24	0.07	0.46	0.22	1.12
Al <sub>2</sub> O <sub>3</sub>	37.87	37.29	38.37	37.37	37.93	37.82	37.18	37.51	32.66
Cr <sub>2</sub> O <sub>3</sub>	0.01	0.01	0.01	0.00	0.00	0.00	0.00	0.00	0.00
MnO	0.01	0.01	0.00	0.02	0.04	0.01	0.01	0.00	0.00
FeO	1.27	1.22	0.51	1.29	1.28	1.29	1.30	1.13	3.28
MgO	0.21	0.26	0.06	0.18	0.19	0.22	0.22	0.19	1.51
BaO	0.00	0.00	0.00	0.00	0.00	0.00	0.00	0.00	0.00
CaO	0.00	0.00	0.00	0.00	0.00	0.00	0.00	0.00	0.24
K <sub>2</sub> O	9.15	9.30	9.99	9.45	9.53	9.35	9.36	9.51	9.26
Na <sub>2</sub> O	1.17	1.29	0.90	1.29	1.06	1.27	1.28	1.18	0.28
F	0.00	0.00	0.00	0.00	0.00	0.00	0.00	0.00	0.00
Cl	0.00	0.00	0.00	0.00	0.00	0.00	0.01	0.00	0.00
Sum	96.77	95.18	95.61	96.08	97.24	95.75	95.13	94.95	96.56
O+F+Cl	0.00	0.00	0.00	0.00	0.00	0.00	0.00	0.00	0.00
Total	96.77	95.18	95.61	96.08	97.24	95.75	95.13	94.95	96.56
Structural Formulae (Based on 22 O)									
Si	6.092	6.024	6.018	6.047	6.083	6.022	6.016	6.009	6.346
Al-iv	1.902	1.976	1.982	1.953	1.917	1.976	1.984	1.991	1.654
Al-vi	3.892	3.849	3.97	3.832	3.872	3.892	3.833	3.884	3.413
Ti	0.012	0.035	0.005	0.044	0.023	0.007	0.046	0.022	0.111
Cr	0.001	0.001	0.001	0	0	0	0	0	0
Fe	0.138	0.135	0.056	0.142	0.139	0.142	0.144	0.126	0.361
Mg	0.041	0.051	0.012	0.035	0.037	0.043	0.044	0.038	0.296
Mn	0.001	0.001	0	0.002	0.004	0.001	0.001	0	0
Ba	0	0	0	0	0	0	0	0	0.012
Ca	0	0	0	0	0	0	0	0	0
Na	0.295	0.332	0.23	0.329	0.266	0.324	0.329	0.304	0.071
K	1.515	1.572	1.677	1.584	1.574	1.571	1.585	1.612	1.555
F	0	0	0	0	0	0	0	0	0
Cl	0	0	0	0	0	0	0.002	0	0
O	22	22	22	22	22	22	22	22	22
Parg	16.27	17.41	12.04	17.18	14.46	17.11	17.21	15.87	4.29
Musc	83.73	82.59	87.96	82.82	85.54	82.69	82.79	84.13	95.61
Marg	0	0	0	0	0	0	0	0	0
Fe/Mg	3.42	2.655	4.769	4.084	3.9	3.316	3.341	3.337	1.219
Fe/Fe+Mg	0.774	0.726	0.827	0.803	0.796	0.768	0.77	0.769	0.549

## Notes.

B028-2: granoblastic Kyanite Zone

B0511-2: contact zone muscovite-biotite granite

TABLE C-3 (cont'd). Microprobe Analyses, Muscovite.

	89-32	89-33	89-34	89-35	89-36	89-37	89-38	89-39	89-40
	B0511-2	B0511-2	B0511-2	B0511-2	B0511-2	B0511-2	B0511-2	B0511-2	B0511-1
SiO <sub>2</sub>	48.55	46.29	50.31	48.90	51.03	48.38	51.96	49.86	50.05
TiO <sub>2</sub>	1.21	1.02	1.04	1.12	0.99	1.21	0.75	1.08	0.97
Al <sub>2</sub> O <sub>3</sub>	33.16	32.03	32.31	34.13	30.74	33.40	31.55	32.45	31.24
Cr <sub>2</sub> O <sub>3</sub>	0.00	0.00	0.00	0.00	0.00	0.00	0.00	0.00	0.00
MnO	0.00	0.05	0.08	0.04	0.09	0.05	0.05	0.00	0.00
FeO	3.09	3.92	3.81	4.17	3.83	4.27	3.56	3.90	5.10
MgO	1.55	1.69	1.95	1.64	2.23	1.57	2.46	1.80	1.72
BaO	0.00	0.00	0.00	0.00	0.00	0.00	0.00	0.00	0.00
CaO	0.24	0.30	0.27	0.27	0.24	0.31	0.25	0.30	0.01
K <sub>2</sub> O	8.90	10.68	9.36	9.27	9.47	8.98	8.93	9.17	9.13
Na <sub>2</sub> O	0.26	0.43	0.26	0.35	0.59	0.40	0.24	0.40	0.27
F	0.00	0.04	0.00	0.00	0.00	0.00	0.00	0.00	0.00
Cl	0.00	0.01	0.01	0.00	0.00	0.00	0.00	0.00	0.00
Sum	96.96	96.46	99.40	99.89	99.21	98.57	99.75	98.96	98.49
O=F+Cl	0.00	0.02	0.00	0.00	0.00	0.00	0.00	0.00	0.00
Total	96.96	96.44	99.40	99.89	99.21	98.57	99.75	98.96	98.49
Structural Formulae (Based on 22 O)									
Si	6.34	6.209	6.442	6.249	6.557	6.267	6.587	6.414	6.488
Al <sub>iv</sub>	1.66	1.791	1.558	1.751	1.443	1.733	1.413	1.586	1.512
Al <sub>vi</sub>	3.441	3.272	3.317	3.388	3.211	3.366	3.3	3.333	3.26
Ti	0.119	0.103	0.1	0.108	0.096	0.118	0.071	0.104	0.095
Cr	0	0	0	0	0	0	0	0	0
Fe	0.337	0.44	0.408	0.446	0.412	0.463	0.377	0.42	0.553
Mg	0.302	0.336	0.372	0.312	0.427	0.303	0.465	0.345	0.332
Mn	0	0.006	0.009	0.004	0.01	0.005	0.005	0	0
Ba	0.012	0.016	0.014	0.014	0.012	0.016	0.012	0.015	0.001
Ca	0	0	0	0	0	0	0	0	0
Na	0.066	0.112	0.065	0.087	0.147	0.1	0.059	0.1	0.068
K	1.482	1.827	1.529	1.511	1.552	1.484	1.444	1.505	1.51
F	0	0.017	0	0	0	0	0	0	0
Cl	0	0.002	0.002	0	0	0	0	0	0
O	22	22	22	22	22	22	22	22	22
Parq	4.25	5.77	4.05	5.43	8.65	6.34	3.92	6.22	4.3
Musc	95.75	94.23	95.95	94.57	91.35	93.66	96.08	93.78	95.7
Marg	0	0	0	0	0	0	0	0	0
Fe/Mg	1.119	1.318	1.12	1.44	0.987	1.544	0.824	1.216	1.664
Fe/Fe+Mg	0.528	0.569	0.528	0.59	0.497	0.607	0.451	0.549	0.625

## Notes

B0511-2 contact zone muscovite-biotite granite

B0511-1 interior muscovite-biotite granite

TABLE C-3 (cont'd). Microprobe Analyses. Muscovite.

	89-41	89-42	89-43
	B0511-1	B0511-1	B0511-1
SiO <sub>2</sub>	45.72	45.91	47.38
TiO <sub>2</sub>	0.99	1.27	1.53
Al <sub>2</sub> O <sub>3</sub>	30.02	30.54	29.93
Cr <sub>2</sub> O <sub>3</sub>	0.00	0.00	0.00
MnO	0.00	0.00	0.00
FeO	4.71	4.97	4.84
MgO	1.63	1.67	1.75
BaO	0.00	0.00	0.00
CaO	0.04	0.08	0.09
K <sub>2</sub> O	11.09	11.10	10.65
Na <sub>2</sub> O	0.32	0.32	0.25
F	0.00	0.00	0.04
Cl	0.00	0.00	0.00
	-----	-----	-----
Sum	94.53	95.86	96.46
O=F+Cl	0.00	0.00	0.02
	-----	-----	-----
Total	94.53	95.86	96.44

## Structural Formulae (Based on 22 O)

Si	6.294	6.242	6.365
Al-iv	1.706	1.758	1.635
Al-vi	3.166	3.136	3.102
Ti	0.102	0.12	0.155
Cr	0	0	0
Fe	0.542	0.565	0.544
Mg	0.334	0.338	0.35
Mn	0	0	0
Ba	0.002	0.004	0.005
Ca	0	0	0
Na	0.085	0.084	0.065
K	1.947	1.925	1.825
F	0	0	0.017
Cl	0	0	0
O	22	22	22
Parg	4.2	4.2	3.45
Musc	95.8	95.8	96.55
Marg	0	0	0
Fe/Mg	1.621	1.67	1.552
Fe/Fe+Mg	0.619	0.625	0.608

## Notes.

B0511-1 interior, muscovite-biotite granite



TABLE C-4. Microprobe Analyses, Biotite

	1	2	3	89-89	89-90	89-91	89-92	89-93	89-94	
	3861-11	3861-11	3861-11	B0512-10	B0512-10	B0512-10	B0512-10	B0512-10	B0512-10	
SiO <sub>2</sub>	37.60	37.52	36.82	36.77	36.54	36.72	36.73	36.30	36.69	
TiO <sub>2</sub>	1.24	1.51	1.37	2.35	2.00	2.20	1.78	1.96	2.12	
Al <sub>2</sub> O <sub>3</sub>	14.97	15.33	15.28	14.74	14.60	14.83	14.59	14.49	15.22	
Cr <sub>2</sub> O <sub>3</sub>	0.00	0.00	0.00	0.05	0.05	0.07	0.03	0.00	0.05	
MnO	0.00	0.00	0.00	0.37	0.41	0.39	0.42	0.31	0.40	
FeO	17.91	17.05	17.92	20.76	20.88	21.43	21.01	20.92	20.51	
MgO	13.04	13.28	12.81	10.73	11.34	10.86	11.23	11.05	10.97	
BaO	0.00	0.07	0.06	0.06	0.04	0.08	0.06	0.14	0.09	
CaO	0.11	0.09	0.12	0.08	0.05	0.03	0.05	0.07	0.05	
K <sub>2</sub> O	9.54	9.02	8.86	9.33	9.48	9.72	9.32	9.24	9.64	
Na <sub>2</sub> O	0.10	0.11	0.11	0.09	0.04	0.05	0.05	0.04	0.07	
F	1.58	1.65	1.53	0.27	0.33	0.27	0.26	0.24	0.21	
Cl	0.00	0.00	0.00	0.01	0.00	0.01	0.02	0.03	0.01	
-----	-----	-----	-----	-----	-----	-----	-----	-----	-----	
Sum	96.09	95.63	94.88	95.61	95.76	96.66	95.55	94.79	96.03	
O=F+Cl	0.67	0.69	0.64	0.12	0.14	0.12	0.11	0.11	0.09	
-----	-----	-----	-----	-----	-----	-----	-----	-----	-----	
Total	95.42	94.94	94.24	95.49	95.62	96.54	95.44	94.68	95.94	
				Structural Formulae (Based on 22 O)						
Si	5.640	5.613	5.583	5.639	5.608	5.601	5.645	5.629	5.604	
Al-iv	2.360	2.387	2.417	2.361	2.392	2.399	2.355	2.371	2.396	
Al-vi	0.286	0.316	0.313	0.303	0.248	0.266	0.288	0.277	0.344	
Ti	0.140	0.170	0.156	0.271	0.231	0.252	0.206	0.229	0.244	
Cr	0.000	0.000	0.000	0.006	0.006	0.008	0.004	0.000	0.006	
Fe	2.247	2.133	2.272	2.663	2.680	2.733	2.701	2.713	2.620	
Mg	2.915	2.961	2.895	2.453	2.594	2.469	2.573	2.554	2.498	
Mn	0.000	0.000	0.000	0.048	0.053	0.050	0.055	0.041	0.052	
Ba	0.006	0.005	0.007	0.004	0.002	0.005	0.004	0.009	0.005	
Ca	0.000	0.011	0.010	0.013	0.008	0.005	0.008	0.012	0.006	
Na	0.029	0.032	0.032	0.027	0.012	0.015	0.015	0.012	0.021	
K	1.825	1.721	1.714	1.825	1.856	1.891	1.827	1.826	1.878	
F	0.750	0.781	0.734	0.131	0.160	0.130	0.126	0.118	0.161	
Cl	0.000	0.000	0.000	0.003	0.000	0.003	0.005	0.008	0.003	
O	22.000	22.000	22.000	22.000	22.000	22.000	22.000	22.000	22.000	
Fe/Mg	0.771	0.720	0.785	1.105	1.054	1.128	1.071	1.078	1.070	
Fe/Fe+Mg	0.435	0.419	0.440	0.525	0.513	0.530	0.517	0.519	0.517	

## Notes:

386-1-11. quartzofeldspathic gneiss of the Tumco Formation

B0512-10. Feldspar Zone

TABLE C-4. Microprobe Analyses, Biotite.

	89-95	89-21	89-23	89-26	89-27	89-29	89-30	89-31	89-33
	B0512-10	B0512-7t	B0512-7t	B0512-7t	B0512-7t	B0512-7t	B0512-7t	B0512-7t	B0512-7t
SiO <sub>2</sub>	36.30	37.25	36.84	37.37	37.06	36.84	37.18	37.00	37.16
TiO <sub>2</sub>	2.31	2.40	2.39	2.77	2.32	2.26	2.27	2.35	2.45
Al <sub>2</sub> O <sub>3</sub>	15.26	16.98	17.02	17.42	17.41	16.82	16.10	16.72	17.25
Cr <sub>2</sub> O <sub>3</sub>	0.03	0.07	0.03	0.02	0.03	0.00	0.00	0.03	0.00
MnO	0.39	0.74	0.66	0.78	0.73	0.59	0.73	0.78	0.67
FeO	21.10	18.15	18.31	18.14	17.89	18.26	18.01	17.75	18.30
MgO	10.65	10.98	10.93	10.98	10.80	10.94	10.94	10.76	10.65
BaO	0.14	0.14	0.15	0.15	0.15	0.15	0.11	0.10	0.14
CaO	0.00	0.01	0.02	0.02	0.03	0.05	0.01	0.06	0.03
K <sub>2</sub> O	9.80	9.90	9.88	9.83	10.02	9.95	9.84	9.80	9.82
Na <sub>2</sub> O	0.05	0.07	0.06	0.07	0.10	0.08	0.07	0.07	0.05
F	0.23	0.64	0.64	0.56	0.62	0.62	0.65	0.64	0.59
Cl	0.01	0.02	0.01	0.01	0.03	0.01	0.01	0.02	0.02
Sum	96.27	97.35	96.94	98.12	97.19	96.59	95.92	96.08	97.13
O=F+Cl	0.10	0.27	0.27	0.24	0.27	0.26	0.28	0.27	0.25
Total	96.17	97.08	96.67	97.88	96.92	96.33	95.64	95.81	96.88
Structural Formulae (Based on 22 O)									
Si	5.558	5.542	5.512	5.509	5.520	5.534	5.615	5.570	5.539
Al-iv	2.442	2.458	2.488	2.491	2.480	2.466	2.385	2.430	2.461
Al-vi	0.312	0.519	0.513	0.535	0.576	0.512	0.481	0.537	0.568
Ti	0.266	0.269	0.269	0.307	0.260	0.255	0.258	0.266	0.275
Cr	0.004	0.008	0.004	0.002	0.004	0.000	0.000	0.004	0.000
Fe	2.702	2.258	2.291	2.236	2.229	2.297	2.275	2.235	2.281
Mg	2.431	2.435	2.438	2.412	2.398	2.450	2.463	2.415	2.360
Mn	0.051	0.092	0.084	0.097	0.092	0.075	0.093	0.099	0.085
Ba	0.008	0.008	0.009	0.009	0.009	0.009	0.007	0.006	0.008
Ca	0.000	0.002	0.003	0.003	0.005	0.006	0.002	0.010	0.005
Na	0.015	0.020	0.017	0.020	0.029	0.023	0.020	0.020	0.014
K	1.914	1.879	1.886	1.848	1.904	1.907	1.896	1.882	1.867
F	0.111	0.301	0.303	0.261	0.292	0.295	0.310	0.305	0.278
Cl	0.003	0.005	0.003	0.002	0.008	0.003	0.003	0.005	0.005
O	22.000	22.000	22.000	22.000	22.000	22.000	22.000	22.000	22.000
Fe/Mg	1.132	0.966	0.974	0.967	0.968	0.968	0.962	0.967	1.000
Fe/Fe+Mg	0.531	0.491	0.493	0.492	0.492	0.492	0.490	0.492	0.500

## Notes:

B0512-10, B0512-7t, Feldspar Zone

TABLE C-4 (cont'd.). Microprobe Analyses. Biotite.

	89-34	89-36	89-37	89-38	89-39	89-45	89-46	89-47	89-48
	B1219-16	B1219-16	B1219-16	B1219-16	B1219-16	B1219-16	B1219-16	B1219-16	B1219-16
SiO <sub>2</sub>	36.16	36.16	35.43	35.36	35.71	36.05	36.00	35.83	35.95
TiO <sub>2</sub>	3.07	2.98	3.03	2.87	2.83	2.74	3.37	3.39	3.29
Al <sub>2</sub> O <sub>3</sub>	17.07	17.39	17.34	16.13	15.77	16.80	17.13	16.46	16.55
Cr <sub>2</sub> O <sub>3</sub>	0.03	0.00	0.01	0.00	0.04	0.02	0.02	0.04	0.02
MnO	0.89	0.92	0.80	0.96	0.91	0.94	0.98	0.89	0.89
FeO	20.85	20.73	21.26	21.77	20.99	21.68	21.89	22.62	21.84
MgO	7.99	7.66	7.53	7.58	7.82	8.05	7.51	7.47	7.44
BaO	0.18	0.20	0.18	0.15	0.12	0.10	0.16	0.12	0.15
CaO	0.05	0.04	0.05	0.05	0.02	0.07	0.04	0.02	0.03
K <sub>2</sub> O	9.62	9.70	9.44	9.34	9.54	9.74	9.85	9.81	9.64
Na <sub>2</sub> O	0.04	0.05	0.05	0.05	0.06	0.05	0.03	0.03	0.03
F	0.61	0.68	0.66	0.63	0.65	0.66	0.58	0.62	0.55
Cl	0.03	0.02	0.01	0.01	0.02	0.02	0.02	0.03	0.01
Sum	96.59	96.53	95.79	94.90	94.48	96.92	97.58	97.33	96.39
O=F+Cl	0.26	0.29	0.28	0.27	0.28	0.28	0.25	0.27	0.23
Total	96.33	96.24	95.51	94.63	94.20	96.64	97.33	97.06	96.16
Structural Formulae (Based on 22 O)									
Si	5.504	5.504	5.450	5.517	5.578	5.496	5.460	5.471	5.516
Al <sup>iv</sup>	2.496	2.496	2.550	2.483	2.422	2.504	2.540	2.529	2.484
Al <sup>vi</sup>	0.565	0.623	0.593	0.483	0.480	0.514	0.521	0.433	0.500
Ti	0.351	0.341	0.351	0.337	0.332	0.314	0.384	0.389	0.380
Cr	0.004	0.000	0.001	0.000	0.005	0.002	0.002	0.005	0.002
Fe	2.654	2.639	2.735	2.841	2.742	2.764	2.776	2.888	2.801
Mg	1.813	1.738	1.726	1.763	1.821	1.829	1.698	1.700	1.701
Mn	0.115	0.119	0.104	0.127	0.120	0.121	0.126	0.115	0.116
Ba	0.011	0.012	0.011	0.009	0.007	0.006	0.010	0.007	0.009
Ca	0.008	0.007	0.008	0.008	0.003	0.011	0.006	0.003	0.005
Na	0.012	0.015	0.015	0.015	0.018	0.015	0.009	0.009	0.009
K	1.867	1.883	1.852	1.859	1.901	1.894	1.905	1.911	1.886
F	0.294	0.317	0.321	0.311	0.321	0.318	0.278	0.299	0.267
Cl	0.008	0.005	0.003	0.003	0.005	0.005	0.005	0.008	0.003
O	22.000	22.000	22.000	22.000	22.000	22.000	22.000	22.000	22.000
Fe/Mg	1.527	1.587	1.644	1.683	1.572	1.577	1.710	1.767	1.715
Fe/Fe+Mg	0.604	0.613	0.622	0.627	0.611	0.612	0.631	0.639	0.632

## Notes:

B1219-16: Feldspar Zone

TABLE C-4 (cont'd.). Microprobe Analyses. Biotite.

	89-49 B1219-16	90-61 B1218-4	90-62 B1218-4	90-63 B1218-4	90-64 B1218-4	90-65 B1218-4	90-66 B1218-4	90-67 B1218-4	90-68 B1218-4
SiO <sub>2</sub>	35.37	37.25	37.64	37.75	37.43	37.21	37.07	37.32	37.16
TiO <sub>2</sub>	3.03	1.70	1.80	1.78	1.71	1.73	1.81	1.89	1.86
Al <sub>2</sub> O <sub>3</sub>	15.99	17.06	17.55	16.35	17.27	17.10	16.99	17.04	16.97
Cr <sub>2</sub> O <sub>3</sub>	0.01	0.01	0.00	0.01	0.02	0.04	0.01	0.06	0.02
MnO	0.77	0.57	0.55	0.47	0.64	0.49	0.54	0.57	0.57
FeO	21.73	17.48	17.30	18.07	17.68	17.23	17.03	17.43	17.33
MgO	7.66	12.38	12.43	12.46	12.54	12.24	12.26	12.26	12.65
BaO	0.19	0.04	0.02	0.03	0.02	0.01	0.04	0.00	0.00
CaO	0.04	0.09	0.05	0.11	0.06	0.16	0.07	0.08	0.08
K <sub>2</sub> O	9.80	9.71	9.94	9.75	9.93	9.99	9.91	10.09	9.42
Na <sub>2</sub> O	0.05	0.09	0.10	0.08	0.09	0.07	0.06	0.07	0.08
F	0.56	0.54	0.49	0.57	0.49	0.52	0.41	0.52	0.56
Cl	0.02	0.02	0.01	0.01	0.01	0.01	0.00	0.00	0.01
Sum	95.22	96.94	97.88	97.44	97.89	96.80	96.20	97.33	96.71
O+F+Cl	0.24	0.23	0.21	0.24	0.21	0.22	0.17	0.22	0.24
Total	94.98	96.71	97.67	97.20	97.68	96.58	96.03	97.11	96.47
Structural Formulae (Based on 22 O)									
Si	5.513	5.536	5.530	5.594	5.517	5.542	5.548	5.533	5.524
Al-iv	2.487	2.464	2.470	2.406	2.483	2.458	2.452	2.467	2.476
Al-vi	0.450	0.524	0.568	0.449	0.516	0.541	0.545	0.511	0.497
Ti	0.355	0.190	0.199	0.198	0.190	0.194	0.204	0.211	0.208
Cr	0.001	0.001	0.000	0.001	0.002	0.005	0.001	0.007	0.002
Fe	2.832	2.173	2.126	2.239	2.179	2.146	2.132	2.161	2.154
Mg	1.780	2.743	2.722	2.752	2.755	2.717	2.735	2.709	2.802
Mn	0.102	0.072	0.068	0.059	0.080	0.062	0.068	0.072	0.072
Ba	0.012	0.005	0.003	0.006	0.003	0.009	0.004	0.005	0.005
Ca	0.007	0.006	0.003	0.005	0.003	0.002	0.006	0.000	0.000
Na	0.015	0.026	0.028	0.023	0.026	0.020	0.017	0.020	0.023
K	1.948	1.841	1.863	1.843	1.867	1.896	1.892	1.906	1.786
F	0.276	0.254	0.228	0.267	0.218	0.245	0.194	0.244	0.267
Cl	0.005	0.005	0.002	0.002	0.002	0.003	0.000	0.000	0.003
O	22.000	22.000	22.000	22.000	22.000	22.000	22.000	22.000	22.000
Fe/Mg	1.649	0.818	0.806	0.835	0.820	0.813	0.804	0.824	0.794
Fe/Fe+Mg	0.622	0.450	0.446	0.455	0.451	0.442	0.446	0.452	0.443

## Notes

B1219-16, B1218-4, Feldspar Zone

TABLE C-4 (cont'd.). Microprobe Analyses. Biotite.

	14	15	16	17	18	19	20	21	91-1
	B0511-1	B0511-1	B0511-1	B0512-4	B0512-4	B0512-4	MT431286	MT431286	MT431286
SiO <sub>2</sub>	37.03	37.07	36.45	37.62	37.50	37.19	36.92	37.44	37.67
TiO <sub>2</sub>	2.48	2.22	2.52	1.53	1.66	1.60	1.88	1.86	1.81
Al <sub>2</sub> O <sub>3</sub>	16.23	15.82	16.32	15.68	16.14	15.97	17.70	17.58	17.84
Cr <sub>2</sub> O <sub>3</sub>	0.00	0.00	0.00	0.05	0.00	0.00	0.00	0.00	0.00
MnO	0.67	0.60	0.62	0.39	0.39	0.34	0.25	0.36	0.35
FeO	19.19	19.23	19.51	19.84	19.60	19.36	16.46	16.32	16.36
MgO	10.85	11.34	10.81	12.23	12.07	12.32	12.81	12.97	11.64
BaO	0.01	0.03	0.01	0.06	0.01	0.08	0.01	0.03	0.46
CaO	0.11	0.13	0.19	0.15	0.10	0.11	0.34	0.34	0.00
K <sub>2</sub> O	10.10	10.06	10.11	9.15	9.53	9.40	9.53	9.59	8.68
Na <sub>2</sub> O	0.05	0.07	0.12	0.07	0.05	0.09	0.15	0.15	0.10
F	1.63	1.68	1.48	0.00	0.42	0.39	0.46	0.43	0.00
Cl	0.00	0.00	0.00	0.00	0.03	0.03	0.02	0.02	0.05
Sum	98.35	98.25	98.14	96.77	97.50	96.88	96.53	97.09	94.96
O+F+Cl	0.69	0.71	0.62	0.00	0.18	0.17	0.20	0.19	0.01
Total	97.66	97.54	97.52	96.77	97.32	96.71	96.33	96.90	94.95
Structural Formulae (Based on 22 O)									
Si	5.490	5.504	5.437	5.649	5.589	5.576	5.483	5.522	5.646
Al-iv	2.510	2.496	2.563	2.351	2.411	2.424	2.517	2.478	2.354
Al-vi	0.325	0.272	0.305	0.424	0.423	0.398	0.580	0.577	0.796
Ti	0.276	0.248	0.283	0.173	0.186	0.180	0.210	0.206	0.204
Cr	0.000	0.000	0.000	0.006	0.000	0.000	0.000	0.000	0.000
Fe	2.379	2.388	2.434	2.492	2.443	2.428	2.044	2.013	2.050
Mg	2.397	2.510	2.403	2.737	2.681	2.753	2.835	2.851	2.600
Mn	0.084	0.075	0.078	0.050	0.049	0.043	0.031	0.045	0.044
Ba	0.006	0.008	0.011	0.009	0.006	0.006	0.020	0.020	0.027
Ca	0.002	0.005	0.002	0.010	0.002	0.013	0.002	0.005	0.000
Na	0.014	0.020	0.035	0.020	0.014	0.026	0.043	0.043	0.029
K	1.910	1.905	1.923	1.753	1.812	1.798	1.805	1.804	1.659
F	0.764	0.789	0.698	0.000	0.198	0.185	0.216	0.201	0.000
Cl	0.000	0.000	0.000	0.000	0.008	0.008	0.005	0.005	0.013
O	22.000	22.000	22.000	22.000	22.000	22.000	22.000	22.000	22.000
Fe/Mg	1.027	0.982	1.045	0.928	0.929	0.897	0.732	0.722	0.806
Fe/Fe+Mg	0.507	0.495	0.511	0.481	0.482	0.473	0.423	0.419	0.446

## Notes.

B0511-1: interior, muscovite-biotite granite

B0512-4: distal hornblende-biotite granodiorite

MT431286: medial hornblende-biotite granodiorite

TABLE C-4 (cont'd.). Macroprobe Analyses. Biotite

	89-58	89-60	89-65	89-4	89-7	89-15	89-16	89-18	89-19
	B0512-1	B0512-1	B0512-1	B0602-1A	B0602-1A	B0602-1A	B0602-1A	B0602-1A	B0602-1A
SiO <sub>2</sub>	38.51	39.09	38.65	39.51	37.46	37.69	36.84	37.21	37.49
TiO <sub>2</sub>	1.58	1.30	1.29	5.58	1.46	1.41	1.46	1.46	1.50
Al <sub>2</sub> O <sub>3</sub>	16.70	17.20	16.95	14.63	18.51	18.70	18.30	18.34	18.29
Cr <sub>2</sub> O <sub>3</sub>	0.03	0.01	0.01	0.00	0.01	0.00	0.00	0.06	0.00
MnO	0.94	0.85	0.71	0.13	0.25	0.26	0.30	0.27	0.24
FeO	10.47	9.60	9.71	11.11	14.90	14.73	15.44	14.96	14.73
MgO	17.51	17.34	17.21	11.53	13.74	13.69	13.99	13.31	13.54
BaO	0.03	0.00	0.00	0.02	0.10	0.11	0.07	0.17	0.11
CaO	0.12	0.02	0.02	9.70	0.02	0.08	0.14	0.06	0.06
K <sub>2</sub> O	9.20	10.03	9.80	1.65	9.83	9.30	8.98	9.17	9.38
Na <sub>2</sub> O	0.08	0.09	0.08	2.83	0.23	0.21	0.19	0.30	0.23
F	0.78	0.81	0.90	0.00	0.91	0.87	0.85	0.76	0.81
Cl	0.02	0.02	0.03	0.03	0.05	0.05	0.06	0.05	0.06
Sum	95.97	96.36	95.36	96.72	97.47	97.10	96.62	96.12	96.44
O=F+Cl	0.33	0.35	0.39	0.01	0.39	0.38	0.37	0.33	0.35
Total	95.64	96.01	94.97	96.71	97.08	96.72	96.25	95.79	96.09
Structural Formulae (Based on 22 O)									
Si	5.576	5.622	5.616	5.641	5.456	5.484	5.413	5.486	5.501
Al-iv	2.424	2.378	2.384	2.359	2.544	2.516	2.587	2.514	2.499
Al-v <sub>2</sub>	0.425	0.537	0.519	0.102	0.633	0.691	0.581	0.673	0.664
Ti	0.172	0.141	0.141	0.599	0.160	0.154	0.161	0.162	0.166
Cr	0.003	0.001	0.001	0.000	0.001	0.000	0.000	0.007	0.000
Fe	1.268	1.155	1.180	1.327	1.815	1.792	1.897	1.845	1.808
Mg	3.779	3.717	3.728	2.454	2.983	2.969	3.064	2.925	2.961
Mn	0.115	0.104	0.087	0.016	0.031	0.032	0.037	0.034	0.030
Ba	0.002	0.000	0.000	0.001	0.006	0.006	0.004	0.010	0.006
Ca	0.019	0.003	0.003	1.484	0.003	0.011	0.021	0.009	0.009
Na	0.022	0.025	0.023	0.783	0.065	0.059	0.054	0.086	0.065
K	1.699	1.840	1.816	0.300	1.826	1.726	1.683	1.724	1.756
F	0.357	0.368	0.414	0.000	0.419	0.400	0.395	0.354	0.376
Cl	0.005	0.005	0.007	0.007	0.011	0.012	0.015	0.012	0.015
O	22.000	22.000	22.000	22.000	22.000	22.000	22.000	22.000	22.000
Fe/Mg	0.366	0.338	0.340	0.547	0.619	0.614	0.621	0.642	0.620
Fe/Fe+Mg	0.268	0.253	0.254	0.354	0.382	0.381	0.387	0.391	0.383

## Notes:

B0512-1: Feldspar Zone

B0602-1A: biotite subzone Muscovite Zone

TABLE C-4 (cont'd.). Microprobe Analyses. Biotite.

	90-6	90-16	90-17	90-18	90-20	89-68	89-70	89-71	89-75
	B0602-1A	B0602-1A	B0602-1A	B0602-1A	B0602-1A	B0430-4	B0430-4	B0430-4	B0430-4
SiO <sub>2</sub>	36.68	37.14	37.58	37.53	37.38	36.14	36.00	35.66	36.01
TiO <sub>2</sub>	1.54	1.43	1.45	1.54	1.45	1.68	1.52	1.55	1.59
Al <sub>2</sub> O <sub>3</sub>	17.78	18.17	18.08	18.45	18.27	19.02	18.94	19.12	19.36
Cr <sub>2</sub> O <sub>3</sub>	0.00	0.00	0.00	0.02	0.00	0.04	0.04	0.01	0.05
MnO	0.32	0.33	0.24	0.33	0.34	0.23	0.25	0.23	0.25
FeO	14.84	15.38	15.09	15.01	14.69	16.11	16.34	15.44	15.74
MgO	13.27	13.29	13.45	13.61	13.52	12.65	12.86	12.73	12.74
BaO	0.11	0.07	0.06	0.01	0.04	0.22	0.21	0.13	0.20
CaO	0.09	0.09	0.14	0.04	0.07	0.07	0.03	0.03	0.01
K <sub>2</sub> O	9.15	9.21	9.21	9.35	9.34	9.05	9.00	8.94	9.25
Na <sub>2</sub> O	0.28	0.25	0.22	0.23	0.25	0.37	0.37	0.42	0.37
F	0.84	0.78	0.85	0.79	0.90	0.40	0.36	0.39	0.37
Cl	0.03	0.03	0.03	0.03	0.05	0.03	0.03	0.02	0.02
Sum	94.93	96.17	96.40	96.94	96.30	96.01	95.95	94.67	95.96
O=F+Cl	0.36	0.34	0.36	0.34	0.39	0.18	0.16	0.17	0.16
Total	94.57	95.83	96.04	96.60	95.91	95.83	95.79	94.50	95.80
Structural Formulae (Based on 22 O)									
Si	5.402	5.404	5.521	5.481	5.493	5.374	5.363	5.359	5.352
Al <sub>iv</sub>	2.518	2.516	2.479	2.519	2.507	2.626	2.637	2.641	2.648
Al <sub>vi</sub>	0.614	0.645	0.650	0.657	0.657	0.706	0.688	0.746	0.743
Ti	0.173	0.159	0.160	0.169	0.160	0.168	0.170	0.175	0.178
Cr	0.000	0.000	0.000	0.002	0.000	0.005	0.005	0.001	0.006
Fe	1.855	1.899	1.854	1.833	1.805	2.003	2.036	1.941	1.956
Mg	2.956	2.925	2.945	2.963	2.961	2.804	2.855	2.852	2.821
Mn	0.041	0.041	0.030	0.041	0.042	0.029	0.032	0.029	0.031
Ba	0.005	0.005	0.008	0.002	0.004	0.013	0.012	0.008	0.012
Ca	0.019	0.011	0.009	0.002	0.006	0.011	0.005	0.005	0.002
Na	0.081	0.072	0.062	0.065	0.071	0.107	0.107	0.122	0.107
K	1.744	1.735	1.726	1.742	1.751	1.716	1.710	1.714	1.754
F	0.397	0.364	0.395	0.365	0.418	0.188	0.170	0.185	0.174
Cl	0.000	0.000	0.007	0.007	0.012	0.000	0.000	0.005	0.005
O	22.000	22.000	22.000	22.000	22.000	22.000	22.000	22.000	22.000
Fe/Mg	0.641	0.663	0.640	0.633	0.624	0.725	0.724	0.691	0.704
Fe/(Fe+Mg)	0.391	0.399	0.390	0.387	0.384	0.420	0.420	0.409	0.413

## Notes:

B0602-1A B0430-4: biotite subzone, Muscovite Zone

TABLE C-4 (cont'd.). Macroprobe Analyses. Biotite.

	89-76	89-80	89-81	89-83	89-84	91-4	91-5	91-30	91-31
	B0430-4	B0430-4	B0430-4	B0430-4	B0430-4	B0430-4	B0430-4	B0430-4	B0430-4
SiO <sub>2</sub>	35.94	35.76	35.60	36.20	36.04	37.44	36.06	35.59	36.27
TiO <sub>2</sub>	1.53	1.54	1.65	1.60	1.54	1.71	1.82	1.74	1.67
Al <sub>2</sub> O <sub>3</sub>	19.30	18.08	19.00	19.25	19.35	18.51	18.73	19.42	19.71
Cr <sub>2</sub> O <sub>3</sub>	0.06	0.04	0.05	0.02	0.03	0.00	0.00	0.00	0.00
MnO	0.26	0.26	0.28	0.31	0.22	0.00	0.00	0.32	0.31
FeO	15.62	16.65	16.08	15.79	16.01	16.68	16.49	16.46	16.37
HgO	12.64	12.71	12.66	12.77	12.46	12.54	11.98	12.24	12.44
BaO	0.14	0.19	0.11	0.10	0.17	0.03	0.00	0.17	0.17
CaO	0.01	0.10	0.04	0.01	0.02	0.23	0.20	0.03	0.00
K <sub>2</sub> O	9.20	8.74	9.10	9.31	9.08	9.09	9.08	8.78	8.96
Na <sub>2</sub> O	0.36	0.33	0.42	0.37	0.37	0.32	0.38	0.30	0.33
F	0.38	0.40	0.31	0.40	0.34	0.48	0.46	0.38	0.29
Cl	0.01	0.02	0.04	0.02	0.02	0.00	0.00	0.02	0.02
Sum	95.45	94.82	95.34	96.15	95.65	97.03	95.20	95.45	96.54
O=F+Cl	0.16	0.17	0.14	0.17	0.15	0.20	0.19	0.16	0.13
Total	95.29	94.65	95.20	95.98	95.50	96.83	95.01	95.29	96.41
Structural Formulae (Based on 22 O)									
Si	5.364	5.401	5.338	5.368	5.372	5.498	5.412	5.325	5.356
Al-iv	2.636	2.599	2.662	2.632	2.628	2.502	2.588	2.675	2.644
Al-vi	0.759	0.618	0.695	0.731	0.771	0.701	0.724	0.750	0.786
Ti	0.172	0.175	0.186	0.178	0.173	0.189	0.205	0.196	0.185
Cr	0.007	0.005	0.006	0.002	0.004	0.000	0.000	0.000	0.000
Fe	1.950	2.103	2.016	1.958	1.996	2.048	2.070	2.060	2.022
Hg	2.812	2.861	2.830	2.822	2.768	2.745	2.680	2.730	2.738
Mn	0.033	0.033	0.036	0.039	0.028	0.000	0.000	0.041	0.039
Ba	0.008	0.011	0.006	0.006	0.010	0.013	0.012	0.010	0.010
Ca	0.002	0.016	0.006	0.002	0.003	0.005	0.000	0.005	0.000
Na	0.104	0.097	0.122	0.106	0.107	0.091	0.111	0.087	0.094
K	1.751	1.684	1.740	1.761	1.726	1.703	1.738	1.676	1.688
F	0.179	0.191	0.147	0.188	0.160	0.223	0.218	0.180	0.135
Cl	0.003	0.005	0.010	0.005	0.005	0.000	0.000	0.005	0.005
O	22.000	22.000	22.000	22.000	22.000	22.000	22.000	22.000	22.000
Fe/Hg	0.705	0.747	0.725	0.708	0.731	0.746	0.772	0.769	0.752
Fe/Fe+Hg	0.414	0.427	0.420	0.414	0.422	0.427	0.436	0.435	0.429

## Notes.

B0430-4: biotite subzone, Muscovite Zone



TABLE C-4 (con'd.). Microprobe Analyses. Biotite.

	91-32	91-33	91-34	91-35	91-36	28	29	6	7
	B0430-4	B0430-4	B0430-4	B0430-4	B0430-4	MT231286	MT231286	B0430-3	B0430-3
SiO <sub>2</sub>	35.90	36.00	35.47	35.72	35.56	36.13	36.60	36.95	36.74
TiO <sub>2</sub>	1.58	1.63	1.66	1.61	1.63	1.38	1.53	1.53	1.40
Al <sub>2</sub> O <sub>3</sub>	18.87	19.06	19.28	19.09	19.23	17.59	17.68	19.40	19.73
Cr <sub>2</sub> O <sub>3</sub>	0.00	0.00	0.00	0.00	0.00	0.00	0.00	0.00	0.00
MnO	0.38	0.39	0.27	0.30	0.30	0.38	0.44	0.00	0.00
FeO	16.25	15.94	15.89	16.23	15.87	15.77	16.36	13.66	14.41
MgO	12.16	12.12	12.03	12.22	11.97	13.24	12.66	13.48	13.76
BaO	0.12	0.16	0.17	0.16	0.10	0.16	0.16	0.00	0.00
CaO	0.12	0.02	0.00	0.00	0.00	0.03	0.02	0.11	0.11
K <sub>2</sub> O	7.65	8.68	9.13	8.97	8.94	9.43	9.25	9.13	9.04
Na <sub>2</sub> O	0.26	0.34	0.30	0.31	0.34	0.21	0.19	0.74	0.72
F	0.38	0.40	0.33	0.42	0.38	1.29	1.31	0.46	0.50
Cl	0.02	0.00	0.00	0.03	0.02	0.03	0.03	0.00	0.00
-----	-----	-----	-----	-----	-----	-----	-----	-----	-----
Sum	93.69	94.74	94.53	95.06	94.34	95.64	96.23	95.46	96.41
O=F+Cl	0.16	0.17	0.14	0.18	0.16	0.55	0.56	0.19	0.21
-----	-----	-----	-----	-----	-----	-----	-----	-----	-----
Total	93.53	94.57	94.39	94.88	94.18	95.09	95.67	95.27	96.20
	Structural Formulae (Based on 22 O)								
Si	5.428	5.407	5.356	5.366	5.372	5.405	5.442	5.443	5.377
Al <sub>iv</sub>	2.572	2.593	2.644	2.634	2.628	2.595	2.558	2.557	2.623
Al <sub>vi</sub>	0.790	0.781	0.787	0.746	0.795	0.506	0.540	0.811	0.779
Ti	0.180	0.184	0.189	0.182	0.185	0.155	0.171	0.170	0.154
Cr	0.000	0.000	0.000	0.000	0.000	0.000	0.000	0.000	0.000
Fe	2.055	2.002	2.007	2.039	2.005	1.973	2.034	1.683	1.764
Mg	2.740	2.713	2.708	2.736	2.695	2.952	2.806	2.960	3.001
Mn	0.049	0.050	0.035	0.038	0.038	0.048	0.055	0.000	0.000
Ba	0.007	0.009	0.010	0.009	0.006	0.009	0.009	0.006	0.006
Ca	0.019	0.003	0.000	0.000	0.000	0.005	0.003	0.000	0.000
Na	0.076	0.099	0.088	0.090	0.100	0.061	0.055	0.211	0.204
K	1.475	1.663	1.759	1.719	1.723	1.799	1.754	1.716	1.687
F	0.182	0.190	0.158	0.200	0.182	0.610	0.616	0.214	0.231
Cl	0.005	0.000	0.000	0.008	0.005	0.006	0.008	0.000	0.000
O	22.000	22.000	22.000	22.000	22.000	22.000	22.000	22.000	22.000
Fe/Mg	0.768	0.756	0.754	0.759	0.758	0.685	0.745	0.569	0.588
Fe/Fe+Mg	0.434	0.431	0.430	0.432	0.431	0.406	0.427	0.362	0.370

## Notes.

B0430-4, MT231286: biotite subzone, Muscovite Zone

B0430-3 granoblastic, staurolite-bearing Kyanite Zone

TABLE C-4 (cont'd.). Microprobe Analyses. Biotite.

	8	9	91-48	91-49	91-50	10	11	12	13
	B0430-3	B0430-3	B0430-3	B0430-3	B0430-3	B0511-2	B0511-2	B0511-2	B0511-1
SiO <sub>2</sub>	36.83	36.86	37.02	36.66	36.55	37.91	37.66	37.44	37.26
TiO <sub>2</sub>	1.48	1.48	1.49	1.49	1.45	2.05	2.25	2.12	2.54
Al <sub>2</sub> O <sub>3</sub>	19.07	19.21	19.35	19.37	19.22	17.09	16.90	17.09	15.64
Cr <sub>2</sub> O <sub>3</sub>	0.00	0.00	0.00	0.00	0.00	0.00	0.00	0.00	0.00
MnO	0.00	0.00	0.28	0.28	0.25	0.00	0.00	0.00	0.64
FeO	14.17	13.90	14.00	14.22	13.93	15.20	14.83	15.01	19.12
MgO	13.80	13.56	13.86	13.47	13.41	12.87	13.20	13.30	10.78
BaO	0.00	0.00	0.04	0.01	0.04	0.00	0.00	0.00	0.01
CaO	0.14	0.08	0.04	0.01	0.01	0.14	0.14	0.13	0.13
K <sub>2</sub> O	8.81	8.45	8.78	8.29	8.58	9.25	9.92	8.79	10.05
Na <sub>2</sub> O	0.67	0.59	0.55	0.50	0.63	0.09	0.15	0.15	0.11
F	0.37	0.38	0.32	0.35	0.30	1.13	1.26	1.29	1.45
Cl	0.00	0.00	0.04	0.03	0.04	0.00	0.00	0.00	0.00
Sum	95.34	94.51	95.77	94.68	94.41	95.73	96.31	95.32	97.73
O=F+Cl	0.16	0.16	0.14	0.15	0.14	0.48	0.53	0.54	0.61
Total	95.18	94.35	95.63	94.53	94.27	95.25	95.78	94.78	97.12
Structural Formulae (Based on 22 O)									
Si	5.440	5.466	5.436	5.435	5.443	5.603	5.554	5.546	5.559
Al-iv	2.560	2.534	2.564	2.565	2.557	2.397	2.446	2.454	2.441
Al-vi	0.760	0.823	0.784	0.819	0.816	0.580	0.490	0.530	0.308
Ti	0.164	0.165	0.165	0.166	0.162	0.228	0.250	0.236	0.285
Cr	0.000	0.000	0.000	0.000	0.000	0.000	0.000	0.000	0.000
Fe	1.750	1.724	1.719	1.763	1.735	1.879	1.829	1.860	2.385
Mg	3.038	2.997	3.033	2.977	2.976	2.835	2.901	2.937	2.397
Mn	0.000	0.000	0.035	0.035	0.032	0.000	0.000	0.000	0.081
Ba	0.008	0.005	0.002	0.001	0.002	0.008	0.008	0.008	0.008
Ca	0.000	0.000	0.006	0.002	0.002	0.000	0.000	0.000	0.002
Na	0.192	0.170	0.157	0.144	0.182	0.026	0.043	0.043	0.032
K	1.660	1.598	1.644	1.568	1.630	1.744	1.866	1.661	1.912
F	0.173	0.178	0.149	0.164	0.141	0.528	0.588	0.604	0.684
Cl	0.000	0.000	0.010	0.008	0.010	0.000	0.000	0.000	0.000
O	22.000	22.000	22.000	22.000	22.000	22.000	22.000	22.000	22.000
Fe/Mg	0.576	0.575	0.578	0.604	0.593	0.663	0.630	0.633	1.029
Fe/Fe+Mg	0.366	0.365	0.366	0.377	0.372	0.399	0.387	0.388	0.507

## Notes:

B0430-3: granoblastic, staurolite-bearing Kyanite Zone

B0511-2: contact zone muscovite-biotite granite

B0511-1: interior, muscovite biotite granite

TABLE C-4 (cont'd.). Microprobe Analyses. Biotite.

	14	15	16	17	18	19	20	21	91-1
	B0511-1	B0511-1	B0511-1	B0512-4	B0512-4	B0512-4	MT431286	MT431286	MT431286
SiO <sub>2</sub>	37.03	37.07	36.45	37.62	37.50	37.19	36.92	37.44	37.67
TiO <sub>2</sub>	2.48	2.22	2.52	1.53	1.66	1.60	1.88	1.86	1.81
Al <sub>2</sub> O <sub>3</sub>	16.23	15.82	16.32	15.68	16.14	15.97	17.70	17.58	17.84
Cr <sub>2</sub> O <sub>3</sub>	0.00	0.00	0.00	0.05	0.00	0.00	0.00	0.00	0.00
MnO	0.67	0.60	0.62	0.39	0.39	0.34	0.25	0.36	0.35
FeO	19.19	19.23	19.51	19.84	19.60	19.36	16.46	16.32	16.36
MgO	10.85	11.34	10.81	12.23	12.07	12.32	12.81	12.97	11.64
BaO	0.01	0.03	0.01	0.06	0.01	0.08	0.01	0.03	0.46
CaO	0.11	0.13	0.19	0.15	0.10	0.11	0.34	0.34	0.00
K <sub>2</sub> O	10.10	10.06	10.11	9.15	9.53	9.40	9.53	9.59	8.68
Na <sub>2</sub> O	0.05	0.07	0.12	0.07	0.05	0.09	0.15	0.15	0.10
F	1.63	1.68	1.48	0.00	0.42	0.39	0.46	0.43	0.00
Cl	0.00	0.00	0.00	0.00	0.03	0.03	0.02	0.02	0.05
-----	-----	-----	-----	-----	-----	-----	-----	-----	-----
Sum	98.35	98.25	98.14	96.77	97.50	96.88	96.53	97.09	94.96
O+F+Cl	0.69	0.71	0.62	0.00	0.18	0.17	0.20	0.19	0.01
-----	-----	-----	-----	-----	-----	-----	-----	-----	-----
Total	97.66	97.54	97.52	96.77	97.32	96.71	96.33	96.90	94.95
Structural Formulae (Based on 22 O)									
Si	5.490	5.504	5.437	5.649	5.589	5.576	5.483	5.522	5.646
Al-iv	2.510	2.496	2.563	2.351	2.411	2.424	2.517	2.478	2.354
Al-vi	0.325	0.272	0.305	0.424	0.423	0.398	0.580	0.577	0.796
Ti	0.276	0.248	0.283	0.173	0.186	0.180	0.210	0.206	0.204
Cr	0.000	0.000	0.000	0.006	0.000	0.000	0.000	0.000	0.000
Fe	2.379	2.388	2.434	2.492	2.443	2.428	2.044	2.013	2.050
Mg	2.397	2.510	2.403	2.737	2.681	2.753	2.835	2.851	2.600
Mn	0.084	0.075	0.078	0.050	0.049	0.043	0.031	0.045	0.044
Ba	0.006	0.008	0.011	0.009	0.006	0.006	0.020	0.020	0.027
Ca	0.002	0.005	0.002	0.010	0.002	0.013	0.002	0.005	0.000
Na	0.014	0.020	0.035	0.020	0.014	0.026	0.043	0.043	0.029
K	1.910	1.905	1.923	1.753	1.812	1.798	1.805	1.804	1.659
F	0.764	0.789	0.698	0.000	0.198	0.185	0.216	0.201	0.000
Cl	0.000	0.000	0.000	0.000	0.008	0.008	0.005	0.005	0.013
O	22.000	22.000	22.000	22.000	22.000	22.000	22.000	22.000	22.000
Fe/Mg	1.027	0.982	1.045	0.928	0.929	0.897	0.732	0.722	0.806
Fe/Fe+Mg	0.507	0.495	0.511	0.481	0.482	0.473	0.423	0.419	0.446

## Notes:

B0511-1. interior, muscovite-biotite granite

B0512-4. distal hornblende-biotite granodiorite

MT431286. medial hornblende-biotite granodiorite

TABLE C-4 (cont'd.). Microprobe Analyses. Biotite.

	91-2	91-3	91-4	91-5	91-6	91-7	91-8	91-9	91-10
	MT431286	MT431286	MT431286	MT431286	MT431286	MT431286	MT431286	MT431286	MT431286
SiO <sub>2</sub>	37.62	36.62	36.44	36.73	36.80	36.24	37.07	36.42	36.82
TiO <sub>2</sub>	1.95	1.77	1.95	1.64	1.82	1.72	1.84	1.85	1.80
Al <sub>2</sub> O <sub>3</sub>	18.41	18.23	17.13	17.23	17.94	17.54	17.53	16.66	16.81
Cr <sub>2</sub> O <sub>3</sub>	0.00	0.00	0.00	0.00	0.00	0.00	0.00	0.00	0.00
MnO	0.31	0.38	0.38	0.32	0.31	0.36	0.41	0.31	0.36
FeO	16.81	15.23	17.02	17.08	16.93	17.42	17.06	16.50	16.06
MgO	11.29	11.83	12.47	12.29	11.99	12.14	12.57	12.29	12.74
BaO	0.39	0.31	0.32	0.34	0.31	0.34	0.22	0.35	0.24
CaO	0.01	0.01	0.00	0.07	0.00	0.02	0.03	0.00	0.02
K <sub>2</sub> O	8.15	9.73	9.00	8.74	9.58	9.56	9.31	9.66	9.12
Na <sub>2</sub> O	0.10	0.09	0.05	0.05	0.07	0.06	0.05	0.08	0.06
F	0.38	0.43	0.57	0.53	0.54	0.44	0.46	0.48	0.58
Cl	0.03	0.01	0.00	0.00	0.01	0.00	0.02	0.02	0.01
-----	-----	-----	-----	-----	-----	-----	-----	-----	-----
Sum	95.45	94.64	95.33	95.02	96.30	95.84	96.57	94.62	94.62
O=F+Cl	0.17	0.18	0.24	0.22	0.23	0.19	0.20	0.21	0.25
-----	-----	-----	-----	-----	-----	-----	-----	-----	-----
Total	95.28	94.46	95.05	94.80	96.07	95.65	96.37	94.41	94.37
Structural Formulae (Based on 22 O)									
Si	5.594	5.520	5.489	5.537	5.488	5.459	5.506	5.540	5.559
Al-iv	2.406	2.480	2.511	2.463	2.512	2.541	2.494	2.460	2.441
Al-vi	0.819	0.758	0.529	0.548	0.641	0.572	0.575	0.527	0.550
Ti	0.218	0.201	0.221	0.186	0.204	0.195	0.206	0.212	0.204
Cr	0.000	0.000	0.000	0.000	0.000	0.000	0.000	0.000	0.000
Fe	2.090	1.920	2.144	2.153	2.112	2.194	2.119	2.009	2.028
Mg	2.502	2.658	2.800	2.761	2.665	2.726	2.783	2.787	2.867
Mn	0.039	0.049	0.048	0.041	0.039	0.046	0.052	0.040	0.046
Ba	0.023	0.018	0.019	0.020	0.180	0.020	0.013	0.021	0.014
Ca	0.002	0.002	0.000	0.011	0.000	0.003	0.005	0.000	0.003
Na	0.029	0.026	0.015	0.015	0.020	0.018	0.014	0.024	0.018
K	1.546	1.871	1.729	1.681	1.822	1.837	1.764	1.874	1.756
F	0.179	0.205	0.272	0.253	0.255	0.210	0.216	0.231	0.277
Cl	0.008	0.003	0.000	0.000	0.003	0.000	0.005	0.005	0.003
O	22.000	22.000	22.000	22.000	22.000	22.000	22.000	22.000	22.000
Fe/Mg	0.851	0.741	0.783	0.795	0.807	0.822	0.780	0.768	0.723
Fe/Fe+Mg	0.460	0.425	0.439	0.442	0.447	0.451	0.438	0.434	0.420

## Notes:

MT431286 medial hornblende-biotite granodiorite

TABLE C-4 (cont'd.). Microprobe Analyses, Biotite.

	91-11 MT431286	91-12 MT431286	91-13 MT431286	91-14 MT431286	91-15 MT431286	91-16 MT431286	91-17 MT431286	91-18 MT431286	91-20 MT431286
SiO <sub>2</sub>	37.18	36.90	36.68	37.34	36.62	36.82	36.76	36.41	37.23
TiO <sub>2</sub>	1.78	1.76	1.72	1.81	1.89	1.74	1.97	1.67	1.35
Al <sub>2</sub> O <sub>3</sub>	15.88	17.57	16.50	17.89	17.22	17.79	17.84	17.82	17.39
Cr <sub>2</sub> O <sub>3</sub>	0.00	0.00	0.00	0.00	0.00	0.00	0.00	0.00	0.00
MnO	0.36	0.26	0.30	0.36	0.41	0.44	0.36	0.31	0.29
FeO	16.43	16.93	16.72	16.78	15.99	16.46	16.75	16.85	14.06
MgO	12.75	12.29	12.19	12.65	12.33	12.70	12.12	12.07	14.30
BaO	0.23	0.32	0.26	0.31	0.25	0.28	0.33	0.40	0.28
CaO	0.00	0.04	0.00	0.00	0.00	0.02	0.00	0.03	0.02
K <sub>2</sub> O	8.80	9.59	8.74	9.06	9.33	9.55	9.64	9.55	9.73
Na <sub>2</sub> O	0.12	0.04	0.17	0.11	0.08	0.10	0.06	0.07	0.09
F	0.53	0.54	0.49	0.54	0.47	0.47	0.46	0.47	0.22
Cl	0.00	0.01	0.02	0.02	0.02	0.01	0.01	0.02	0.01
Sum	94.06	96.25	93.79	96.87	94.63	96.38	96.30	95.67	94.97
O=F+Cl	0.22	0.23	0.21	0.23	0.20	0.20	0.20	0.20	0.09
Total	93.84	96.02	93.58	96.64	94.43	96.18	96.10	95.47	94.88
Structural Formulae (Based on 22 O)									
Si	5.648	5.507	5.598	5.509	5.535	5.479	5.484	5.475	5.497
Al <sup>iv</sup>	2.352	2.493	2.402	2.491	2.465	2.521	2.516	2.525	2.503
Al <sup>vi</sup>	0.490	0.598	0.565	0.620	0.603	0.598	0.619	0.633	0.686
Ti	0.203	0.198	0.197	0.201	0.215	0.195	0.221	0.189	0.173
Cr	0.000	0.000	0.000	0.000	0.000	0.000	0.000	0.000	0.000
Fe	2.087	2.113	2.134	2.070	2.021	2.048	2.090	2.119	1.989
Mg	2.887	2.734	2.773	2.782	2.778	2.817	2.695	2.705	2.826
Mn	0.046	0.033	0.039	0.045	0.052	0.055	0.045	0.039	0.038
Ba	0.014	0.019	0.016	0.018	0.015	0.016	0.019	0.024	0.020
Ca	0.000	0.006	0.000	0.000	0.000	0.003	0.000	0.005	0.002
Na	0.035	0.012	0.050	0.031	0.023	0.029	0.017	0.020	0.026
K	1.705	1.826	1.701	1.705	1.799	1.812	1.834	1.832	1.727
F	0.255	0.255	0.236	0.252	0.225	0.221	0.217	0.224	0.240
Cl	0.000	0.003	0.005	0.005	0.005	0.003	0.003	0.005	0.005
O	22.000	22.000	22.000	22.000	22.000	22.000	22.000	22.000	22.000
Fe/Mg	0.739	0.785	0.784	0.760	0.747	0.747	0.792	0.798	0.717
Fe/Fe+Mg	0.425	0.440	0.439	0.432	0.427	0.428	0.442	0.444	0.418

## Notes.

MT431286 medial hornblende-biotite granodiorite

TABLE C-4 (cont'd.). Microprobe Analyses. Biotite.

	90-84 B0628-1	90-88 B0628-1	90-89 B0628-1	90-91 B0628-1	90-94 B0628-1	91-20 B0628-1	91-21 B0628-1	91-22 B0628-1	91-23 B0628-1
SiO <sub>2</sub>	36.73	36.83	36.77	36.39	36.26	37.23	37.51	36.92	36.88
TiO <sub>2</sub>	1.24	1.30	1.48	1.31	1.23	1.35	1.39	1.32	1.42
Al <sub>2</sub> O <sub>3</sub>	17.80	17.42	17.23	17.41	17.60	17.39	17.88	17.84	17.92
Cr <sub>2</sub> O <sub>3</sub>	0.04	0.00	0.00	0.03	0.03	0.00	0.00	0.00	0.00
MnO	0.32	0.33	0.29	0.31	0.23	0.29	0.25	0.25	0.26
FeO	14.29	14.03	15.20	14.88	14.63	14.06	14.05	14.44	15.72
MgO	14.68	14.68	13.86	14.35	13.99	14.30	14.51	14.49	13.62
BaO	0.00	0.00	0.00	0.00	0.03	0.28	0.22	0.25	0.27
CaO	0.28	0.27	0.22	0.24	0.30	0.02	0.01	0.00	0.00
K <sub>2</sub> O	9.95	9.85	9.82	9.64	9.60	9.73	9.70	8.91	9.25
Na <sub>2</sub> O	0.12	0.10	0.11	0.15	0.12	0.09	0.13	0.15	0.14
F	0.30	0.33	0.32	0.30	0.31	0.22	0.29	0.30	0.29
Cl	0.01	0.03	0.02	0.01	0.01	0.01	0.02	0.02	0.02
Sum	95.76	95.17	95.32	95.02	94.34	94.97	95.96	94.87	95.79
O=F+Cl	0.13	0.15	0.14	0.13	0.13	0.09	0.13	0.13	0.13
Total	95.63	95.02	95.18	94.89	94.21	94.88	95.83	94.74	95.66
Structural Formulae (Based on 22 O)									
Si	5.460	5.499	5.509	5.463	5.475	5.559	5.531	5.501	5.487
Al-iv	2.540	2.501	2.491	2.537	2.525	2.441	2.469	2.499	2.513
Al-vi	0.577	0.564	0.551	0.543	0.607	0.619	0.637	0.633	0.629
Ti	0.139	0.146	0.167	0.148	0.140	0.152	0.154	0.148	0.154
Cr	0.005	0.000	0.000	0.004	0.004	0.000	0.000	0.000	0.000
Fe	1.776	1.752	1.905	1.868	1.847	1.756	1.733	1.799	1.956
Mg	3.252	3.267	3.095	3.211	3.149	3.183	3.189	3.218	3.020
Mn	0.040	0.042	0.037	0.039	0.029	0.037	0.031	0.032	0.033
Ba	0.016	0.016	0.013	0.014	0.018	0.016	0.013	0.015	0.016
Ca	0.000	0.000	0.000	0.000	0.005	0.003	0.002	0.000	0.000
Na	0.035	0.029	0.032	0.044	0.035	0.026	0.037	0.042	0.040
K	1.886	1.876	1.877	1.846	1.849	1.853	1.824	1.692	1.755
F	0.141	0.156	0.152	0.142	0.148	0.104	0.135	0.141	0.136
Cl	0.003	0.008	0.005	0.003	0.003	0.003	0.005	0.000	0.005
O	22.000	22.000	22.000	22.000	22.000	22.000	22.000	22.000	22.000
Fe/Mg	0.559	0.549	0.627	0.594	0.596	0.563	0.553	0.569	0.658
Fe/Fe+Mg	0.358	0.354	0.385	0.373	0.373	0.360	0.356	0.363	0.397

## Notes:

B0628-1. proximal hornblende-biotite granodiorite, adjacent to muscovite-biotite granite

TABLE C-4 (cont'd.). Microprobe Analyses. Biotite.

	91-24 B0628-1	91-25 B0628-1	91-26 B0628-1	91-27 B0628-1
SiO <sub>2</sub>	36.55	36.31	37.05	37.37
TiO <sub>2</sub>	1.20	1.32	1.47	1.30
Al <sub>2</sub> O <sub>3</sub>	17.71	18.22	18.50	17.99
Cr <sub>2</sub> O <sub>3</sub>	0.00	0.00	0.00	0.00
MnO	0.24	0.25	0.32	0.24
FeO	14.46	15.21	14.81	14.96
HgO	14.01	13.93	13.92	14.42
BaO	0.18	0.20	0.24	0.22
CaO	0.00	0.08	0.02	0.01
K <sub>2</sub> O	8.82	9.12	9.22	8.82
Na <sub>2</sub> O	0.10	0.13	0.11	0.17
F	0.29	0.28	0.32	0.26
Cl	0.02	0.00	0.02	0.05
-----	-----	-----	-----	-----
Sum	93.59	95.05	96.00	95.81
O=F+Cl	0.13	0.12	0.14	0.12
-----	-----	-----	-----	-----
Total	93.46	94.93	95.86	95.69
Structural Formulae (Based on 22 O)				
Si	5.520	5.432	5.468	5.516
Al-iv	2.480	2.568	2.532	2.484
Al-vi	0.671	0.643	0.686	0.645
Ti	0.136	0.146	0.163	0.144
Cr	0.000	0.000	0.000	0.000
Fe	1.826	1.903	1.828	1.847
Hg	3.154	3.106	3.062	3.172
Mn	0.031	0.032	0.040	0.030
Ba	0.011	0.012	0.014	0.013
Ca	0.000	0.013	0.003	0.002
Na	0.029	0.038	0.031	0.049
K	1.699	1.740	1.736	1.660
F	0.139	0.132	0.149	0.121
Cl	0.005	0.000	0.005	0.013
O	22.000	22.000	22.000	22.000
Fe/Hg	0.589	0.623	0.610	0.592
Fe/Fe+Hg	0.371	0.384	0.379	0.372

## Notes.

B0628 1: proximal hornblende-biotite granodiorite, adjacent to muscovite-biotite granite

TABLE C-5. Microprobe Analyses, Garnet.

	1	2	3	4	5	6	7	8	9
	MT431286	MT431286	MT431286	MT431286	MT431286	MT431286	MT431286	MT431286	MT431286
SiO <sub>2</sub>	36.92	37.01	36.75	36.94	37.31	37.27	36.83	36.94	36.47
TiO <sub>2</sub>	0.15	0.11	0.06	0.14	0.09	0.14	0.16	0.10	0.18
Al <sub>2</sub> O <sub>3</sub>	20.27	20.52	20.23	20.17	21.03	21.42	21.25	21.29	21.21
FeO	19.47	20.56	19.58	19.78	19.73	20.48	20.21	20.38	20.17
MnO	15.07	15.53	15.34	15.12	15.67	14.82	15.42	15.38	15.13
MgO	2.54	2.40	2.51	2.58	2.54	2.63	2.53	2.57	2.61
CaO	3.29	3.31	3.20	3.18	3.21	3.13	3.11	3.07	3.20
Total	97.71	99.44	97.67	97.91	99.58	99.89	99.51	99.58	98.97
Structural Formulae (Based on 24 O)									
Si	6.06	6.00	6.05	6.06	6.01	5.98	5.95	5.96	5.93
Al-iv	0.00	0.00	0.00	0.00	0.00	0.02	0.05	0.04	0.08
Al-vi	3.92	3.92	3.92	3.90	3.99	4.03	4.00	4.01	3.99
Ti	0.02	0.01	0.01	0.02	0.01	0.02	0.02	0.01	0.02
Mg	0.62	0.58	0.62	0.63	0.61	0.63	0.61	0.62	0.63
Fe	2.67	2.79	2.69	2.71	2.66	2.75	2.73	2.75	2.74
Ca	0.58	0.58	0.56	0.56	0.55	0.54	0.54	0.53	0.56
Mn	2.09	2.13	2.14	2.10	2.14	2.01	2.11	2.08	2.08

## Notes:

MT431286: medial hornblende-biotite granodiorite

	10	11	12	13	14	15	16	17	18
	MT431286	MT431286	MT431286	MT431286	MT431286	MT431286	MT431286	MT431286	B0628-1
SiO <sub>2</sub>	36.70	36.66	36.35	36.44	36.61	36.57	36.60	36.46	37.18
TiO <sub>2</sub>	0.11	0.13	0.12	0.13	0.13	0.12	0.13	0.11	0.13
Al <sub>2</sub> O <sub>3</sub>	21.42	20.77	20.70	20.71	21.16	21.24	20.41	20.88	21.18
FeO	20.86	20.42	20.39	20.51	20.74	20.59	19.48	20.39	22.85
MnO	15.56	15.38	15.13	15.41	15.16	15.37	15.16	15.30	10.98
MgO	2.35	2.45	2.32	2.33	2.48	2.30	2.62	2.44	3.23
CaO	3.42	3.39	2.97	2.99	3.29	3.25	3.53	3.26	4.02
Total	100.42	99.20	97.98	98.52	99.57	99.44	97.93	98.84	99.57
Structural Formulae (Based on 24 O)									
Si	5.90	5.96	5.98	5.97	5.93	5.93	6.00	5.95	5.97
Al-iv	0.10	0.04	0.03	0.03	0.07	0.07	0.00	0.05	0.03
Al-vi	3.96	3.94	3.99	3.96	3.96	3.99	3.95	3.96	3.97
Ti	0.01	0.02	0.02	0.02	0.02	0.02	0.02	0.01	0.02
Mg	0.56	0.59	0.57	0.57	0.60	0.56	0.64	0.59	0.77
Fe	2.81	2.70	2.80	2.81	2.81	2.79	2.67	2.78	3.07
Ca	0.59	0.59	0.52	0.53	0.57	0.57	0.62	0.57	0.69
Mn	2.12	2.12	2.11	2.14	2.08	2.11	2.11	2.11	1.49

## Notes:

MT431286: medial hornblende-biotite granodiorite

B0628-1: proximal hornblende-biotite granodiorite



TABLE C-5 (cont'd.). Microprobe Analyses. Garnet.

	19	20	21	22	23	24	25	26	27
	B0628-1	B0628-1	B0628-1	B0628-1	B0628-1	B0628-1	B0628-1	MT231286	MT231286
SiO <sub>2</sub>	37.18	36.85	37.23	36.56	36.85	36.85	36.90	36.50	36.23
TiO <sub>2</sub>	0.09	0.10	0.09	0.17	0.08	0.09	0.08	0.10	0.09
Al <sub>2</sub> O <sub>3</sub>	21.57	21.31	21.34	21.40	21.48	21.37	21.39	20.68	20.55
FeO	23.84	23.06	23.00	22.25	23.09	23.06	23.29	21.05	19.81
MnO	10.47	10.90	10.69	12.79	10.54	10.46	10.95	16.59	15.83
MgO	3.71	3.00	3.45	2.55	3.22	3.41	3.64	2.00	1.94
CaO	3.03	4.28	3.47	4.24	3.93	4.01	3.28	2.65	2.49
Total	99.89	99.50	99.27	99.96	99.19	99.25	99.53	99.57	96.94
Structural Formulae (Based on 24 O)									
Si	5.94	5.93	5.99	5.89	5.93	5.93	5.93	5.95	6.02
Al-iv	0.06	0.07	0.02	0.11	0.07	0.07	0.07	0.05	0.00
Al-vi	4.00	3.97	4.02	3.95	4.01	3.98	3.98	3.93	4.02
Ti	0.01	0.01	0.01	0.02	0.01	0.01	0.01	0.01	0.01
Mg	0.88	0.72	0.83	0.61	0.77	0.82	0.87	0.49	0.48
Fe	3.19	3.10	3.09	3.00	3.11	3.10	3.13	2.87	2.75
Ca	0.52	0.74	0.60	0.73	0.68	0.69	0.56	0.46	0.44
Mn	1.42	1.49	1.45	1.75	1.44	1.43	1.49	2.29	2.23

## Notes:

B0628-1: proximal hornblende-biotite granodiorite  
 MT231286: biotite subzone, Muscovite Zone

	28	29	30	31	32	33	34	35	36
	MT231286	B0430-4	B0430-4	B0430-4	B0430-4	B0430-4	B0430-4	B0430-4	B0430-4
SiO <sub>2</sub>	36.43	36.29	36.25	36.47	36.49	36.39	36.14	36.32	36.96
TiO <sub>2</sub>	0.06	0.18	0.07	0.07	0.11	0.18	0.04	0.11	0.31
Al <sub>2</sub> O <sub>3</sub>	21.17	20.92	21.21	21.19	21.10	20.90	21.15	21.16	21.20
FeO	20.70	23.38	24.01	24.49	24.01	23.98	24.33	24.39	22.89
MnO	16.99	11.84	11.67	11.93	11.85	11.15	11.65	11.79	13.65
MgO	2.05	3.07	2.95	2.87	2.97	2.96	3.10	3.08	2.70
CaO	2.54	2.52	2.13	2.49	2.42	3.02	2.06	2.66	3.13
Total	99.94	98.20	98.29	99.51	98.95	98.58	98.47	99.51	100.27
Structural Formulae (Based on 24 O)									
Si	5.91	5.94	5.93	5.91	5.93	5.94	5.91	5.89	5.90
Al-iv	0.09	0.06	0.07	0.09	0.07	0.07	0.09	0.11	0.10
Al-vi	3.96	3.97	4.02	3.96	3.98	3.95	3.98	3.93	3.90
Ti	0.01	0.02	0.01	0.01	0.01	0.02	0.01	0.01	0.04
Mg	0.50	0.75	0.72	0.69	0.72	0.72	0.76	0.74	0.64
Fe	2.81	3.20	3.28	3.32	3.27	3.27	3.33	3.31	2.98
Ca	0.44	0.44	0.37	0.43	0.42	0.53	0.36	0.46	0.54
Mn	2.34	1.64	1.62	1.64	1.63	1.54	1.61	1.62	1.85

## Notes:

MT231286, B0430-4: biotite subzone, Muscovite Zone

TABLE C-5 (cont'd.). Microprobe Analyses. Garnet.

	37	38	39	40	41	42	43	44	45
	B0430-4	B0430-4	B0430-4	B0430-4	B0430-4	B0430-4	B0430-4	B0430-4	B0430-4
SiO <sub>2</sub>	36.73	37.18	36.87	36.94	36.11	36.00	37.38	36.94	36.92
TiO <sub>2</sub>	0.06	0.06	0.06	0.06	1.34	1.34	1.34	1.34	0.06
Al <sub>2</sub> O <sub>3</sub>	21.06	20.86	21.17	20.85	20.76	20.76	20.83	20.77	21.51
FeO	24.81	24.81	24.89	25.48	24.53	24.13	24.35	24.24	25.03
MnO	11.20	12.14	11.69	11.67	11.68	11.73	12.22	11.95	11.61
MgO	2.87	2.95	2.95	2.97	2.95	2.85	3.03	2.84	2.92
CaO	3.07	3.08	3.00	2.35	2.69	2.80	2.24	2.24	3.05
Total	99.80	100.95	100.63	100.32	100.06	99.61	101.39	100.32	101.10
Structural Formulae (Based on 24 O)									
Si	5.93	5.95	5.92	5.94	5.83	5.83	5.93	5.92	5.89
Al-iv	0.07	0.05	0.08	0.06	0.17	0.17	0.07	0.08	0.11
Al-vi	3.94	3.88	3.92	3.89	3.78	3.80	3.83	3.85	3.94
Ti	0.01	0.01	0.01	0.01	0.16	0.16	0.16	0.16	0.01
Mg	0.69	0.70	0.71	0.71	0.71	0.69	0.72	0.68	0.69
Fe	3.35	3.32	3.34	3.42	3.31	3.27	3.23	3.25	3.34
Ca	0.53	0.52	0.52	0.46	0.47	0.49	0.38	0.38	0.52
Mn	1.53	1.64	1.59	1.59	1.60	1.61	1.64	1.62	1.57

## Notes:

B0430-4 biotite subzone. Muscovite Zone

	46	90-3	90-4	90-8	90-9	90-10	90-11	90-13	90-14
	B0430-4	B0430-4	B0430-4	B0430-4	B0430-4	B0430-4	B0430-4	B0430-4	B0430-4
SiO <sub>2</sub>	36.91	36.21	36.69	37.51	37.42	37.31	36.95	36.86	36.09
TiO <sub>2</sub>	0.06	0.31	0.06	0.06	0.06	0.06	0.06	0.06	0.06
Al <sub>2</sub> O <sub>3</sub>	21.41	21.20	21.06	20.76	21.42	21.57	20.44	20.75	20.66
FeO	25.30	22.89	23.79	24.81	25.48	25.05	24.33	25.29	24.09
MnO	11.63	11.97	12.95	11.99	12.16	11.98	11.81	12.23	11.21
MgO	2.98	2.62	2.66	2.91	3.04	2.88	2.84	2.81	2.82
CaO	2.35	2.28	2.19	2.77	2.29	2.28	2.94	3.05	2.73
Total	100.52	97.48	99.40	100.81	101.87	101.13	99.37	101.05	97.66
Structural Formulae (Based on 24 O)									
Si	5.92	5.95	5.95	6.00	5.93	5.94	6.00	5.92	5.95
Al-iv	0.08	0.05	0.05	0.00	0.07	0.06	0.00	0.08	0.05
Al-vi	3.95	4.06	3.98	3.91	3.93	3.99	3.91	3.85	3.96
Ti	0.01	0.04	0.01	0.01	0.01	0.01	0.01	0.01	0.01
Mg	0.71	0.64	0.64	0.69	0.72	0.68	0.69	0.67	0.69
Fe	3.40	3.15	3.23	3.32	3.38	3.34	3.30	3.40	3.32
Ca	0.40	0.40	0.38	0.47	0.39	0.39	0.51	0.52	0.48
Mn	1.58	1.67	1.78	1.62	1.63	1.62	1.62	1.66	1.57

## Notes:

B0430-4: biotite subzone. Muscovite Zone

TABLE C-5 (cont'd.). Microprobe Analyses, Garnet.

	90-17	90-18	90-19	90-45	90-46	90-51	47	48	49
	B0430-4	B0430-4	B0430-4	B0430-4	B0430-4	B0430-4	B0430-3	B0430-3	B0430-3
SiO <sub>2</sub>	37.14	36.37	36.98	37.25	36.66	36.24	36.46	36.58	36.26
TiO <sub>2</sub>	0.06	0.06	0.06	1.34	1.34	1.34	0.16	0.07	0.15
Al <sub>2</sub> O <sub>3</sub>	21.41	21.13	21.13	20.92	21.35	20.77	21.10	21.40	20.69
FeO	25.25	24.97	24.34	24.46	24.40	24.13	21.55	22.70	19.75
MnO	12.11	12.07	12.72	12.68	12.32	12.06	13.38	11.88	16.60
MgO	2.95	3.02	2.68	2.56	2.78	2.87	2.58	3.53	1.77
CaO	2.19	2.12	2.26	2.27	2.19	2.00	3.12	2.70	3.32
Total	101.11	99.74	100.17	101.48	101.04	99.41	98.35	98.86	98.54

## Structural Formulae (Based on 24 O)

Si	5.93	5.89	5.96	5.92	5.85	5.88	5.95	5.92	5.96
Al-iv	0.07	0.11	0.04	0.08	0.15	0.12	0.48	0.08	0.04
Al-vi	3.96	3.93	3.97	3.84	3.86	3.84	4.01	4.00	3.96
Ti	0.01	0.01	0.01	0.16	0.16	0.16	0.02	0.01	0.02
Mg	0.70	0.73	0.64	0.61	0.66	0.69	0.63	0.85	0.43
Fe	3.37	3.38	3.28	3.25	3.26	3.27	2.94	3.07	2.71
Ca	0.37	0.37	0.39	0.39	0.37	0.35	0.55	0.47	0.58
Mn	1.64	1.66	1.74	1.71	1.67	1.66	1.85	1.63	2.31

## Notes:

B0430-4: biotite subzone, Muscovite Zone

B0430-3: granoblastic, staurolite-bearing Kyanite Zone

	50	51	52	53	54	55	90-20	90-21	90-23
	B0430-3	B0430-3	B0430-3	B0430-3	B0430-3	B0430-3	B0430-3	B0430-3	B0430-3
SiO <sub>2</sub>	36.56	36.89	36.99	36.92	36.66	36.20	36.63	37.37	36.89
TiO <sub>2</sub>	0.09	0.06	0.06	1.52	1.34	1.34	0.06	0.06	0.06
Al <sub>2</sub> O <sub>3</sub>	21.00	20.82	20.72	20.66	20.60	20.47	20.87	21.44	20.82
FeO	23.08	18.60	20.62	18.75	18.54	18.70	18.44	23.41	18.60
MnO	11.53	18.83	16.38	18.66	19.25	18.85	19.50	12.17	18.83
MgO	3.18	1.65	1.99	1.47	1.64	1.79	1.76	3.69	1.65
CaO	3.09	3.56	3.47	3.92	3.40	2.87	2.78	2.01	3.56
Total	98.53	100.41	100.23	101.90	101.43	100.22	100.04	100.15	100.41

## Structural Formulae (Based on 24 O)

Si	5.95	5.96	5.98	5.89	5.88	5.87	5.95	5.97	5.96
Al-iv	0.05	0.04	0.02	0.11	0.12	0.13	0.05	0.03	0.04
Al-vi	3.98	3.93	3.95	3.77	3.77	3.79	3.94	4.00	3.93
Ti	0.01	0.01	0.01	0.18	0.16	0.16	0.01	0.01	0.01
Mg	0.77	0.40	0.48	0.35	0.39	0.43	0.43	0.88	0.40
Fe	3.14	2.51	2.79	2.50	2.49	2.54	2.51	3.13	2.51
Ca	0.54	0.62	0.60	0.67	0.58	0.50	0.48	0.34	0.62
Mn	1.59	2.58	2.24	2.52	2.61	2.58	2.68	1.65	2.58

## Notes:

B0430-3: granoblastic, staurolite-bearing Kyanite Zone

TABLE C-5 (cont'd.). Microprobe Analyses. Garnet.

	90-25	90-26	90-27	90-28	90-29	90-30	90-31	90-32	90-33
	B0430-3	B0430-3	B0430-3	B0430-3	B0430-3	B0430-3	B0430-3	B0430-3	B0430-3
SiO <sub>2</sub>	36.66	36.98	37.13	37.46	37.04	37.38	37.74	37.18	37.40
TiO <sub>2</sub>	0.06	0.06	0.06	0.06	0.06	1.45	1.50	1.51	1.51
Al <sub>2</sub> O <sub>3</sub>	21.40	20.79	21.15	21.15	21.24	21.35	21.66	21.47	21.61
FeO	21.41	23.53	22.94	23.56	23.15	23.13	23.43	23.39	23.08
MnO	15.51	12.79	13.51	12.80	13.99	13.67	12.41	12.19	12.32
MgO	2.24	3.20	3.10	3.27	2.87	3.12	3.40	3.52	3.50
CaO	3.46	2.27	2.16	2.06	2.03	1.10	1.87	1.94	1.99
Total	100.74	99.62	100.05	100.36	100.38	101.20	102.01	101.20	101.41
Structural Formulae (Based on 24 O)									
Si	5.89	5.98	5.97	5.99	5.95	5.92	5.91	5.88	5.89
Al-iv	0.11	0.02	0.03	0.01	0.05	0.08	0.09	0.12	0.11
Al-vi	3.94	3.93	3.97	3.98	3.97	3.91	3.91	3.88	3.90
Ti	0.01	0.01	0.01	0.01	0.01	0.17	0.18	0.18	0.18
Mg	0.54	0.77	0.74	0.78	0.69	0.74	0.79	0.83	0.82
Fe	2.88	3.18	3.08	3.15	3.11	3.07	3.07	3.09	3.04
Ca	0.60	0.39	0.37	0.35	0.35	0.19	0.31	0.33	0.34
Mn	2.11	1.75	1.84	1.73	1.90	1.83	1.65	1.63	1.64

## Notes:

B0430-3: granoblastic, staurolite-bearing Kyanite Zone

	90-34	90-35	90-37	90-38	90-39	90-40	90-41	90-42	90-43
	B0430-3	B0430-3	B0430-3	B0430-3	B0430-3	B0430-3	B0430-3	B0430-3	B0430-3
SiO <sub>2</sub>	37.18	36.98	37.43	36.97	36.93	36.77	36.90	36.20	36.66
TiO <sub>2</sub>	1.51	1.34	1.34	1.34	1.34	1.34	1.34	1.34	1.34
Al <sub>2</sub> O <sub>3</sub>	21.18	21.66	20.85	21.09	20.63	21.10	21.01	20.47	20.60
FeO	23.74	23.21	22.99	22.57	19.67	17.85	17.12	18.70	18.54
MnO	11.65	12.65	12.31	12.97	16.39	12.65	20.95	18.85	19.25
MgO	3.52	3.46	3.19	3.29	2.07	1.47	1.23	1.79	1.64
CaO	2.96	2.05	2.61	2.55	3.57	3.15	3.93	2.87	3.40
Total	101.74	101.35	100.72	100.78	100.60	101.33	102.48	100.22	101.43
Structural Formulae (Based on 24 O)									
Si	5.86	5.85	5.95	5.89	5.93	5.88	5.86	5.87	5.88
Al-iv	0.14	0.15	0.05	0.11	0.07	0.12	0.14	0.13	0.12
Al-vi	3.80	3.89	3.86	3.84	3.83	3.86	3.80	3.79	3.77
Ti	0.18	0.16	0.16	0.16	0.16	0.16	0.16	0.16	0.16
Mg	0.83	0.82	0.76	0.78	0.50	0.35	0.29	0.43	0.39
Fe	3.13	3.07	3.06	3.01	2.64	2.39	2.27	2.54	2.49
Ca	0.50	0.35	0.44	0.44	0.61	0.54	0.67	0.50	0.58
Mn	1.56	1.69	1.66	1.75	2.23	2.66	2.82	2.59	2.61

## Notes:

B0430-3: granoblastic, staurolite-bearing Kyanite Zone

TABLE C-6. Microprobe Analyses, Tourmaline.

	1	2	3	4	5	6	7	8	9
	MT-4	MT-4	MT-4	MT-4	MT-4	MT-4	MT-4	MT-4	MT-4
SiO <sub>2</sub>	35.99	35.40	35.72	34.43	36.24	36.37	36.23	34.85	34.95
TiO <sub>2</sub>	0.21	0.24	0.24	0.33	0.23	0.16	0.23	0.25	0.40
Al <sub>2</sub> O <sub>3</sub>	31.35	31.96	32.70	32.57	33.15	32.93	33.19	32.64	32.74
Cr <sub>2</sub> O <sub>3</sub>	0.04	0.02	0.00	0.04	0.00	0.00	0.00	0.00	0.00
MnO	0.03	0.02	0.02	0.00	0.00	0.05	0.00	0.00	0.01
FeO	7.05	7.09	7.39	10.12	7.04	6.79	7.88	9.48	10.29
MgO	6.80	6.73	6.51	4.71	6.30	6.85	6.02	5.17	4.67
CaO	0.14	0.33	0.11	0.24	0.13	0.17	0.11	0.23	0.24
BaO	0.00	0.00	0.00	0.00	0.00	0.00	0.00	0.00	0.00
K <sub>2</sub> O	0.00	0.00	0.00	0.00	0.00	0.00	0.00	0.00	0.00
Na <sub>2</sub> O	2.41	2.19	2.32	2.10	2.07	2.28	2.41	2.20	2.14
F	0.00	0.10	0.07	0.10	0.09	0.00	0.02	0.06	0.06
Cl	0.00	0.00	0.00	0.00	0.00	0.00	0.01	0.03	0.00
B <sub>2</sub> O <sub>3</sub> <sup>a</sup>	10.38	10.38	10.50	10.28	10.57	10.61	10.61	10.35	10.39
Total	94.40	94.46	95.58	94.92	95.82	96.21	96.71	95.26	95.89
-O=F+Cl	0.00	0.04	0.03	0.04	0.04	0.00	0.01	0.03	0.03
Total	94.40	94.50	95.61	94.97	95.86	96.21	96.72	95.30	95.91
Structural Formulae (Based on 29 O, 3B, and 4 OH+F+Cl)									
B	3.000	3.000	3.000	3.000	3.000	3.000	3.000	3.000	3.000
Si	6.026	5.928	5.913	5.820	5.958	5.959	5.935	5.851	5.849
Al-t	0.000	0.072	0.087	0.180	0.042	0.041	0.065	0.149	0.151
Al-z	6.000	6.000	6.000	6.000	6.000	6.000	6.000	6.000	6.000
Al-y	0.214	0.237	0.294	0.311	0.384	0.319	0.345	0.311	0.308
Ti	0.026	0.030	0.030	0.042	0.028	0.020	0.028	0.032	0.050
Fe	0.987	0.993	1.023	1.431	0.968	0.930	1.080	1.331	1.440
Mn	0.000	0.000	0.000	0.000	0.000	0.000	0.000	0.000	0.000
Mg	1.697	1.679	1.606	1.187	1.544	1.673	1.470	1.294	1.165
Cr	0.005	0.003	0.000	0.005	0.000	0.000	0.000	0.000	0.000
Y-total	2.930	2.942	2.953	2.975	2.924	2.942	2.923	2.968	2.964
Ca	0.025	0.059	0.020	0.043	0.023	0.030	0.019	0.041	0.043
Na	0.782	0.711	0.745	0.688	0.660	0.724	0.766	0.716	0.694
K	0.000	0.000	0.000	0.000	0.000	0.000	0.000	0.000	0.000
X-total	0.808	0.770	0.764	0.732	0.683	0.754	0.785	0.758	0.737
F	0.000	0.053	0.037	0.053	0.047	0.000	0.010	0.032	0.032
Cl	0.000	0.000	0.000	0.000	0.000	0.000	0.003	0.009	0.000
Fe/Fe+Mg	0.368	0.372	0.389	0.547	0.385	0.357	0.423	0.507	0.553

<sup>a</sup>B<sub>2</sub>O<sub>3</sub> calculated according to the methods of Henry and Guidotti (1985).  
MT-4, schistose to mylonitic Kyanite Zone.

TABLE C-6 (cont'd). Microprobe Analyses, Tourmaline.

	10	11	12	13	14	15	16	25	17
	MT-4	MT-4	MT-4	MT-4	MT-4	MT-4	MT-4	MT-4	MT-4
SiO <sub>2</sub>	35.73	35.89	35.39	35.34	35.30	34.92	35.25	34.94	35.23
TiO <sub>2</sub>	0.18	0.19	0.26	0.35	0.42	0.48	0.47	0.48	0.15
Al <sub>2</sub> O <sub>3</sub>	32.82	32.87	32.61	31.95	31.82	32.00	32.32	32.49	32.01
Cr <sub>2</sub> O <sub>3</sub>	0.01	0.01	0.02	0.00	0.01	0.00	0.03	0.03	0.03
MnO	0.00	0.01	0.03	0.00	0.02	0.00	0.00	0.00	0.00
FeO	6.84	7.78	9.72	10.29	10.84	10.14	10.28	10.46	6.80
MgO	6.74	5.86	5.19	4.94	4.49	4.72	4.76	4.81	7.14
CaO	0.15	0.11	0.25	0.26	0.29	0.20	0.24	0.24	0.21
BaO	0.00	0.00	0.00	0.00	0.01	0.00	0.00	0.00	0.00
K <sub>2</sub> O	0.00	0.00	0.00	0.00	0.00	0.00	0.00	0.00	0.00
Na <sub>2</sub> O	2.24	2.28	2.20	2.18	2.16	2.03	2.12	2.18	2.24
F	0.03	0.00	0.03	0.03	0.20	0.11	0.16	0.13	0.27
Cl	0.00	0.00	0.00	0.00	0.00	0.00	0.00	0.00	0.00
B <sub>2</sub> O <sub>3</sub> *	10.50	10.49	10.44	10.37	10.36	10.29	10.41	10.40	10.39
Total	95.24	95.49	96.14	95.71	95.92	94.89	96.04	96.16	94.47
-O=F+Cl	0.01	0.00	0.01	0.01	0.08	0.05	0.07	0.05	0.11
Total	95.25	95.49	96.16	95.72	96.00	94.94	96.10	96.22	94.59
Structural Formulae (Based on 29 O, 3B, and 4 OH+F+Cl)									
B	3.000	3.000	3.000	3.000	3.000	3.000	3.000	3.000	3.000
Si	5.918	5.950	5.890	5.926	5.923	5.899	5.889	5.840	5.893
Al-t	0.082	0.050	0.110	0.074	0.077	0.101	0.111	0.160	0.107
Al-z	6.000	6.000	6.000	6.000	6.000	6.000	6.000	6.000	6.000
Al-y	0.326	0.374	0.289	0.242	0.218	0.273	0.254	0.242	0.205
Ti	0.022	0.024	0.033	0.044	0.053	0.061	0.059	0.060	0.019
Fe	0.947	1.079	1.353	1.443	1.521	1.433	1.436	1.462	0.951
Mn	0.000	0.000	0.000	0.000	0.001	0.000	0.000	0.000	0.000
Mg	1.664	1.448	1.287	1.234	1.123	1.188	1.185	1.198	1.780
Cr	0.001	0.001	0.003	0.000	0.001	0.000	0.004	0.004	0.004
Y-total	2.961	2.926	2.965	2.963	2.917	2.955	2.939	2.966	2.958
Ca	0.027	0.020	0.045	0.047	0.052	0.036	0.043	0.043	0.038
Na	0.719	0.733	0.710	0.709	0.703	0.665	0.687	0.707	0.726
K	0.000	0.000	0.000	0.000	0.000	0.000	0.000	0.000	0.000
X-total	0.746	0.752	0.755	0.755	0.755	0.701	0.730	0.749	0.764
F	0.016	0.000	0.016	0.016	0.106	0.059	0.085	0.069	0.143
Cl	0.000	0.000	0.000	0.000	0.000	0.000	0.000	0.000	0.000
Fe/Fe+Mg	0.363	0.427	0.512	0.539	0.575	0.547	0.548	0.550	0.348

\*B<sub>2</sub>O<sub>3</sub> calculated according to the methods of Henry and Guidotti (1985).  
 MT-4: schistose to mylonitic Kyanite Zone.

TABLE C-6 (cont'd). Microprobe Analyses, Tourmaline.

	18	19	20	21	22	23	26	27	28
	MT-4	MT-4	MT-4	MT-4	MT-4	MT-4	MT-4	MT-4	MT-4
SiO <sub>2</sub>	35.93	36.07	35.86	35.83	34.96	34.75	34.68	35.47	36.04
TiO <sub>2</sub>	0.17	0.21	0.20	0.23	0.37	0.33	0.46	0.23	0.18
Al <sub>2</sub> O <sub>3</sub>	33.24	32.41	32.61	32.93	32.25	32.66	31.76	33.23	32.86
Cr <sub>2</sub> O <sub>3</sub>	0.00	0.01	0.04	0.00	0.00	0.02	0.03	0.00	0.00
MnO	0.02	0.00	0.02	0.00	0.04	0.00	0.02	0.00	0.00
FeO	6.77	7.39	8.56	10.00	12.14	9.82	12.39	7.03	7.24
MgO	6.60	6.46	5.47	5.09	3.99	4.68	4.13	6.50	6.11
CaO	0.15	0.13	0.14	0.25	0.31	0.22	0.31	0.15	0.13
BaO	0.00	0.00	0.00	0.00	0.00	0.00	0.00	0.00	0.00
K <sub>2</sub> O	0.00	0.00	0.00	0.00	0.00	0.00	0.00	0.00	0.00
Na <sub>2</sub> O	2.32	2.30	2.12	2.17	2.16	2.08	2.04	2.23	2.17
F	0.19	0.20	0.16	0.15	0.13	0.13	0.19	0.00	0.10
Cl	0.00	0.00	0.00	0.00	0.00	0.00	0.00	0.00	0.00
B <sub>2</sub> O <sub>3</sub> *	10.58	10.52	10.47	10.56	10.38	10.32	10.32	10.50	10.50
Total	95.97	95.70	95.65	97.27	96.73	95.01	96.33	95.34	95.33
-O=F+Cl	0.08	0.08	0.07	0.06	0.05	0.05	0.08	0.00	0.04
Total	96.05	95.79	95.71	97.34	96.78	95.06	96.41	95.34	95.37
Structural Formulae (Based on 29 O, 3B, and 4 OH+F+Cl)									
B	3.000	3.000	3.000	3.000	3.000	3.000	3.000	3.000	3.000
Si	5.903	5.960	5.956	5.896	5.856	5.855	5.844	5.874	5.965
Al-t	0.097	0.040	0.044	0.104	0.144	0.145	0.156	0.126	0.035
Al-z	6.000	6.000	6.000	6.000	6.000	6.000	6.000	6.000	6.000
Al-y	0.341	0.273	0.340	0.284	0.224	0.342	0.153	0.362	0.377
Ti	0.021	0.026	0.025	0.036	0.047	0.042	0.058	0.029	0.022
Fe	0.930	1.021	1.189	1.376	1.701	1.384	1.746	0.974	1.002
Mn	0.000	0.000	0.000	0.000	0.000	0.000	0.000	0.000	0.000
Mg	1.616	1.591	1.354	1.248	0.996	1.175	1.037	1.604	1.507
Cr	0.000	0.001	0.005	0.000	0.000	0.003	0.004	0.000	0.000
Y-total	2.909	2.913	2.913	2.945	2.967	2.945	2.999	2.969	2.909
Ca	0.026	0.023	0.025	0.044	0.056	0.040	0.056	0.027	0.023
Na	0.739	0.737	0.683	0.692	0.702	0.679	0.667	0.716	0.696
K	0.000	0.000	0.000	0.000	0.000	0.000	0.000	0.000	0.000
X-total	0.765	0.760	0.708	0.736	0.757	0.719	0.723	0.743	0.719
F	0.099	0.105	0.084	0.078	0.069	0.069	0.101	0.000	0.052
Cl	0.000	0.000	0.000	0.000	0.000	0.000	0.000	0.000	0.000
Fe/Fe+Mg	0.365	0.391	0.468	0.524	0.631	0.541	0.627	0.378	0.399

\*B<sub>2</sub>O<sub>3</sub> calculated according to the methods of Henry and Guidotti (1985).  
 MT 4. schistose to mylonitic Kyanite Zone.

TABLE C-6 (cont'd). Microprobe Analyses. Tourmaline.

	29	30	31	32	33	34	35	36	37
	MT-4	TOP-1	TOP-1	TOP-1	TOP-1	TOP-1	TOP-1	B0501-4	B0501-4
SiO <sub>2</sub>	35.12	35.11	35.14	35.93	34.52	33.60	35.20	38.42	34.39
TiO <sub>2</sub>	0.37	0.22	0.35	0.31	0.31	0.23	0.32	0.43	0.39
Al <sub>2</sub> O <sub>3</sub>	32.44	34.80	33.75	34.71	33.66	29.05	33.08	31.53	33.73
Cr <sub>2</sub> O <sub>3</sub>	0.00	0.00	0.00	0.00	0.01	0.00	0.00	0.01	0.00
MnO	0.07	0.00	0.02	0.00	0.00	0.00	0.01	0.08	0.05
FeO	10.54	9.21	8.97	9.88	10.23	9.52	9.37	9.24	9.55
MgO	4.91	4.88	4.81	4.40	4.66	4.59	4.45	5.41	5.19
CaO	0.26	0.06	0.12	0.12	0.26	0.09	0.11	0.70	0.76
BaO	0.00	0.00	0.01	0.02	0.00	0.00	0.00	0.00	0.00
K <sub>2</sub> O	0.00	0.00	0.00	0.00	0.00	0.00	0.00	0.00	0.00
Na <sub>2</sub> O	2.24	1.91	1.95	1.88	1.92	2.11	2.00	1.97	1.96
F	0.20	0.05	0.12	0.12	0.19	0.12	0.11	0.00	0.00
Cl	0.00	0.00	0.01	0.00	0.01	0.01	0.02	0.01	0.01
B <sub>2</sub> O <sub>3</sub> *	10.44	10.58	10.46	10.69	10.43	9.65	10.37	10.77	10.47
Total	96.59	96.82	95.71	98.06	96.20	88.97	95.04	98.56	96.50
-O=F+Cl	0.08	0.02	0.05	0.05	0.08	0.05	0.05	0.00	0.00
Total	96.67	96.84	95.76	98.11	96.28	89.03	95.09	98.56	96.50
	Structural Formulae (Based on 29 O, 3B, and 4 OH+F+Cl)								
B	3.000	3.000	3.000	3.000	3.000	3.000	3.000	3.000	3.000
Si	5.849	5.771	5.841	5.842	5.754	6.050	5.903	6.201	5.712
Al-t	0.151	0.229	0.159	0.158	0.246	0.000	0.097	0.000	0.288
Al-z	6.000	6.000	6.000	6.000	6.000	6.000	6.000	6.000	6.000
Al-y	0.217	0.514	0.454	0.496	0.368	0.217	0.442	0.207	0.317
Ti	0.046	0.027	0.044	0.038	0.039	0.031	0.040	0.052	0.049
Fe	1.468	1.266	1.247	1.344	1.426	1.434	1.314	1.248	1.327
Mn	0.000	0.000	0.001	0.001	0.000	0.000	0.000	0.000	0.000
Mg	1.219	1.195	1.192	1.066	1.158	1.232	1.112	1.302	1.285
Cr	0.000	0.000	0.000	0.000	0.001	0.000	0.000	0.001	0.000
Y-total	2.950	3.003	2.937	2.945	2.992	2.914	2.909	2.804	2.977
Ca	0.046	0.011	0.021	0.021	0.046	0.017	0.020	0.121	0.135
Na	0.723	0.609	0.628	0.593	0.621	0.737	0.650	0.617	0.631
K	0.000	0.000	0.000	0.000	0.000	0.000	0.000	0.000	0.000
X-total	0.770	0.619	0.650	0.614	0.667	0.754	0.670	0.738	0.767
F	0.105	0.026	0.063	0.062	0.100	0.068	0.058	0.000	0.000
Cl	0.000	0.000	0.003	0.000	0.003	0.003	0.006	0.003	0.003
Fe/Fe+Mg	0.546	0.514	0.511	0.558	0.552	0.538	0.542	0.489	0.508

\*B<sub>2</sub>O<sub>3</sub> calculated according to the methods of Henry and Guidotti (1985)  
 MT-4. schistose to mylonitic Kyanite Zone  
 TOP-1: granoblastic Kyanite Zone  
 B0501-4. schistose Kyanite Zone.



TABLE C-6 (cont'd). Microprobe Analyses. Tourmaline.

	38	39	40	41	42	43	44	45	46
	B0501-4	B0501-4	B0501-4	B0501-4	H0319-10	H0319-10	H0319-10	H0319-10	H0319-10
SiO <sub>2</sub>	34.86	34.62	34.56	34.33	36.18	34.86	36.17	35.10	35.21
TiO <sub>2</sub>	0.36	0.45	0.32	0.43	0.14	0.16	0.08	0.22	0.34
Al <sub>2</sub> O <sub>3</sub>	32.66	33.82	33.21	34.64	34.48	33.21	33.58	33.28	32.42
Cr <sub>2</sub> O <sub>3</sub>	0.00	0.00	0.00	0.00	0.00	0.00	0.00	0.00	0.00
MnO	0.07	0.00	0.00	0.00	0.00	0.00	0.00	0.00	0.00
FeO	9.38	10.06	8.98	9.87	6.93	8.19	6.40	8.20	7.22
MgO	5.48	5.19	5.56	5.17	6.04	6.16	7.03	6.28	6.93
CaO	0.63	0.80	0.63	0.95	0.02	0.05	0.11	0.14	0.30
BaO	0.00	0.00	0.00	0.00	0.00	0.00	0.00	0.00	0.00
K <sub>2</sub> O	0.00	0.00	0.00	0.00	0.00	0.00	0.00	0.00	0.00
Na <sub>2</sub> O	2.15	1.91	2.16	1.78	1.83	2.41	2.14	2.41	2.45
F	0.00	0.00	0.00	0.00	0.04	0.09	0.00	0.05	0.26
Cl	0.02	0.01	0.00	0.01	0.00	0.02	0.00	0.00	0.00
B <sub>2</sub> O <sub>3</sub> *	10.42	10.54	10.42	10.59	10.66	10.45	10.63	10.51	10.48
Total	96.03	97.40	95.84	97.77	96.32	95.60	96.14	96.19	95.61
-O=F+Cl	0.00	0.00	0.00	0.00	0.02	0.04	0.00	0.02	0.11
Total	96.04	97.41	95.84	97.77	96.33	95.64	96.14	96.21	95.72
Structural Formulae (Based on 29 O, 3B, and 4 OH+F+Cl)									
B	3.000	3.000	3.000	3.000	3.000	3.000	3.000	3.000	3.000
Si	5.815	5.708	5.764	5.634	5.901	5.799	5.913	5.804	5.839
Al-t	0.185	0.292	0.236	0.366	0.099	0.201	0.087	0.196	0.161
Al-z	6.000	6.000	6.000	6.000	6.000	6.000	6.000	6.000	6.000
Al-y	0.239	0.282	0.294	0.337	0.532	0.313	0.385	0.292	0.177
Ti	0.045	0.056	0.040	0.053	0.017	0.020	0.010	0.027	0.042
Fe	1.309	1.387	1.253	1.355	0.945	1.140	0.875	1.134	1.001
Mn	0.000	0.000	0.000	0.000	0.000	0.000	0.000	0.000	0.000
Mg	1.362	1.275	1.382	1.265	1.468	1.527	1.713	1.548	1.713
Cr	0.000	0.000	0.000	0.000	0.000	0.000	0.000	0.000	0.000
Y-total	2.955	3.001	2.969	3.009	2.963	3.000	2.983	3.001	2.934
Ca	0.113	0.141	0.113	0.167	0.003	0.009	0.019	0.025	0.053
Na	0.695	0.611	0.699	0.566	0.579	0.777	0.678	0.773	0.788
K	0.000	0.000	0.000	0.000	0.000	0.000	0.000	0.000	0.000
X-total	0.808	0.752	0.811	0.734	0.582	0.786	0.698	0.798	0.841
F	0.000	0.000	0.000	0.000	0.021	0.047	0.000	0.026	0.136
Cl	0.006	0.003	0.000	0.003	0.000	0.006	0.000	0.000	0.000
Fe/Fe+Mg	0.490	0.521	0.475	0.517	0.392	0.427	0.338	0.423	0.369

\*B<sub>2</sub>O<sub>3</sub> calculated according to the methods of Henry and Guidotti (1985).  
 B0501-4, H0319-10: schistose Kyanite Zone

TABLE C-6 (cont'd). Microprobe Analyses, Tourmaline.

	47	48	49	50	51	53	54	55	56
	H0319-10	B0501-5	B0501-5	B0501-5	B0501-5	B0602-1A	B0602-1A	B0602-1A	B0602-1A
SiO <sub>2</sub>	35.36	36.25	35.38	34.47	35.19	35.01	35.72	36.02	35.32
TiO <sub>2</sub>	0.32	0.22	0.42	0.39	0.37	0.38	0.13	0.25	0.39
Al <sub>2</sub> O <sub>3</sub>	32.47	34.23	34.20	33.53	33.20	33.19	34.27	33.25	33.40
Cr <sub>2</sub> O <sub>3</sub>	0.00	0.03	0.00	0.00	0.01	0.00	0.00	0.00	0.00
MnO	0.00	0.00	0.04	0.10	0.03	0.00	0.01	0.02	0.00
FeO	5.84	8.24	9.49	9.34	9.21	7.28	6.00	7.02	7.61
MgO	8.24	5.53	5.30	5.40	5.33	7.30	7.53	7.32	7.04
CaO	0.34	0.24	0.49	0.38	0.27	0.67	0.49	0.66	0.71
BeO	0.00	0.00	0.00	0.00	0.00	0.00	0.00	0.00	0.00
K <sub>2</sub> O	0.00	0.00	0.00	0.00	0.00	0.00	0.00	0.00	0.00
Na <sub>2</sub> O	2.42	1.82	2.14	2.41	2.23	2.24	2.01	2.32	2.18
F	0.38	0.00	0.00	0.00	0.00	0.00	0.00	0.00	0.00
Cl	0.00	0.01	0.01	0.01	0.00	0.00	0.00	0.01	0.00
B <sub>2</sub> O <sub>3</sub> *	10.58	10.68	10.67	10.47	10.49	10.58	10.71	10.71	10.64
Total	95.95	97.25	98.14	96.50	96.33	96.65	96.87	97.58	97.29
-O=F+Cl	0.16	0.00	0.00	0.00	0.00	0.00	0.00	0.00	0.00
Total	96.11	97.26	98.14	96.50	96.33	96.65	96.87	97.58	97.29
Structural Formulae (Based on 29 O, 3B, and 4 OH+F+Cl)									
B	3.000	3.000	3.000	3.000	3.000	3.000	3.000	3.000	3.000
Si	5.810	5.899	5.765	5.725	5.834	5.751	5.797	5.845	5.768
Al-t	0.190	0.101	0.235	0.275	0.166	0.249	0.203	0.155	0.232
Al-z	6.000	6.000	6.000	6.000	6.000	6.000	6.000	6.000	6.000
Al-y	0.101	0.465	0.336	0.290	0.323	0.179	0.354	0.206	0.199
Ti	0.040	0.027	0.051	0.049	0.046	0.047	0.016	0.031	0.048
Fe	0.803	1.121	1.293	1.297	1.277	1.000	0.814	0.953	1.039
Mn	0.000	0.000	0.000	0.000	0.000	0.000	0.000	0.000	0.000
Mg	2.018	1.341	1.287	1.337	1.317	1.787	1.821	1.770	1.713
Cr	0.000	0.004	0.000	0.000	0.001	0.000	0.000	0.000	0.000
Y-total	2.961	2.959	2.968	2.973	2.964	3.013	3.006	2.960	2.999
Ca	0.060	0.042	0.086	0.068	0.048	0.118	0.085	0.115	0.124
Na	0.771	0.574	0.676	0.776	0.717	0.714	0.633	0.730	0.690
K	0.000	0.000	0.000	0.000	0.000	0.000	0.000	0.000	0.000
X-total	0.831	0.616	0.762	0.844	0.765	0.831	0.718	0.845	0.815
F	0.197	0.000	0.000	0.000	0.000	0.000	0.000	0.000	0.000
Cl	0.000	0.003	0.003	0.003	0.000	0.000	0.000	0.003	0.000
Fe/Fe+Mg	0.285	0.455	0.501	0.493	0.492	0.359	0.309	0.350	0.378

\*B<sub>2</sub>O<sub>3</sub> calculated according to the methods of Henry and Guidotti (1985).  
H0319-10: schistose Kyanite Zone  
B0602-1A: magnetite subzone, Muscovite Zone

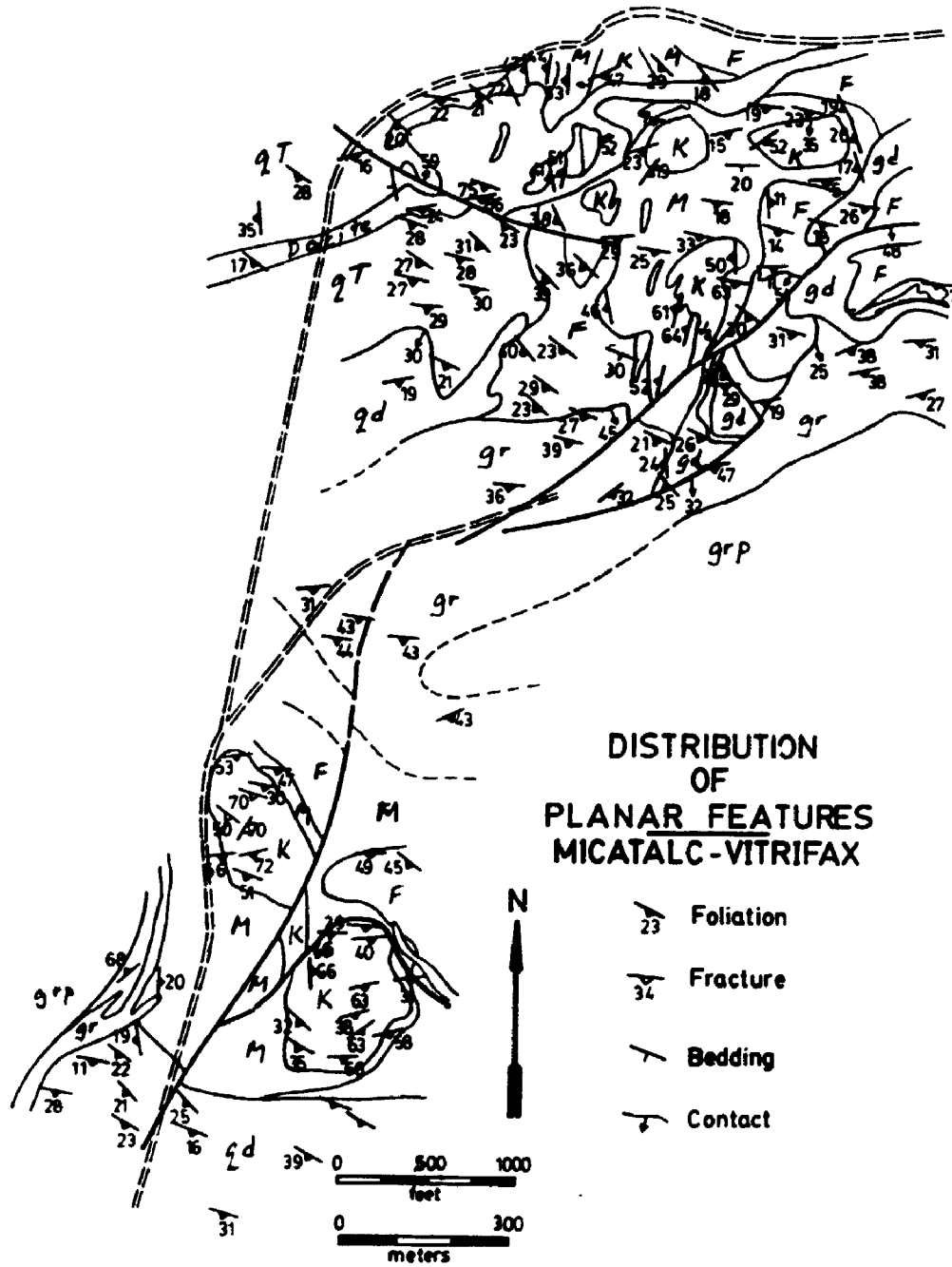
TABLE C-6 (cont'd). Microprobe Analyses. Tourmaline.

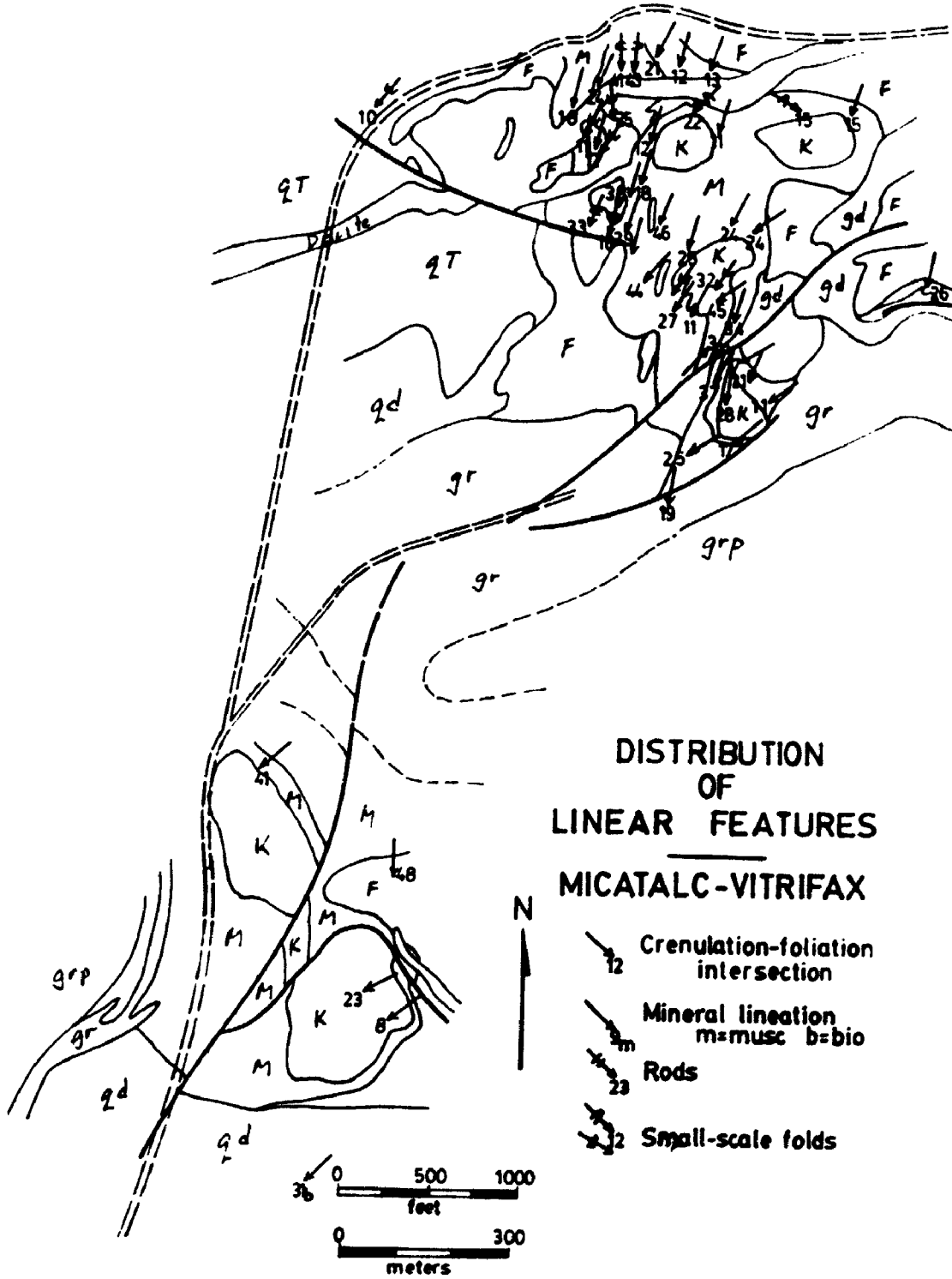
	57	58	60	61	62	63	64
	B0602-1A	B0602-1A	H0412-4	H0412-4	H0412-4	H0412-4	H0412-4
SiO <sub>2</sub>	35.85	35.60	35.88	35.89	35.91	36.08	35.44
TiO <sub>2</sub>	0.00	0.41	0.32	0.26	0.29	0.22	0.33
Al <sub>2</sub> O <sub>3</sub>	34.48	33.33	34.91	33.86	32.69	33.16	33.31
Cr <sub>2</sub> O <sub>3</sub>	0.00	0.00	0.00	0.08	0.01	0.03	0.03
MnO	0.00	0.00	0.00	0.02	0.03	0.03	0.02
FeO	5.90	7.34	9.19	5.17	7.37	5.13	6.32
MgO	7.12	7.31	4.92	8.48	6.96	8.73	7.59
CaO	0.40	0.63	0.22	0.37	0.07	0.28	0.35
BaO	0.00	0.00	0.00	0.00	0.00	0.00	0.00
K <sub>2</sub> O	0.00	0.00	0.00	0.00	0.00	0.00	0.00
Na <sub>2</sub> O	1.88	2.20	1.77	2.34	2.31	2.41	2.40
F	0.00	0.00	0.00	0.00	0.00	0.00	0.00
Cl	0.00	0.00	0.01	0.00	0.01	0.00	0.00
B <sub>2</sub> O <sub>3</sub> *	10.68	10.69	10.71	10.77	10.57	10.72	10.62
Total	96.31	97.51	97.93	97.24	96.22	96.79	96.41
-O=F+Cl	0.00	0.00	0.00	0.00	0.00	0.00	0.00
Total	96.31	97.51	97.93	97.24	96.22	96.79	96.41
Structural Formulae (Based on 29 O, 3B, and 4 OH+F+Cl)							
B	3.000	3.000	3.000	3.000	3.000	3.000	3.000
Si	5.837	5.792	5.823	5.793	5.906	5.849	5.803
Al-t	0.163	0.208	0.177	0.207	0.094	0.151	0.197
Al-z	6.000	6.000	6.000	6.000	6.000	6.000	6.000
Al-y	0.456	0.184	0.503	0.236	0.245	0.187	0.233
Ti	0.000	0.050	0.039	0.032	0.036	0.027	0.041
Fe	0.803	0.999	1.247	0.698	1.014	0.696	0.865
Mn	0.000	0.000	0.000	0.000	0.000	0.000	0.000
Mg	1.728	1.772	1.190	2.040	1.706	2.109	1.852
Cr	0.000	0.000	0.000	0.010	0.001	0.004	0.004
Y-total	2.907	3.005	2.980	3.016	3.002	3.022	2.995
Ca	0.070	0.110	0.038	0.064	0.012	0.049	0.061
Na	0.594	0.694	0.557	0.732	0.737	0.758	0.762
K	0.000	0.000	0.000	0.000	0.000	0.000	0.000
X-total	0.663	0.804	0.595	0.796	0.749	0.806	0.823
F	0.000	0.000	0.000	0.000	0.000	0.000	0.000
Cl	0.000	0.000	0.003	0.000	0.003	0.000	0.000
Fe/Fe+Mg	0.317	0.360	0.512	0.255	0.373	0.248	0.318

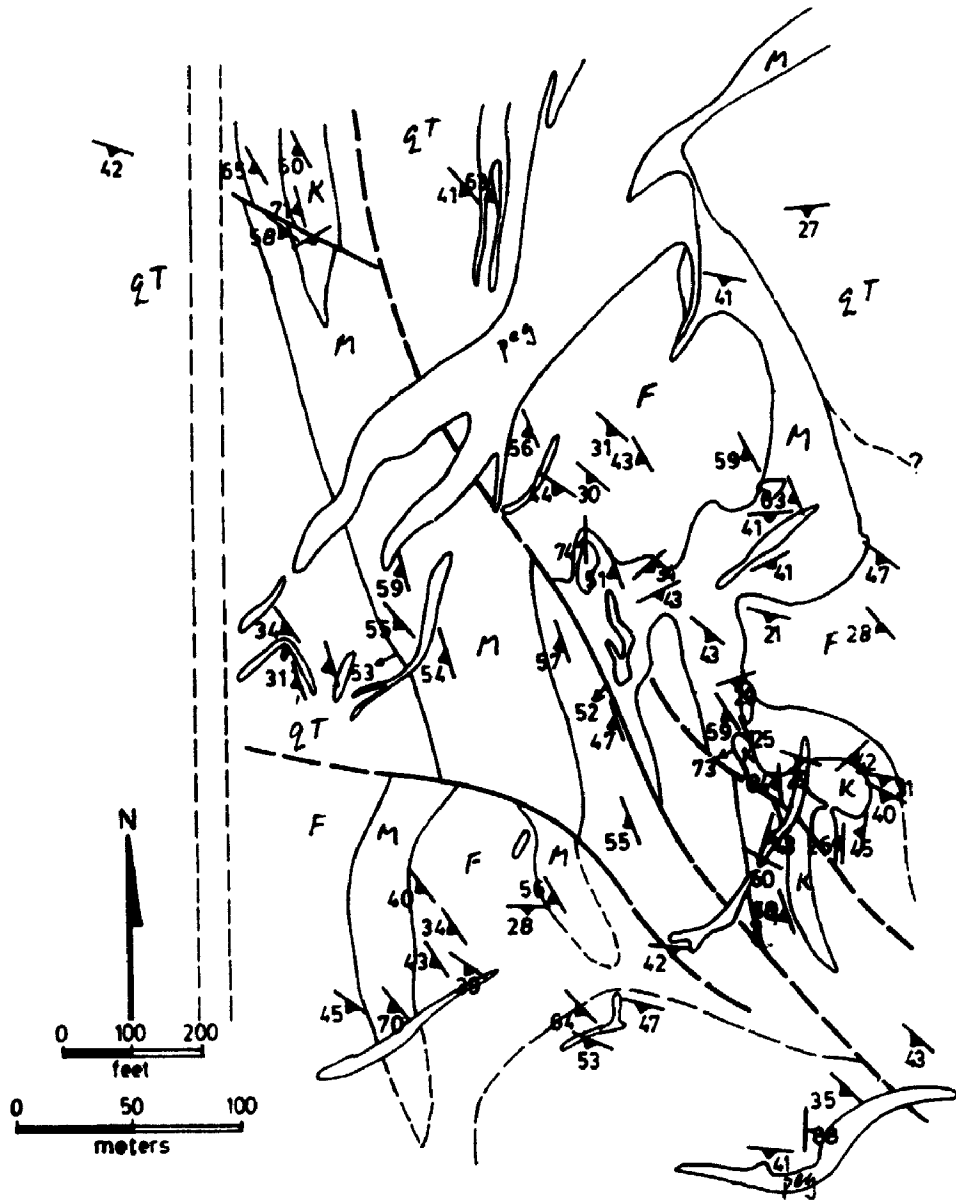
\*B<sub>2</sub>O<sub>3</sub> calculated according to the methods of Henry and Guidotti (1985).  
 B0602-1A, H0412-4: magnetite subzone, Muscovite Zone

**APPENDIX D. Foliation and Lineation Data.**

The following maps provide foliation and lineation data for Micatalc Hill, Vitrifax Hill and Hedges.





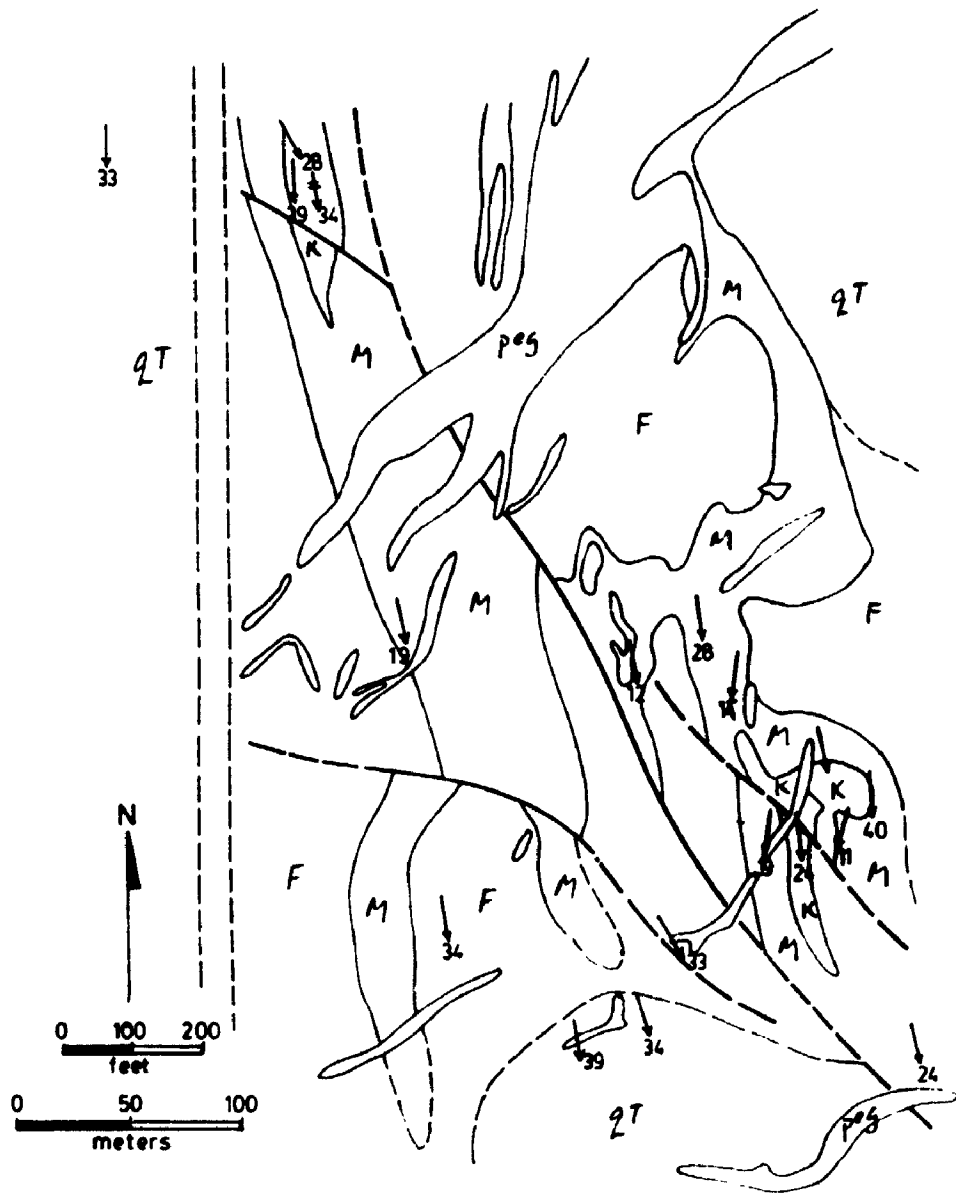




30A

### DISTRIBUTION OF PLANAR FEATURES WEST HEDGES

-  Foliation
-  Bedding



### DISTRIBUTION OF LINEAR FEATURES WEST HEDGES

- ↘<sub>34</sub> Crenulation-foliation intersection
- ↘<sub>23m</sub> Mineral lineation  
m=musc b=bio



## BIBLIOGRAPHY

- Allison, I.; Barnett, R.L.; and Kerrich, R., 1979, Superplastic flow and changes in crystal chemistry of feldspars; *Tectonophys.*, T41-T46.
- Anderson, G.M.; and Burnham, C. Wayne, 1983, Feldspar solubility and the transport of aluminum under metamorphic conditions; *Am. J. Sci.*, 283A, 283-297.
- Anderson, T.H.; and Silver, L.T., 1979, The role of the Mohave-Sonora megashear in the tectonic evolution of northern Sonora; in *Geology of northern Sonora* (Anderson, T.H., and Roldan-Q, J., eds.) *Geol. Soc. Am. Ann. Mtg. Guidebook 27* (Univ. of Pittsburg), 59-68.
- Baldelli, Carla; Franceschelli, Marcello; Leoni, Leonardo; and Memmi, Isabella, 1989, Ferrimuscovite and celadonite substitutions in muscovite from Fe<sup>3+</sup>-rich low grade psammitic rocks (Northern Appenines, Italy); *Lithos*, 23, 201-208.
- Banerji, A.K., 1981, Ore genesis and its relationship to volcanism, tectonism, granitic activity, and metasomatism along the Singhbhum Shear Zone, eastern India; *Econ. Geol.*, 76, 905-912.
- Barton, Mark D.; Battles, Denise A.; Debout, Gray E.; Capo, Rosemary C.; Christensen, John N.; Davis, Samuel, R.; Hanson, Brooks; Michelson, Carl J.; and Trim, Heather E., 1988, Mesozoic contact metamorphism in the western United States; in *Metamorphism and Crustal Evolution of the*

- Western United States (Ernst, W.G., ed.), 110-178.
- Beach, A., 1980, Retrogressive metamorphic processes in shear zones with special reference to the Lewisian complex; *J. Struct. Geol.*, 2, 257-263.
- Beane, Richard E., 1982, Hydrothermal alteration in silicate rocks; in *Advances in Geology of the Porphyry Copper Deposits, Southwestern North America* (Titley, Spencer R., ed.); The University of Arizona Press, Tucson, Ariz., 117-137.
- Beane, R.E.; and Titley, S.R., 1980, Porphyry copper deposits: Part 2. Hydrothermal alteration and mineralization; *Econ. Geol.*, 75th Ann. Issue, Economic Geology Publishing Co., El Paso, 235-269.
- Berger, B.R.; and Bethke, P.M., 1985, Geology and Geochemistry of Epithermal Systems; *Reviews in Economic Geology*, vol. 2, Economic Geology Publishing Co., El Paso, 298p.
- Bennet, D.G.; and Barker, A.J., 1992, High salinity fluids: the result of retrograde metamorphism in thrust zones; *Geochim. Cosmochim. Acta*, 56, 81-95.
- Bowers, T.S.; Jackson, K.J.; and Helgeson, H.C., 1986, Equilibrium Activity Diagrams, for Coexisting Minerals and Aqueous Solutions at Pressures and Temperatures to 5 Kb and 600°C; Springer-Verlag, 397p.
- Bowman, J.R.; Parry, W.T.; Kropp, W.P.; and Kruer, S.A., 1987, Chemical and isotopic evolution of Hydrothermal solutions at Bingham, Utah; *Econ. Geol.*, 82, 395-428.

- Branham, Alan David, 1988, Gold mineralization in low angle faults, American Girl Valley, Cargo Muchacho Mountains, California; Unpubl. MSc. Thesis, Washington State Univ, 144pp.
- Brodie, K.H., 1981, Variation in amphibole and plagioclase composition with deformation; *Tectonophys.*, 78, 385-402.
- Brodie, K.H.; and Rutter, E.H., 1985, On the relationship between deformation and metamorphism, with special reference to the behavior of basic rocks; in *Metamorphic Reactions: Kinetics, Textures and Deformation* (Thompson, A.B., and Rubie, D.C., eds.), Springer-Verlag, New York, 138-179.
- Brown, William L.; and Parsons, Ian, 1981, Towards a more practical two-feldspar geothermometer; *Contr. Min. Pet.*, 76, 369-377.
- Burnham, C. Wayne, 1962, Facies and types of hydrothermal alteration; *Econ. Geol.*, 57, 768-784.
- Cameron, Eion M.; and Hattori, Keiko, 1987, Archean gold mineralization and oxidized hydrothermal fluids; *Econ. Geol.*, 82, 1177-1191.
- Chatterjee, Niranjana D.; and Flux, Susanne, 1986, Thermodynamic mixing properties of muscovite-paragonite crystalline solutions at high temperatures and pressures, and their geological applications; *J. Petrol.*, 27, 677-693.
- Chivas, Allan R., 1981, Geochemical evidence for magmatic fluids in porphyry copper mineralization; *Contr. Min. Pet.*, 78, 389-403.

- Coney, Peter J., 1981, Accretionary tectonics in western North America: in Relations of Tectonics to Ore Deposits in the Southern Cordillera (Dickinson, William R., and Payne, William D., eds.), Arizona Geological Soc. Digest, v. XIV, 23-37.
- Crowe, B.M., 1978, Cenozoic volcanic geology and probable age of inception of basin-range faulting in the southernmost Chocolate Mountains, California; Geol. Soc. America Bull., 89, 251-264.
- Crowell, John C., 1981, An outline of the tectonic history of southeastern California: in The Geotectonic Development of California (Ernst, W.G., ed.), Prentice Hall, Inc., Englewood Cliffs, New Jersey, 583-600.
- Czamanske, G.K.; and Wones, D.R., 1973, Oxidation during magmatic differentiation, Finnmark Complex, Oslo area, Norway: Part 2, the mafic silicates; J. Pet., 14, 349-380.
- Damon, P.E.; Shafiqullah, M.; and Clark, K.F., 1981, Age trends of igneous activity in relation to metallogenesis in the southern Cordillera; in Relations of Tectonics to Ore Deposits in the Southern Cordillera (Dickinson, William R. and Payne, William D., eds.), Arizona Geol. Soc. Digest, vol. 14, 137-154.
- Dennis, A.J.; and Secor, D.T., 1987, A model for the development of crenulations in shear zones with applications from the Southern Appalachian Piedmont; J. Struct. Geol., 9, 809-817.

- Dickinson, William R., 1981a, Plate tectonic evolution of the southern Cordillera: in Relations of Tectonics to Ore Deposits in the Southern Cordillera (Dickinson, William R., and Payne, William D., eds.), Arizona Geological Soc. Digest, v. XIV, 113-135.
- Dickinson, William R., 1981b, Plate tectonics and the continental margin of California: in The Geotectonic Development of California, Rubey Volume 1 (Ernst, W.G., ed.), Prentice Hall, Inc., Englewood Cliffs, New Jersey, 1-28.
- Dillon, John Thomas, 1976, Geology of the Chocolate and Cargo Muchacho Mountains, Southeasternmost California; PhD. Diss., University of California, Santa Barbara, 405 pp.
- Dyar, M. Darby, 1990, Mossbauer spectra of biotite from metapelites; Am. Min., 75, 656-666.
- Ferry, J.M.; and Spear, F.S., 1978, Experimental calibration of the partitioning of Fe and Mg between biotite and garnet; Contr. Min. Pet., 66, 113-117.
- Frost, Eric G.; and Okaya, David A., 1986, Application of seismic reflection profiles to tectonic analysis in mineral exploration; in Frontiers in Geology and Ore Deposits of Arizona and the Southwest (Beatty, Barbara, and Wilkinson, P.A.K., eds.), Arizona Geol. Soc. Digest, v. 16, 137-152.
- Fuhrman, Miriam L.; and Lindsley, Donald H., 1988, Ternary feldspar modeling and thermometry; Am. Min., 73, 201-215.

- Fyfe, W.S.; Price, N.J.; and Thompson, A.B., 1978, Fluids in the Earth's Crust; Elsevier-North Holland, 383p.
- Gallagher, V., 1988, Coupled substitutions in schorl-dravite tourmaline: new evidence from SE Ireland; *Min. Mag.*, 52, 637-658.
- Ganguly, Jibamitra; and Saxena, Surendra K., 1984, Mixing properties of aluminosilicate garnets: constraints from natural and experimental data, and applications to geothermobarometry; *Am. Min.*, 69, 88-97.
- Garner, Welford E.; Frost, Eric G.; Tanges, Susan E.; and Germinario, Mark P., 1982, Mid-Tertiary detachment faulting and mineralization in the Trigo Mountains, Yuma County, Arizona: in *Mesozoic-Cenozoic Tectonic Evolution of the Colorado River Region, California, Arizona, and Nevada*, Anderson-Hamilton volume (Frost, Eric G., and Martin, Donna L., eds.), Cordilleran Publishers, San Diego, California, 158-172.
- Geiger, Per, 1963, Genetic relationships of the paragenesis  $Al_2SiO_5$ -lazulite-rutile; *Arkiv fur Min. Geol.*, 3, 423-464.
- Ghiorso, M.S., 1984, Activity/composition relations in the ternary feldspars; *Contr. Min. Pet.*, 87, 282-296.
- Grant, James A., 1986, The isocon diagram -- a simple solution to Gresens' equation for metasomatic alteration; *Econ. Geol.*, 81, 1976-1982.
- Gresens, Randall L., 1967, Composition-volume relationships of metasomatism; *Chem. Geol.*, 2, 47-65.

- Gresens, Randall L., 1971, Application of hydrolysis equilibria to the genesis of pegmatite and kyanite deposits in northern New Mexico; *Mountain Geologist*, 8, 3-16.
- Green, N.L.; and Usdansky, S.I., 1986, Ternary-feldspar mixing relations and thermobarometry; *Am. Min.*, 71, 1100-1108.
- Guidotti, Charles V., 1984, Micas in metamorphic rocks; in *Micas* (Bailey, S.W., ed.), *Min. Soc. Am. Reviews in Mineralogy*, v. 13, 357-467.
- Guidotti, C.V.; and Sassi, F.P., 1976, Muscovite as a petrogenetic indicator mineral in pelitic schists; *N. Jahrb. Mineral. Abh.*, 127, 97-142.
- Guilbert, John M.; and Parks, Charles F., Jr, 1986, *The Geology of Ore Deposits*; W.H. Freeman and Co., New York, 985p.
- Gustafson, L.B.; and Hunt, J.P., 1975, The porphyry copper deposit at El Salvador, Chile; *Econ. Geol.*, 70, 857-912.
- Haas, H.; and Holdaway, M.J., 1973, Equilibria in the system  $Al_2O_3-SiO_2-H_2O$  involving the stability limits of pyrophyllite; *Am. J. Sci.*, 273, 449-464.
- Hamilton, Warren, 1987, Mesozoic geology and tectonics of the Big Maria Mountains region, southeastern California; in *Mesozoic Rocks of Southern Arizona and Adjacent Areas* (Dickinson, William R., and Klute, Margaret A., eds.), *Ariz. Geol. Soc. Digest*, v. 18, 33-48.
- Harding, Lucey E.; and Coney, Peter J., 1985, The geology of the McCoy Mountains Formation, southeastern California

and southwestern Arizona: Geol. Soc. Am. Bull., 96, 755-769.

Haselton, H.T.; Hovis, Guy L.; Hemingway, Bruce S.; and Robie, Richard A., 1983, Calorimetric investigation of the excess entropy of mixing in analbite-sanidine solid-solutions: lack of evidence for Na, K short-range order and implications for two-feldspar thermometry; Am. Min., 68, 398-414.

Haxel, Gordon Blair, 1977, The Orocochia Schist and the Chocolate Mountain Thrust, Picacho-Peter Kane Mountain area, southeasternmost California; PhD. Dissertation, University of California, Santa Barbara, 277 pp.

Haxel, G.B.; and Dillon, J.T., 1978, The Pelona-Orocochia Schist and Vincent Chocolate Mountains thrust system, southern California; Pacific Sec. Soc. Econ. Paleontologists and Mineralogists, Pacific Coast Paleogeography Symposium 2, 453-469.

Haxel, Gordon B.; Tosdal, Richard M.; May, Daniel J.; and Wright, James E., 1984, Latest Cretaceous and early Tertiary orogenesis in south-central Arizona: Thrust faulting, regional metamorphism, and granitic plutonism; Geol. Soc. Am. Bull., 95, 631-653.

Haxel, Gordon B.; Tosdal, Richard M.; and Dillon, John T., 1985, Tectonic setting and lithology of the Winterhaven Formation: a new Mesozoic stratigraphic unit in southeasternmost California and southwestern Arizona: U.S. Geol. Survey, Bull. 1599, 19pp.



- Hayes, Elizabeth M., 1989, Mid-crustal Mesozoic plutonism in the Cargo Muchacho Mountains, southeasternmost California; Geol. Soc. Am. Abstr. w programs, v. 21, p. 92.
- Helgeson, H.C., 1974, Chemical interaction of feldspars and aqueous solutions; in The Feldspars (MacKenzie, W.S., and Zussman, J., eds.), Manchester University Press, NY, 184-217.
- Hem, J.D.; and Roberson, C.E., 1967, Form and stability of aluminum hydroxide complexes in dilute solutions; U.S. Geol. Survey Water Supply Paper 1827-A, 55p.
- Hemley, J. Julian, 1959, Some mineralogical equilibria in the system  $K_2O-Al_2O_3-SiO_2-H_2O$ ; Am. J. Sci., 257, 241-270.
- Hemley, J.J.; and Jones, W.R., 1964, Chemical aspects of hydrothermal alteration with emphasis on hydrogen ion metasomatism; Econ. Geol. 59, 538-569.
- Hemley, J.J.; Montoya, J.W.; Marinenko, J.W.; and Luce, R.W., 1980, Equilibria in the system  $Al_2O_3-SiO_2-H_2O$  and some general implications for alteration mineralization processes; Econ. Geol., 75, 210-228.
- Henley, R.W.; Truesdell, A.H.; and Barton, P.B., 1984, Fluid-Mineral Equilibria in Hydrothermal Systems; Reviews in Economic Geology, vol. 1, Economic Geology Publishing Co., El Paso, 267p.
- Henry, Darrel J.; and Guidotti, Charles V., 1985, Tourmaline as a petrogenetic indicator mineral: an example from the staurolite-grade metapelites of NW Maine; Am. Min., 70, 1-15.

- Henshaw, Paul C., 1942, Geology and mineral deposits of the Cargo Muchacho Mountains, Imperial County, California; California Div. Mines Rept. 38, 147-196.
- Hyndman, Donald W., 1972, Petrology of Igneous and Metamorphic Rocks; McGraw-Hill Book Co., New York, 533p.
- Jacobs, David C.; and Parry, William T., 1979, Geochemistry of biotite in the Santa Rita Porphyry Copper Deposit, New Mexico; Econ. Geol., 74, 860-887.
- Johnson, J.W.; Oelkers, E.H.; and Helgeson, H.C., 1992, SUPCRT 92, A software package for calculating the standard molal thermodynamic properties of minerals, gases, aqueous species, and reactions from 1 to 5000 bars and 0° to 1000°C; Computers and Geosciences (submitted for publication).
- Kerrick, R.; Fyfe, W.S.; Barnett, R.L.; Blair, B.B.; and Willmore, L.M., 1987, Corundum, Cr-muscovite rocks at O'Briens, Zimbabwe: the conjunction of hydrothermal desilicification and LIL-element enrichment -- geochemical and isotopic evidence: Contrib. Mineral. Petrol., 95, 481-498.
- Kerrick, D.M., 1972, Experiments on the upper stability limits of pyrophyllite at 1.8 kb and 3.9 kb water pressure; Am. J. Sci., 266, 204-215.
- Kerrick, Derrill M., 1988, Al<sub>2</sub>SiO<sub>5</sub>-bearing segregations in the Lepontine Alps, Switzerland: Aluminum mobility in metapelites; Geology, 16, 636-640.

- King, R.W., 1987, Tourmaline from Archean lode gold deposits: chemical, textural and isotopic relationships; Geol. Soc. Am., Abstr. w Programs, 19, 727.
- Lister, G.S.; and Snoke, A.W., 1984, S-C mylonites; J. Struct. Geol., 6, 617-638.
- Marquis, P.; Brown, A.L.; Hubert, C.; and Rigg, D.M., 1990, Progressive alteration associated with auriferous massive sulfide bodies at the Dumagami Mine, Abitibi Greenstone Belt, Quebec; Econ. Geol., 85, 746-764.
- Mason, D.R., 1978, Compositional variations in ferromagnesian minerals from porphyry copper-generating and barren intrusions of the western highlands, Papua New Guinea; Econ. Geol., 73, 878-890.
- Meillon, J.J., 1978, Economic geology and tropical weathering; Can. Inst. Min. Metall. Bull., 71, 61-70.
- Meyer, C.; and Hemley, J.J., 1967, Wall rock alteration, in Geochemistry of Hydrothermal Ore Deposits (Barnes, H.L., ed.), 1st ed., Holt, Rinehart and Winston, 166-235.
- Miller, Calvin; Stoddard, Edward; Bradfish, Larry J.; and Dollase, Wayne A., 1981, Composition of plutonic muscovite: genetic implications; Can. Min., 19, 25-34.
- Monier, Gilles; and Robert, Jean-Louis, 1986, Muscovite solid solutions in the system  $K_2O-MgO-FeO-Al_2O_3-SiO_2-H_2O$ : an experimental study at 2 kbar  $PH_2O$  and comparison with natural Li-free white micas; Min. Mag., 50, 257-266.
- Moore, William J.; and Czamanske, Gerald K., 1973, Compositions of biotites from the unaltered and altered

- monzonitic rocks in the Bingham Mining District, Utah; *Econ. Geol.*, 68, 269-280.
- Murphy, G.P.; Tosdal, R.M.; Wooden, J.L.; Kent, J.; Vaughn, R.B.; and Hayes, E.M., 1990, Chemical and isotopic character of Jurassic granitoids, Cargo Muchacho Mountains, SE California; *Geol. Soc. Am. Abstr. w programs*, 22, 71.
- Murray, Kent, 1982, Tectonic implications of Cenozoic volcanism in southeastern California; in *Mesozoic-Cenozoic Tectonic Evolution of the Colorado River Region, California, Arizona, and Nevada* (Frost, Eric G., and Martin, Donna L., eds.); Cordilleran Publishers, San Diego, 77-83.
- Norrish, K.; and Hutton, J.T., 1969, An accurate X-ray spectrographic method for the analysis of a wide range of geological samples; *Geochim. Cosmochim. Acta*, 33, 431-453.
- Norton, S.A., 1973, Laterite and bauxite formation; *Econ. Geol.*, 68, 353-361.
- O'Hara, Kieran, 1988, Fluid flow and volume loss during mylonitization: an origin for phyllonite in an overthrust setting, North Carolina, USA; *Tectonophys.*, 156, 21-36.
- Olmsted, F.H.; Loeltz, O.S.; and Ireland, B., 1973, Geohydrology of the Yuma area; *U.S. Geol. Survey Prof. Paper* 486-H.
- Olsen, Terkel Svava; and Kohlstedt, David L., 1985, Natural deformation and recrystallization of some intermediate feldspars; *Tectonophys.*, 111, 107-131.

- Price, Jonathan G., 1985, Ideal site mixing in solid solutions, with an application to two-feldspar geothermometry; *Am. Min.*, 70, 696-701.
- Ramsay, John G.; and Huber, Martin I., 1988, *The Techniques of Modern Structural Geology, Vol. 2: Folds and Fractures*; Academic Press, London, 309-700.
- Rankin, A.H.; Ransey, M.H.; Coles, B.; Langvelde, F. Van; and Thomas, C.R., 1992, The composition of hypersaline granitic fluids based on laser-ICP and Synchrotron-XRF microprobe analyses of individual fluid inclusions in topaz, Mole Granite, eastern Australia; *Geochim. Cosmochim. Acta*, 56, 67-79.
- Rehrig, William A., 1982, Metamorphic core complexes of the southwestern United States -- An updated analysis; in *Mesozoic-Cenozoic Tectonic Evolution of the Colorado River Region, California, Arizona, and Nevada* (Frost, Eric G., and Martin, Donna L., eds.), Anderson-Hamilton Volume, 551-560.
- Richardson, S.W., 1968, Staurolite stability in part of the system Fe-Al-Si-O-H; *J. Petrol.*, 9, 467-488.
- Richardson, S.W., Gilbert, M.C., and Bell, P.M., 1969, Experimental determination of kyanite-andalusite and andalusite-sillimanite equilibria: The aluminum silicate triple point; *Am. J. Sci.*, 267, 259-272.
- Ririe, G. Todd, 1990, A comparison of alteration assemblages associated with Archean gold deposits in Western Australia and Paleozoic gold deposits in the southeast United

- States; *Can. J. Earth Sci.*, 27, 1560-1576.
- Robie, R.A.; Bethke, P.M.; and Beardsley, K.M., 1967, Selected x-ray crystallographic data, molar volumes, and densities of minerals and related substances; *U.S. Geol. Surv. Bull* 1248.
- Romberger, Samuel B., 1986, The solution chemistry of gold applied to the origin of hydrothermal deposits; in *Gold in the Western Shield* (Clark, Lloyd A., ed.), *Can. Inst. Min. Met.*, Sp. Vol. 38, 168-186.
- Rose, Arthur W.; and Burt, Donald M., 1979, Hydrothermal alteration; in *Geochemistry of Hydrothermal Ore Deposits* (Barnes, Hubert Lloyd, ed.), 2nd ed., John Wiley and Sons, New York, 173-235.
- Rutherford, Malcolm J., 1973, The phase relations of aluminous iron biotites in the system  $KAlSi_3O_8$ - $KAlSiO_4$ - $Al_2O_3$ - $Fe-O-H$ ; *J. Petrol.*, 14, 159-180.
- Schmidt, Robert G., 1985, High alumina hydrothermal systems in volcanic rocks and their significance to mineral prospecting in the Carolina Slate Belt; *U.U. Geol. Survey, Bull.* 1562, 59p.
- Shade, John W., 1974, Hydrolysis reactions in the  $SiO_2$ -excess portion of the system  $K_2O-Al_2O_3-SiO_2-H_2O$  in chloride fluids at magmatic conditions; *Econ. Geol.*, 69, 218-228.
- Silver, L.T.; Bickford, M.E.; Van Schmus, W.R.; Anderson, J.L.; Anderson, T.H.; and Medaris, L.G., 1977, The 1.4-1.4 b.y. transcontinental anorogenic plutonic perforation of North America; *Geol. Soc. Abstr. w. Programs*, 9, 1176-

1177.

Simpson, Carol; and Schmid, Stefan M., 1983, An evaluation of criteria to deduce the sense of movement in sheared rocks; *Geol. Soc. Am. Bull.*, 94, 1281-1288.

Slack, John F.; and Coad, Paul R., 1989, Multiple hydrothermal events in the Kidd Creek volcanogenic massive sulfide deposit, Timmins, Ontario,: evidence from tourmalines and chlorites; *Can. J. Earth Sci.*, 26, 694-715.

Smith, Joseph V.; and Brown, William L., 1988, *Feldspar Minerals, Volume 1: Crystal Structures, Physical, Chemical, and Microtextural Properties*; Springer-Verlag, Berlin, 828p.

Sokolova, N.T.; and Khodakovskiy, I.L., 1977, The mobility of aluminum in hydrothermal systems; *Geochem. Int.*, 77, 105-112.

Spry, Alan, 1969, *Metamorphic Textures*; Pergamon Press, Oxford, 352 pp.

Steeffel, Carl I.; and Atkinson, William F., Jr., 1983, Hydrothermal andalusite and corundum in the Elkhorn District, Montana; *Geol. Soc. Am., Abstr. w. Progr.*, 15(6), 695.

Stevens, Rollin E.; and Carron, Maxwell K., 1948, Simple field test for distinguishing minerals by abrasion pH; *Am. Min.*, 33, 31-49.

Stoffregen, Roger, 1987, Genesis of acid-sulfate alteration and Au-Cu-Ag mineralization at Summitville, Colorado;

- Econ. Geol., 82, 1575-1591.
- Strong, D.F., 1989, A review and model for granite-related mineral deposits; in Recent Advances in the Geology of Granite-Related Mineral Deposits (Taylor, R.P. and Strong, D.F., eds.), Can. Inst. Min. Met., Proceedings of the CIM Conference on Granite-Related Deposits, 424-445.
- Sykes, Martha L.; and Moody, Judith B., 1978, Pyrophyllite and metamorphism in the Carolina Slate Belt; Am. Min., 63, 96-108.
- Thomas, Warren M.; Clark, H. Steve; Young, Edward D.; Orrell, Suzanne E.; and Anderson, J. Lawford, 1988, Proterozoic high-grade metamorphism in the Colorado River region, Nevada, Arizona, and California; in Metamorphism and Crustal Evolution of the Western United States (Ernst, W.G., ed.), Rubey Volume VII, 526-537.
- Tourigny, Ghislain; Hubert, Claude; Brown, Alex C.; and Crepeau, Robert, 1989, Synvolcanic and syntectonic gold mineralization at the Bousquet mine, Abitibi Greenstone Belt, Quebec; Econ. Geol., 84, 1875-1890.
- Tosdal, R.M., 1986a, Gneissic host rocks to gold mineralization in the Cargo Muchacho Mountains, southeastern California; in Cenozoic Stratigraphy, Structure, and Mineralization in the Mojave Desert, Geol. Soc. Am. 82nd Ann. Mtg., Field trip Guidebook, 139-142.
- Tosdal, Richard M., 1986b, Mesozoic ductile deformations in the southern Dome Rock Mountains, northern Trigo Mountains, Trigo Peak, and Livingston Hills, southwestern



- Arizona, and Mule Mountains, southeastern California; in *Frontiers in Geology and Ore Deposits of Arizona and the Southwest*, Ariz. Geol. Soc. Digest, v. 16, 62-71.
- Tosdal, R.M., 1990, Jurassic low angle ductile shear zones, SE California and SW Arizona: Thrust faults, extensional faults, or rotated high-angle faults?; *Geol. Soc. Am. Abstr. w programs*, 22, 89.
- Tosdal, R.M., and Haxel, G.B., 1987, Late Jurassic regional metamorphism and Deformation, Southeastern California and Southwestern Arizona; *Geol. Soc. Am., Abstr. w Programs*, 19, 870.
- Tosdal, R.M., and Wooden, J.L., 1991, Middle Jurassic plutons, SE California and SW Arizona; *Geol. Soc. Am. Abstr. w Programs*, 23, no. 5, A308.
- Turner, F.J.; and Weiss, L.E., 1963, *Structural Analysis of Metamorphic Tectonites*: New York, McGraw Hill Book Company, 524 pp.
- Valliant, R.I.; Barnett, R.L.; and Hodder, R.W., 1983, Aluminum silicate-bearing rock and its relation to gold mineralization; Bousquet Mine, Bousquet Township, Quebec; *Canadian Inst. Min. Met. Bull.*, 76, 811-819.
- Vernon, R.H., 1979, Formation of late sillimanite by hydrogen metasomatism (base-leaching) in some high-grade gneisses; *Lithos*, 12, 143-152.
- Vernon, R.H., 1986, Oriented growth of sillimanite in andalusite, Placitas -- Juan Tabo area, New Mexico, U.S.A.; *Can. J. Earth Sci.*, 24, 580-590.

- Vernon, R.H., Flood, R.H., and D'Arcy, W.F., 1987, Sillimanite and andalusite produced by base-cation leaching and contact metamorphism of felsic igneous rocks; *J. Meta. Geol.*, 5, 439-450.
- Walker, J. Douglas, 1987, Permian to Middle Triassic rocks of the Mojave Desert; in *Mesozoic Rocks of Southern Arizona and Adjacent Areas* (Dickinson, William R., and Klute, Margaret A., eds.), *Arizona Geol. Soc. Digest*, vol. 18, 1-14.
- Whitney, J.A., 1988, The origin of granite: the role and source of water in the evolution of granitic magmas; *Geol. Soc. Am. Bull.*, 100, 1886-1897.
- Whitney, James A.; and Stormer, John C., 1977, The distribution of  $\text{NaAlSi}_3\text{O}_8$  between coexisting microcline and plagioclase and its effects on geothermometric calculations; *Am. Min.*, 62, 687-691.
- Wilkins, Joe, 1984, The distribution of gold- and silver-bearing deposits in the Basin and Range Province, Western United States; in *Gold and Silver Deposits of the Basin and Range Province, Western U.S.A.* (Wilkins, Joe, ed.), *Arizona Geological Society Digest*, vol. 15, 1-27.
- Williams, Michael L.; and Grambling, Jeffrey A., 1990, Manganese ferric iron, and the equilibrium between garnet and biotite; *Am. Min.*, 75, 886-908.
- Wintsch, R.P., 1975a, Feldspathization as a result of deformation; *Geol. Soc. Am. Bull.*, 86, 35-38.

- Wintsch, Robert P., 1975b, Solid-fluid equilibria in the system  $KAlSi_3O_8$ - $NaAlSi_3O_8$ - $Al_2SiO_5$ - $SiO_2$ - $H_2O$ - $HCl$ ; *J. Petrol.*, 16, part 1, 57-79.
- Wintsch, R.P., 1980, Supercritical pE-pH diagrams, with application to the stability of biotite; *Contr. Min. Pet.*, 73, 421-428.
- Wintsch, R.P., 1981, Syntectonic oxidation; *Am. J. Sci.*, 281, 1223-1239.
- Wintsch, R.P., 1985, The possible effects of deformation on chemical processes in metamorphic fault zones; *in* *Metamorphic Reactions: Kinetics, Textures, and Deformation* (Thompson, A. B., and Rubie, D. C., eds.), Springer-Verlag, NY, 251-268.
- Wintsch, Robert P.; and Dunning, Jeremy, 1985, The effect of dislocation density on the aqueous solubility of quartz and some geologic applications: A theoretical approach; *J. Geophys. Res.*, 90 (B5), 3649-3657.
- Wise, William S., 1974, The origin of the assemblage: quartz + Al-silicate + rutile + Al-phosphate; *Fortschr. Miner.*, 52, 151-159.
- Wones, David R.; and Eugster, Hans P., 1965, Stability of biotite: Experiment, theory and application; *Am. Min.*, 50, 1228-1272.